Effect of composition and processing on the microstructure and formability of aluminium automotive body sheet alloys

A Thesis Submitted for the Degree of Doctor of Philosophy

by

Hao Zhong

Department of Materials Engineering

Monash University

June 2014

Statement of Originality

This thesis does not contain material that has been submitted or accepted for the award of another degree, diploma or qualification at this or any other university or institution. To the best of my knowledge and belief, it does not contain any materials that have been previously published or written by any other person, except where dues reference is made in the text of the thesis.

Hao Zhong

June 2014

Acknowledgements

Finally, I would like to express my cordial gratitude to my family for their persistent support and encouragement. They are always my driver for completing my PhD study.

Abstract

Stretch forming is a common deformation mode during the stamping of 6xxx series Al-Mg-Si(-Cu) automotive body panels. Good formability in this mode requires high work hardening and strain rate hardening capabilities, which are controlled by the alloy composition and processing (particularly heat treatments) through their influence on the microstructure. The influence of composition and heat treatment on the formability of 6xxx alloys has been previously investigated, but systematic research is still needed in order to provide a deeper understanding of the underlying mechanisms for the purpose of maximising the formability of 6xxx alloys, whenever possible, by composition and heat treatment modifications.

Therefore, in this PhD project, the effects of alloy composition (Si, Mg and Cu contents) and heat treatment (natural ageing and/or pre-ageing at 100 ºC for 2 h or at 200 ºC for 20 s) on the formability of eight 6xxx alloys were systematically studied. The microstructure of these alloys was investigated by scanning electron microscopy (SEM) and transmission electron microscopy (TEM). The macro-texture was characterised by X-ray diffraction. A surface profilometer was used to characterise the strain localisation. Tensile testing was used to determine the uniaxial tensile properties, and to study the work hardening and strain rate hardening behaviour of these alloys, which were used to correlate the microstructural features with the formability results. The use of Kocks-Mecking-Estrin model enabled a separation of the contributions of different microstructural features to the work hardening capability of the alloys studied. Furthermore, based on the knowledge from the experimental and constitutive modelling results, thermodynamic modelling was employed to predict the microstructure that could improve the formability of a high Mg content alloy.

In this work it was found that solutes in solution are the most important factor that influences the stretch formability. It increases the work hardening capability by increasing the dislocation storage rate and impeding the dynamic recovery. For instance, Cu atoms were found to have a significant influence on the dislocation storage rate while having little influence on the dynamic recovery rate; conversely, Mg atoms have a substantial influence on the dynamic recovery rate while having little effect on the dislocation storage rate; and,

finally, Si atoms have a slight influence on both the dynamic recovery rate and the dislocation storage rate. It should be noted that increasing Si content also leads to a high number density of dispersoids, although the contribution of dispersoids to work hardening is much smaller than that of solute atoms in solution. In terms of strain rate hardening behaviour, solute atoms in solution (particularly Mg atoms) reduce the strain rate sensitivity (SRS). However, if the addition of solutes promotes the natural ageing kinetics, then a high SRS is observed after extended natural ageing. This is the case in the high Si content alloys. By contrast, high Mg content alloys normally show a sluggish natural ageing kinetics, thus a larger negative contribution to SRS associated with dynamic strain ageing (DSA) can be observed. It was also found that Cu additions can retard the natural ageing kinetics regardless of the magnitude of the Mg/Si ratio in the alloys. The degree of retardation does depend on the Mg/Si ratio, though. This is particularly the case in the alloys with a high Mg/Si ratio where serrated yielding can still be observed in the alloy after one week of natural ageing. This is at variance with other alloys where serrated yielding disappeared within one day of natural ageing after quenching, which can be associated with the depletion of solutes and quenched-in vacancies.

Vacancies were also found to influence the formability. This is particularly important in pre-aged samples. After one week of natural ageing, pre-aged samples showed a lower SRS than those without pre-ageing, which is probably due to a higher vacancy concentration in the pre-aged samples. The excess vacancies may exist as solute-vacancy complexes or be bound with solute clusters depending on pre-ageing time. A model was proposed to account for the decreased SRS in the pre-aged samples.

Stretch formability is a property that is crucial in the selection of Al alloys for targeted applications. It was investigated in the course of the project in great detail. The overall effect of the alloy composition on the formability is that increasing Si content or decreasing Mg/Si ratio can improve the stretch formability due to the increased work hardening and strain rate hardening capabilities. The addition of Cu can significantly enhance the stretch formability of alloys with Mg/Si > 1, which is because the magnitude of the work hardening is more important than that of the strain rate hardening.

An important property that influences acceptance of an alloy of the 6xxx series by industry is its bake-hardening response. This aspect of alloy development was also studied in the thesis. It was shown that although pre-ageing can improve the paint-bake response of the 6xxx alloys, pre-ageing was found to reduce their stretch formability due to the decreased work hardening and strain rate hardening capabilities. This effect is especially pronounced in the case when the samples are pre-aged at 100 ºC for 2 h, as pre-ageing reduces the strain rate hardening appreciably. Therefore, this work suggests that any attempts at improving the stretch formability of 6xxx alloys must also consider their effects on the paint-bake response.

Finally, thermodynamic modelling results show that the stretch formability of the excess Mg alloy A2, which has a relatively poor stretch formability, can be improved by increasing the Si and Mn contents and/or decreasing the Mg content.

Thus, a tangible outcome of the PhD project is a detailed set of reliable experimental results on the effect of the alloy composition and heat treatment of 6xxx alloys studied on their strength and ductility characteristics, stretch formability, and bake-hardening response. Moreover, practically, this PhD project not only explains why most of the commercial 6xxx alloys for automotive outer panels are Si-rich alloys, but also provides guidance for the development of Mg-rich 6xxx alloys for automotive panel applications.

Publications and presentations

Publications:

H. Zhong, P.A. Rometsch, L.F. Cao, F.A Guo and B.C. Muddle. *Tensile properties and work hardening behaviour of alloy 6016 in naturally aged and pre-aged conditions.* The 12th International Conference on Aluminium Alloys Proceedings. Yokahama, Japan, 2010, pp. 2203-2208.

H. Zhong, P.A. Rometsch and Y. Estrin. *The influence of alloy composition on the microstructure, tensile ductility and formability of 6xxx alloys.* Proceedings of the 13th International Conference on Aluminium alloys. Pittsburgh, USA, 2012, pp. 687-692.

H. Zhong, P.A. Rometsch and Y. Estrin. *Effect of alloy composition and heat treatment on the mechanical performance of 6xxx alloys.* Proceedings of the First International Conference on Aluminium alloys, Beijing, China, 2013, pp. 235-243.

H. Zhong, P.A. Rometsch and Y. Estrin. *The influence of Si and Mg content on the microstructure, tensile ductility and stretch formability of 6xxx alloys.* Metallurgical and Materials Transaction A, 44, 2013, pp. 3970-3983.

L.F. Cao, B.C. Muddle, P.A. Rometsch, **H. Zhong**, S. Gao, Y.L. Ji, P. Hu, F.A. Guo. An aluminium alloy for automotive panels and heat treatment thereof. Chinese patent, CN103060632A.

H. Zhong, P.A. Rometsch and Y. Estrin. *The influence of Mg/Si ratio and Cu content on the tensile ductility and stretch formability of 6xxx alloys*, in preparation.

H. Zhong, P.A. Rometsch and Y. Estrin. *The increased dynamic strain ageing in 6xxx alloys by pre-ageing,* in preparation.

H. Zhong, P.A. Rometsch and Y. Estrin. *The influence of heat treatment on the mechanical performance of 6xxx alloys,* in preparation.

H. Zhong, L.F. Cao, P.A. Rometsch and Y. Estrin. *The apparent relationship between the strain rate sensitivity and paint-bake response*, in preparation.

Presentations:

The 12th International Conference on Aluminium Alloys
Yokahama, Japan, 5th - 9th September 2010

The 2011 Monash Materials Engineering Postgraduate Winter Conference
Melbourne, Australia, 8th June 2011

The 13th International Conference on Aluminium alloys
Pittsburgh, USA, 3rd - 7th June 2012

The First International Conference on Aluminium alloys
Beijing, China, 13th - 17th October 2013

Table of Contents

List of Figures

List of Tables

Chapter 1: Introduction

Steel has been the dominant material used in manufacturing automobiles since the 1920s, due to its all-round versatility (i.e. high strength and formability) and low processing cost [1, 2]. However, the increasing requirement to improve fuel economy triggered by concerns about global warming and energy usage has compelled the use of lighter metals than steel in automotive applications [1].

Weight reduction is particularly important because the average mass of vehicle is expected to increase (see Fig. 1-1), due to more stringent legislative requirements and customer demands (increased luxury, convenience, performance and safety, etc) [1, 3]. In order to invert this weight increase, a reduction of the whole vehicle weight is therefore necessary. Besides the effort on improving design and power train efficiency, the substantial use of light-weight materials is believed to be an effective way for a significant reduction in overall vehicle weight [1]. According to one rule of thumb, a 10% weight reduction approximately equals a 5.5% improvement in fuel economy [1]. Moreover, this weight reduction by using light-weight metals would allow further weight saving due to drivetrain, motor and chassis downsizing [3]. Therefore a 10% vehicle weight reduction could result in an 8-10% fuel economy improvement [1].

The characteristic properties of aluminium alloys - high strength and stiffness to weight ratio, good formability, good corrosion resistance, and recycling potential - make it the ideal candidate to replace heavier materials in cars to respond to the weight reduction demands within the automotive industry [1, 4]. Therefore, the use of aluminium alloys in automotive applications has consistently increased in recent years, as shown in Fig. 1-2. Fig. 1-3 shows the typical use of aluminium in the construction of an Audi A8.

Among several types of aluminium alloys that meet the requirements for automotive sheet applications, Al-Mg-Si alloys of the 6xxx series stand out owing to their remarkable strengthening potential during the paint-bake cycle [5].
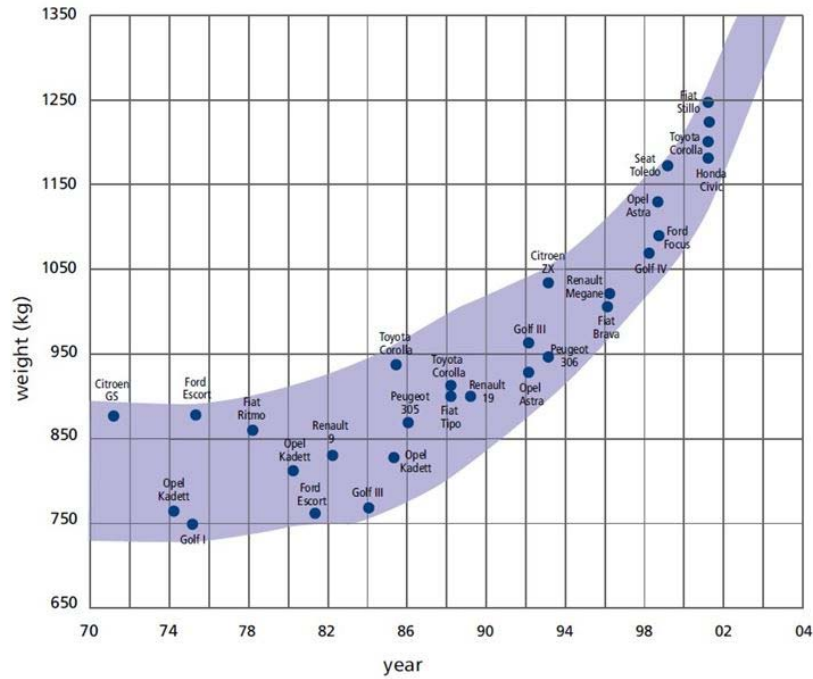
Fig. 1-1 Evolution of weight in the compact class of European cars [3].

Stretch forming is a common deformation mode in the production of 6xxx exterior automotive body panels [6]. Good formability in this mode requires high work hardening and strain rate hardening capabilities [7, 8], which are controlled by the alloy composition and processing (i.e. heat treatment) through their influence on the microstructure [9]. The influence of composition and heat treatment on the formability of 6xxx alloys has been previously investigated to some degree [9-12], but controversies still exist. For instance, increasing the Si content was reported to either increase [9, 13, 14] or decrease the stretch formability [10]. The addition of Mg is believed to deteriorate the plane strain stretching performance [13]. Moreover, although the addition of Cu has a positive influence on the work hardening [15], it appears that the influence of Cu on the formability depends on the Mg/Si ratios in the alloys [13]. As for the effect of heat treatment on the formability of 6xxx alloys, it is generally accepted that a higher formability is achieved in the naturally aged condition than in the artificially aged (i.e. peak aged and/or over aged) conditions [16, 17] due to a higher work hardening capability in the naturally aged condition [16]. However, pre-ageing is effectively an under-ageing treatment that is used to stabilise the material after solution treatment and quenching [5]. Moreover, after pre-ageing, the materials will be naturally aged for a significant but variable amount of time before forming. The natural

ageing after the pre-ageing treatment is expected to further modify the microstructure and thus influence the formability of the materials. It should be noted that some researches did study the influence of pre-ageing on the formability of 6xxx alloys [12, 18]. In their studies, Erichsen dome height was used as a formability index. However, Erichsen test was believed to be an inappropriate method for the formability evaluation [19]. Moreover, it appears that pre-ageing always led to an unbalanced combination between the formability and the paint bake response [20]. Most importantly, the underlying mechanisms of how the composition and heat treatment influence the formability of 6xxx alloys are still unclear. Moreover, previous studies showed that different microstructural features, such as the grain structure, solute in solution and dispersoids, all have different influences on the formability. However, in practice, several microstructural features may act together to generate the macroscopic response. This makes it difficult to directly correlate an individual feature with the formability. The poor understanding on the effect of composition and heat treatment on the formability of 6xxx alloys would impede the development of new 6xxx alloys with improved formability for automotive applications.

Practically, most current Al-Mg-Si alloys used for automotive panel applications are Si-excess alloys, e.g. alloys AA6016 and AA6022 [21]. However, high Si alloys are not recycling-friendly since Si is difficult to control in recycled metal [22]. The Si content tends to increase slightly with subsequent recycling steps. In contrast, high Mg alloys are more recyclable than high Si alloys [22]. Therefore, it is of interest to investigate the stretch formability of 6xxx alloys with an excess of Mg to see whether such alloys could perform similarly or better than Si-excess alloys. This is expected to provide information for the development of new aluminium alloys for automotive panel applications.

In summary, the major objective of this PhD study is to obtain a comprehensive understanding of the effects of alloy composition and heat treatment on the formability of 6xxx alloys for automotive auto panel applications for the purpose of developing new aluminium alloys with improved formability for automotive panel applications.
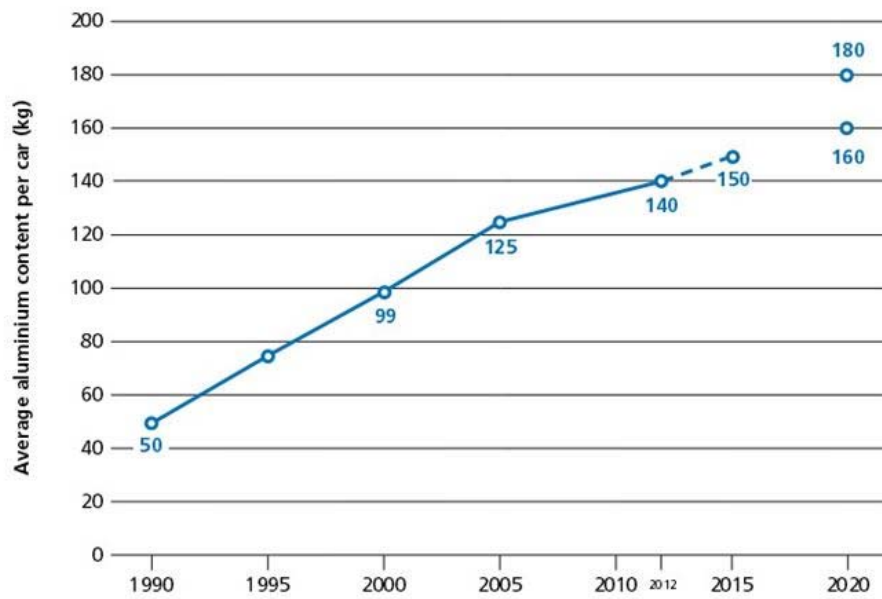
Fig. 1-2 Evolution of average aluminium content per car produced in Europe [23].
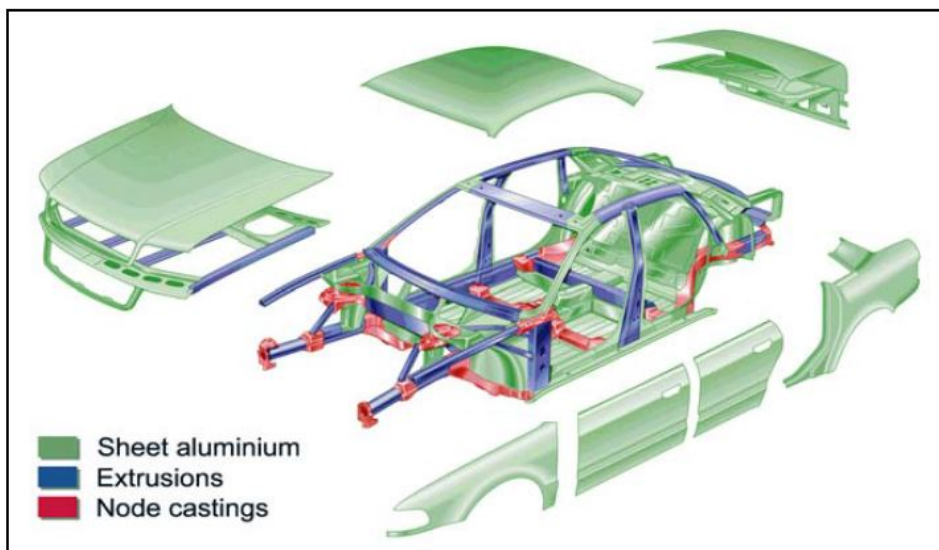
Fig. 1-3 Audi A8-Al space frame and semi materials distribution [24].

Chapter 2: Literature review

2.1 Aluminium alloys used for automotive panel applications

For automotive panel applications, the main aluminium alloy classes are the non-heat treatable Al-Mg (5xxx series) and the heat treatable Al-Mg-Si(-Cu) (6xxx series) alloy systems [4]. Some Al body sheet materials are especially tailored by modifications in chemical composition and processing, e.g. 6016 variants for outer panels have been designed for improved formability (HF100), and/or age hardening response (DR100 or DR130) [25]. Fig. 2-1 illustrates the key properties of 5xxx and 6xxx alloys used in automotive body sheet applications.
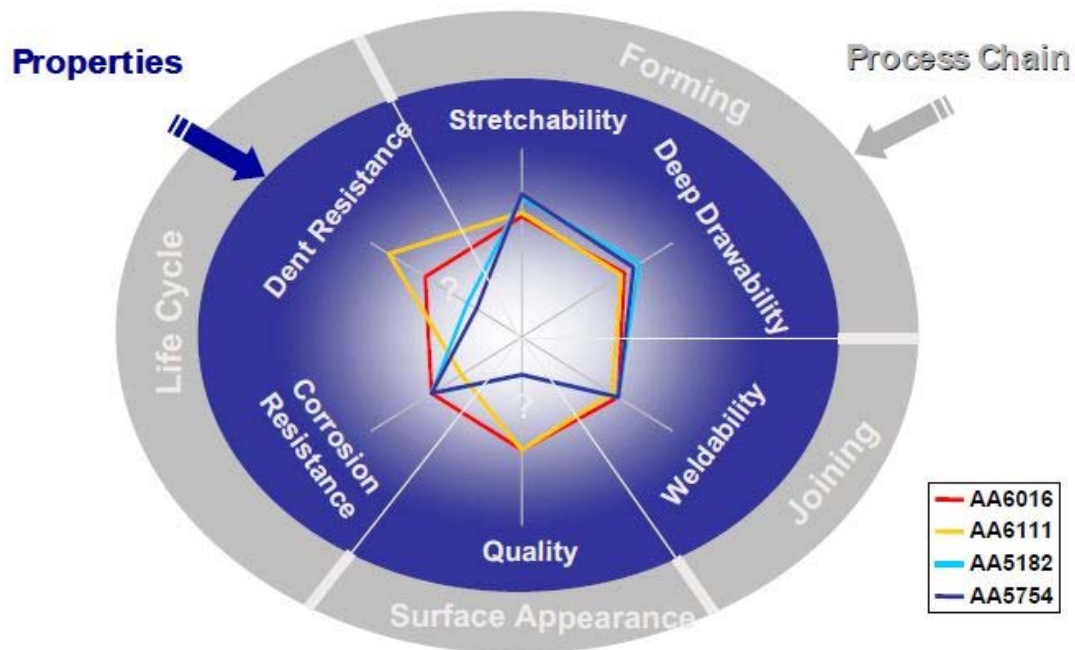
Fig. 2-1 Properties of some 5xxx and 6xxx alloys competing for car body applications [24].

The 5xxx alloy system gives a good combination of superior formability with sufficient strength achieved by the mechanism of solid solution hardening, which can be enhanced by deformation due to the high work hardening behaviour [24]. Due to their problems with strain markings (PLC effect, Lüders-lines) after sheet forming/stretching operations [24], Al-Mg 5xxx alloys are mostly used for inner panel applications [1].

The heat treatable 6xxx alloys are the primary choice for outer panel applications since these alloys exhibit a good balance of formability, paint-baked strength, and a high surface quality after forming and paint-bake cycle [1]. The 6xxx series alloys contain Mg and Si, either with or without additions of Cu. Current 6xxx alloys used for autobody sheets include AA6016, AA6111, AA6022 [13, 21] and AA6181A was developed for recycling purpose [24]. Table 2-1 lists the composition limits of these 6xxx alloys for automotive applications. In the USA, AA6111 is often used for outer panels, combining high strength with good formability [24]. In Europe, EN-6016 is preferred [24]. It shows a superior formability, better filiform corrosion resistance than the higher Cu alloys (e.g. AA6111), and allows flat hems even on parts with local pre-deformation [21]. However, the bake-hardened strength of 6016 is significantly lower than that of AA6111 [13]. Alloy AA6022 was developed by Alcoa [21] and shows a better combination of formability, paint-baked strength and corrosion resistance than AA6016 and AA6111 [13, 21]. It should be noted that all these four alloys are Si-excess alloys with respect to Mg_2Si balanced alloys (in this case, the amount of Si consumed by Fe-containing particles are not considered), as illustrated in Fig. 2-2.
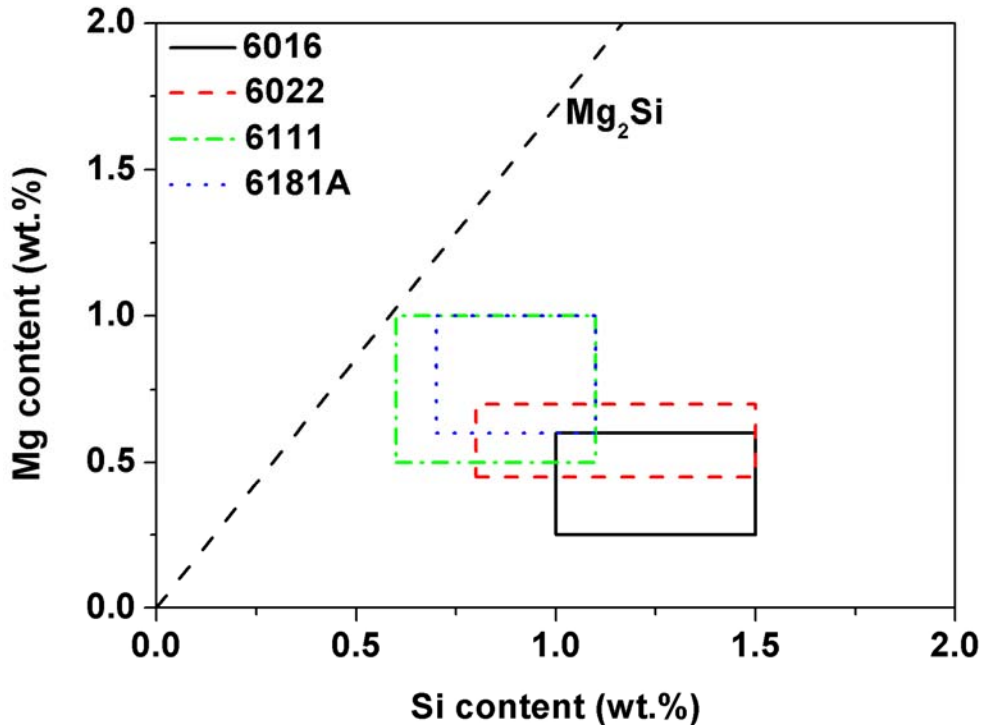
Fig. 2-2 Si and Mg ranges in the main 6xxx alloys used for automotive applications.

Table 2-1 Composition ranges (in wt.%) of aluminium alloys used for automotive closure panel applications [21, 26]. (Note: single numbers refer to the maximum values)

Alloy	Si	Mg	Cu	Fe	Mn	Ti	Al
6111	0.6-1.1	0.50-1.0	0.5-0.9	0.4	0.1-0.45	0.1	Bal.
6016	1.0-1.5	0.25-0.6	0.2	0.5	0.2	0.1	Bal.
6022	0.8-1.5	0.45-0.7	0.01-0.11	0.05-0.2	0.02-0.1	0.15	Bal.
6181A	0.7-1.1	0.6-1.0	0.25	0.15-0.5	0.4	0.25	Bal.

2.2 Typical processing route for aluminium automotive outer panels

In the commercial production of AA6xxx sheets the material goes through a specific production route (DC casting, hot and cold rolling and final anneal treatment) before reaching the final gauge in the materials factory. Such a sequence was described by Engler and Hirsch [26], and is shown schematically in Fig. 2-3. After final anneal (or solution treatment) the sheets are pre-aged to stabilise the properties during storage and shipment at room temperature, and improve the age hardening response during paint-bake cycle [5]. Then the sheet will be delivered to the automotive manufactures after an extended period of storage and shipment at room temperature. In the automotive plant, the sheets are stretched over a punch to form the auto body components. The final in-service strength of the manufactured parts is achieved after the forming operations by means of age hardening, typical during the final automotive paint-baking cycles, which may be approximated as under-ageing treatments of 20-30 min at temperatures between about 160 and 200 °C [26].

The basic requirements for the 6xxx alloys used for automotive outer panels are a high stretch formability for stamping and a high paint-bake response during the paint-bake treatment, although it appears that a high stretch formability tends to correspond with a low paint-baked strength [20]. The formability and paint-bake response are influenced by the whole production chain shown in Fig. 2-3, especially by the processing after final cold rolling (i.e. solution treatment [27] and/or natural ageing [16] and/or pre-ageing [20]).

(a) DC casting   (b) preheating (homogenization)

(c) breakdown hot rolling   (d) multistand hot rolling

(e) cold rolling   (f) continuous annealing (recrystallization)
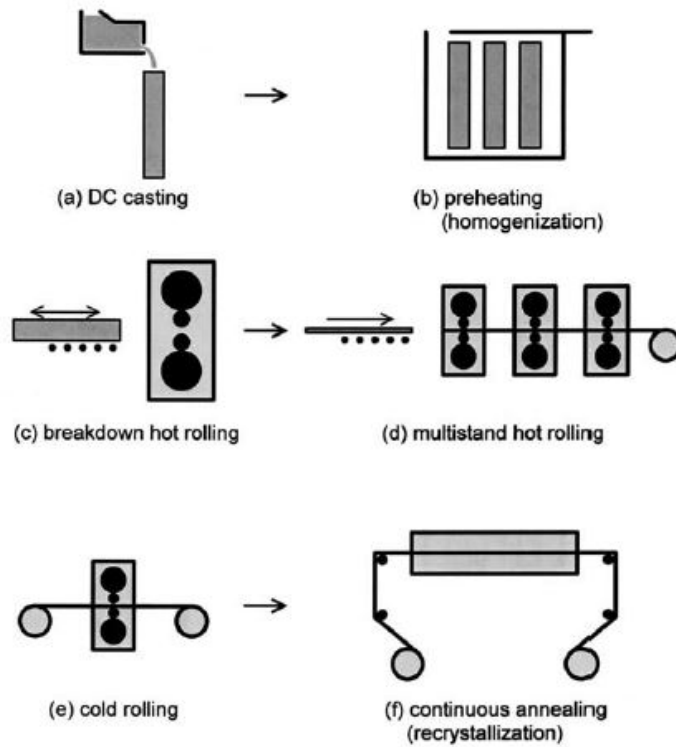
Fig. 2-3 Schematic diagram illustrating the typical steps of thermo-mechanical processing of AA6xxx sheet alloys [26].

2.3 The relationship between microstructural features, work hardening, strain rate hardening and formability

The most common mode of failure in the stretching of sheet metal components is the development of a localised (through-thickness) necking or tearing, which occurs generally over a punch radius as the sheet surface area is increased to conform to the punch shape [8]. It is important to distribute deformation uniformly throughout the sheet, since a punch radius acts as a strain-concentrator by virtue of its curvature and frictional resistance [8]. A peak develops in the strain distribution and ultimately produces a neck or tear. Therefore the material's ability to distribute deformation uniformly throughout the sheet is crucial for a superior stretch formability [6, 8]. Two primary sources of hardening during deformation can help to maintain a uniform distribution of strain, namely: (i) work hardening, and (ii) strain rate hardening. A simplified constitutive description is given by [7]

$$\sigma = K \varepsilon^n \dot{\varepsilon}^m \tag{2-1}$$

8

where K is a constant, ε is the strain, $\dot{\varepsilon}$ is the strain rate, n is the work hardening exponent, and m is the strain rate hardening index (i.e. strain rate sensitivity, or SRS). In a workpiece, the region undergoing thinning work hardens and becomes resistant to further deformation, and thereby forces the deformation to the less deformed neighbouring elements [8]. Similarly, as the local strain-rate increases in areas undergoing thinning, the strain rate hardening of such regions forces deformation to occur in areas experiencing a slowdown in the rate of deformation [8]. Both processes thus resist strain localisation. Moreover, the work hardening exponent, n, is believed to be the most important factor in the distribution of strain prior to the onset of necking [8]. The presence of a positive strain rate sensitivity has an important stablising influence on the deformation beyond the onset of necking [8, 28]. Fig. 2-4 illustrates the influence of work hardening and strain rate hardening on the initial of necking and neck development in several metals. Improving the stretch formability by increasing the work hardening and strain rate hardening capabilities is well documented [7, 8, 28, 29], and work hardening capabilities are believed to be the predominant factor that influences stretch formability [6]. Obviously, the work hardening and strain rate hardening capabilities of the materials are controlled by alloy composition and processing parameters through their influence on the microstructural features.
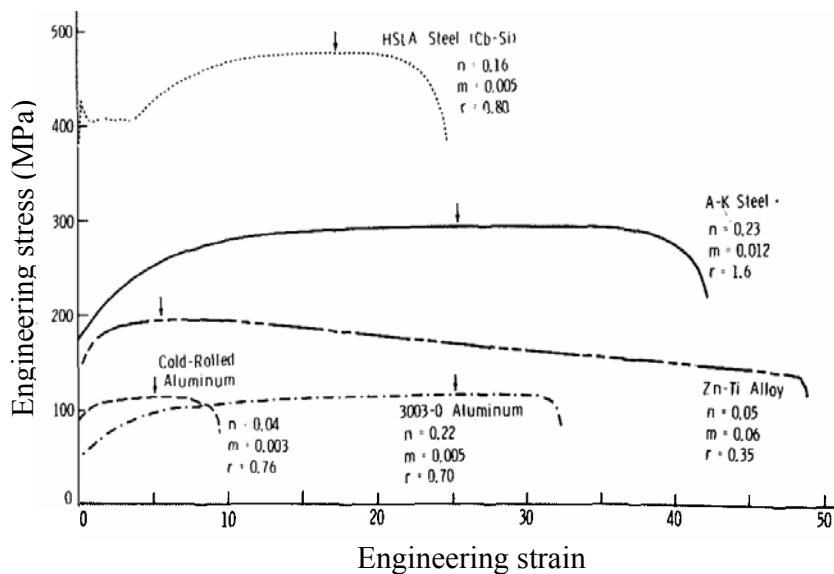
Fig. 2-4 Engineering stress-strain curves in uniaxial tension for a number of test materials [8]. Maximum load points are indicated by short vertical arrows.

2.3.1 Work hardening theory

Work hardening, also known as strain hardening or cold working, is the strengthening of a metal by plastic deformation. The work hardening of Al alloys is very important from a practical viewpoint, for instance, in optimising formability and in the production of specific products. It is also important from a more fundamental viewpoint in terms of understanding the interaction between strengthening mechanisms and the appropriate descriptions of work hardening for a variety of microstructures [30].

Many approaches can be used to express work hardening. Some of the most general measures are ($\sigma_{UTS} - \sigma_Y$), the stress difference between the yield stress, σ_Y and the ultimate tensile strength (σ_{UTS}), or the ratio (σ_{UTS}/σ_Y), and the work hardening exponent, *n* [31-33]. However, these methods cannot describe what is happening inside the microstructure during deformation. Therefore, they are only normally used to express degrees of work hardening for engineering purposes. Indeed, work hardening of single crystals is associated with the evolution of a dislocation substructure, which can be divided into a number of different stages of work hardening [34, 35]. In general, four stages (Stages I-IV) of classification have been widely accepted to identify the work hardening behaviour. A common way to represent work hardening is to use a Kocks-Mecking plot [36]; i.e. work hardening rate θ or Θ ($\partial\sigma/\partial\varepsilon_p$) *vs* true stress σ, where ε_p is the true plastic strain. Fig. 2-5 illustrates three stages of work hardening that can be observed from a Kocks-Mecking plot.
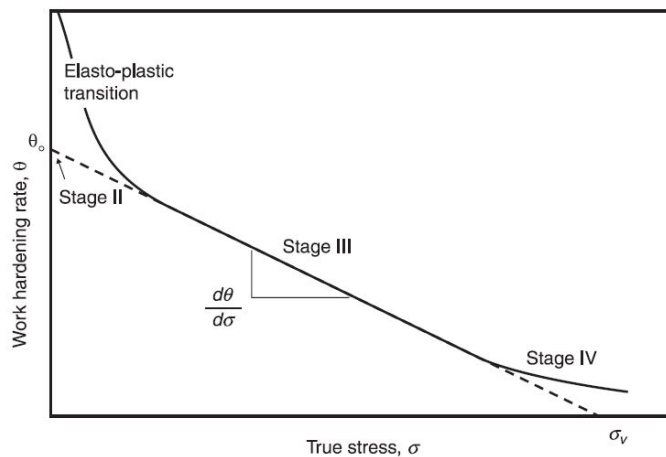
Fig. 2-5 Schematic diagram illustrating the various stages of work hardening and the elasto-plastic transition [35].

Stage I, or 'easy glide', depends very strongly on the orientation of the crystal and does not occur when the deformation takes place by multiple slip from the beginning [34]. This stage is characterised by a slight linear hardening and a low level of work hardening [37].

Stage II refers to the steepest rate of work hardening and occurs in both single crystals and polycrystals. Stage II is material insensitive [34]. In this stage, the rate of work hardening for pure metals is due to dislocation storage. For polycrystalline FCC metals, the Stage II work hardening amounts to approximately $\mu/20$, where μ is the shear modulus for the material, i.e. the initial work hardening rate, θ_0 is approximately 1200-1500 MPa for aluminium at ambient temperature [35].

Stage III exhibits a decreasing slope and is very sensitive to the temperature, rate of deformation and stacking fault energy (SFE) [34]. Stage III is also known as dynamic recovery process in which there exists a competition between dislocation accumulation and annihilation [34, 37].

Stage IV illustrates a breakdown of the linear decrease in the work hardening rate with stress in stage III. This stage corresponds to slight linear hardening with the same order of magnitude as in Stage I [37]. The rate of work hardening in Stage IV is low (usually below 100 MPa at ambient temperature) but this can be very important for large strain processes such as extrusion, rolling or equal channel angular extrusion (ECAE) [35].

The Kocks-Mecking approach is the most well-known approach to model the work hardening. It describes the concurrent processes of dislocation accumulation and annihilation in the pure material [34], and allows for terms to describe the role of additional features such as grain size, solute, non-shearable particles [38] etc.

The approach is based on the assumption that the kinetics of plastic flow are determined by a single structure parameter, the average dislocation density ρ, through the relation [39]

$$\sigma = \sigma_0 + M\alpha Gb\sqrt{\rho} \qquad (2\text{-}2)$$

where α is a constant of the order of unity and is 0.3 for FCC metals, G is the shear modulus, b is the Burger's vector and σ_0 is the friction stress. The second term in the equation

represents the contribution of dislocation strengthening to the flow stress (σ_D). The increase of the flow stress with strain is, then, determined by the evolution of the dislocation density. The evolution of the dislocation density is assumed to be the sum of two independent contributions [38, 39]:

$$\frac{d\rho}{d\varepsilon_p} = M(k_1\sqrt{\rho} - k_2\rho) \qquad (2\text{-}3)$$

The production term, $k_1\sqrt{\rho}$, is associated with the athermal storage (k_1 = constant) of moving dislocations which become immobilised after having travelled a distance proportional to the average spacing between the dislocations, $\rho^{-1/2}$, the process believed to account for the athermal hardening (stage II) [39]. The second term, $k_2\rho$, is associated with dynamic recovery (stage III), which is assumed to be linear with ρ.

By combining equation (2-2) and (2-3), the evolution equation for the dislocation strengthening can be obtained as following:

$$\frac{d\sigma_D}{d\varepsilon_p} = \Theta_0(1 - \frac{\sigma}{\sigma_v}) \qquad (2\text{-}4)$$

with $\Theta_0 = \alpha G b k_1 / 2$ and $\sigma_v = \alpha G b k_1 / k_2$

According to equation (2-4) the stress evolves during the plastic deformation towards the steady state value σ_v, i.e., $d\sigma/d\varepsilon = 0$ (see Fig. 2-5).

If geometric obstacles (i.e. fine grain size, non-shearable particles) exist, an additional term should be added in equation (1), as suggested by Estrin [39]

$$\frac{d\rho}{d\varepsilon_p} = M(k + k_1\sqrt{\rho} - k_2\rho) \qquad (2\text{-}5)$$

where k is a constant which represents the storage rate of geometrically necessary dislocations at geometric obstacles.

Integration of equation (2-5) for constant plastic strain rate yields, in combination with equation (2-2),

$$\Theta\sigma_D = \Theta_0\left(1 - \frac{\sigma}{\sigma_v}\right)\sigma + \frac{M^3(\alpha Gb)^2 k}{2} \qquad (2\text{-}6)$$

If the geometric obstacles have no influence on dislocation accumulation, the second term in equation (2-6) is absent, a plot of $\Theta\sigma_D$ *vs.* σ_D is an inverted parabola passing through the origin, and the initial slope of the curve is Θ_0, with a maximum in the plot ($\Theta_0\sigma_v/4$) occurring at $\sigma_D = \sigma_v/2$. By contrast, if the geometric obstacles do affect dislocation accumulation significantly, then the intercept of the $\Theta\sigma_D$ *vs.* σ_D plot with the ordinate axis is non-zero and corresponds to $\dfrac{M^3(\alpha Gb)^2 k}{2}$. Fig. 2-6 schematically shows the effect of geometric obstacles on the work hardening.
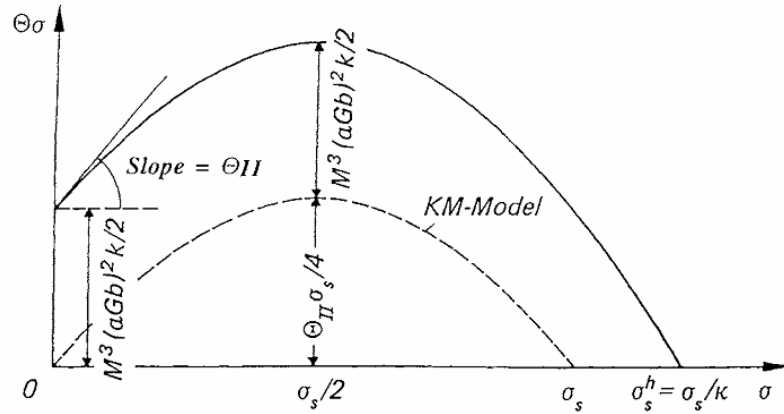
Fig. 2-6 $\Theta\sigma$ *vs.* σ plot showing the effect of geometric obstacles [38].

It should be noted that in Eq. 2-2, the flow stress is taken as a linear sum of the different contributions. However, for situations where multiple sets of objects are present such as solutes, precipitates and dislocations, Cheng *et al* [40] have proposed that another more general form for the flow stress addition laws should be considered when examining work-hardening behaviour, i.e.

$$\sigma = \sigma_0 + \sigma_{ss} + (\sigma_D{}^w + \sigma_{ppt}{}^w)^{1/w} \qquad (2\text{-}7)$$

where σ_{ss} is the solid solution strengthening contribution, σ_{ppt} is the contribution of precipitates and w can vary between 1 and 2. Moreover, Cheng et al [40] suggested that w = 1 only applies when there is a high density of week obstacles and a low density of strong obstacles (i.e. the early stages of precipitation). On the other hand, a value of w = 2 would be appropriate when the obstacle strength of the precipitates and the average obstacle strength for cutting for forest dislocations would be identical during the later stages of ageing (i.e. over-ageing) [40]. At intermediate cases, the appropriate value of w falls between these two extremes.

Moreover, for the tensile ductility and stretch formability, it is the work hardening at large strains (i.e. at strains close to necking) that matters [7]. Obviously, a high initial work hardening rate and a low dynamic recovery rate can result in a high work hardening rate at large strains.

The work hardening behaviour of aluminium alloys is influenced by microstructural features, such as solutes, non-shearable precipitates/particles and a fine grain size.

- **Solute**

Solutes may influence work hardening in the following three ways: a) precipitation during deformation, e.g. dynamic precipitation; b) enhancement of dislocation multiplication; c) retardation of dynamic recovery.

a. Dynamic precipitation

Precipitation may occur by the interaction of solutes and dislocations during deformation, which can increase the work hardening rate of the metals. For instance, Deschamps et al [41] studied a deformed supersaturated solid solution of a commercial 7010 alloy by in-situ small-angle X-ray scattering (SAXS) measurements. The authors found dynamic precipitation occurred during deformation, which was believed to be the mechanism for the increased work hardening rate since no non-shearable precipitates were observed to act as a dislocation storage medium. Another contribution may be due to retarded dynamic recovery since the

14

solute content is significantly high in the as-quenched 7010 alloy. Dynamic precipitation was also suggested to be the origin of a high work hardening rate in a naturally aged Al-Zn-Mg alloy [42]. Fig. 2-7 shows a comparison of Kocks-Mecking plots for as-quenched 7010 alloy and pure aluminium. As shown in Fig. 2-10, as quenched 7010 alloy showed a high stage II work hardening rate.
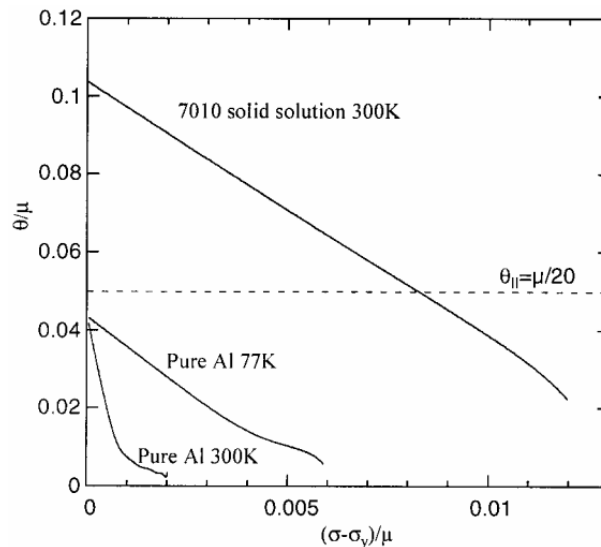
Fig. 2-7 Work hardening rate diagram for aluminium alloy 7010 deformed in solid solution, compared with the stage II work hardening rate and the work hardening rate behaviour of pure aluminium deformed at 300 and 77 K [41].

b. Enhancement in the dislocation multiplication

In the classic theory, it is generally believed that solutes in solution have no effect on the dislocation multiplication [36, 39]. In other words, the initial work hardening rate is independent of the solute concentration in solution, and is in the order of $\mu/20$ for polycrystalline aluminium. The influence of solutes on the work hardening is thought to be mainly through their influence on the dynamic recovery. However, recent studies showed that solutes in solution can influence both dislocation multiplication and dynamic recovery [15, 43, 44]. This is the case in the Al-Mg [15, 44], Al-Cu [15, 45], Ti alloy [46], Fe-Mn and Fe-N systems [43]. Indeed, solutes can influence the dislocation multiplication through their influence on the dislocation junction strength (α) [47] or dislocation storage rate (k_1) [15]. For the former mechanism, the variation in α may be explained by the formation of solute aggregates near the dislocation cores that increase the apparent strength of the forests by

pinning the mobile dislocations and by making more difficult the unzipping of the mobile dislocations from the forest [47]. For the latter mechanism, Zolotorevsky *et al* [15] suggested that foreign atoms diffuse from forest dislocations to a mobile dislocation while the latter is stopped before a barrier; this contributes to a pinning of the mobile dislocation and causes its transition to the category of forest dislocations. Fig. 2-8 shows the influence of Mg, Cu, Si and Zn concentrations on the initial work hardening rate. It is evident that solutes can influence the initial work hardening rate.
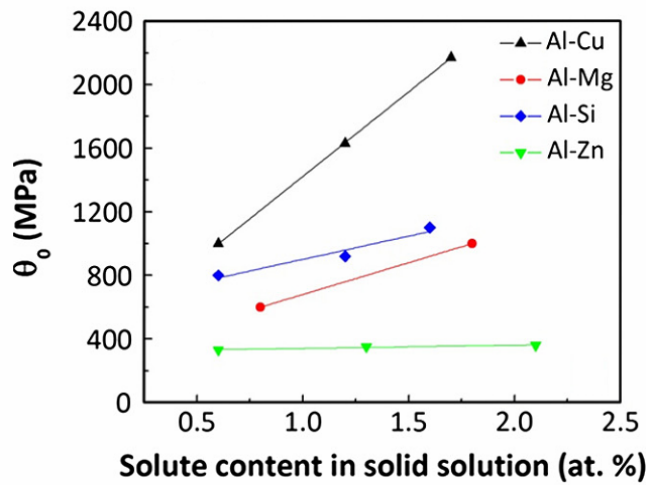
Fig. 2-8 Effect of solute concentration on the initial work hardening rate [48].

Fig. 2-9 shows the effect of normal alloying additions on the work hardening capability of aluminium. As shown in Fig. 2-9, with an increase of solute concentration, the work hardening capability increases. Out of the most common solutes in aluminium alloys, Cu is the most efficient element in promoting work hardening capability, due to its large influence on the initial work hardening rate.
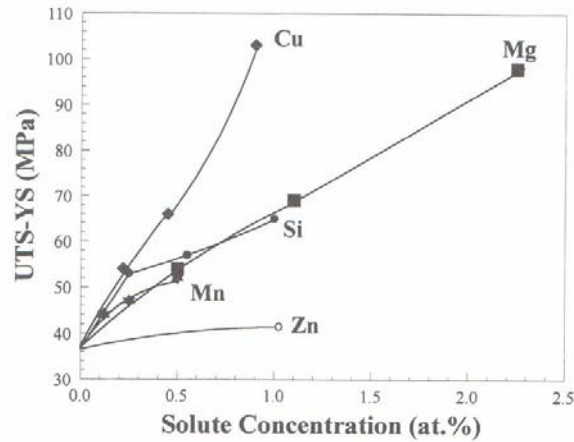
Fig. 2-9 The difference between the ultimate strength (UTS) and yield strength obtained in a tensile test for various alloying addition in aluminium [49].

c. Retardation of dynamic recovery

As for dynamic recovery, solutes drastically reduce the stacking fault energy of aluminium, which together with pinning effects, inhibits cross-slip and reduces cell formation by dynamic recovery [28]. Fig. 2-10 shows the effect of Mg, Cu, Si and Zn content on the dynamic recovery rate. It can be seen that solutes, especially Si, can influence the dynamic recovery rate.
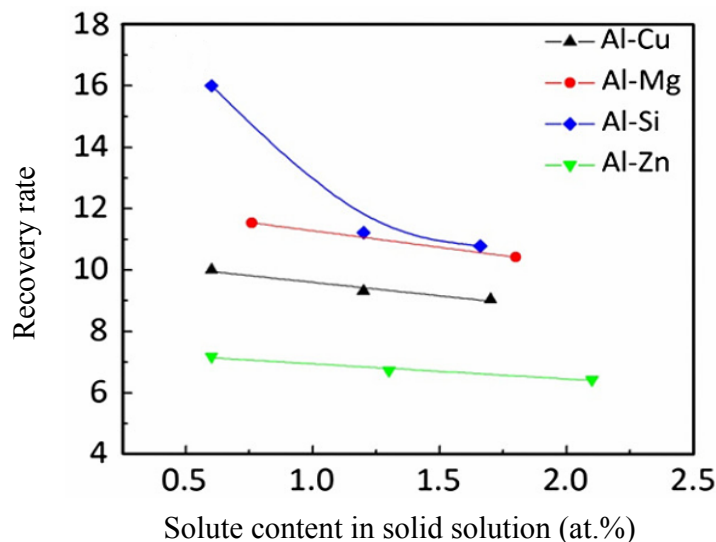
Fig. 2-10 Effect of solute concentration on the dynamic recovery rate [48].

- **Fine grain size**

The strength of polycrystalline materials increases as the grain size is reduced. Empirically this strengthening effect is often described as

$$\sigma_Y = \sigma_1 + KD^{-N} \tag{2-8}$$

where σ_Y is the yield stress and/or flow stress, D is the grain diameter, and σ_1, K and N are constants. Hall and Petch first correlated the yield stress of mild steels with the inverse square root of the grain diameter [50]. This so-called Hall-Petch equation can be applied not only to the yield stress, but also to the flow stress [51].

The mechanism for the contribution of grain boundaries to work hardening is as follows [50]: because of the difference in crystallographic orientation between neighbouring grains, geometrically necessary dislocations are introduced, in addition to statistically stored dislocations, to accommodate the incompatibility of deformation between grains. Estrin *et al* [39] has proposed a model (Eq. 2-5) that can describe the grain-size dependence of dislocation density. Moreover, Narutani *et al* [50] used this model to study the effect of grain size on the work hardening behaviour of Ni, as shown in Fig. 2-11.
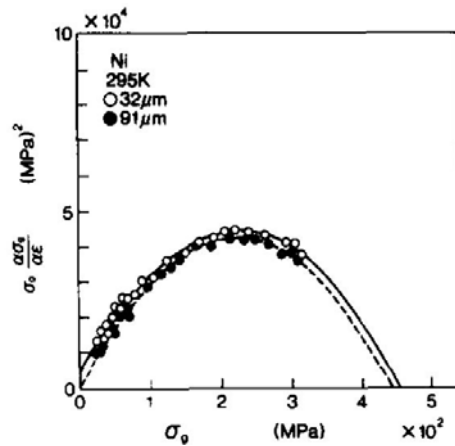
Fig. 2-11 The grain size effect on strain hardening for polycrystalline Ni [50].

- **Precipitates**

The influence of precipitates on the work hardening depends on the nature of the precipitates, i.e. shearable or non-shearable [40]. When the precipitates are small and coherent with the matrix, the precipitates are expected to be easily sheared by gliding dislocations, which produces local softening along the glide plane [52]. Therefore, further deformation will be localised in those glide planes. On the other hand, the presence of non-shearable precipitates can homogenise the slip distribution [53]. Indeed, dislocation debris left by a gliding dislocation around non-shearable precipitates in its slip plane increases the slip resistance there, thus promoting slip on other planes. As a result, more uniform slip has been observed in alloys with high number densities of non-shearable precipitates [53-55]. Cheng *et al* [40] and Poole *et al* [53] studied the influence of precipitates on the work hardening behaviour of AA6111 alloys. They found that the initial work hardening rate decreases as the artificial ageing proceeds and then increases when the alloy was over-aged, as shown in Fig. 2-12a. By contrast, the dynamic recovery rate hardly changed with the artificial ageing time, as shown in Fig. 2-12b. However, when non-shearable precipitates formed, the dynamic recovery rate suddenly decreased.
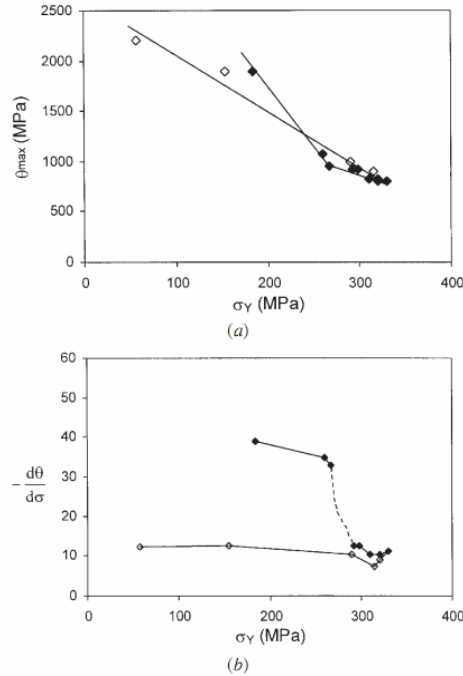
Fig. 2-12 The dependence of (a) initial work hardening rate and (b) dynamic recovery rate on the yield stress [40]. Note: open symbols are for under-aged samples and closed symbols are for over-aged samples.

2.3.2 Strain rate hardening theory

The strain rate hardening behaviour of the materials is controlled by the dispersed local obstacles. The strain-rate $\dot{\varepsilon}$ produced by the glide of a density ρ of mobile dislocations with the Burgers vector b and average velocity v is given by the Orowan relation [56]:

$$\dot{\varepsilon} = \rho b v / M \qquad (2\text{-}9)$$

where M is the Taylor factor. When the dislocations are held up by a dispersion of local obstacles, the glide velocity v is determined by the rate at which local thermal activation allows pinned dislocation segments to overcome the energy barriers of individual obstacles [56, 57]. The apparent activation volume V is defined as

$$V = -\frac{\partial \Delta G}{\partial \sigma} = bdl / M \qquad (2\text{-}10)$$

where ΔG is the stress dependent Gibbs free energy of activation, σ is the applied stress, d is the so called activation distance given by the distance between two equilibrium positions of a dislocation in the stress field of a localised obstacle, and l is the average obstacle spacing. The apparent activation volume can be related to the strain rate sensitivity parameter m ($= \frac{\partial \ln \sigma}{\partial \ln \dot{\varepsilon}} \mid$ T,structure) using an Arrhenius equation for the plastic strain rate $\dot{\varepsilon}$, of the form [58]

$$\dot{\varepsilon} = \dot{\varepsilon}_0 \exp(-\frac{\Delta G}{kT}) \qquad (2\text{-}11)$$

where $\dot{\varepsilon}_0$ can be considered as a constant, k is the Boltzmann constant and T is the absolute temperature. It follows that

$$V = kT \frac{\partial \ln \dot{\varepsilon}}{\partial \sigma} = \frac{kT}{m\sigma} \qquad (2\text{-}12)$$

By combining Eqs. (2-10) and (2-12), one gets

$$m = \frac{kT}{V\sigma} = \frac{MkT}{bdl\sigma} \qquad\qquad (2\text{-}13)$$

If the local obstacles are mainly dislocation junctions, then l is inversely proportional to the square root of the dislocation density. If σ is largely controlled by a dislocation-related contribution, which is proportional to the square root of the dislocation density, then the product $l\sigma$ will be stress-independent, and the stress dependence of m will be given by the activation distance d. With increasing dislocation strengthening, d will slightly decrease. In other words, higher dislocation strengthening will result in a larger value of m.

If the local obstacles are mobile solute atoms, which means the mechanism of dynamic strain ageing (DSA) is operating, then equation (2-13) is no longer applicable. DSA is the dynamic interaction between mobile dislocations and diffusing solute atoms [59], which gives a negative contribution to the SRS of the flow stress. The first model for DSA was developed by Cottrell [60, 61] who considered that, above a certain temperature, solute atoms are mobile enough to move along with dislocations. If the deformation rate is low, this mechanism would lead to an increased applied force. However, at higher deformation rates, the dislocation may lose its cloud, hence requiring a smaller resolved shear stress for gliding. This leads to a negative contribution to the SRS. In the early models, dislocations were assumed to move in a viscous manner [62]. This led to a numerical inconsistency, i.e., a too low value of solute diffusivity in particular in substitutional alloys [61, 62]. To resolve this inconsistency, Cottrell [61] proposed that the diffusivity of substitutional solutes is enhanced by vacancies generated during plastic deformation in excess of thermal equilibrium. Subsequently, dislocations were suggested to move in a discontinuous manner [63, 64]. Thermally activated jumps through forest dislocations alternate in time with free-flight motion between two such obstacles [62]. Therefore, DSA occurs during a waiting time when the dislocations are temporarily locked by other forest dislocations through their slip plane. Nevertheless, the vacancy hypothesis is still needed to account for the occurrence of DSA [64], since mobile solutes need vacancies to aid them diffuse to dislocation cores. Meanwhile, other authors [65] suggested that solute atmospheres form on the forest dislocations and are then drained by pipe diffusion from the forest dislocations to mobile dislocations during the time spent by the mobile dislocations while they are waiting at the forest dislocations.

Furthermore, within the range of existence of DSA, the SRS may become negative and thereby provide conditions for the occurrence of the Portevin-Le Châtelier (PLC) effect [59, 62] (also known as serrated yielding or discontinuous yielding). Thus, the PLC effect is a subregion of the DSA domain. The boundary of this subregion can be roughly represented by the condition m = 0, though in practice the onset of the PLC effect is often associated with m dropping below a finite negative value [59]. Within the PLC domain, deformation curves are serrated and in some favourable cases a propagating pattern of deformation bands can be observed [62]. Three major types of serrations, labelled A, B, and C, are shown schematically in Fig. 2-13. Their characteristics have been described in Reference [59, 66]. Both substitutional and interstitial solutes can give rise to the PLC effect [67, 68]. However, for each solute species there appears to exist a limited range of strain rates and temperatures for which the PLC effect occurs, as shown in Fig. 2-14. For the onset of serrations in substitutional alloys, a critical strain ε_c is required [66]. The critical strain is dependent on both the strain rate and temperature in a non-monotonic way [59, 66]. The existence of critical strain is attributed to enhanced solute diffusivity due to the deformation induced vacancies and increased mobile dislocation density [67, 69]. In the high strain rate/low temperature range, ε_c increases with increasing strain rate and decreasing temperature. This most commonly observed behaviour referred to as *normal*, is illustrated in Fig. 2-15. In the low strain rate/high temperature range, the opposite trend, known as *inverse behaviour*, is observed. This trend can be caused by the interaction between DSA and concurrent precipitation in concentrated solid solutions [70]. Apart from the genuine PLC effect, a 'pseudo-Portevin-Le Châtelier effect' was attributed to the discontinuous yielding observed in Al-Li alloys, due to the repeated shearing of shearable precipitates [71].
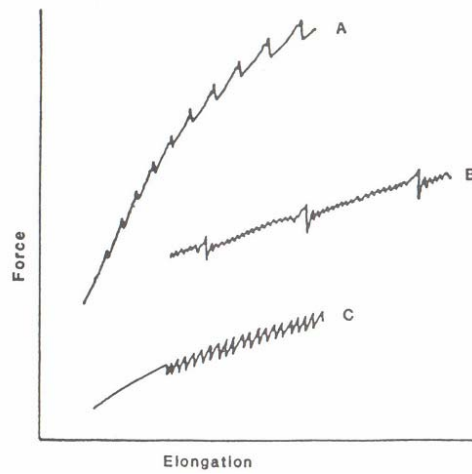
Fig. 2-13 Typical forms of serrated yielding [72].
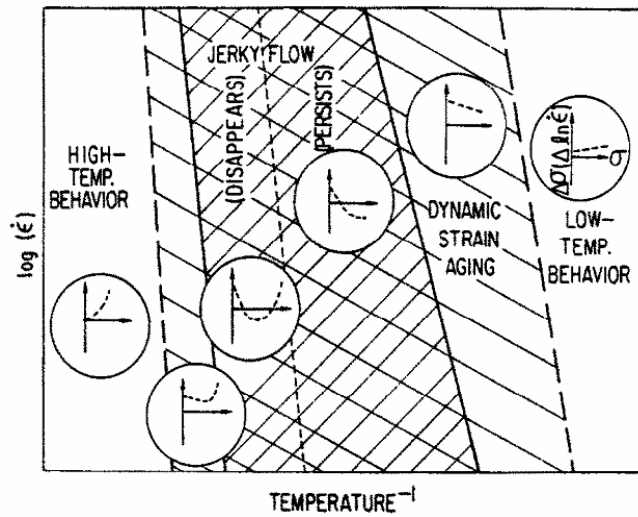
Fig. 2-14 Schematic diagram of the temperature and strain rate regions of DSA and of PLC effect [65]. The behaviour of $\Delta\sigma/(\Delta\ln\dot{\varepsilon})$ *vs* σ in each region is indicated.
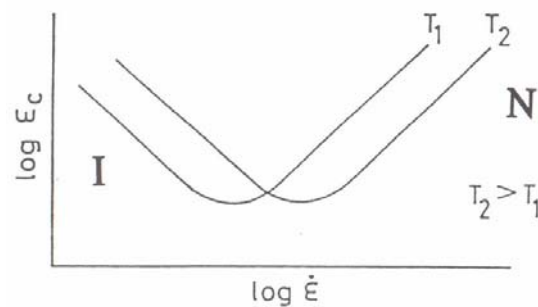
Fig. 2-15 Normal (N) and inverse (I) behaviour of ε_c (schematic) [59].

23

Dynamic strain ageing causes a decrease in the strain rate sensitivity of the flow stress, which can be so severe that serrated yielding occurs. But even before dynamic strain ageing becomes visible in such an extreme manifestation, the mechanical properties of the alloy will show some unusual characteristics [59], as shown in Fig. 2-16.
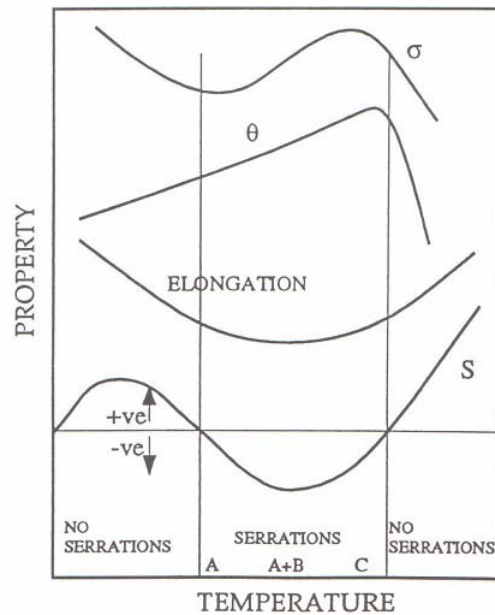
Fig. 2-16 Schematic diagram showing correlations between the temperature dependence of the strain rate sensitivity S and the temperature dependence of stress σ, work hardening rate θ and the elongation [59].

In summary, the major microstructural features that influence the strain rate hardening behaviours are:

- Dislocation junctions

Dislocation junctions give a positive contribution to the strain rate hardening of the materials. Therefore, without DSA, the rate sensitivity was found to increase with increasing strain [65].

- Mobile solutes

Mobile solutes give a negative contribution to the strain rate hardening of the materials due to DSA. This effect is strong when Mg is added to Al. This is because DSA occurs when the characteristic waiting time of dislocations on pinning points is comparable to the characteristic diffusion time of solutes to pinned dislocations. For the common ranges of

strain rate and temperature, the two characteristic times happen to be comparable in the presence of Mg.

- Precipitates

The formation of precipitates during ageing would deplete mobile solutes and/or vacancies from the matrix, which are critical for the occurrence of DSA, therefore increasing the strain rate hardening capability [73]. However, if the precipitates can be repeatedly sheared by mobile dislocations, then a 'pseudo-Portevin-Le Châtelier effect' may occur, which was attributed to the discontinuous yielding observed in the Al-Li alloys [71]. Moreover, the interplay between DSA and concurrent precipitation in concentrated solute solutions will lead to an 'inverse' behaviour of the critical strain ε_c [70].

2.3.3 Microstructural features and formability

Different microstructural features influence the stretch formability primarily through their influence on the work hardening and strain rate hardening behaviour of the metals.

- **Solutes and clusters**

Solutes (i.e. Mg, Cu and Si) in solution can significantly increase the degree of work hardening by enhancing the dislocation multiplication and impeding the dynamic recovery process [9, 30]. At the same time, they also tend to decrease the strain rate hardening capability [74] by promoting the occurrence of dynamic strain ageing [73]. By the combined effect of work hardening and strain rate hardening capability, solutes generally do not improve the formability [74, 75].

Clusters are shearable and are therefore expected to decrease the work hardening rate. However, it is interesting to find that the sample with clusters showed a higher work hardening rate than as-quenched or artificially aged samples [16, 76], possibly due to the dynamic precipitation that occurred in the former material [76]. Therefore, the former material exhibited a higher formability than as-quenched or artificially aged material [16]. It should be noted that the serrated yielding should also contribute the inferior formability of as-quenched material [16].

- **Second particles**

Second particles may be divided into three categories: precipitates up to several nanometers in size, dispersoids about 50 to 500 nm in diameter and micron-sized coarse particles.

Precipitates: If precipitates are shearable, the shearing of them would cause a decrease of the work hardening capability [40, 74]. Although the formation of precipitates would deplete the solute in solution and thus improve the strain rate hardening capability [77], coherent precipitates normally decrease the formability [16, 74, 78]. When precipitates become non-shearable, geometrically necessary dislocations will be generated at particle-matrix interfaces [40], therefore increasing the work hardening capability and thereby improving the formability [16, 78].

Dispersoids: Dispersoids are non-shearable, and known to promote the generation of geometrically necessary dislocations [79, 80], therefore improving the work hardening capability [55]. With increasing volume faction of dispersoids, an improved formability was reported in alloy 2036 [11]. However, high volume faction of dispersoids was reported to decrease the stretch formability of 6xxx alloys [9]. The most commonly encountered dispersoids in the 6xxx alloys are Al(Fe,Mn)Si [53], which are believed to be formed during homogenisation [81].

Coarse particles: Micron-sized coarse particles do not have an influence on the work hardening or strain rate hardening behaviour and thus have a negligible influence on diffuse instability [9]. However, these particles are strain concentration sites that decrease the final fracture strains due to nucleation of voids either at their interfaces or due to their facture [74, 82]. Therefore, although coarse particles would have no influence on the plane strain stretching behaviour, they may decrease the forming limit in balanced biaxial stretching since a low facture strain was predicted to decrease the performance in the balanced biaxial stretching condition [8].

- **Grain size**

Although grain boundaries are known to be an important factor in the work hardening process by promoting the generation of geometrically necessary dislocations [38, 50], it

appears a finer grain size does not ensure a high work hardening rate [83], especially when the grain size is smaller than 5 μm [74, 84]. Moreover, the SRS of the flow stress was also reported to decrease with decreasing grain size when both coarse grains, nanocrystalline grains and ultra-fine grains are considered [85]. Therefore, the material with ultra-fine grains showed a lower formability than the material with coarse grains [86]. Despite this, for the materials with relatively coarse grains, literature data show that the formability improves significantly with decreasing grain size [87, 88]. This may be attributed to a more homogeneous distribution of strain in the material with fine grain size [89] and the ability of the material with fine grains to maintain a high work hardening to strains beyond plastic instability [87]. Meanwhile, it was reported that the sheet thickness to grain size ratio is more important than the grain size itself [9, 87, 90]. For a superior formability, the grain size should be at least around 20 times smaller than the sheet thickness [9]. Thus, for 1 mm sheet, the grain size should be below 50 μm. It should be noted that the grain size range of 20 to 100 μm in normal commercial alloys was proposed to have little effect on the necking or fracture limits of aluminium alloys at room temperature [74].

- **Texture**

Many studies showed that texture can have a significant influence on the deep drawing ability of the material through its influence on the r-value [91, 92]. As for stretch forming, the stretchability of a material is determined much more by work hardening and strain-rate hardening capabilities of the material rather than by the r-value [6]. However, Pedersen *et al* [93] suggested that a strong cube texture can lead to a high stretch formability, although no information about the work hardening and strain rate hardening characteristics of the materials was provided. Furthermore, Yoshida *et al* [94] modelled the effect of major texture components in aluminium alloys on the biaxial formability, and also found a strong cube texture would contribute to a high stretch formability due to the enhanced work hardening rate.

2.4 Effect of alloy composition and heat treatment on the tensile ductility and formability of 6xxx alloys

- **Alloy composition**

Mg and Si are the major solutes in the 6xxx alloys; they increase the strength of the material by the formation of precursors of Mg_2Si during artificial ageing [95]. Moreover, Cu is often added to enhance the precipitation kinetics [96], although the corrosion resistance tends to be degraded by the addition of copper [97]. A minor addition of Mn serves to control the grain size through the formation of non-shearable dispersoids [9, 55]. The effect of alloy composition on the formability of 6xxx alloys has been previously investigated to some degree [9, 10, 13, 14], but the research is fragmented and controversies still exist. For instance, it is generally accepted that increasing Si content usually enhances the tensile ductility and stretch formability [9, 14], probably due to a more complete removal of Mg from the matrix with the formation of clusters [98]. However, other researchers proposed that increased Si content would reduce the stretch formability of the alloys [10]. Mg is believed to deteriorate the plane strain stretching performance [13], while the tensile ductility of the alloy was found to increase with higher Mg content [9]. Although the addition of Cu has a positive influence on the work hardening [13], it appears the influence of Cu on the tensile ductility and formability depends on the Mg/Si ratio in the alloys [13]. Although Mn was found to decrease the formability [9], the tensile ductility was reported to be either increased [55] or decreased [9] by Mn additions.

- **Heat treatment**

The effect of heat treatment on the stretch formability of 6xxx alloys has been studied by forming limit diagram (FLD) tests and hydraulic bulge test in reference [16]. It was shown that the formability is poor in the freshly-quenched condition due to the serrated yielding effect, but improved when the sample was over-aged. Moreover, sample in the T4 temper showed a higher formability than as-quenched or artificially aged samples due to the high work hardening rate in the T4 temper [16]. Furthermore, Ozturk *et al* [99] studied the effect of artificial ageing on the Erichsen Index of 6061 alloy. The authors claimed that the formability decreased with increasing artificial ageing time, since the Erichsen Index decreased with increasing ageing time. However, the Erichsen test may be an inadequate method for evaluating the stretch formability [100, 101].

Practically, for automotive panel applications, after artificial ageing (pre-ageing), the 6xxx alloys will be naturally aged before forming. The natural ageing after pre-ageing is expected to influence the formability of 6xxx alloys since clustering will occur during natural ageing, which will further influence the solute/vacancy concentration in the matrix. Unfortunately, there is limited available data on the effect of pre-ageing on the formability of 6xxx alloys. Although Liu *et al* [12, 18] studied the effect of pre-ageing on the stretch formability of 6111 type alloys by Erichsen testing, the Erichsen test may be an improper method for stretch formability evaluation. The shortcoming of the Erichsen test will be discussed in Section 2.5.1. Moreover, Daniel *et al* [20] found that a 6xxx alloy with a high paint-bake strength would have a low limiting dome height under plane strain condition (LDH_0). In other words, a high formability sacrifices a high paint-bake performance.

Most importantly, until now, the underlying mechanisms of how the composition and heat treatment influence the tensile ductility and stretch formability of 6xxx alloys are still unclear.

2.5 Methods for formability evaluation

The formability of a material is the extent to which it can be deformed in a particular process without fracturing or without the formation of a localised neck or tear [102]. Sheet metal forming processes can be characterised by two basic types of deformation patterns: bending and drawing. Bending is essentially a plane strain process [74]. Concerning drawing one has to distinguish stretching and deep drawing. Deep drawing can be defined as processes which change the shape of a product by pushing or pulling it through a die whereas stretching consists of clamping the edge of the sheet and stretching it over a rigid punch to the desired shape [102]. The basic difference between deep drawing and stretching is that the former involves deformation under tension-compression condition whereas the latter involves tension-tension straining [74, 102]. It should be noted that stretching is the most common deformation mode in the production of automotive outer panels [6].

Various methods for evaluating sheet metal formability have been developed. One may subdivide them into four classes [103]: simulative tests, uniaxial tensile tests, limiting dome height tests and methods based on forming limit diagrams.

2.5.1 Simulative tests

The typical simulative test for stretching is the Erichsen test, in which a sheet is stretched over a 20 mm diameter punch until the occurrence of fracture [104], as shown in Fig. 2-17. The depth of the punch indentation in the specimen, when fracture occurs, expressed in millimeters is the so-called Erichsen index (IE). This is the most commonly used parameter for expressing the stretch formability of sheet metals. Olsen introduced a test similar to that proposed by Erichsen but with a slightly different size of the tools [104, 105]. The Erichsen test has been widely used in Europe and the Olsen test in North America [106]. In theory, the Erichsen/Olsen test is a pure biaxial stretch test [105]. Therefore, the Erichsen/Olsen index should correlate with common stretchability parameters, especially the work hardening exponent (n-value) [100]. However, available literature data show extreme scatter and little correlation is seen as a function of the n-value [19, 100, 107]. Hecker [19] proposed that it is virtually impossible to reproduce Olsen cup test results even within the same laboratory due to experimental scatter being, in most instances, larger than the material differences to be measured. Moreover, neither of the Erichsen/Olsen indexes correlate well with press performance for several reasons [106, 108]: some draw-in is always possible, the biaxiality of the stress state is significant and difficult to control, and the small punch radius introduces a considerable bending component and makes results greatly dependent on the sheet thickness. This last reason probably explains why the Olsen index had a good correlation with bending performance [100].
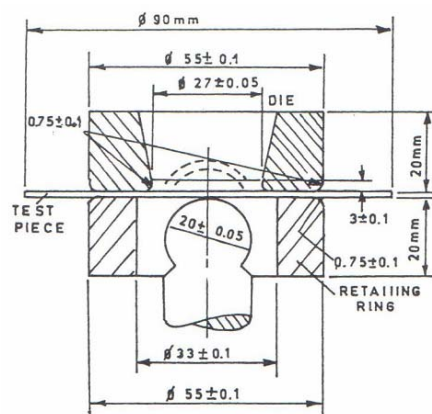
Fig. 2-17 Schematic of Erichsen test [109].

The typical simulative test for deep drawing is the Swift flat-bottom test, as shown in Fig. 2-18. This test consists of deep-drawing cylindrical parts having different diameters and determining the limit drawing ratio (LDR), i.e. the ratio of the maximum diameter of the specimen that is draw without tearing and the diameter of the punch [109]. And LDR was shown to very dependant on the plastic strain ratio (r value) [101]. The Swift flat-bottom test is well suited to predict the performance of sheet metals in deep-drawing conditions [108]. Therefore this method has been widely used and is considered as a standard test by the International Deep-Drawing Research Group (IDDRG) [105]. However, the shortcoming of Swift test is one has to conduct several experiments to obtain the LDR. Fukui proposed a deep-drawing test using a conical die, in which test the diameter ratio as a measure of formability may be established by a single test [105].
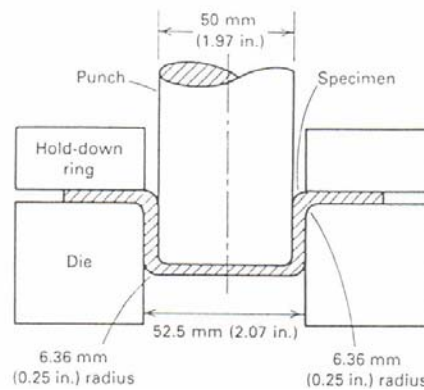
Fig. 2-18 Swift flat-bottom test [105]

Also some simulative tests combining deep-drawing and stretching have been developed, i.e. Swift round-bottom test in which test deformation takes place by stretching at the center of the part and by deep-drawing in the region of the blank [105].

The simulative tests described above cannot simulate the condition of plane strain stretching, where the minor strain is zero. This imposes a limitation on the use of these tests as the most common mode of final failure in sheet metal parts is in conditions of plane strain [110, 111]. Therefore, simulative tests have been gradually abandoned as the way for assessing

formability and only considered as a cheap, rapid method for materials properties checking [101].

2.5.2 Uniaxial tensile test

A drawback of simulative tests is that they require special equipment and the obtained information applies only to a special forming process [105]. This shortcoming can be overcome by the use of material parameters determined by the uniaxial tensile test as a measure of formability. The uniaxial tensile test is perhaps the most informative single test available for assessing formability [102]. It is generally accepted that the plastic strain ratio (i.e. the r-value), determines the deep-drawability whereas the work hardening exponenet (i.e. the n-value), determines stretchability [6]. These two parameters can easily be determined by uniaxial tensile testing based on ASTM standards [112, 113]. However, even in deep-drawing, a large part of the deformation consists of stretching and so the central importance for the r-value for the forming limits has to be questioned [105], and comparison of n-value with other stretch forming tests such as Erichsen/Olsen cup test and forming limit diagrams, sometime show serious departures [19, 107]. Moreover, the uniform elongation and the total elongation have also been used to roughly estimate the formability [100, 101, 114].

The tensile testing still provides a convenient basis for comparisons between various materials, and can also be used for evaluating new materials based on a general knowledge of sheet metal formability.

2.5.3 Limiting dome height test

The limiting dome height (LDH) test is similar to Erichsen/Olsen tests in that dome height at failure is used as the measure of formability. However, the critical difference is that the strain state at failure in the dome test is varied in a precise manner so that it duplicates the strain state at failure in a stamping [105, 111]. This is partly made possible through the use of a significantly larger dome in this test as compared to the Olsen cup test. Furthermore, the dome height of the LDH test is controlled by the amount of stretching over the dome since a lock bead in the die plates prevents any draw-in from the flange, as shown in Fig. 2-19. Furthermore, this method combines the advantages of simulative tests and of the forming

limit diagram [105]. In this method, the heights of the deformed parts stretched on a hemispherical punch until fracture are recorded as functions of the minor strains occurring in the specimens. By drawing a curve through the experimental points obtained in the specimens with different width, a diagram is obtained, as shown in Fig. 2-20. The height of the part, corresponding to plane strain, is a formability index denoted by LDH_0. Ayres *et al* [111] compared the LDH and Olsen tests, and found only the LDH tests can successfully predict the formability of both steel and aluminium. However, subsequently, due to the large dispersion of the LDH_0 values and large amount of experimental work, this method has been little used in industry [105]. More recently, the OSU test was introduced in order to overcome the applicability limits of the LDH method [105, 108, 115]. In the OSU test, the shape of the tools was optimised by FE simulations aiming to achieve as close as possible a state of plane strain [105]. The results showed a reduced dispersion and good agreement with industrial practice [115].
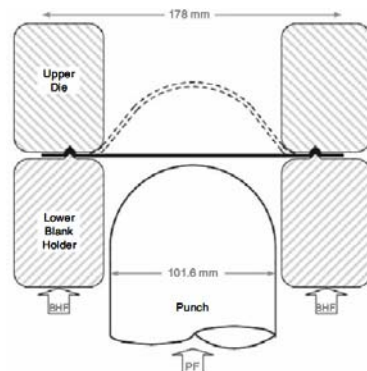
Fig. 2-19 Hemispherical punch and die set for LDH measurements [111].
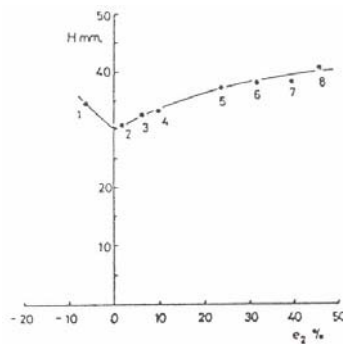
Fig. 2-20 Limit dome height curve [105].

2.5.4 Forming limit diagrams

The formability of sheet metals is limited by localised necking or non-uniform strains that may occur within a small region in the plane of the sheet. The amount of strain that a sheet metal can tolerate just before localised necking is called the limit strain [116]. These maximum values of the major strain ε_1 and minor strain ε_2 can be determined by measuring the strains on sheet components covered with grids of circles [6]. On this basis, forming limit diagrams (FLDs) represent limiting major and minor available principal strains on the surface of the deformed sheet in the different deformation modes that can be achieved, as shown in Fig. 2-21. FLDs were introduced by Keeler and Goodwin in the 1960s [116]. Later research showed that the forming limits in sheet metal forming can be evaluated well by determining the forming limit curves in laboratory tests [6].
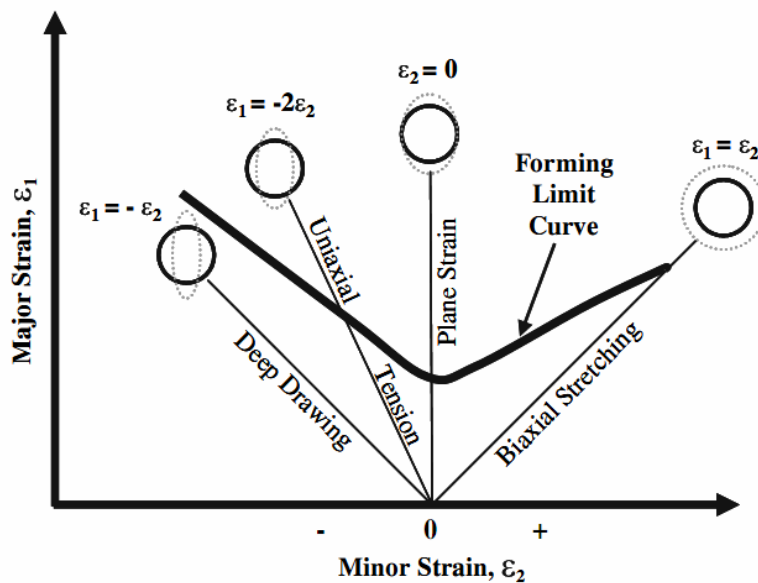
Fig. 2-21. Scheme of forming limit diagram [117]

FLDs should provide as much as possible the deformation modes that occur in industrial sheet metal forming processes. The diagrams are established by experiments that provide pairs of values of the limit strains ε_1 and ε_2 obtained for various loading patterns (equi-biaxial, biaxial, uniaxial etc.) . There are several kinds of tests [105, 118], such as in-plane tests, out-of-plane tests (punch stretching test) and hydraulic bulge tests, that can be used for constructing FLDs. However, from a practical standpoint, the FLD determined by punch

stretching test is more realistic, since it simulates the type of instability conditions that are encountered in stamping sheets with rigid tooling [118].

FLDs are influenced by materials parameters. A material with high work hardening and strain rate hardening capabilities would have a high forming limit [7, 8, 118]. Moreover, FLDs are also influenced by experimental parameters. For instance, with 3-mm grids or a 50-mm punch, the level of the forming limit curve obtained would be higher than that obtained with 5-mm grids or a 110 mm punch [119].

2.6 Summary

Forming of 6xxx series sheet alloys is typically carried out in the naturally-aged or pre-aged conditions. The formability of the 6xxx alloys are influenced by alloy composition and heat treatment through their influence on the work hardening and strain rate hardening capabilities. The literature survey showed that although the effect of alloy composition and heat treatment on the formability of 6xxx alloys have been studied to some degree, controversies still exist. Most importantly, the underlying mechanism is still unclear, which would impede the development of new 6xxx alloy with improved formability for automotive outer panel applications. Therefore, a more comprehensive and systematic study of the effects of alloy composition and heat treatment on the formability of 6xxx alloys is needed. This is expected to provide information for the development of new 6xxx alloys for automotive outer panel applications. Moreover, the literature survey suggests that, along with uniaxial tensile testing, forming limit diagram testing is likely to be the most convincing method of formability evaluation for the purpose of this work.

Chapter 3: Experimental procedures

3.1 Alloy composition

Eight alloys whose compositions are shown in Table 3-1 were studied. It should be noted that the total atomic percentages of Mg and Si in the alloys A2, A4 and A6 is nearly the same. Furthermore, alloys A7, A8, A10 are Cu-containing versions of alloys A2, A6 and A4, respectively. Fig. 3-1 shows an isothermal section of the Al-Mg-Si phase diagram at 550 ºC together with the Si and Mg contents of the alloys studied. It can be seen that the Mg and Si contents in the alloys A4 and A6 are within the composition limit of alloys 6016 and 6111, respectively.

Table 3-1 Alloy compositions

Alloy	Fe wt.%	Mn wt.%	Ti wt.%	Zn wt.%	Cu wt.%	Mg		Si		Mg+Si	Mg/Si	Comment
						wt.%	at.%	wt.%	at.%	at.%	at. ratio	
A2	0.07	0.12	0.10	0.12	/	1.06	1.18	0.50	0.48	1.66	2.46	High Mg/Si
A3	0.06	0.12	0.11	0.11	/	0.43	0.48	0.45	0.43	0.91	1.12	/
A4	0.07	0.12	0.11	0.13	/	0.41	0.46	1.26	1.21	1.67	0.38	Low Mg/Si
A5	0.07	0.12	0.12	0.10	/	0.41	0.46	1.50	1.44	1.90	0.32	/
A6	0.06	0.11	0.12	0.11	/	0.70	0.78	0.80	0.77	1.55	1.01	Medium Mg/Si
A7	0.08	0.12	0.11	0.12	0.29	0.96	1.07	0.48	0.46	1.53	2.33	High Mg/Si
A8	0.07	0.11	0.11	0.10	0.29	0.65	0.72	0.85	0.82	1.54	0.88	Medium Mg/Si
A10	0.09	0.12	0.11	0.11	0.27	0.35	0.39	1.22	1.18	1.57	0.33	Low Mg/Si
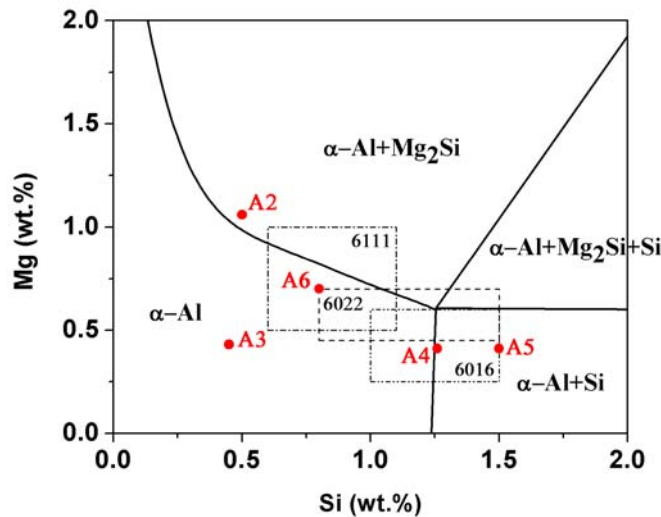
Fig. 3-1 Isothermal section of Al-Mg-Si phase diagram at 550 ºC determined using Thermocalc. The red points represent the compositions of the Cu-free alloys. The dashed rectangles represent the Mg and Si composition limits of some commercial 6xxx alloys used for auto panels.

3.2 Material preparation and heat treatment

Ingots were cast into permanent moulds, homogenised at 460 ºC for 6 h and then at 540 ºC for 24 h, followed by hot rolling and subsequent cold rolling to 1 mm thick sheet.

The sheets were solution treated at 550 °C for 0.5 h in a salt bath, followed by water quenching (Asq). The as-quenched samples were divided into three groups. The first group of samples were naturally aged (NA) for one hour (NA1h), 24 h (NA1d), one week (NA1w) or one month (NA1m); the second group samples were immediately pre-aged (PA) at 100 °C for 5 min (PA100x5min), 30 min (PA100x30min), 1 h (PA100x1h), 2 h (PA100x2h) or 4 h (PA100x4h), respectively, then naturally aged for one week; the third group of samples were immediately pre-aged at 200 °C for 20 s (PA200x20s), 40 s (PA200x40s) and 60 s (PA200x60s), then naturally aged for one week. For comparison, some pre-aged samples were naturally aged for one month, and some samples were solution treated at 500 °C for 0.5 h before one week of natural ageing. Furthermore, the naturally aged and/or pre-aged alloys were isothermally aged at 170 °C for 30 min to simulate the paint-bake cycle (PB) used in automotive applications. It should be noted that pre-ageing at medium temperatures for a long time (i.e. 100 °C for 2 h) is normally more suitable for batch pre-ageing, while pre-ageing at high temperature for a short time (i.e. 200 °C for 20 s) is suitable for in-line heat treatment.

3.3 Microstructural characterisation

The grain structure of the solution treated alloys was studied by scanning electron microscopy (SEM) using a JEOL-JSM-6480 with electron backscattered diffraction (EBSD). The microstructures of the solution treated alloys were studied by field emission gun SEM (JEOL 7001F). Quantitative data for undissolved coarse particles and dispersoids were determined using high contrast back scattered electron images (from JEOL 7001F) and Imagej 1.32j image analysis software. Ten random views on each alloy were examined for coarse particle analysis, and six random views with 200 dispersoids in total for each alloy were examined for dispersoid analysis. The volume fraction of dispersoids in the different alloys was assumed to be the same as the area fraction based on the Delesse principle. The mean planar spacing, L, of the dispersoids was estimated by [120]:

$$L = \left((\frac{2\pi}{3f})^{1/2} - (\frac{8}{3})^{1/2} \right) r \qquad (3\text{-}1)$$

where f is the volume fraction and r is the radius of the dispersoids.

To find out the influence of dispersoids on dislocation accumulation, transmission electron microscopy (TEM) using a FEI-G2-T20, at 200 KV, was employed on the naturally aged alloy A2 after 2% straining. Thin foils for microstructural characterisation in the TEM were made using a 1/3 nitric-2/3 methanol solution in a Struer Tenupol 5 unit. A surface profilometer (Veeco-Wyko-Nt1100) was used to characterise the degree of deformation localisation in the alloys strained by 30%, i.e. after necking.

3.4 Texture characterisation

The texture of the solution treated alloys was studied using XRD technology. The macrotextures were measured at the sheet surface by the Schulz reflection method on a X'pert MRD X-ray goniometer with a Co target. The beam was reflected off planes comprising rolling direction and long transverse direction. Three incomplete pole figures {111}, {200} and {220} were measured and subsequently corrected for defocusing errors and background intensity. The volume fractions of the various texture components were calculated by an integration method.

3.5 Hardness measurements and tensile testing

Hardness testing was carried out by using a Vickers hardness tester with a 5 kg load and an indentation time of 15 s. The mean of 5 impressions was taken as the hardness of the corresponding condition, and one standard deviation was chosen for error bars. Tensile tests and strain rate jump tests were conducted on the naturally aged and/or pre-aged samples. The samples for tensile tests and strain rate jump tests were dog-bone samples with a gauge length of 10 mm, as shown in Fig. 3-2. To determine the uniaxial tensile properties, a screw-driven Instron machine was used at a nominal strain rate of 2×10^{-3} s^{-1}. The average value of the tensile testing results of three samples was reported for each alloy. The maximum and the minimum value were taken for the upper and the lower ends of the error bars, respectively. The work-hardening rate was determined by numerically differentiating the true stress-true

plastic strain data using a moving regression method. Each data point on the σ-ε^p curve, and the six adjacent data points (three on each side), were used to obtain a best-fit linear regression line, and the slope of this line was treated as the work-hardening rate at that point. The resulting values of derivative were then smoothed to reduce the noise in the data. For some samples with strong PLC effect, the work hardening rate was calculated by fitting the true stress – strain curves with a polynomial function, and differentiating this function with respect to true strain. Strain rate jump tests were performed with the strain rate being changed by a factor of 10 (between the nominal strain rates of 2 x 10^{-4} s^{-1} and 2 x 10^{-3} s^{-1}). The extrapolation used to calculate the SRS, $\log(\sigma_2 / \sigma_1)/\log(\dot{\varepsilon}_2/\dot{\varepsilon}_1)$, is defined in Fig. 3-3.
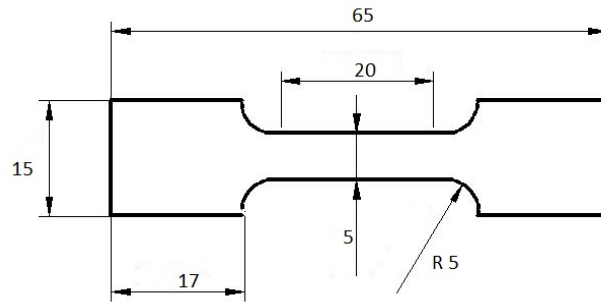
Fig. 3-2 Schematics showing the dimension of specimen for tensile testing (mm)
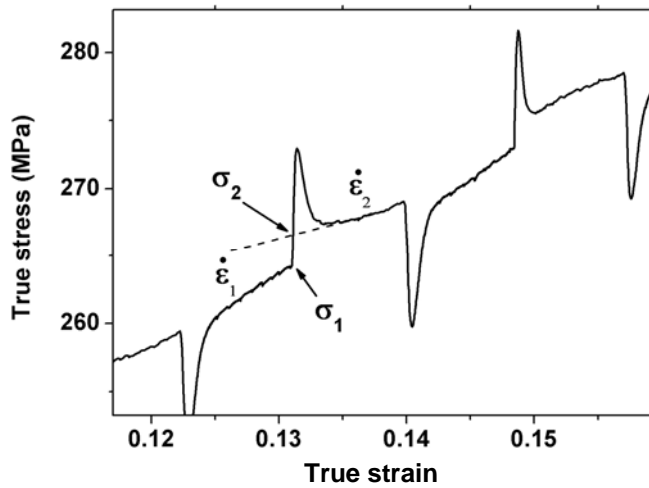
Fig. 3-3 Illustration of the results of a strain-rate jump test for alloy A4

3.6 Formability tests

Forming limit diagram (FLD) tests were used to evaluate the formability of naturally aged samples using an Erichsen sheet metal tester with a 48 mm diameter punch. The dimensions of specimens for FLD tests are shown in Fig. 3-4. The specimens were electrochemically etched to produce a grid pattern with circles measuring 2 mm in diameter. Three samples were used for each deformation mode (from plane strain stretching to biaxial stretching). For each test, a sandwich construction of oil (lithium complex based greases - Liplex EP2) together with three polypropylene foils was used for lubrication. During the test, the specimens were clamped on the edges with a blank-holder force of 100 kN and stretched by the hemispherical punch until localised necking occurred. Each trial started with a punch velocity of 12 mm/min, while at the end of each test the velocity was decreased to 1 mm/min to facilitate the observation of localised necking. The deformation of the grid circles was evaluated using a grid pattern analyser (GPA 3.0), and the FLD was obtained by drawing a line between the strains in the regions where the occurrence of necking and the lack of necking were clearly identified. Fig. 3-5 shows typical experimental FLDs for some naturally aged alloys.
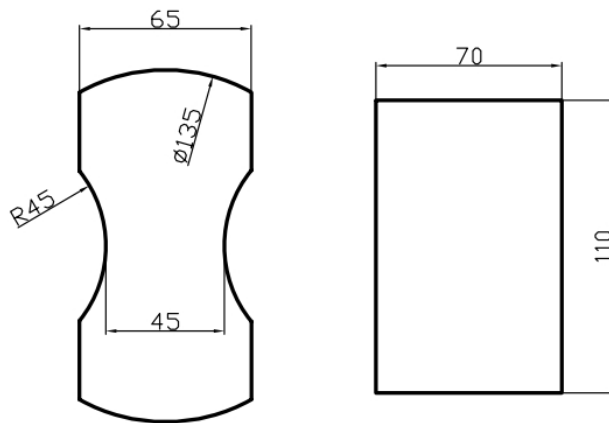
Fig. 3-4 Schematics showing the dimensions of specimens for FLD tests (mm).
Note: left sample is for plane strain stretching, and the right sample is for biaxial stretching.
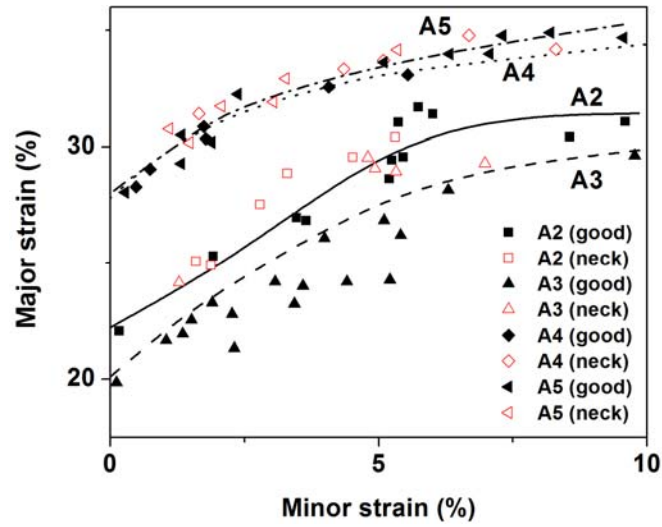
Fig. 3-5 Right-hand side of FLD for the alloys A2-A5 after 1 week of natural ageing

3.7 Thermodynamic modelling

The thermodynamic software package, ThermoCalc, with the TTAL6 database [121], was employed to calculate the amounts of the various phases and the solute concentrations in the matrix at different temperatures.

Chapter 4 Microstructure and formability of naturally aged Al-Mg-Si alloys

4.1 Introduction

In this chapter, five alloys (whose compositions are indicated in Table 3-1) with increasing Si content from alloy A3 to A4 to A5 and/or increasing Mg content from alloy A3 to A2 and/or decreasing Mg/Si ratio from alloy A2 to A6 to A4 were studied. Microstructural features such as grain size, intermetallic particles and texture of these five alloys were characterised. Moreover, the natural ageing response was investigated to find out when the properties of these alloys were stable. Based on these results, the tensile properties and formability of the alloys after one week of natural ageing (a relatively stable state) was evaluated. Work hardening and strain rate hardening characteristics of these alloys were used to correlate the microstructural features with tensile ductility and formability.

4.2 Results

4.2.1 Microstructure and texture of solution treated alloys

4.2.1.1 Coarse particles and dispersoids

After solution treatment, undissolved coarse particles with the size being larger than 1 μm in diameter, mainly α-Al(Fe,Mn)Si particles [122], were observed in all the alloys, as shown in Fig. 4-1. In the high Mg content alloy A2 and medium Mg/Si ratio alloy A6, undissolved Mg_2Si could also be observed (Fig. 4-1a, e). This is at variance with observations on the high Si content alloy A5, where undissolved Si particles were found instead (Fig. 4-1d). For higher alloy contents, a larger area fraction of coarse particles was observed except in alloy A6, see Table 4-1.

The backscattered SEM images in Fig. 4-2 show the distribution of dispersoids with the size being smaller than 1 μm in diameter in the alloys, and Fig. 4-3 displays the typical morphology and EDS results of dispersoids in alloy A4. It should be noted that in Fig. 4-2, the white dots are dispersoids, while the grey contrast in the matrix may be caused by the

colloidal silica polishing suspension, which has a pH value of 9.8. As shown in Fig. 4-2, the high Si content alloys A4 and A5 have a higher number density of dispersoids than the other alloys. Table 4-2 lists quantitative data for those dispersoids in the alloys. Energy dispersive X-ray analysis (EDS) of the dispersoids and the matrix revealed that the dispersoids contain Al, Mn, Si and Fe (see Fig. 4-3b). They are most likely α-Al(Fe,Mn)Si phases often observed in the 6xxx alloys [53] and are believed to be formed during homogenisation in 6xxx alloys [81]. Furthermore, it appears that the large dispersoids have a smaller Mn/Fe ratio than the small dispersoids.
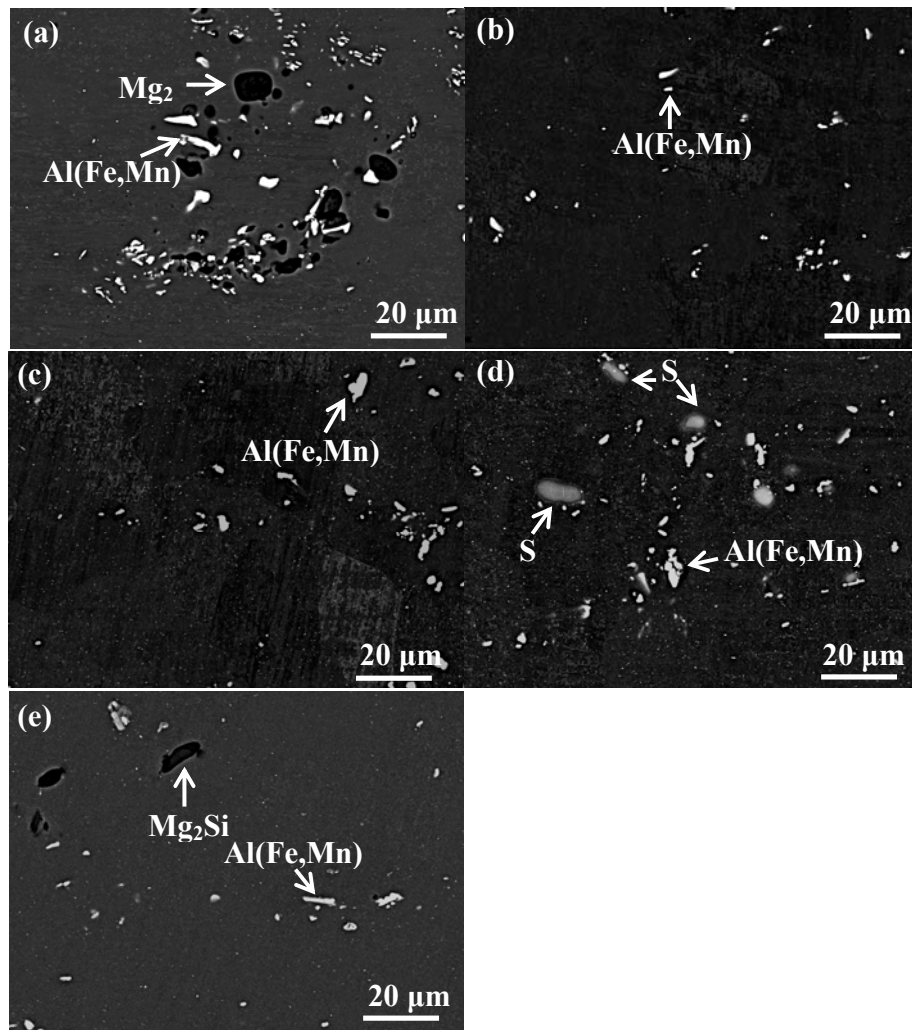
Fig. 4-1 Backscattered electron images showing undissolved coarse particles in the solution treated alloys (a) A2 (b) A3 (c) A4 (d) A5 (e) A6

Table 4-1 Area fraction of coarse constituent particles in the different alloys

Alloy	Total	Mn-containing
A2	0.54	0.40
A3	0.36	0.36
A4	0.45	0.45
A5	0.58	0.37
A6	0.36	0.31
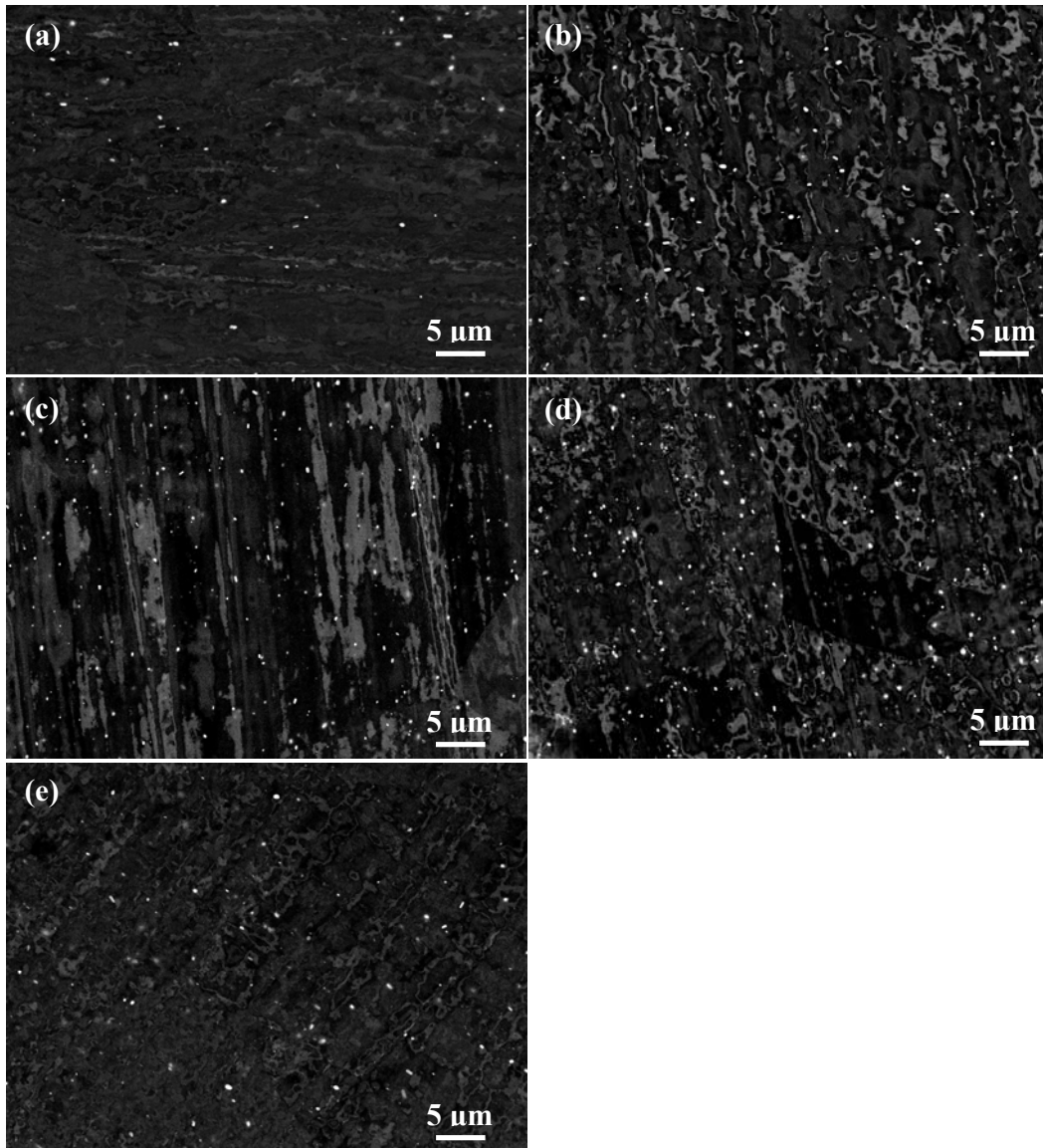
Fig. 4-2 Backscattered SEM images showing the distribution of dispersoids in the solution treated alloys: (a) A2 (b) A3 (c) A4 (d) A5 (e) A6.
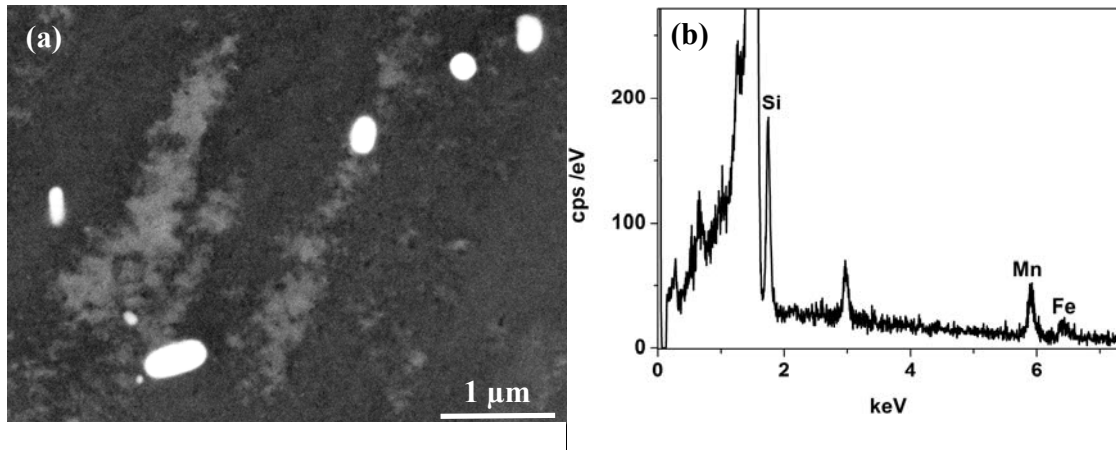
Fig. 4-3 (a) Backscattered electron image showing the morphology of the dispersoids in alloy A4 (b) EDS results of dispersoids.

Table 4-2 Quantitative data for dispersoids determined by image analysis.

Alloy	Area %	Number density per mm^2	Average diameter (μm)	Interparticle distance (μm)
A2	0.52	2.1 x 10^5	0.17	1.59
A3	0.93	2.6 x 10^5	0.18	1.23
A4	1.14	3.1 x 10^5	0.21	1.23
A5	1.25	3.6 x 10^5	0.20	1.13
A6	1.13	2.5 x 10^5	0.22	1.30

4.2.1.2 Grain structure

As shown in Fig. 4-4, with increasing Mg and/or Si content and/or Mg/Si ratio, the grain size of the alloys decreases and becomes more uniformly distributed. In general, the low solute content alloy A3 exhibits a more heterogeneous grain size distribution and the largest average grain size among the studied alloys. On the other hand, the high Si content alloy A5 shows the finest average grain size and a more homogeneous grain size distribution.
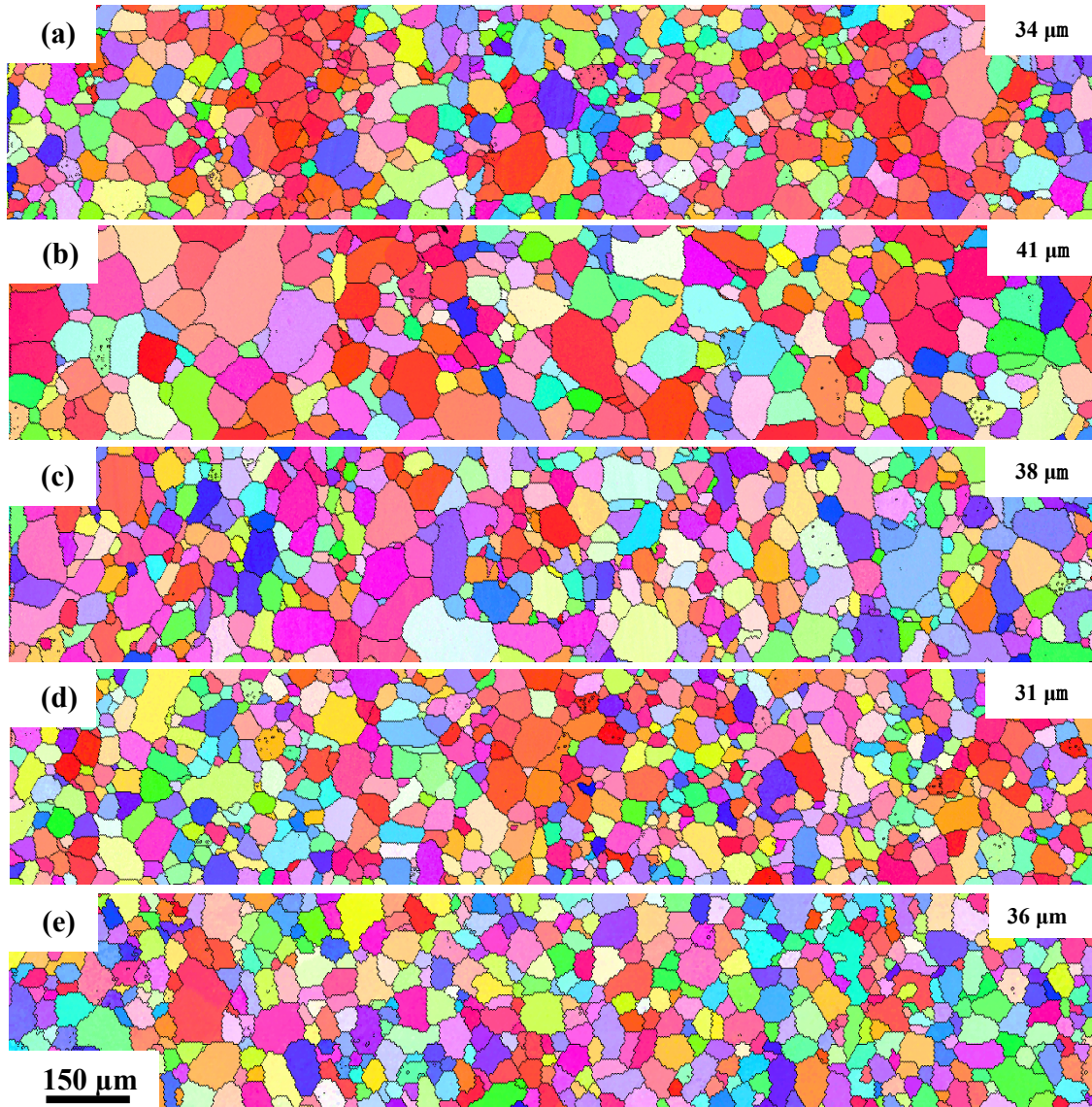
Fig. 4-4 EBSD grain structure of the alloys: (a) A2 (b) A3 (c) A4 (d) A5 (e) A6
(Note: numbers in the upper right corners indicate the average grain size.)

4.2.1.3 Texture

Furthermore, the macro-texture of the solution treated alloys was analysed. As shown in Fig. 4-5, the maximum texture intensity across different alloys is similar. The volume faction of the main texture components: cube $\{001\}<100>$, RD rotated cube $\{013\}<100>$ and ND rotated cube $\{001\}<250>$ components are listed in Table 4-3.

A2 (3.0)

A3 (2.0)

A4 (2.5)

A5 (2.3)

A6 (2.1)
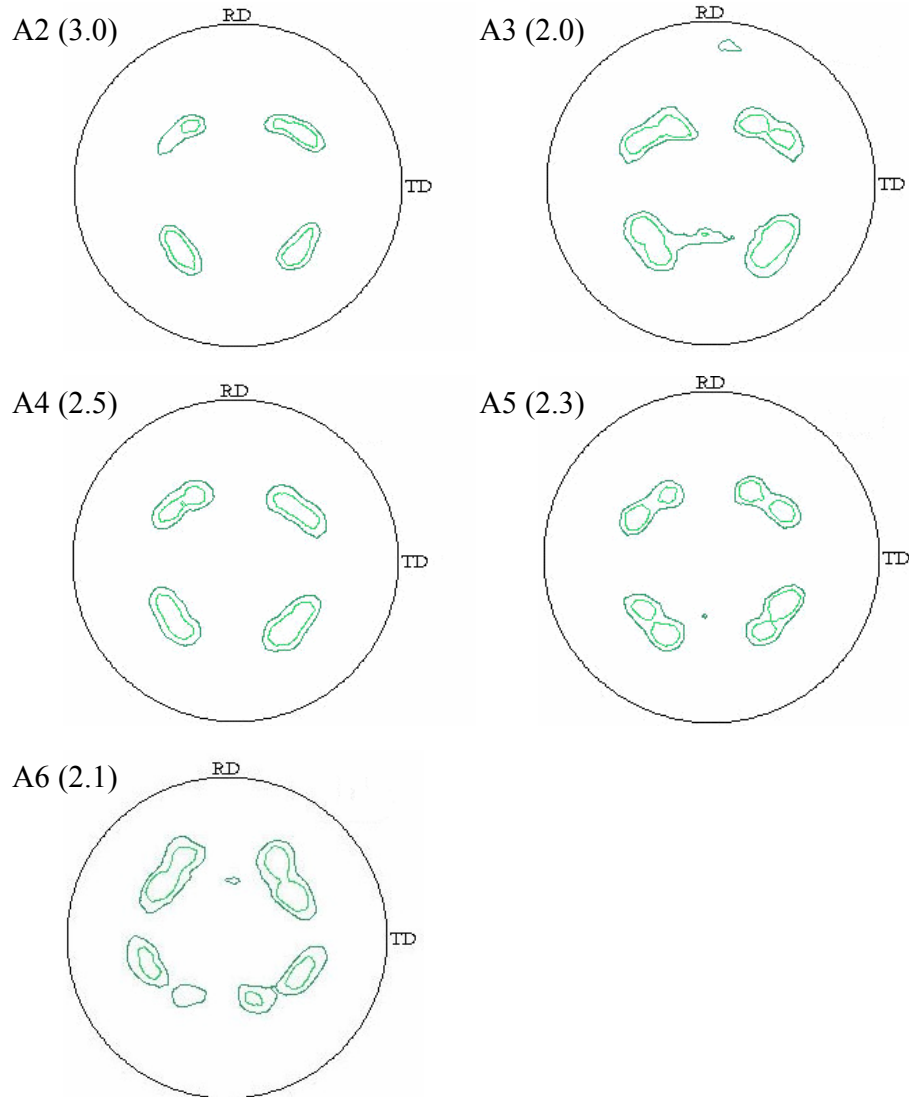
Fig. 4-5 {111} pole figures of experimental alloys in the T4 condition.
The number in parentheses represents the maximum texture intensity for
each alloy.

Table 4-3 Volume fractions of the main texture components based on bulk texture analysis

Alloy	Texture components		
	{001}<100>	{001}<250>	{013}<100>
A2	10.13	12.00	6.17
A3	6.09	7.93	5.40
A4	8.77	10.79	5.57
A5	7.31	10.25	5.12
A6	5.79	8.58	4.3

4.2.2 Natural ageing response

4.2.2.1 Effect of solution treatment parameters on the natural ageing response

The hardness evolution of alloy A2 after solution treatment at 550 ºC for different times is shown in Fig. 4-6. As seen in Fig. 4-6, it appears solution treatment for 10 minutes is sufficient to make the matrix supersaturated, since solution treatment times longer than 10 minutes cannot notably increase both the as-quenched hardness and the hardness after one week of natural ageing. Moreover, the solution treatment time at 550 ºC has little influence on the natural ageing response after quenching.

However, if the tensile properties of the materials are measured, an improvement in both the strength and elongation, with increasing solution treatment time can be observed, as shown in Fig. 4-7. This result suggests that a longer solution treatment time at 550 ºC is still needed to make the matrix fully supersaturated.
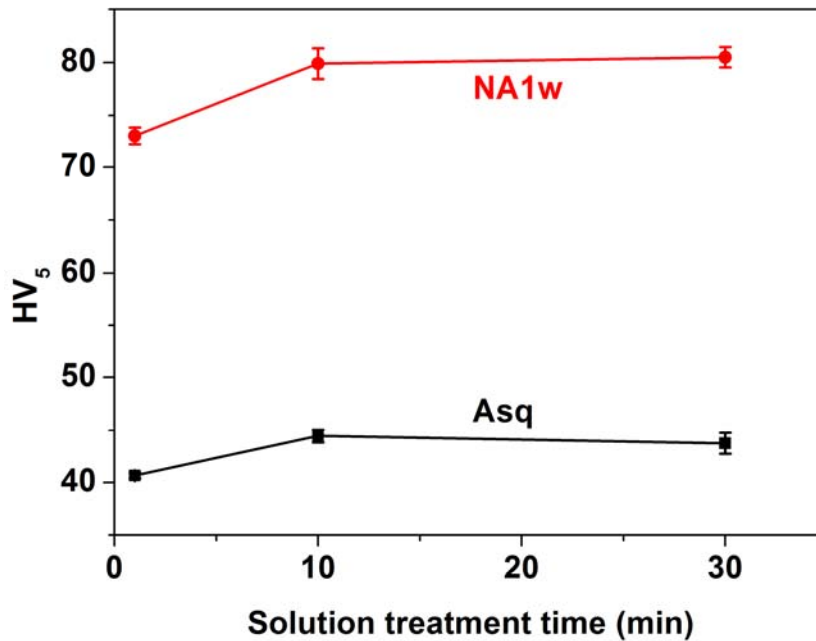
Fig. 4-6 Effect of solution time at 550 ºC on the hardness of alloy A2
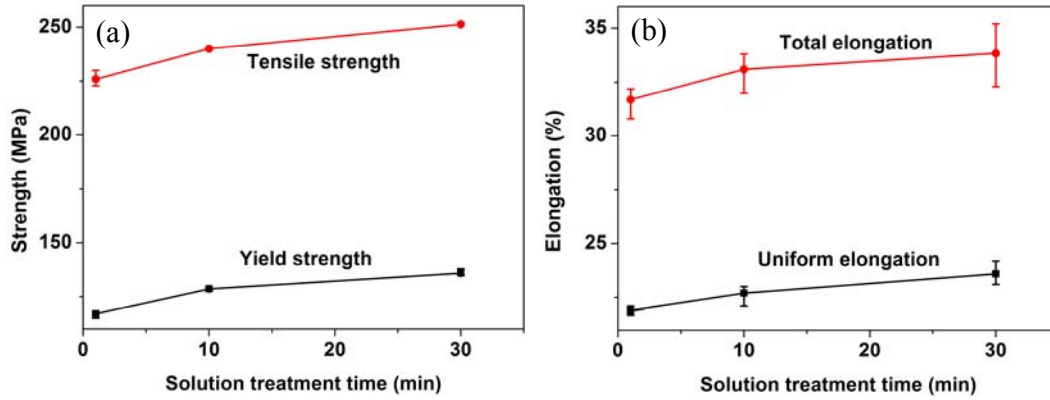
Fig. 4-7 Effect of solution treatment time on the tensile properties of alloy A2 after one week of natural ageing.

As regards strain rate sensitivity, an increase of the SRS of the flow stress can be observed with increasing solution treatment time, as shown in Fig. 4-8. However, the SRS at strains close to the onset of necking, which matters for the tensile ductility and formability, does not change with the solution treatment time.
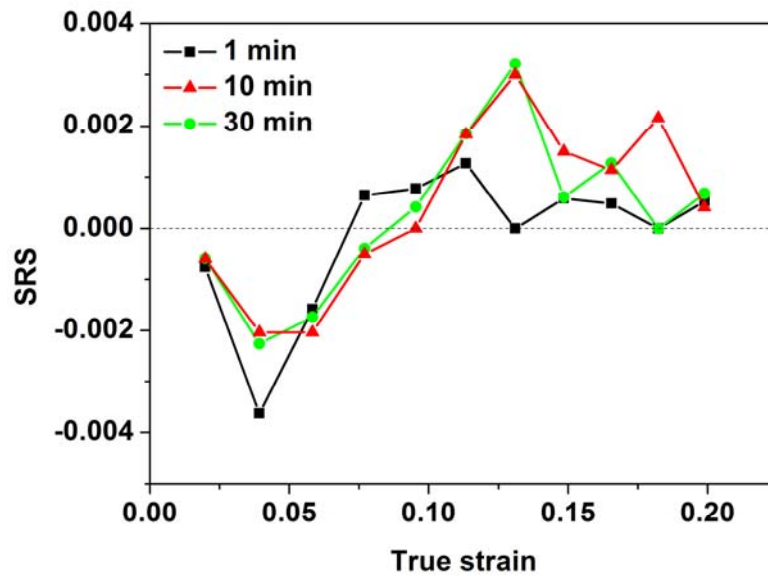
Fig. 4-8 Effect of solution treatment time on the SRS of the flow stress of alloy A2 after one week of natural ageing.

Furthermore, if the solution temperature is decreased from 550 ℃ to 500 ℃, although there is a little difference in the hardness after 30 minutes exposure in a salt bath, it is interesting to observe a smaller natural ageing response after 1 week of natural ageing in the material solution treated at 500 ℃, as shown in Fig. 4-9. This result is not unexpected since the degree

of supersaturation of both solutes and vacancies in the material solution treated at 500 ºC is expected to be lower than in the material solution treated at 550 ºC, which leads to a smaller natural ageing response in the former material. Moreover, an unexpected feature for the material solution treated at 500 ºC is that after one week of natural ageing, the PLC effect was observed, while such serrated yielding was not observed in the material solution treated at 550 ºC, as shown in Fig. 4-10. One possible mechanism for this phenomenon is that the smaller natural ageing response is associated with more mobile solutes/vacancies being retained in the material that was solution treated at 500 ºC after one week of natural ageing than in the material solution treated at 550 ºC after one week of natural ageing. In the Chapter 5, a pre-ageing treatment was also found to promote the occurrence of the PLC effect, which was associated with a smaller natural ageing response after pre-ageing. The possible mechanism for the occurrence of the PLC effect observed in the material solution treated at 500 ºC will be explained in detail and discussed together with the observed PLC effect caused by pre-ageing in the Chapter 5. Moreover, it should be noted that the serrated yielding is believed to be detrimental to the formability of 6xxx alloys [16].

Therefore, based on above results, the solution treatment of 6xxx alloys is suggested to be performed at high temperature for a long time, i.e., at 550 ºC for 30 min.
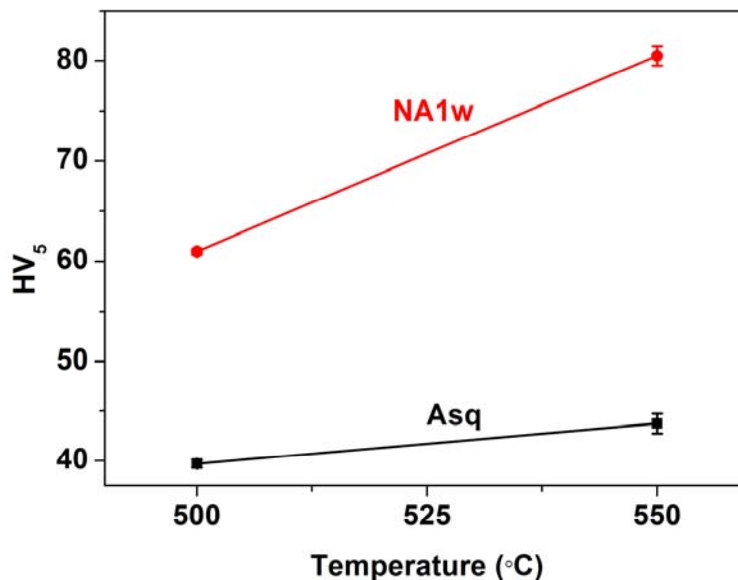
Fig. 4-9 Effect of solution temperature on the hardness of alloy A5.
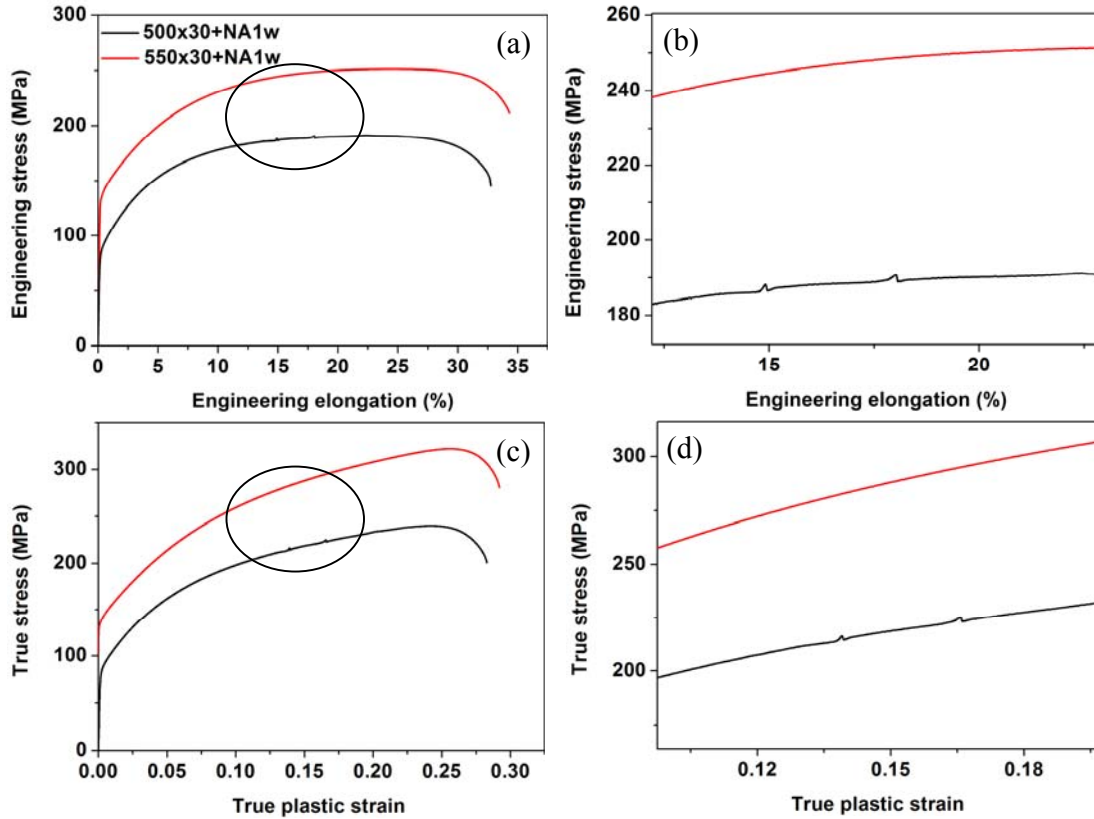
Fig. 4-10 (a) Effect of solution temperature on the engineering stress-strain curves of alloy A2 (b) enlarged view of (a), and (c-d) on the corresponding true stress-plastic strain curves.

4.2.2.2 Effect of alloy composition on the natural ageing response

In practice, 6xxx alloys are stamped in the T4 or T4P conditions [5]. In these conditions, the mechanical properties of the alloys are quite stable. In other words, the mechanical properties of the alloys do not change after an extended natural ageing (i.e. one week) before forming. To find out how the natural ageing influences mechanical properties of these Al-Mg-Si alloys and when the mechanical properties are stable, the evolution of hardness and tensile properties during natural ageing was studied.

- **Hardness**

As shown in Fig. 4-11, with increasing Mg and/or Si content, the natural ageing response of the alloys becomes greater and more rapid. With the same total atomic Mg plus Si content, low Mg/Si ratio alloy A4 and medium Mg/Si ratio alloy A6 showed faster ageing kinetics

than high Mg/Si ratio alloy A2 during the first few hours of natural ageing. With prolonged natural ageing (i.e. 1 week), the hardness values of alloys A2, A4 and A5 saturated to a similar hardness level of about 82 HV_5, while A6 attained slightly higher hardness values. The highest hardness value for alloy A6 after one week of natural ageing is not unexpected since the Mg/Si atomic ratio in alloy A6 is close to 1, which is supposed to promote the formation of hardening clusters [123].
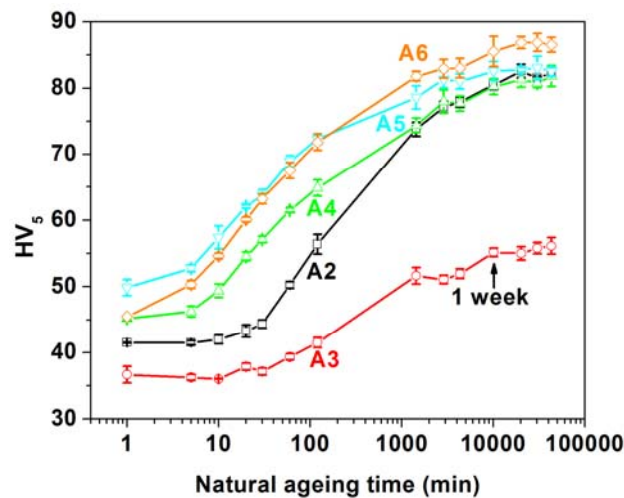
Fig. 4-11 Natural ageing curves for the alloys studied

- **Tensile properties**

As for the tensile properties, the typical engineering stress-strain curves for the high Mg content alloy A2 after different natural ageing times are shown in Fig. 4-12. It can be seen that the flow stress of alloy A2 increases with natural ageing time. Moreover, significant serrated yielding is only seen in alloy A2 with natural ageing time being equal to or less than one hour. Table 4-4 summarises the observation of the PLC effect in these five alloys in the different tempers. It appears the observation of the PLC effect after one hour of natural ageing can be related to the natural ageing kinetics observed in the Fig. 4-11. More precisely, the high Si content alloys (A4 and A5) and medium Mg/Si ratio alloy A6 have faster early natural ageing kinetics (i.e. within the first hour of natural ageing), which is associated with the faster removal of mobile solutes and/or vacancies from the matrix, compared to the low Si content alloys A2 and A3. Therefore, serrated yielding is more notable after a given natural ageing time in the latter alloys than in the former alloys. Since the poor formability of as-quenched 6xxx alloys was attributed to the serrated yielding [16], forming of 6xxx alloys

is therefore suggested to be performed on the alloys after longer natural ageing time (i.e., one day or more).

Fig. 4-13 shows the mechanical property evolution during natural ageing for alloy A2. It can be seen that the strength increased with the natural ageing time and saturated after one week of natural ageing. It is interesting to see that the uniform/total elongation decreased with the natural ageing time and saturated after one week of natural ageing, as well. This suggests that forming of 6xxx alloys can be performed on the alloys after one week of natural ageing when the mechanical properties of the alloys are stable.
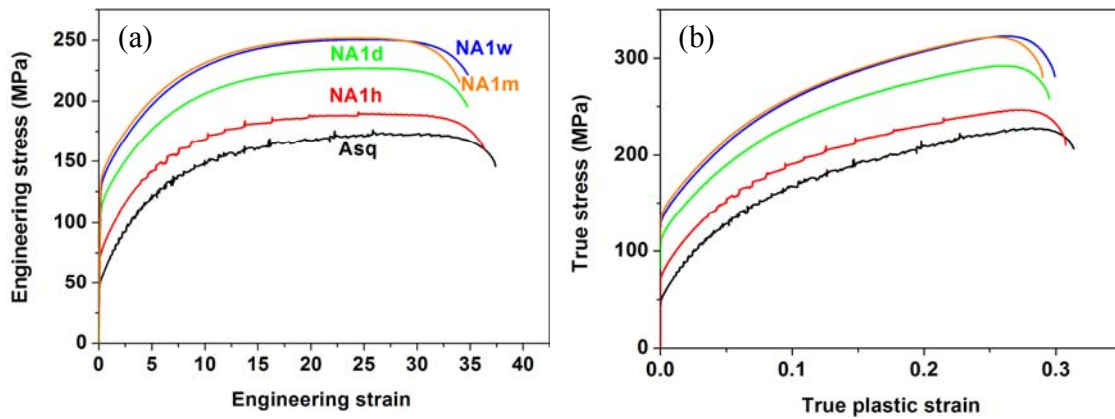
Fig. 4-12 (a) Engineering stress *vs.* strain plots for alloy A2 in different conditions, and (b) corresponding true stress-plastic strain plots.

Table 4-4 Summary of the onset strain for the PLC effect in the alloys

Alloy	Conditions				
	Asq	NA1h	NA1d	NA1w	NA1m
A2	0.008	0.04	/	/	/
A3	0.007	0.02	0.13	/	/
A4	0.006	0.1	/	/	/
A5	0.010	0.1	/	/	/
A6	0.011	0.12	/	/	/
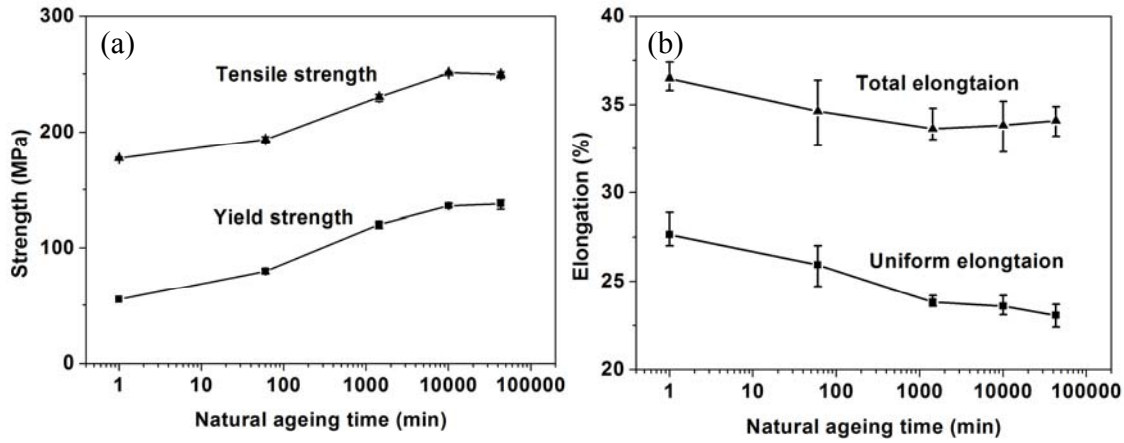
Fig. 4-13 The evolution of mechanical properties of alloy A2 during natural ageing (a) strength (b) elongation.

- **Work hardening and strain-rate sensitivity**

The work hardening curves for alloy A2 in the as-quenched and/or naturally aged conditions are shown in Fig. 4-14. It can be seen that the material in the as-quenched and/or naturally aged for 1 h conditions shows a lower work hardening rate than the material with longer natural ageing time (i.e. more than one day of natural ageing), especially at strains close to the onset of necking. After one week of natural ageing, the work hardening curve almost has no change with prolonged natural ageing.
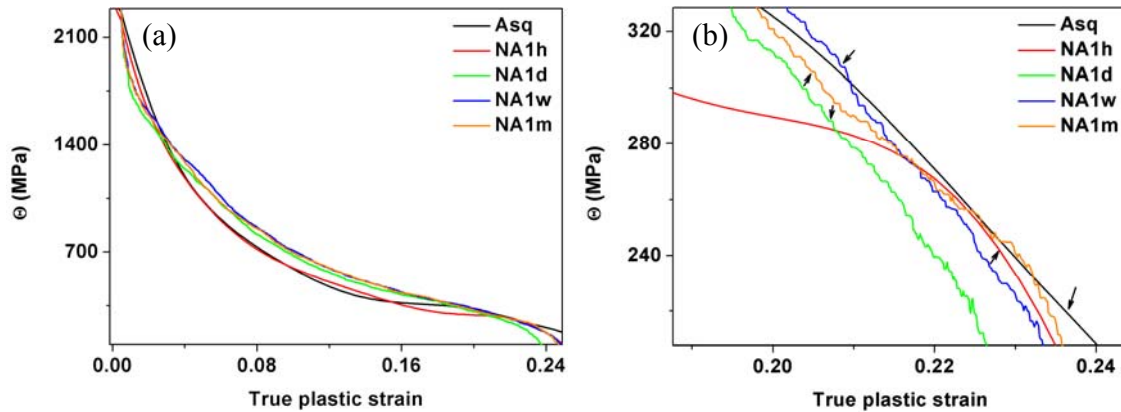
Fig. 4-14 (a) Work hardening curves for alloy A2 in the as-quenched and/or naturally aged conditions (b) enlarged view of (a) at strains close to the onset of necking. The arrows in (b) indicate uniform strains.

Kocks-Mecking plots for alloy A2 in the different conditions are shown in Fig. 4-15. Both the initial work hardening rate and dynamic recovery rate were observed to decrease with natural ageing time increasing. Θ_{II} is believed to be dependent on the solute concentration in

the matrix, and a high solute concentration is expected to lead to a high initial work hardening rate [15, 45]. Thus, it is not surprising that as-quenched material has a higher initial work hardening rate than naturally aged material, since as-quenched material contains more solute atoms in solution than naturally aged material. As for the dynamic recovery rate, a high solute concentration in the matrix is expected to decrease the dynamic recovery rate. This may suggest that the dynamic recovery rate in the as-quenched material should be lower than that in naturally aged material. However, the trend in this study is opposite, which was also reported by Zolotorevsky *et al* [15]. This is probably attributed to the occurrence of dynamic precipitation in the naturally aged material [42], which may decrease the dynamic recovery rate.
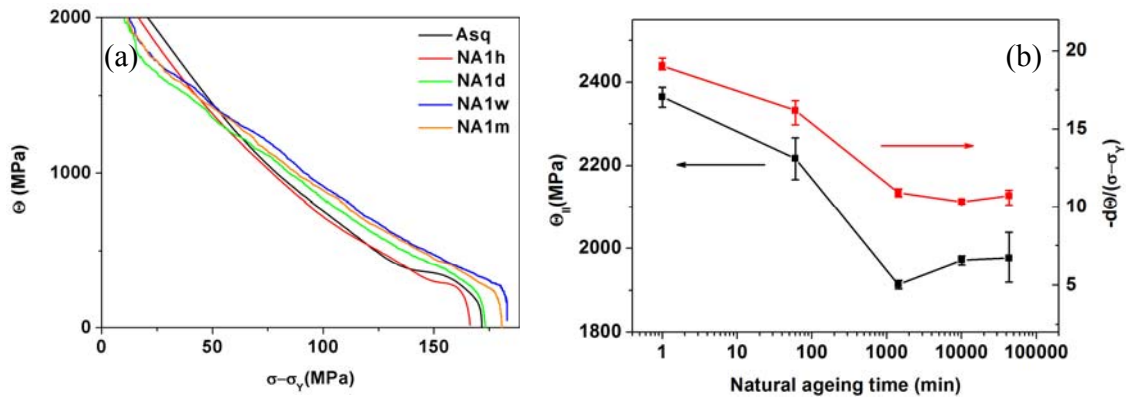
Fig. 4-15 (a) Kocks-Mecking plots, (b) Θ_{II} and $d\Theta/d(\sigma - \sigma_Y)$ for alloy A2 in the as-quenched and/or naturally aged conditions.

For the SRS of the flow stress, an increase in the SRS with increasing natural ageing time is expected since the PLC effect gradually disappeared with prolonged natural ageing (see Fig. 4-12), which suggests a decreased negative contribution of DSA to the SRS of the flow stress. As shown in Fig. 4-16, the improvement in the SRS of the flow stress is significant if the material was further naturally aged after one hour of natural ageing, (i.e., when the serrated yielding disappears after one hour of natural ageing).
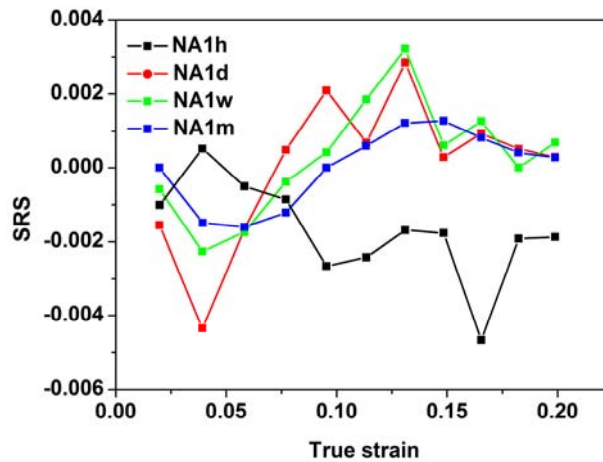
Fig. 4-16 Dependence of the SRS on the true strain for the naturally aged alloy A2.

4.2.3 Effect of Si, Mg and Mg/Si ratio on the tensile properties of 6xxx alloys

The naturally aged strength of the alloys increases with increasing total Mg + Si content (from A3 to A2 and A4, and further to A5), as shown in Fig. 4-17. As for the tensile ductility, Mg has almost no effect on it. However, an increase in the Si content raises the average ductility slightly, although at the highest Si levels this enhancement disappears. As regards the effect of Mg/Si ratio, alloys with high and low Mg/Si ratios (i.e. alloys A2 and A4, respectively) were found to have similar strengths at a level of about 10-15 MPa lower than that achieved by the alloy with medium Mg/Si ratio (A6). It is evident that the uniform and total elongations both decrease slightly with increasing Mg/Si ratio.
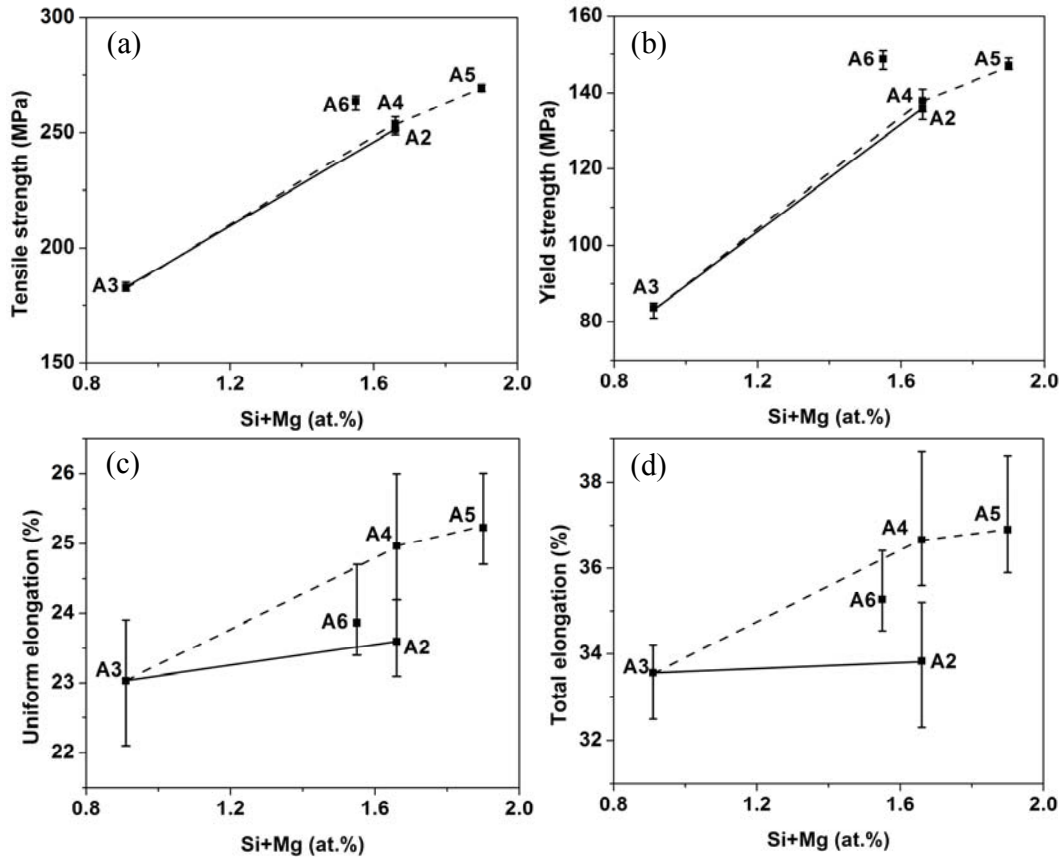
Fig. 4-17 Tensile properties of the alloys naturally aged for one week.
Note: dashed lines connect the alloys with different Si contents, while solid lines connect the alloys with different Mg contents

4.2.4 Formability results

Increased Mg and Si content was shown to improve the stretch forming performance of the alloys (see Fig. 4-18). A noticeable effect was found for the forming limit in the plane strain stretching condition (FLD_0), which is very important for automotive stamping lines since most of the forming failures occur in this mode [110]. It is noted that the formability enhancement by increasing the Si content is more significant than that achieved by increasing the Mg content. Notably, the FLD_0 of the alloys studied is within the range of values for 6xxx alloys reported in the literature [6, 16, 124] . For instance, FLD_0 for the high Si content alloys A4 and A5 is close to the value for alloy 6016 reported in [124]. Similarly, FLD_0 for the high Mg content alloy A2 is equivalent to the value for alloy 6061 reported in [6], although the latter alloy has relatively high Fe and Cu contents.
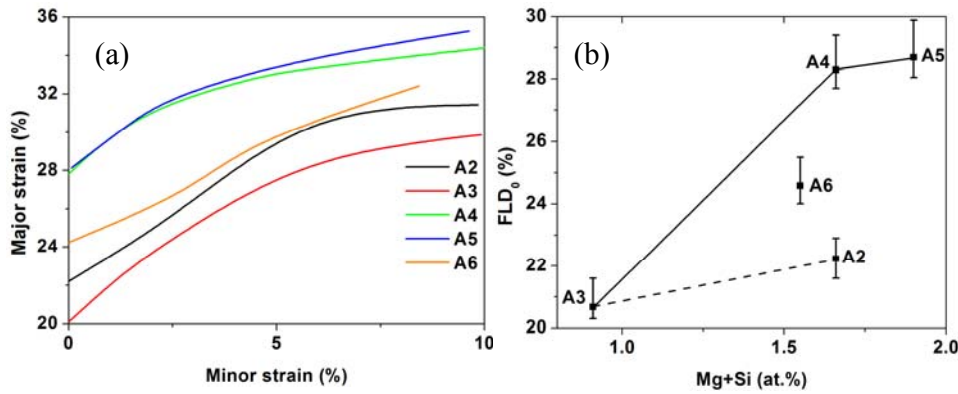
Fig. 4-18 (a) Right-hand side of FLD and (b) FLD of the alloys after 1 week of natural ageing.

4.3 Discussion

4.3.1 Effect of grain size

Grain size is known to be an important factor in the localised necking process, since correlated shear bands spreading across a specimen cross-section are formed at lower strains in materials with a coarse grain size [89]. Literature data [87, 88] show that the formability improves significantly with decreasing grain size. For a superior formability, the grain size should be at least around 20 times smaller than the sheet thickness [9]. Thus, for 1 mm sheet, the grain size should be below 50 μm. In this study, the average grain size of the alloys was in the range from 31 to 41 μm. Furthermore, one may think that the grain size should also have an effect on the formability, as the formability of the alloys was found to increase in the sequence A3 to A4 to A5 and A3 to A2, i.e. in the same sense as the grain size decreased (cf. Fig. 4-4). However, the formability of alloy A2 with a grain size of 34 μm was lower than that of alloy A4 with a similar grain size of 38 μm, which suggests that the grain size is not the major factor that affects formability. Morris *et al* {Morris, 1982 #133} also proposed that grain size in the normal commercial alloy range of 20 to 100 microns has little effect on the necking or fracture limits of aluminium alloys at room temperature. Similarly, the grain size should also have little effect on the tensile ductility of the alloys studied, since the tensile ductility and the formability have similar trends with respect to grain size variation.

The variation in grain size may be attributed to a different volume fraction and distribution of coarse particles and dispersoids in the alloys. Coarse particles are important in that they tend

to refine the grain size in the final T4 state by providing nucleation sites for particle-stimulated nucleation [26]. Moreover, dispersoids restrict grain growth during the final solutionising treatment [26]. In the present study, the volume fraction of both coarse particles and dispersoids increased with increasing Si content, resulting in a refined grain structure. An increase in Mg content and the ensuing increase of the volume fraction of coarse particles may counteract the reduced negative effect on grain refinement caused by the low number density of dispersoids. As a result, a refined grain structure can be observed. The increased volume fraction of dispersoids in the alloy A6 is expected to attribute the finer grain size compared to alloy A3. Furthermore, a larger solute drag effect by solute atoms in the matrix may also contribute to the grain size refinement in the high solute content alloys [125].

4.3.2 Effect of texture

Many studies showed that texture can have significant influence on the deep drawing ability of the material through it's influence on the r-value [91, 92] . As for stretch forming, the stretchability of a material is determined by work hardening and strain-rate hardening capability of the material rather than r-value [6, 7]. However, Pedersen *et al* [93] suggested that a strong cube texture can lead to a high stretch formability, although no information about the work hardening and strain-rate hardening characteristics of the materials was provided. Furthermore, Yoshida *et al* [94] modelled the effect of major texture components in aluminium alloys on the biaxial formability, and also found a strong cube texture would contribute the high stretch formability due to the enhanced work hardening rate.

In this study, the major texture components in the alloys are cube texture, and the variation in maximum texture intensity across the different alloys is small. Therefore, texture should not be considered as an important factor that influence on the stretch formability of the studied alloys.

4.3.3 Effect of solute and clusters

Solutes in solution tend to increase the yield strength and retard dynamic recovery [98], which results in an increased work hardening capacity [126] . Cheng *et al* [40] proposed that the slope of the linear part of the Θ *vs.* (σ-σ_Y) plot is inversely proportional to the rate of

dynamic recovery, where Θ is the work hardening rate and σ_Y is the yield stress. Fig. 4-19 shows the Θ *vs.* (σ-σ_Y) plots for the alloys after one week of natural ageing. High solute content alloys were found to have a higher work hardening rate at large stresses (Fig. 4-19a) and a lower dynamic recovery rate than that in the low solute content alloys (Fig. 4-19b). Furthermore, it appears the Mg/Si ratio has little influence on the dynamic recovery rate.
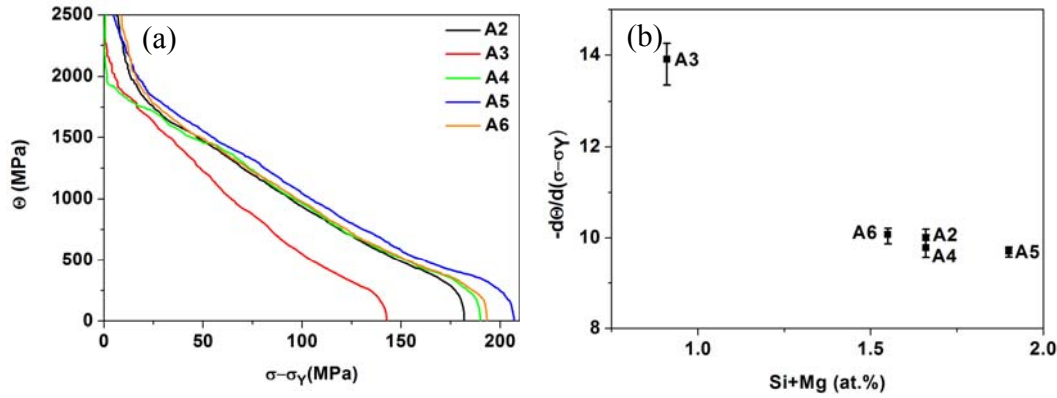
Fig. 4-19 (a) Θ *vs* (σ-σ_Y) plots, and (b) rate of dynamic recovery of the alloys. The alloys were naturally aged for one week.

Accordingly, the increased work hardening capacity represented by the *average* work hardening exponent (n-value) increases slightly with increasing Si content (Fig. 4-20a). The Mg content, however, has a lesser effect on the n-value. With the same total solute content, low Mg/Si ratio alloy A4 shows a higher n-value than alloys A2 and A6. According to Considère necking criterion, the n-value should be exactly equal to uniform strain provided that the true stress- plastic strain curves of the alloys studied conform to Hollomon equation. In other words, the dependence of n-value and uniform elongation on the compositions should be similar. However, comparing Fig. 4-20 (a) with Fig. 4-17 (c), some differences can be found (i.e. the dependence of n-value of A2, A4, and A6 on the compositions is not the same as the dependence of uniform elongation of these alloys on the compositions). In addition, the work hardening capacity can also be represented by (UTS-YS)/YS. As shown in Fig. 4-20 (b), it is interesting to see that the low solute content alloy A3 exhibits a largest work hardening capacity than another four high solute content alloys, however, alloy A3 has a lowest uniform elongation among the alloys studied. These differences arising from Fig. 4-20 can be explained in terms of the *instantaneous* work hardening exponent, n_i defined as the derivative of the logarithms of true stress with respect to the logarithm of true plastic strain at

a given point on the true stress-plastic strain curve. As shown in Fig. 4-21 (a), at the beginning of plastic deformation, n_i increases sharply with strain, but then drops off gradually until the onset of necking. After that, a rapid decrease in n_i can be observed. At small strains below 0.1, A3 exhibits significantly larger values of n_i than the other alloys. However, at strains close to the onset of necking, n_i for alloy A3 is lower than that for the other alloys (Fig. 4-21b). Also, from Fig. 4-21b it can be found that n_i at the point corresponding to uniform strain ($n_{\varepsilon u}$) is almost the same as the uniform strain itself – in keeping with the Considère necking criterion ($\Theta = \sigma$). As listed in Table 4-5, the overall work hardening exponent (average value from strains of 0.002 to uniform strain, $n_{0.002\sim\varepsilon u}$) of alloy A3 is higher than for the other alloys, which is consistent with the results if the work hardening capacity is expressed as (UTS-YS)/YS (as shown in Fig. 4-20b). However, if the average n_i between the strains of 0.002 and 0.1 ($n_{0.002\sim0.1}$), and between the strains of 0.1 and uniform strain ($n_{0.1\sim\varepsilon u}$) are measured, then it can be found that the high n_i of alloy A3 only refers to the low strains below 0.1. At large strains, alloy A3 loses its ability to maintain a high work hardening capacity. In other words, it is the work hardening at low strains (0.002 to 0.1) that causes a high overall work hardening capacity in alloy A3. However, for ductility and stretch formability, the work hardening capacity at high strains, especially close to the onset of necking, is more important than the overall one. By using the *instantaneous* work hardening exponent, the consistence can be found about the uniform elongation and $n_{\varepsilon u}$ on the compositions, as shown in Fig. 4-17 and Fig. 4-22.

It should be noted that both the average work hardening exponent and (UTS-YS)/YS are normally used for representing the work hardening capability for engineering purposes. However, this study shows that both of them are not suitable for describing the work hardening capability of the alloys that were investigated. By contrast, the *instantaneous* work hardening exponent at the uniform strain may be considered as a suitable way for evaluating the work hardening capability. However, the *instantaneous* work hardening exponent cannot tell us why various materials have different work hardening behaviour. Therefore, the Kocks-Mecking-Estrin model will additionally be employed to study the work hardening behaviours of the alloys studied. Nevertheless, the *instantaneous* work hardening exponent at uniform strain is still used in this PhD study for representing work hardening capability and for the purpose of ranking materials, as this is a common practice in this industry.
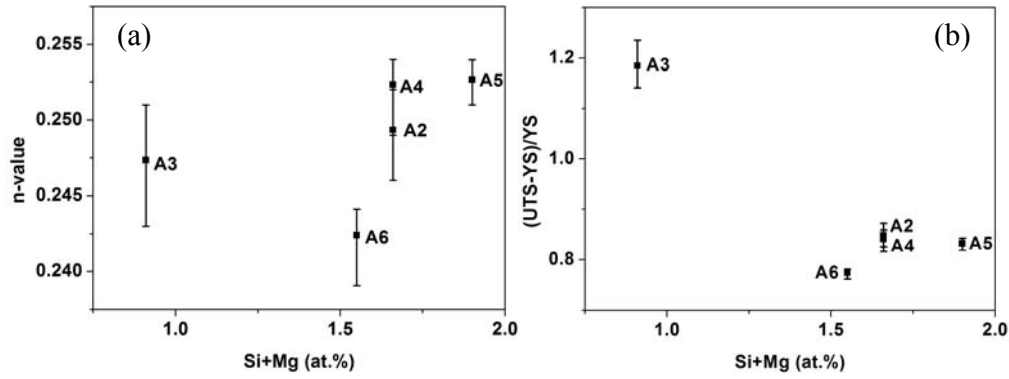
Fig. 4-20 Effect of composition on (a) n-value and (b) (UTS-YS)/YS.
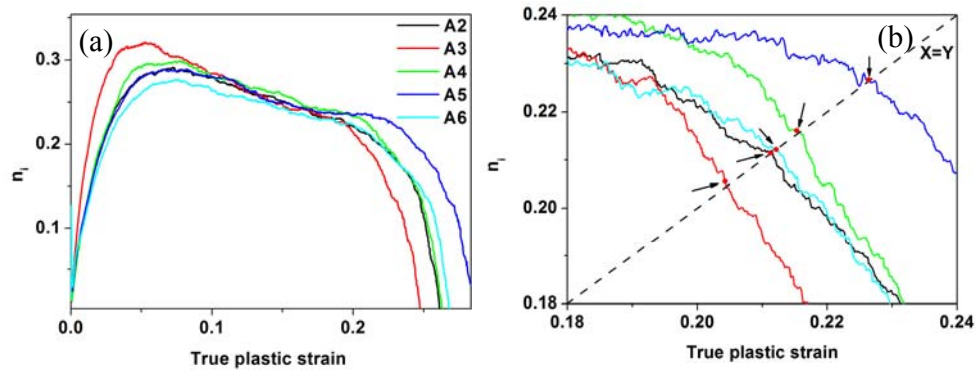
Fig. 4-21 (a) The dependence of n_i on the true plastic strain of the different alloys; (b) an enlarged view of (a) at strains close to uniform strains. The alloys were naturally aged for one week. Arrows and red dots in (b) indicate the uniform strain determined by the Considère necking criterion.

Table 4-5. Average n_i value at different levels of true plastic strain for alloys A2 to A6 after one week of natural ageing.

Alloy	$n_{0.002\sim\varepsilon u}$	$n_{0.002\sim0.1}$	$n_{0.1\sim\varepsilon u}$
A2	0.245	0.244	0.247
A3	0.266	0.282	0.248
A4	0.252	0.253	0.252
A5	0.247	0.243	0.252
A6	0.236	0.231	0.242
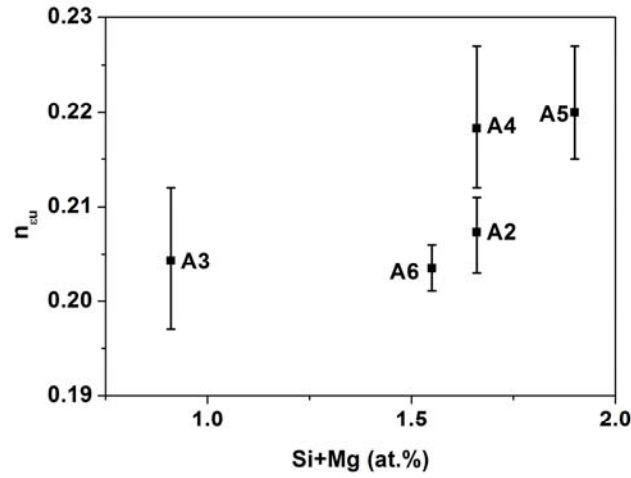
Fig. 4-22 Effect of compositions on $n_{\varepsilon u}$

Furthermore, the work hardening rate (Θ) curves of the alloys were examined. As shown in Fig. 4-23a, at first glance, the strain dependence of the work hardening rate is very similar for all the alloys, although alloy A3 shows a lowest work hardening level among the alloys studied. However, if the region near the onset of necking is enlarged, some differences are observed. As shown in Fig. 4-23b, increasing Si (from alloys A3 to A4, and further to A5) and/or Mg contents (from alloys A3 to A2) was found to increase the work hardening rate at the uniform strain. With the same total atomic Mg plus Si content, low Mg/Si ratio alloys A4 and A6 exhibited a higher work hardening rate at the uniform strain than high Mg/Si ratio alloy A2.
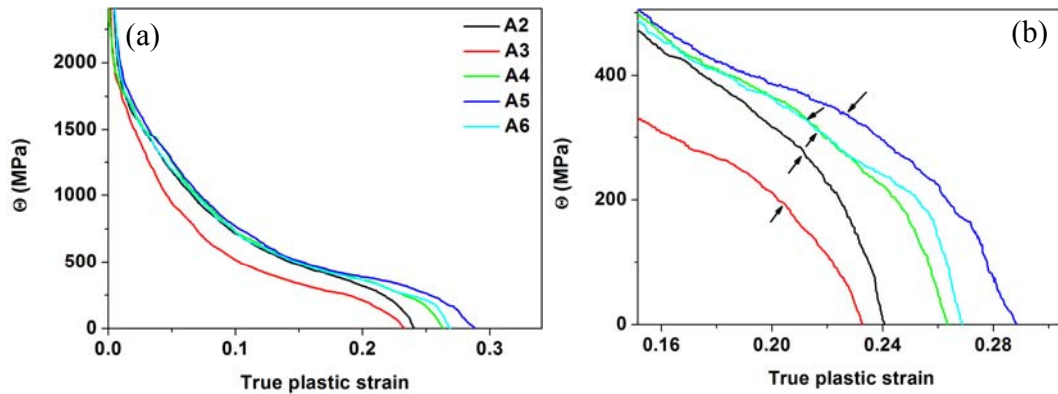
Fig. 4-23 (a) The dependence of work hardening rate on true plastic strain for different alloys and (b) an enlarged view of (a) at strains close to uniform strains. The alloys were naturally aged for one week. Arrows in (b) indicate the uniform strain determined by the Considère necking criterion.

Solutes in solution also influence the strain rate sensitivity (SRS) of the flow stress of the alloys. A high SRS is expected to decrease the tendency for strain localization [127]. As shown in Fig. 4-24, the SRS of the Si-rich alloys A4 and A5 after one day of natural ageing is larger than that of the Mg-rich alloy A2 and the low Si alloy A3, especially at the large strains that are relevant for tensile ductility and formability. The decrease of Mg/Si ratio (from alloys A2 to A6, and further to A4) also increases the SRS at the large strains. It should be noted that at low strains (i.e. around 0.02), the SRS of all the alloys is negative and/or zero, which is a manifestation of dynamic strain ageing. With prolonged natural ageing (from one day to one week), the SRS of the alloys increases. At low strains, the SRS of alloys A4, A5 and A6 becomes positive, while that of alloys A2 and A3 is still negative. Mobile atoms are believed to give rise to a negative contribution to the SRS due to dynamic strain ageing, with the effect being stronger for higher Mg concentrations in solid solution [74]. Therefore, a low SRS was found in the high Mg content alloy A2. Meanwhile, high Si contents and/or low Mg/Si ratio accelerate the ageing kinetics (as seen in Fig. 4-11) associated with the removal of mobile atoms from solid solution; therefore alloys A4 and A5 exhibit a higher SRS than alloys A2 and A3, and the SRS increases with decreasing Mg/Si ratio. Accordingly, the alloys with higher strain rate sensitivity systematically exhibit a larger post-uniform elongation (Fig. 4-25). This is consistent with reports in literature [8].
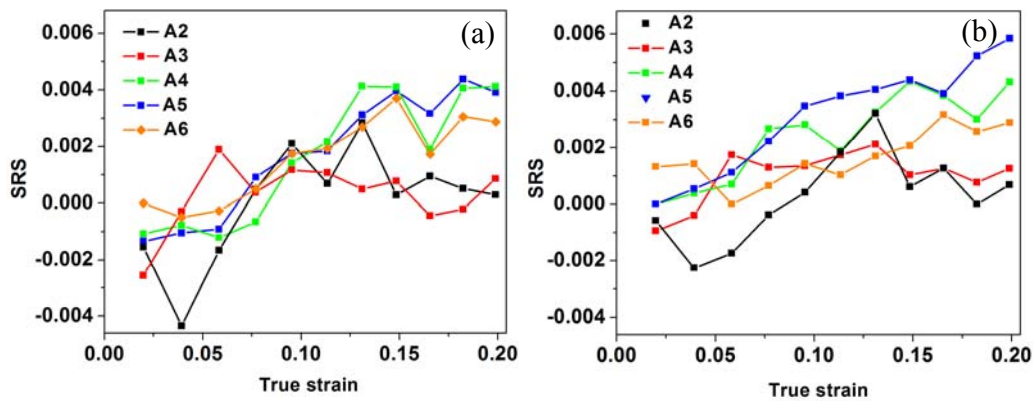
Fig. 4-24 Dependence of the SRS on the true strain for the alloys naturally aged for (a) one day and (b) one week.
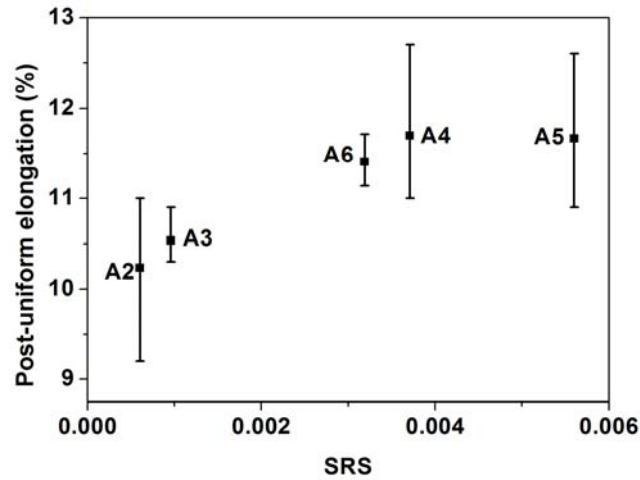
Fig. 4-25 The dependence of post-uniform elongation on the SRS for the alloys naturally aged for one week. The SRS was determined at a strain of 0.2, which is close to the onset of necking.

Dynamic strain ageing and dislocation strengthening are the major factors that influence the SRS of the flow stress of the alloys. Dynamic strain ageing results in a negative contribution to the SRS, while dislocation strengthening provides a positive contribution. At small strains (e.g. 0.02), the SRS is negative for alloys A2 and A3, which suggests that the contribution of dynamic strain ageing is predominant. The SRS is zero for alloys A4, A5 and A6. With increasing strain, the SRS increases, especially in alloys A4, A5 and A6. This suggests that the positive contribution of dislocation strengthening becomes predominant there. For alloys A2, A4 and A6 with the same total solute content level, the dislocation strengthening is similar, as shown in Fig. 4-26. Therefore, dynamic strain ageing is the only major factor that makes the SRS different in these three alloys. On the other hand, for the alloys A3, A4 and A5, increasing the Si content enhances the natural ageing kinetics, which in turn weakens the negative contribution of dynamic strain ageing to the SRS. The increased Si content also increases the dislocation strengthening compared to alloy A3, which decreases the activation distance. As a result, a larger contribution of dislocation strengthening to the SRS can be obtained in Si-rich alloys than in the low Si content alloy A3.

From the above analysis it can be recognised that a low dynamic recovery rate in the high solute content alloys influences both the work hardening and the strain rate hardening. The low dynamic recovery rate in the high solute content alloys is due to the decrease of the

stacking fault energy (SFE), which reduces the activity of cross-slip as a dynamic recovery process [128, 129].
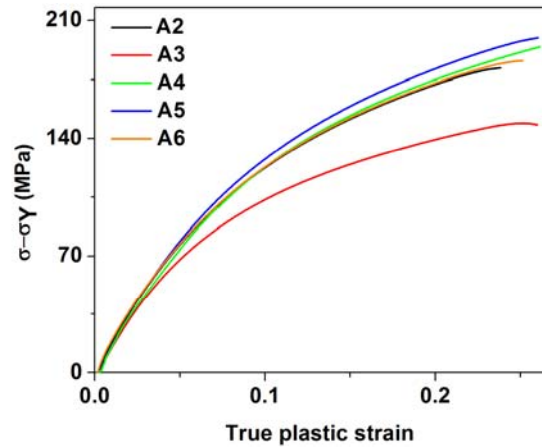
Fig. 4-26 (σ-σ_Y) *vs.* plastic strain plots for the alloys naturally aged for one week.

The difference in the SRS across different alloys can be reflected by the deformed microstructures. As shown in Fig. 4-27, after 30% straining (at which necking already occurred), the necking in the high Mg content alloy A2 is more prominent than in the high Si content alloy A4. This result is not unexpected since the deformation beyond the onset of necking is controlled by strain rate hardening. Alloy A4 has a higher SRS than alloy A2 (see Fig. 4-24); therefore a low tendency for strain localisation was observed. Furthermore, a surface profilometer was used to quantitatively study the strain localisation in these alloys. As shown in Fig. 4-28, with increasing Si content (from alloys A3 to A4, and further to A5), the deformation localisation became less prominent. Meanwhile, with increasing Mg/Si ratio (from alloys A4 to A6, and further to A2), an increase in the degree of deformation localisation was observed. It appears Mg content has little influence on the deformation localisation.

During natural ageing after quenching, clusters are expected to be formed. Clusters are shearable, and sheared by mobile dislocations during the course of deformation. Therefore, a decrease in the work hardening capability is seen when the material was naturally aged, compared to that of as-quenched alloy (see Fig. 4-13b). Furthermore, the formation of clusters would consume the mobile solutes from the matrix, thus decreasing the negative

contribution of DSA on the SRS. This process can enhance the SRS of the flow stress of the materials, as shown in Fig. 4-16.
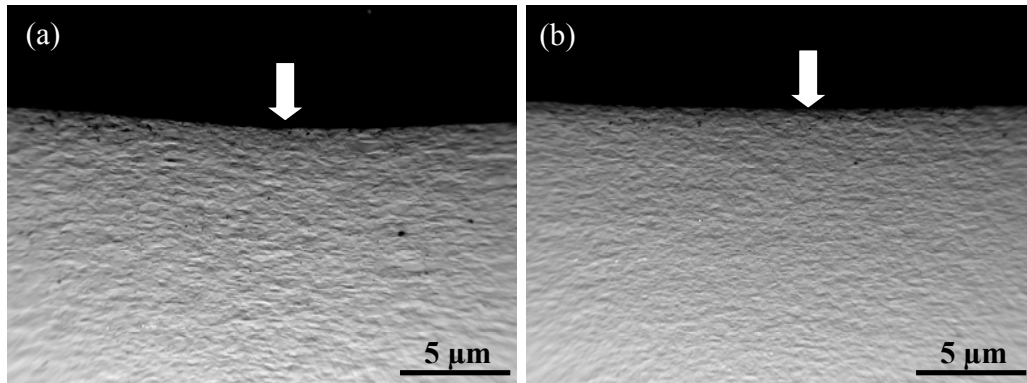
Fig. 4-27 SEM images showing the necked region in the alloys (a) A2 and (b) A4. The alloys were naturally aged for 1 week, and then strained by 30%. The arrows indicate the necked region.
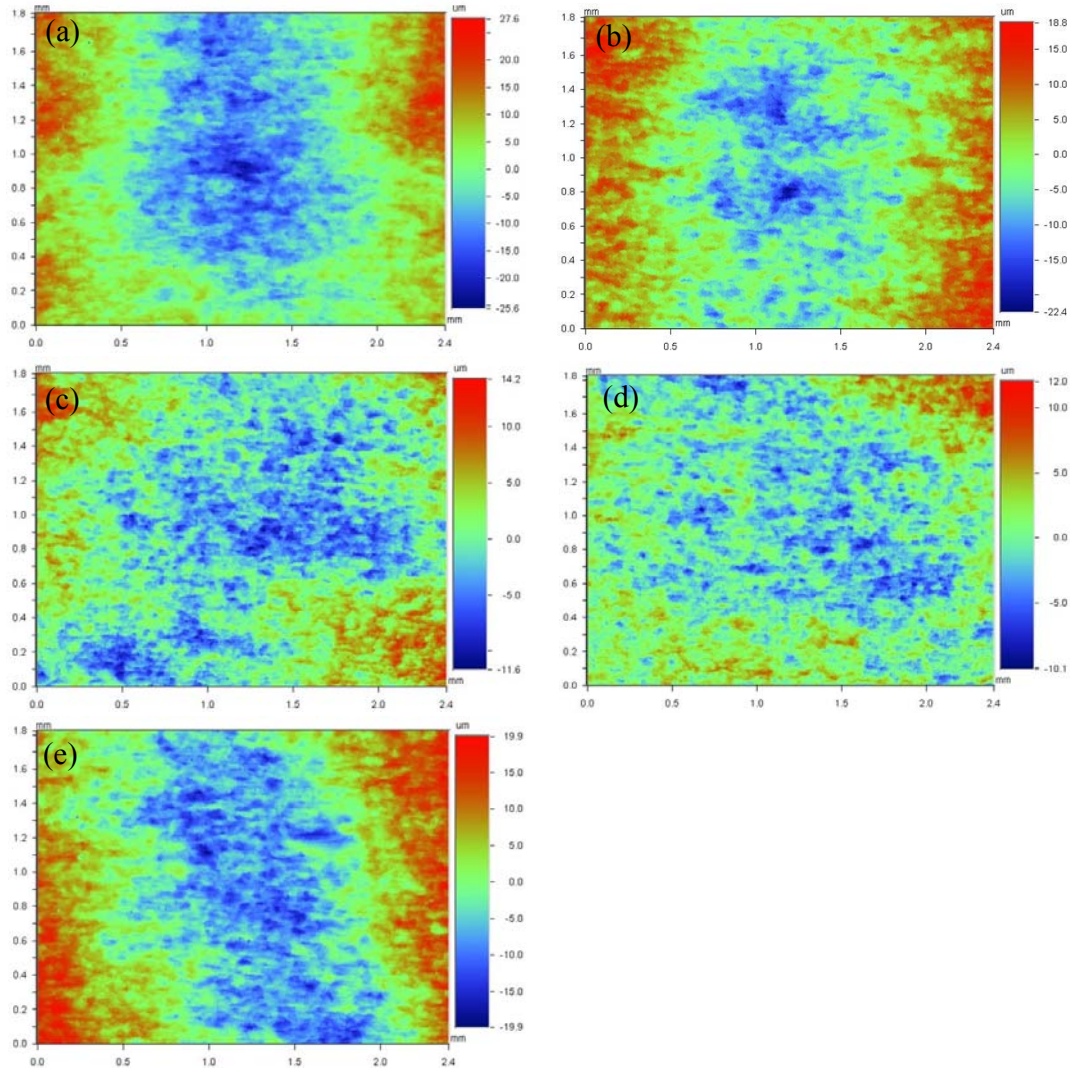
Fig. 4-28 Effect of alloy composition on the necking in (a) A2, (b) A3, (c) A4, (d) A5 and (e) A6. The alloys were naturally aged for 1 week, and then strained by 30%.

4.3.4 Effect of dispersoids

The presence of dispersoids can homogenise the slip distribution. Indeed, dislocation debris left by a gliding dislocation around non-shearable dispersoid particles in its slip plane increases the slip resistance there, thus promoting slip on other planes. As a result, more uniform slip can be observed [54].

The effect of dispersoids on the work hardening behaviour can be studied by means of the Kocks-Mecking-Estrin model [39]. To model the influence of dispersoids on the work

hardening behaviour, the following superposition law for the flow stress encompassing the various contributions was used:

$$\sigma = \sigma_o + \sigma_{ss} + \sigma_{clusters} + (\sigma_D{}^2 + \sigma_n{}^2)^{1/2} \qquad (4\text{-}1)$$

where σ_o is an intrinsic 'friction' stress, σ_{ss} is the solid solution strengthening contribution, $\sigma_{clusters}$ is the strengthening contribution arising from solute clusters, and σ_n is the contribution of non-shearable dispersoids. The term $(\sigma_o + \sigma_{ss} + \sigma_{clusters})$ equals $(\sigma_Y - \sigma_n)$, where σ_Y is the yield stress, and its magnitude for the different alloys is listed in Table 4-6. As shown in the table, the contribution of dispersoids to the yield stress is around 5 MPa, which is similar to the value reported in Reference [82].

Table 4-6 Yield strength and σ_n of the alloys after 1 week of natural ageing

Alloy	Yield strength (MPa)	σ_n *(Mpa)
A2	136	3.9
A3	84	5.0
A4	138	5.0
A5	147	5.5
A6	149	4.8

*σ_n is obtained by using quantitative data in Table 2 and the Orowan equation [120]

Fig. 4-29 shows the dependence of k, k_1 and k_2, determined by fitting the experimental curves to Eq. 2-4, on the combined content of Mg and Si of the alloys. It is seen that the high Si content alloys (A4 and A5) have a higher k-value than the low Si content alloy A3. This is attributed to the high number density of dispersoids in alloys A4 and A5 (Table 4-2). Similarly, decreasing Mg/Si ratio (from alloys A2 to A6, and further to A4) increases the number density of dispersoids, which also increase the k-value. Increasing the Mg content (from alloy A3 to A2) has no influence on k_1, while k_1 has a weak dependence on the Si content (from alloys A3 to A4, and further to A5) and Mg/Si ratio (from alloys A2 to A6, and further to A4). In the classic work hardening theory, k_1 is independent of the solute content [39], although recent study showed that k_1 can be influenced by the solute content (e.g. Cu and Mg contents in Al alloys) [15]. A possible mechanism was suggested by Zolotorevsky *et al* [15] foreign atoms diffuse from forest dislocations to mobile dislocations while the latter

are stopped before a barrier; this contributes to the pinning of mobile dislocations and their transition to the category of forest dislocations, thus enhancing the amount of athermal hardening. The dynamic recovery rate k_2 is seen to be strongly influenced by the amount of Mg and Si in the alloy. This implies that alloys with a higher solute content exhibit a lower dynamic recovery rate. The Mg/Si ratio was found to have little influence on k_2.
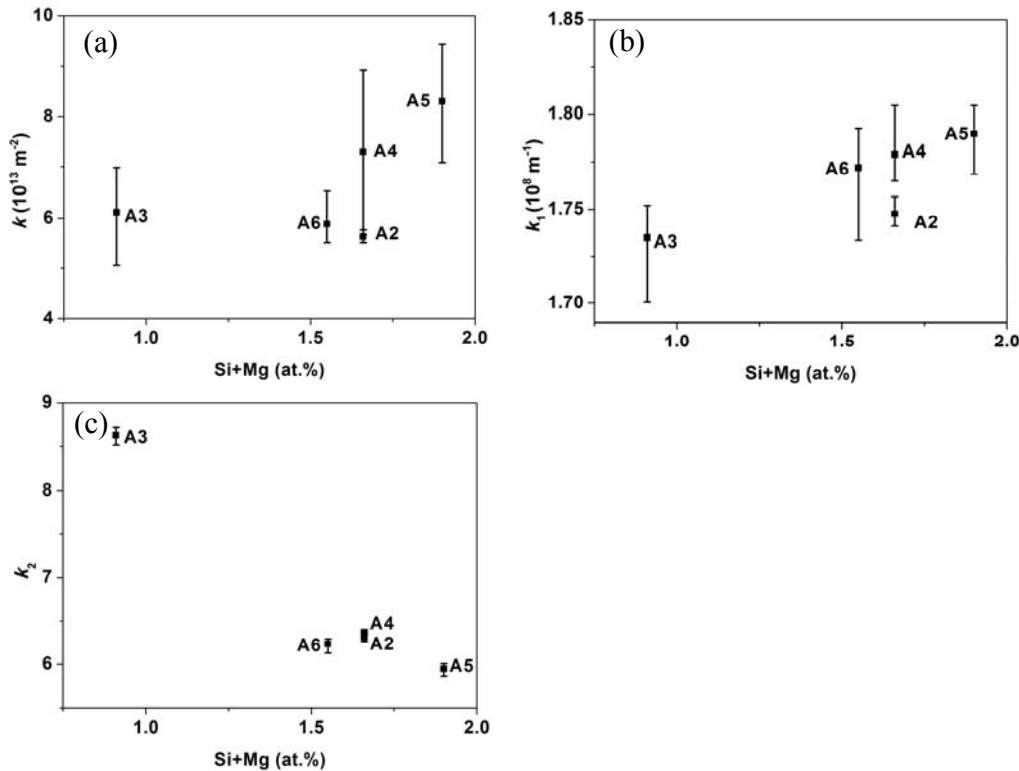
Fig. 4-29 Effect of alloying element content on (a) k, (b) k_1 and (c) k_2. The alloys were naturally aged for one week.

These results suggest that, to maintain a high work hardening rate, the alloy should have a high Si content (or low Mg/Si ratio) and a high number density of dispersoids. However, it should be emphasised that the contribution of solutes in the solution to the work hardening is predominant over the contribution of dispersoids to the work hardening. Fig. 4-30 shows a comparison of stress-strain curves of alloy A4 with dispersoids (experimental result) and without dispersoids (modelling result). As shown in this figure, the contribution of dispersoids on the amount of work hardening increases with increasing strain. However, the dispersoids only provide a small contribution to the amount of work hardening. The contribution of solutes on the amount of work hardening is still predominant.
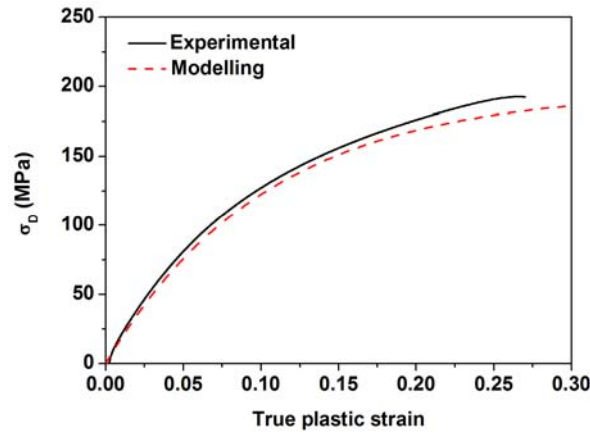
Fig. 4-30 The dependence of σ_D on the true plastic strain for alloy A4. The solid line presents experimental results, and the dashed line presents modelling results assuming the dispersoids do not have any influence on the work hardening behaviour.

To find out whether the dispersoids in the alloys have an influence on the work hardening (as suggested by the work hardening modelling), the microstructure of naturally aged alloy A2 after 2% tensile straining was characterised by TEM. As shown in Fig. 4-31, dispersoids do have an influence on the dislocation accumulation, although it appears this effect is weak.
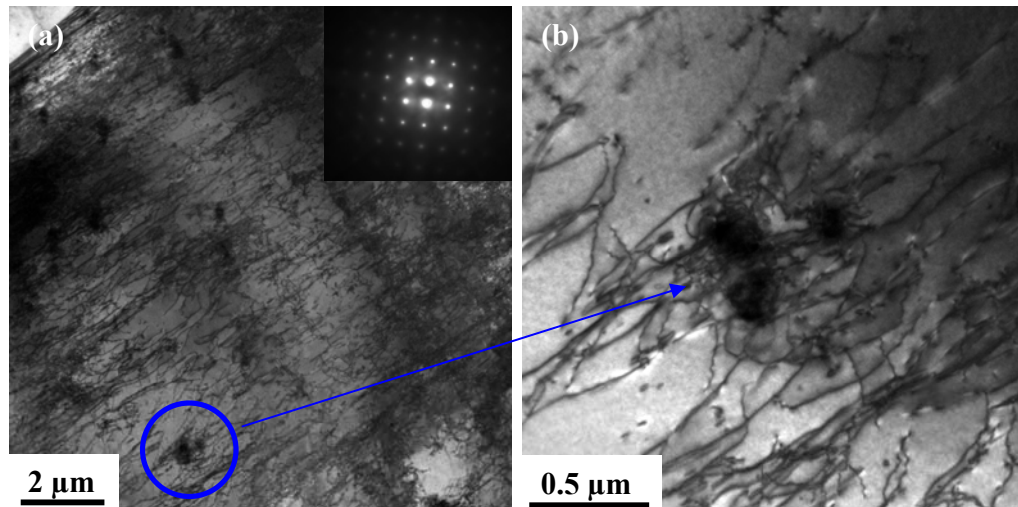
Fig. 4-31 (a) TEM image showing the interaction between dispersoids and dislocations in the alloy A2 deformed by 2% (b) enlarged view of (a). The alloy A2 was naturally aged for 1 week before deformation. The pictures were taken from [001] zone axis.

Dowling *et al* [54] reported that the volume fraction of Mn-containing dispersoids increases with increasing Mn content. However, in the present study, the Mn content in the different

alloys was the same; only the Mg and Si contents were different. This still results in a different number density of Al(Fe,Mn)Si dispersoids in the alloys (Fig. 4-2). Note that the volume fraction of coarse Mn-containing particles in all the alloys was similar, which may suggest that the amount of Mn trapped in them was nearly the same as well. Therefore, it is not the variation in volume fraction of coarse Mn-containing particles that causes different distributions of Mn-containing dispersoids. Gupta *et al* [130] found that increased Si content can promote the formation of β'' precipitates (precursors of Mg_2Si). The Si variation in the alloys studied may also have a similar influence on the formation of Al(Fe,Mn)Si dispersoids. Increased Si contents (from alloys A3 to A5) may increase the amount of Al(Fe,Mn)Si dispersoids due to more Si being available for the formation of dispersoids. On the other hand, the existence of undissolved coarse Mg_2Si particles in the high Mg content alloy A2 may reduce the amount of available Si for the formation of dispersoids. It is therefore not surprising that a more homogeneous distribution of dispersoids was observed in the high Si content alloys A4 and A5 than in the low Si content alloys A3 and A2. The influence of alloy composition on the amount of intermetallics will be modelled by thermodynamic modelling in the Chapter 7.

4.4 Summary

In this chapter, the effects of Si content, Mg content and Mg/Si ratio on the microstructure, tensile ductility and stretch formability were studied for five different 6xxx alloys designed with systematically varying Si and Mg contents. In particular, three among the five alloys studied had about the same total atomic percentage of Mg plus Si. It was found that the tensile ductility and stretch formability are affected by the microstructural features of the alloys. Not only does an increase in the Si content raise the work hardening capacity of an alloy due to a decrease in the dynamic recovery rate, but it also enhances strain rate hardening by facilitating the formation of clusters that remove mobile solute atoms and/or vacancies from the solid solution. Furthermore, by increasing the Si content of the alloy, the occurrence of a high number density of dispersoids is promoted, which increases the storage rate of geometrically necessary dislocations. Collectively, these effects act to improve the tensile ductility and stretch formability of sheet products manufactured from these alloys. By contrast, increasing the Mg content of the alloy has little influence on the tensile ductility and

stretch formability. For the same combined Mg and Si level, the alloy with lower Mg/Si ratio shows a greater tensile ductility and stretch formability than high Mg/Si ratio alloy. This is due to an increased strain rate sensitivity of the flow stress and an improved distribution of dispersoids in the high Si alloy. The present study also suggests that it is the work hardening and the strain rate hardening close to the onset of necking that matter for ductility and formability, rather than the overall values of these material characteristics. Furthermore, the deformed microstructures also reflect the difference in the mechanical characteristics between these alloys, namely, the materials with high strain rate sensitivity show a low tendency for deformation localisation.

Chapter 5: Formability of Pre-aged Al-Mg-Si Alloys

5.1 Introduction

Although the effect of artificial ageing on the stretch formability of 6xxx alloys has been studied [16, 99, 131] to some degree, relatively little attention has been paid to the influence of pre-ageing treatment on the stretch formability of 6xxx alloys [18].

In this chapter, five Cu-free alloys (A2-A6) were pre-aged at 100 ℃ for 2 h or at 200 ℃ for 20 s, followed by one week of natural ageing. The former pre-ageing treatment is suitable for batch treatment, while the latter is suitable for in-line treatment. To understand the influence of pre-ageing on the strain rate hardening behaviour of the alloys, high Mg content alloy A2 and high Si content alloy A4 were pre-aged at 100 ℃ or 200 ℃ for different times. The work hardening and strain rate hardening behaviour of the pre-aged alloys was used to understand the formability results. Furthermore, a model for the observed strain rate hardening behaviour of the pre-aged alloys was proposed.

5.2 Results

5.2.1 The influence of pre-ageing treatment parameters on the natural ageing and paint bake responses

5.2.1.1 Hardness

Effects of pre-ageing time at 100 ℃ on the hardness of alloys A2 and A4 are presented in Fig. 5-1. It can be seen that pre-ageing at 100 ℃ can significantly enhance the paint-bake response of the alloys, compared to the paint-bake response of the material without pre-ageing. The dependence of hardness on the pre-ageing time is quite similar between these two alloys. More precisely, the hardness, measured immediately after pre-ageing, increases with increasing pre-ageing time. The effect of pre-ageing on the natural ageing response was also studied. After one week of natural ageing, the hardness of pre-aged samples was observed to drop firstly, and then to increase gradually. The overall result is a decreased natural ageing response after pre-ageing with increasing pre-ageing time. Particularly, after pre-ageing for 2 h, there is almost no natural ageing response during further room

temperature storage. In other words, the material is very stable after pre-ageing in terms of hardness. Moreover, the paint-baked hardness always increases with increasing pre-ageing time, although after a long pre-ageing, the increment tends to saturate.
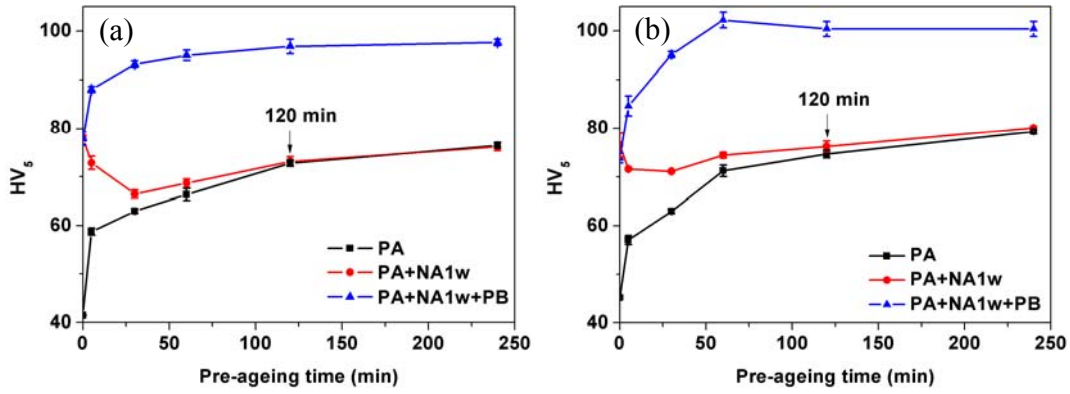
Fig. 5-1 Effect of pre-ageing time at 100 ºC on the hardness of alloys (a) A2 and (b) A4.

The influence of pre-ageing time at 200 ºC on the hardness of alloys A2 and A4 is quite similar to that observed at 100 ºC (cf. Fig. 5-1 and 5-2). However, pre-ageing at 200 ºC for 20 - 60 seconds cannot suppress the natural ageing response after pre-ageing, thus a limited improvement in the paint-bake response was observed, compared to the improvement obtained if the material was pre-aged at 100 ºC. Nevertheless, it appears pre-ageing at 200 ºC for 20 s provides a good combination of properties (i.e. a low hardness after natural ageing and high hardness after paint-bake treatment) compared to pre-ageing at 200 ºC for 40 s and 60 s.
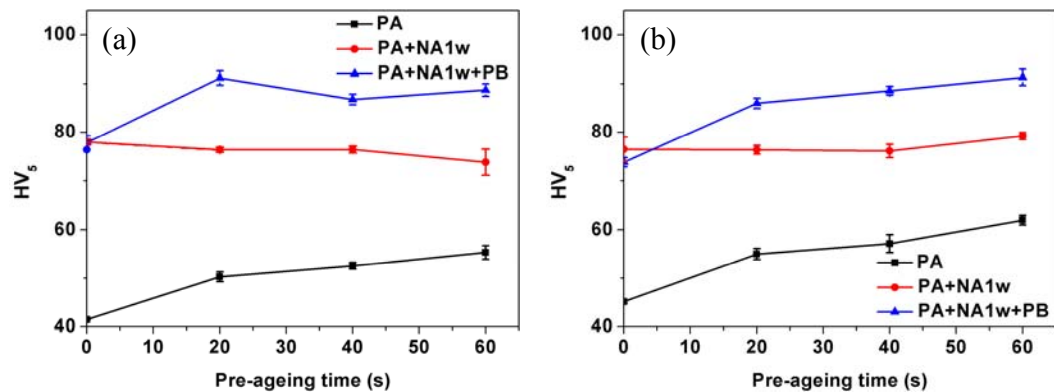
Fig. 5-2 Effect of pre-ageing time at 200 ºC on the hardness of alloys (a) A2 and (b) A4.

5.2.1.2 Tensile properties

The typical stress-strain curves for alloys A2 and A4 pre-aged at 100 ºC for different times are shown in Fig. 5-3. It can be seen that, with increasing pre-ageing time, the serrated yielding gradually disappears in both alloys due to the depletion of mobile solutes/vacancies from the supersaturated solid solution. The PLC effect was observed to disappear faster in the high Si content alloy A4 than in the high Mg content alloy A2.
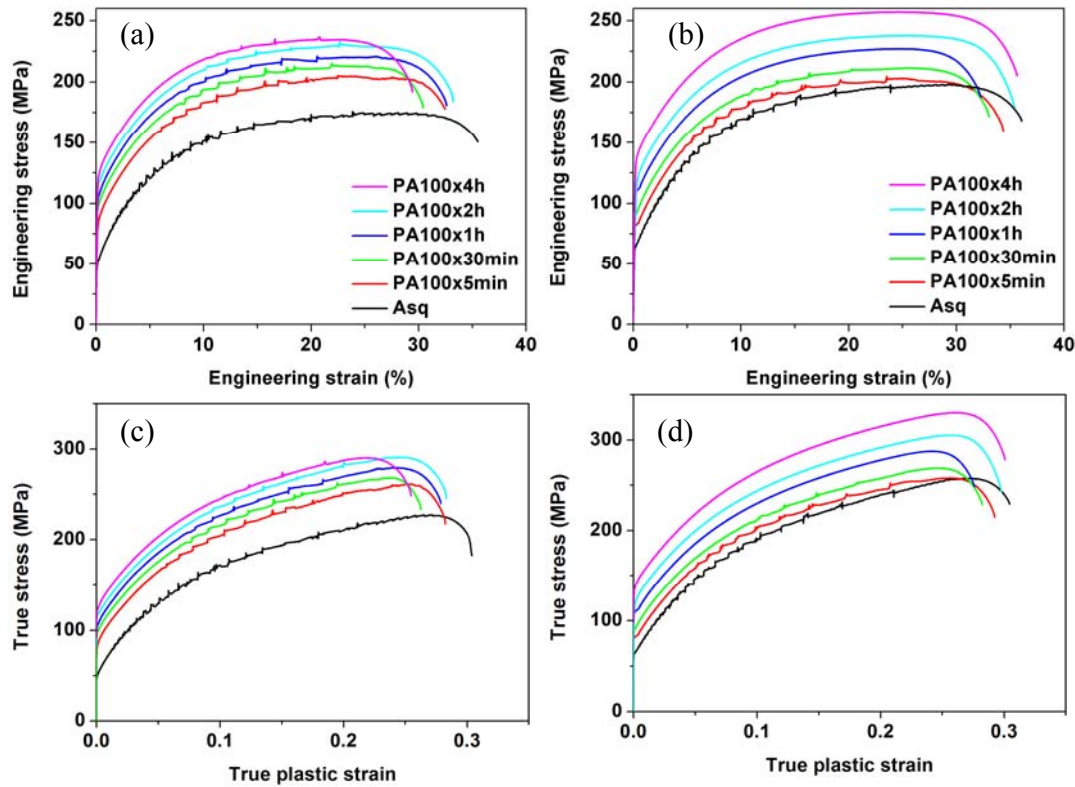
Fig. 5-3 Engineering stress-strain curves for alloys (a) A2 and (b) A4 aged at 100 ºC for different times, and corresponding true stress-plastic strain curves for alloys (c) A2 and (d) A4.

Upon one week of natural ageing after pre-ageing, it is interesting to observe that the serrated yielding can still be found in alloy A2, even if alloy A2 was pre-aged for 4 h at 100 ºC (Fig. 5-4). By contrast, the stress-strain curve for as-quenched alloy A2 after one week of natural ageing is smooth. Similarly, the stress-strain curves for pre-aged alloy A4 are smooth after one week of natural ageing, as shown in Fig. 5-5. The serrated yielding in the pre-aged alloy A2 suggests a more negative SRS than that for the naturally aged material without pre-ageing,

as shown in Fig. 5-6a. Pre-ageing also decreases the SRS of the flow stress in the alloy A4 (Fig. 5-6b), although this decrease in the SRS is not sufficient to promote the occurrence of serrated yielding. Fig. 5-7 shows tensile property results for pre-aged alloys A2 and A4 after one week of natural ageing, together with mechanical properties of as-quenched alloys after one week of natural ageing. As shown in Fig. 5-7, the dependence of the yield and tensile strength on the pre-ageing time is quite similar, i.e., with increasing pre-ageing time, the strength firstly decreases and then increases. For the tensile ductility, there is little variation in uniform elongation and total elongation with respect to pre-ageing time.
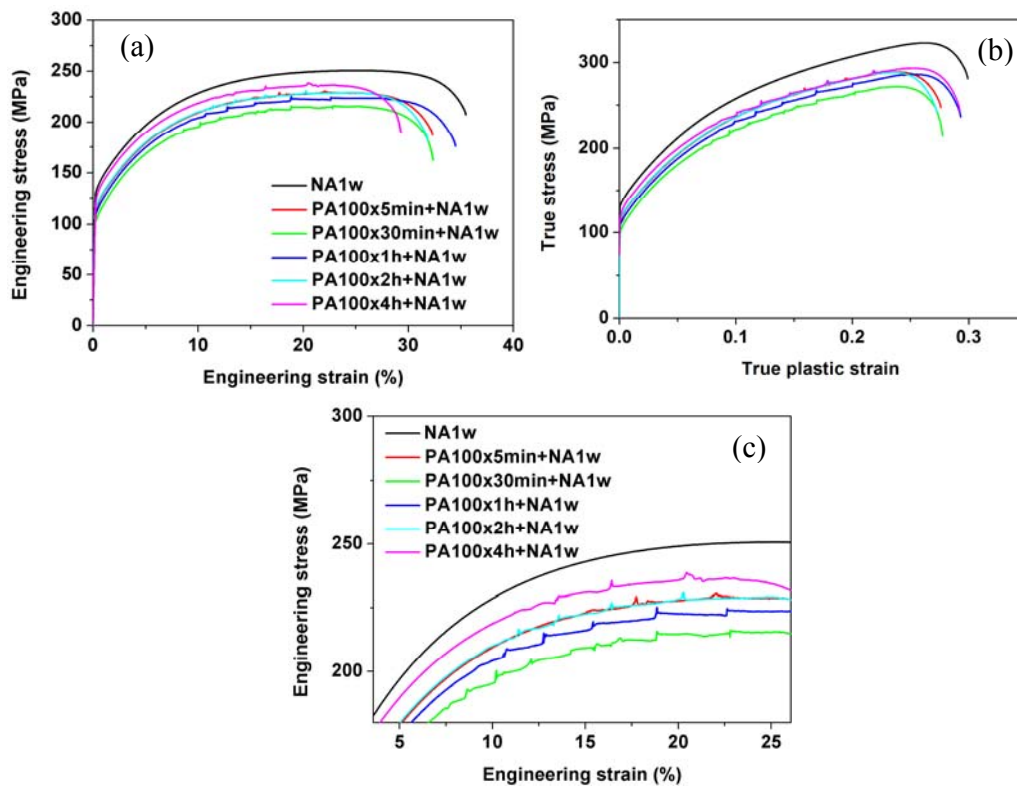
Fig. 5-4 (a) Engineering and (b) true stress-strain curves for alloy A2 (c) enlarged view of (a).
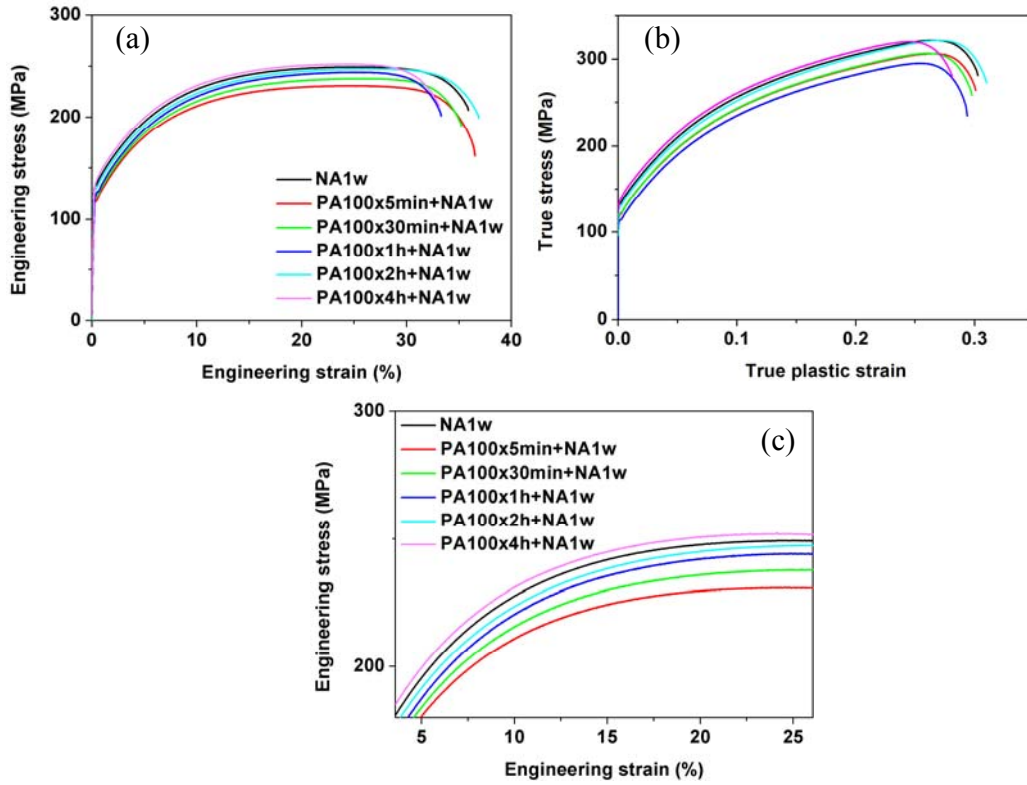
Fig. 5-5 (a) Engineering and (b) true stress-strain curves for alloy A2 (c) enlarged view of (a).
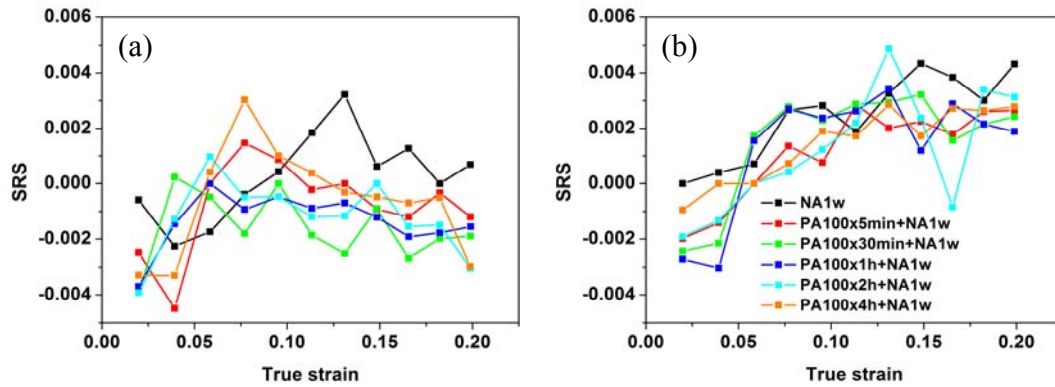
Fig. 5-6 Dependence of the SRS of the flow stress on the true strain in (a) alloys A2 and (b) A4.
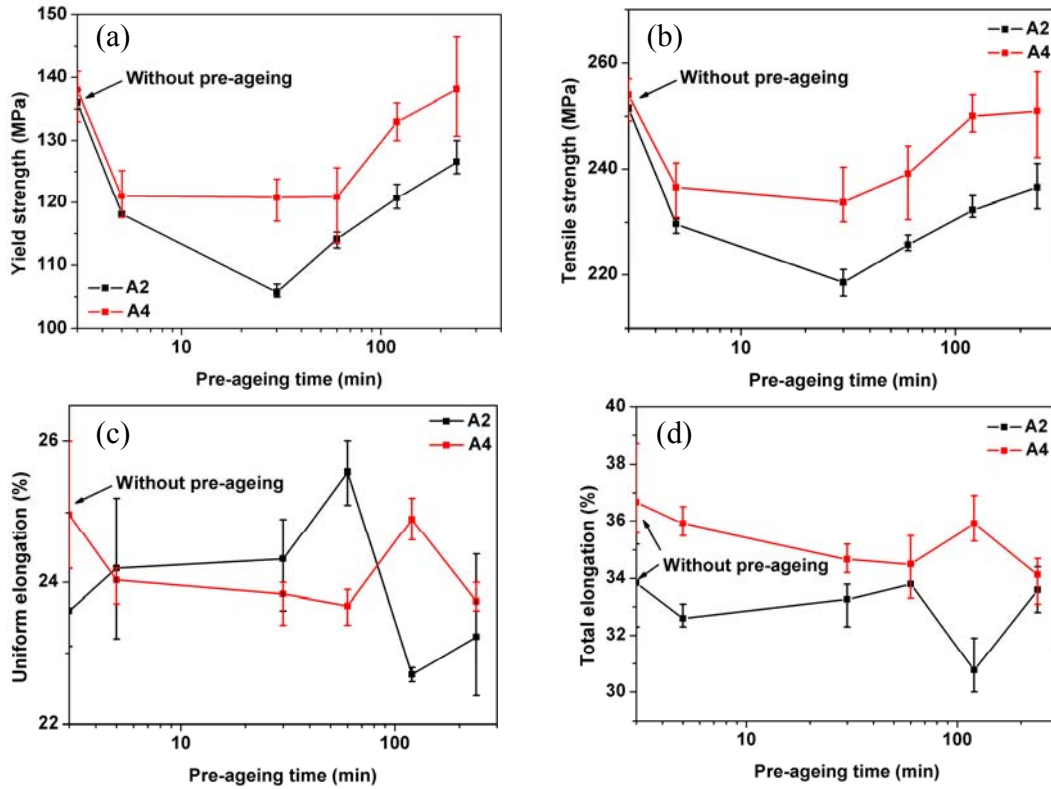
Fig. 5-7 Mechanical properties of alloys A2 and A4 pre-aged at 100 ºC. The pre-aged samples were further naturally aged for one week before tensile testing.

Fig. 5-8 shows the stress-strain curves for alloys A2 pre-aged at 200 ºC for different times. As shown in Fig. 5-8, with increasing pre-ageing time, the PLC effect becomes more significant in pre-aged alloy A2 after one week of natural ageing. By contrast, no PLC effect was observed in alloy A4, as shown in Fig. 5-9. This trend is similar to that observed in the samples pre-aged at 100 ºC. Fig. 5-10 shows the SRS of pre-aged alloys A2 and A4 after one week of natural ageing. A decreased SRS of the flow stress can be found in both alloys with increasing pre-ageing time. As for the tensile properties, as shown in Fig. 5-11, it is evident that, with increasing pre-ageing time at 200 ºC, both the tensile strength and the ductility decrease.
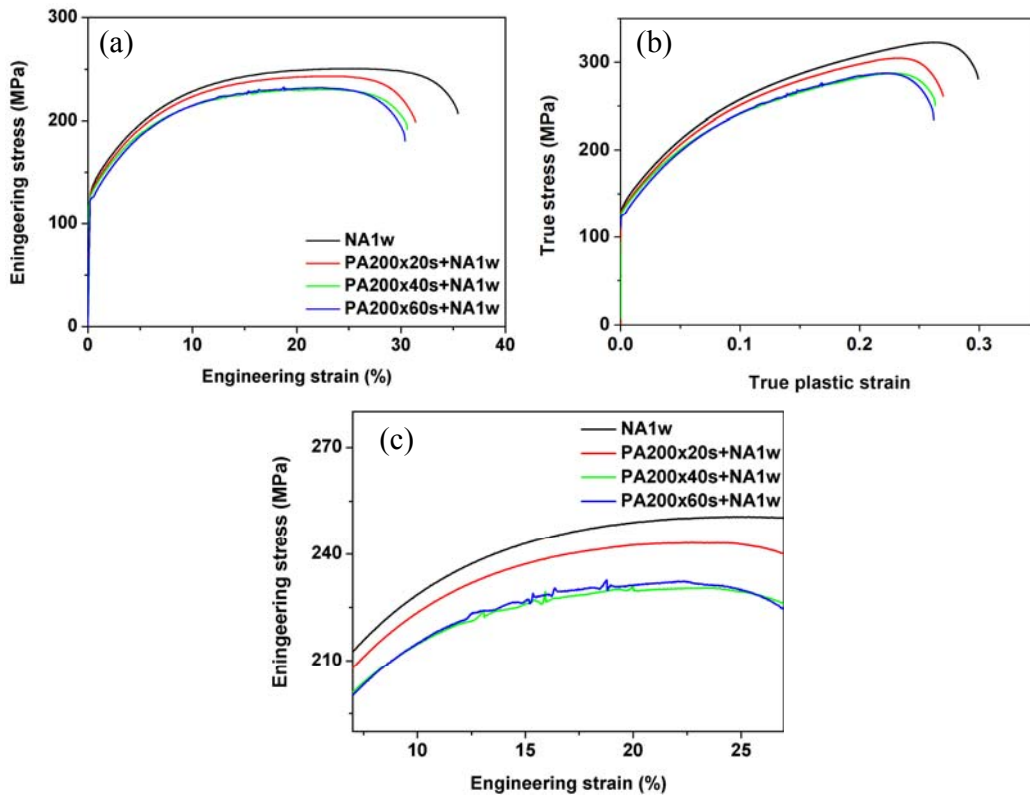
Fig. 5-8 (a) Engineering and (b) true stress-strain curves for alloy A2 pre-aged at 200 ºC, and (c) enlarged view of (a).
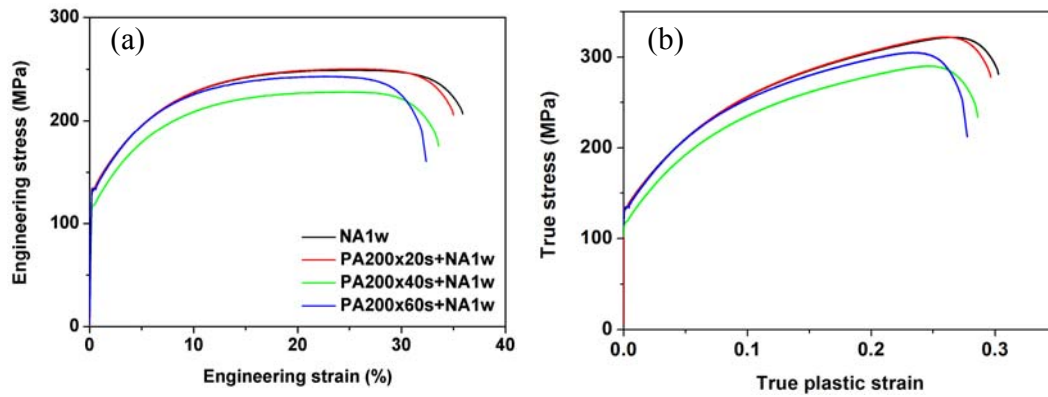
Fig. 5-9 (a) Engineering and (b) true stress-strain curves for alloy A4 pre-aged at 200 ºC
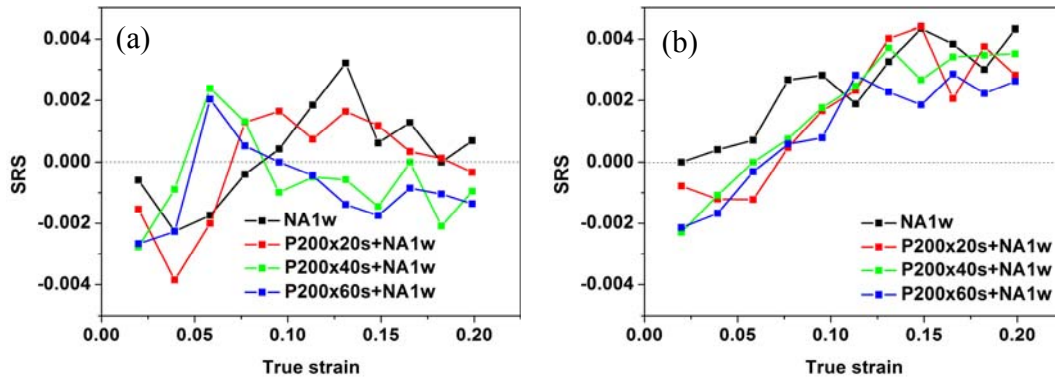
Fig. 5-10 Dependence of the SRS of the flow stress on the true strain in (a) alloys A2 and (b) A4 pre-aged at 200 ºC.
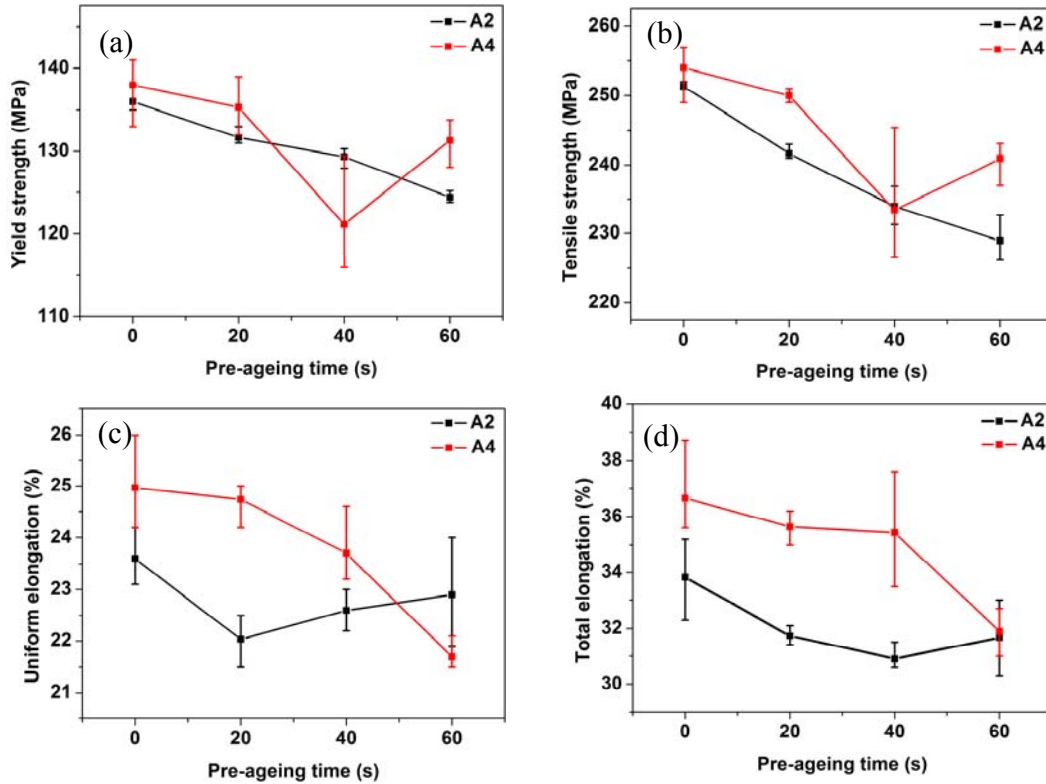
Fig. 5-11 Effect of pre-ageing time at 200 ºC on the mechanical properties of alloy A2 after one week of natural ageing.

5.2.2 The hardness and tensile properties of different pre-aged alloys

As shown in Fig. 5-12, a pre-ageing treatment can significantly inhibit the natural ageing process and improve the paint bake response of the materials, compared to the materials that

did not undergo a pre-ageing treatment. Pre-ageing at 100 ºC is more efficient in promoting a good paint bake response than pre-ageing at 200 ºC. The tensile properties after different heat treatments are shown in Fig. 5-13. As shown in Fig. 5-13, similarly to the hardness results, pre-ageing was found to reduce the strength of the materials after natural ageing. As for the tensile ductility, in most cases, pre-ageing was found to reduce the uniform and total elongation or to have little influence on these quantities. However, for alloy A3, it is interesting to observe that pre-ageing at 100 ºC for 2h can improve the tensile ductility.
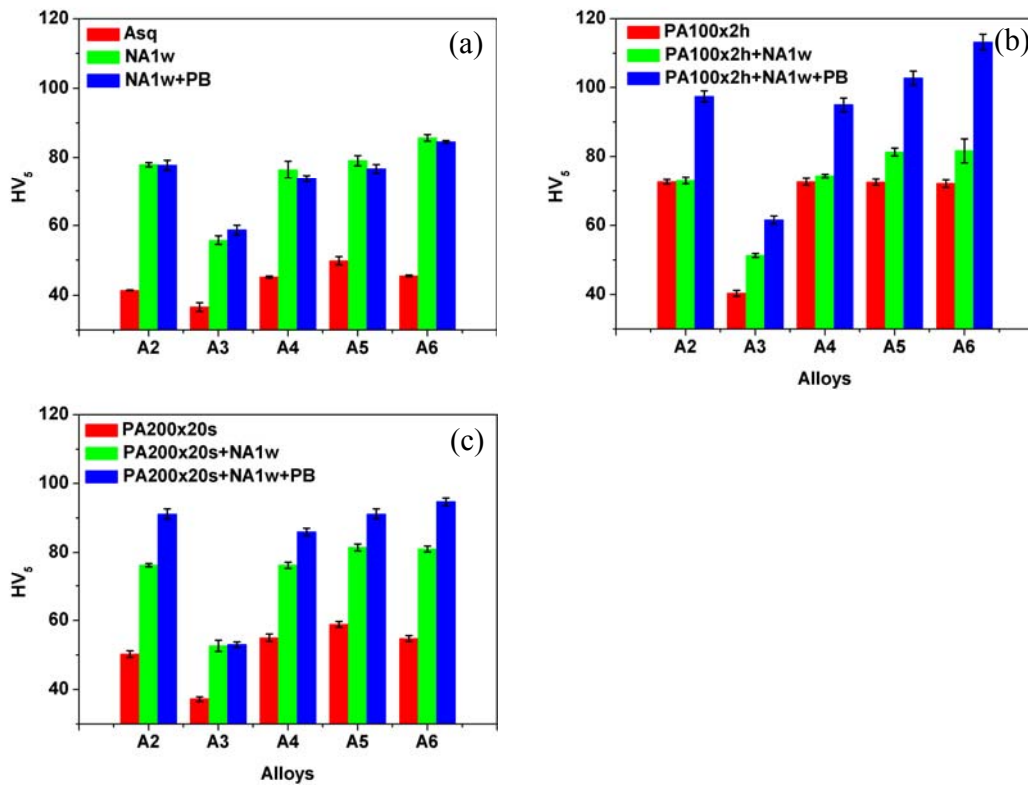
Fig. 5-12 Effect of heat treatment on the hardness of the alloys
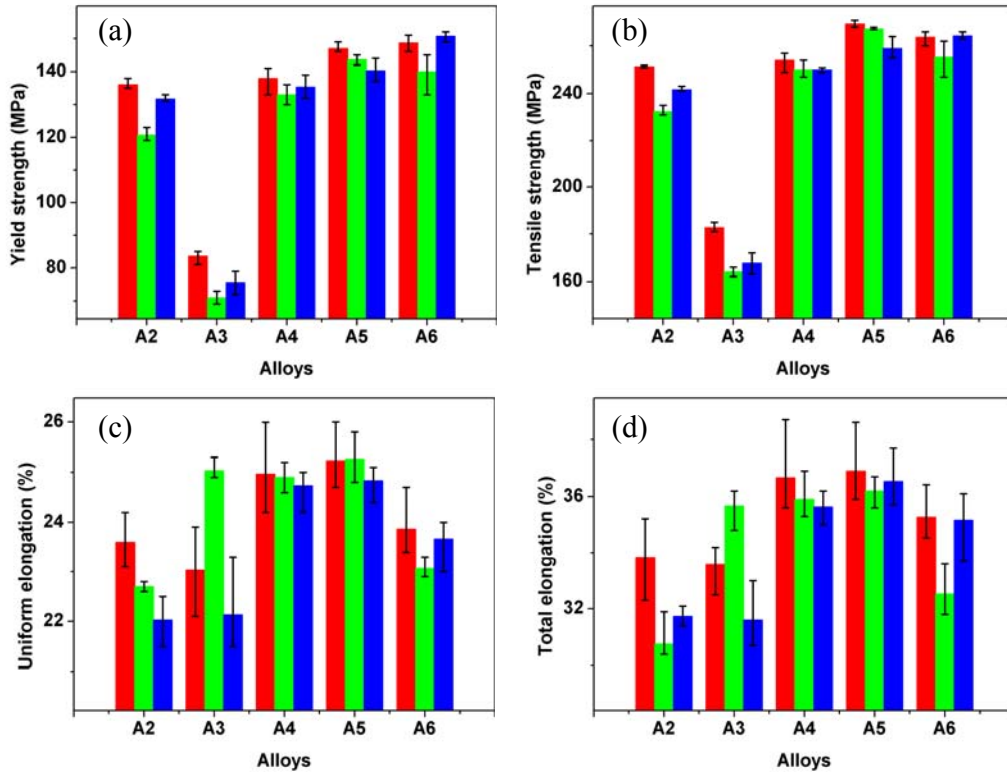
Fig. 5-13 Mechanical properties of the alloys in different tempers

NA1w   PA100x2h+NA1w   PA200x20s+NA1w

5.2.3 Effect of pre-ageing on the stretch formability

Effects of heat treatment on the right hand side of FLD of the alloys are shown in Fig. 5-14. Pre-ageing was found to reduce FLD_0 for all the materials tested, except for alloy A3, as shown in Fig. 5-15. In alloy A3, pre-ageing has little influence on FLD_0. The decrease in FLD_0 is more significant in the alloys pre-aged at 100 ºC for 2 h than in the alloys pre-aged at 200 ºC for 20 s. It is also more pronounced in the excess Si alloys A4 and A5.
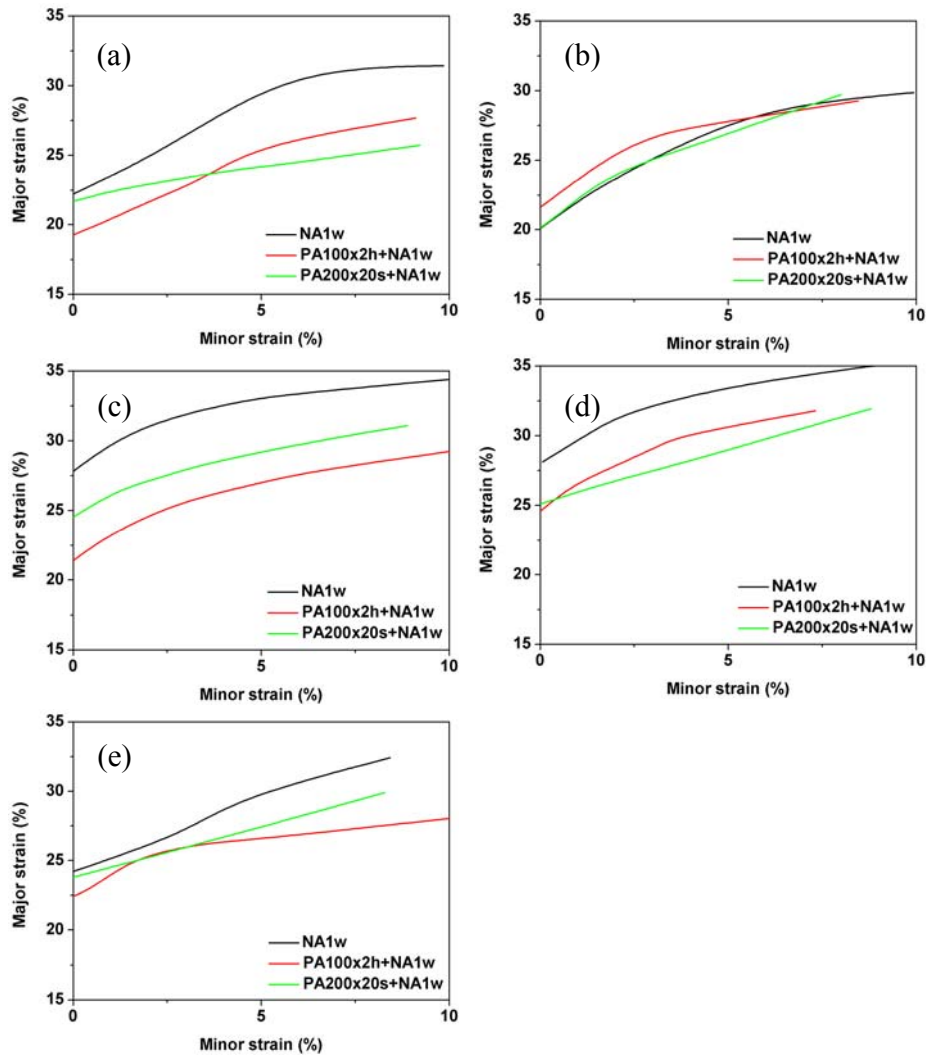
Fig. 5-14 Effect of heat treatment on the right hand side of FLDs for alloys (a) A2, (b) A3, (c) A4, (d) A5 and (e) A6
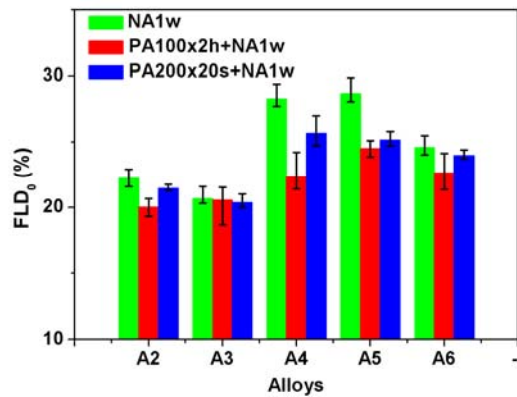
Fig. 5-15 Effect of heat treatment on FLD0 for different alloys

5.3 Discussion

5.3.1 Strain rate hardening behaviour

A decrease in the SRS of the flow stress was seen in pre-aged alloys A2 and A4 after one week of natural ageing, compared to that of the as-quenched alloys after one week of natural ageing. Actually, this phenomenon was also observed in the other three Cu-free alloys, as shown in Fig. 5-16. In particular, the PLC effect, which is a manifestation of negative SRS, was also observed in the pre-aged alloy A3. Table 5-1 summarises the observation of the PLC effect in these five alloys. It can be seen that after pre-ageing the low Si content alloys A2 and A3 were more prone to the PLC effect. These two alloys with sluggish natural ageing kinetics showed the occurrence of DSA after one week of natural ageing if they were not pre-aged before natural ageing, as shown in Fig. 4-24b. It appears pre-ageing promoted the development of DSA, and finally led to the occurrence of serrated yielding (the PLC effect) in these two alloys.

Table 5-1 The observation of serrated yielding in the alloys in the different conditions.

Alloys	NA1w	PA100x2h+NA1w	PA200x20s+NA1w
A2	-	+	-
A3	-	+	+
A4	-	-	-
A5	-	-	-
A6	-	-	-

Note: The "-" sign shows that no serrated yielding was observed, while "+" sign indicates the occurrence of serrations.
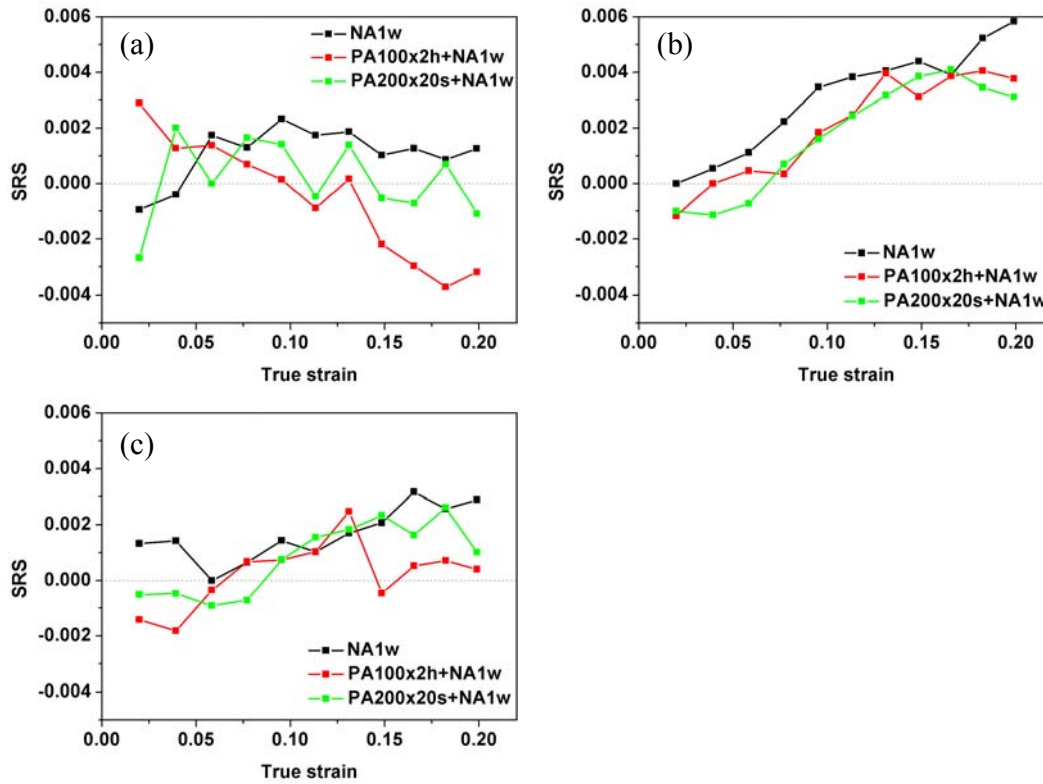
Fig. 5-16 The SRS of the flow stress of alloys (a) A3, (b) A5 and (c) A6

A decrease in the SRS of the flow stress in the pre-aged samples with a further one week of natural ageing can be unexpected, since pre-ageing is supposed to deplete the solute and vacancy concentration in the matrix. Therefore, the serrated yielding was observed to gradually disappear with prolonged pre-ageing (as shown in Fig. 5-3 and in Reference [132]), and the SRS of the flow stress of the pre-aged alloys was observed to be higher than that of as-quenched samples [77]. After one week of natural ageing, the SRS of pre-aged alloys was expected to be still higher than that of the naturally aged alloys without pre-ageing. However, the trend is opposite, which suggests that natural ageing after pre-ageing may have different influences on the SRS of pre-aged samples and the samples without pre-ageing. Furthermore, two factors can influence the SRS of the flow stress, namely, dislocation strengthening and dynamic strain ageing. Dislocation strengthening (e.g. through the mechanism of cutting of forest junctions) is expected to give a positive contribution to the SRS, while DSA is believed to give a negative contribution to the SRS [133]. Therefore, the decreased SRS in pre-aged alloys may be caused by either reduced dislocation strengthening or increased DSA.

However, a detailed study showed that pre-ageing has little influence on the dislocation strengthening (the difference between the flow stress and the yield strength) at a strain of 0.02, as shown in Fig. 5-17. Therefore, the decreased SRS after pre-ageing should be caused by the increased DSA contribution. It should be noted that the SRS at a strain of 0.02 was chosen because the difference in the SRS at a strain of 0.02 is significant across different tempers. Furthermore, the increased DSA can be caused by the interaction between mobile dislocations and diffusing solutes (i.e. classic DSA) or the repeated shearing of shearable clusters/precipitates (i.e. pseudo PLC) [71].
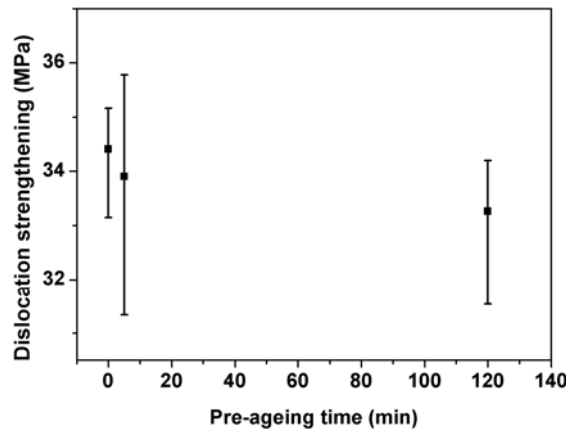
Fig. 5-17 Effect of pre-ageing time on dislocation strengthening at a strain of 0.02 in pre-aged alloy A4 after one week of natural ageing.

Therefore, two possible mechanisms may account for the increased DSA and observed PLC effect:

● After one week of natural ageing, pre-aged samples may contain more solute/vacancies than sample without pre-ageing, which causes the increased DSA (Mechanism I). This mechanism implies that natural ageing process should be faster in pre-aged samples than in samples without pre-ageing, if pre-aged samples are further naturally aged after one week of natural ageing, since, after one week of natural ageing, pre-aged samples contain more solutes/vacancies than samples without pre-ageing. Moreover, longer natural ageing (i.e. 1 month of natural ageing) after pre-ageing should increase the SRS of the flow stress due to further removal of solute/vacancies from the matrix and the ensuing reduction of the DSA contribution to stress. It should be noted that, after one month of

natural ageing, most of solutes (~ 80%) are expected to be still retained in the matrix of the samples with/without pre-ageing [134]. This may suggest, for a specific alloy and for the conditions tested, solute concentration in the matrix may be not so critical for the DSA. Thus the importance of vacancies for the DSA can be highlighted.

● Alternatively, after one week of natural ageing pre-aged samples may contain more clusters/precipitates than samples without pre-ageing. The repeated shearing of these shearable clusters/precipitates by gliding dislocations may give rise to the serrated yielding (Mechanism II).

In order to test Mechanism I, alloys A2 and A4 were naturally aged for either one week or one month after pre-ageing. As shown in Fig. 5-18, although the natural ageing effect was retarded during one week of natural ageing after pre-ageing, it was more significant in the pre-aged samples during one week to one month of natural ageing if the samples were pre-aged at 100 ºC for less than 2 h. However, it is interesting to see that the natural ageing response during one week to one month of natural ageing is almost the same for the samples pre-aged for more than 2 h as for the samples without pre-ageing. These results appear to support Mechanism I for the decrease in the SRS in the pre-aged alloys after one week of natural ageing, especially when samples were pre-aged for a short time (i.e. less than 2 h at 100 ºC). For longer pre-ageing time, Mechanism I may be still valid or the other mechanism (Mechanism II) may become predominant. Furthermore, the hardness results in Fig. 5-18 suggest that one month of natural ageing has a more significant influence on the SRS of the flow stress of the samples pre-aged for a short time (eg 5 min) than of the alloys pre-aged for a long time (eg 2 h). In fact, after one month of natural ageing, the PLC effect disappeared in alloy A2 samples that were pre-aged for 5 min. By contrast, the PLC effect was still observed in alloy A2 pre-aged for 5 min after one week of natural ageing, as shown in Fig. 5-19. It should be noted, however, that one month of natural ageing did not have any significant effect on the PLC effect observed in alloy A2 pre-aged for 2 h, although it appears the onset strain for the PLC effect increased slightly with increasing natural ageing time, as shown in Fig. 5-20. The improvement (that is, an increment) in the SRS (i.e. the SRS at a strain of 0.02) by longer natural ageing was more significant in samples pre-aged for 5 min than in samples pre-aged for 2 h, as shown in Fig. 5-21. (It should be noted that due to the serrated yielding,

the uncertainty for the SRS determination becomes large. Therefore, the SRS results from three tests are presented in Fig. 5-21.) As for alloy A4, no PLC effect was observed in the pre-aged samples after one week or one month of natural ageing, Figs. 5-22 and 5-23. However, an increase in the SRS of the flow stress can be seen in the pre-aged alloy A4 when the samples were naturally aged from one week to one month after pre-ageing, as shown in Fig. 5-24. An enhancement of the SRS by longer natural ageing was also observed in the alloys pre-aged at 200 ℃ for 20 s, see Fig. 5-25. Moreover, even after one month of natural ageing, the SRS of pre-aged samples was still lower than that of samples without pre-ageing. These results further suggest that the decrease in the SRS in the pre-aged alloys after natural ageing should be caused by Mechanism I if samples were pre-aged for a short time (i.e. less than 2 h at 100 ℃ or 200 ℃ for 20 s).
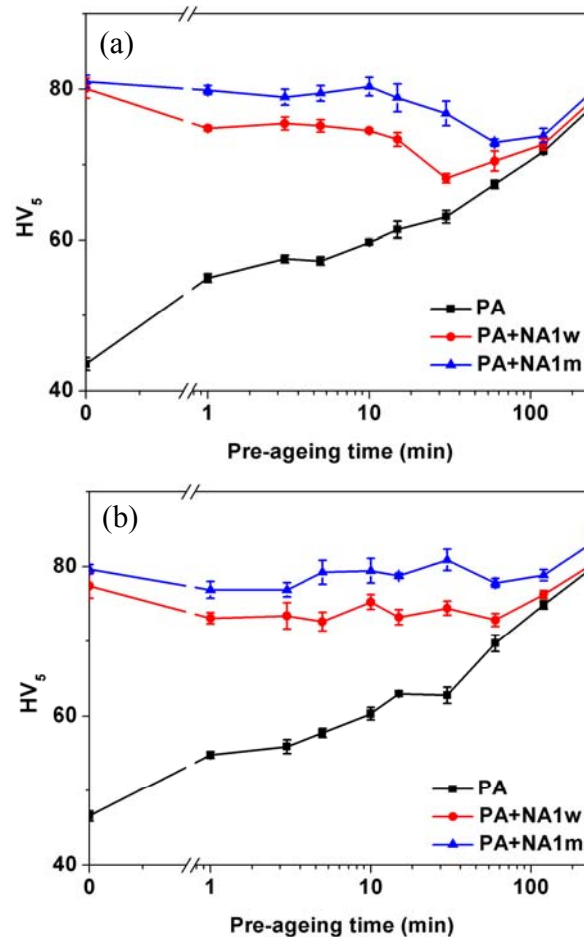
Fig. 5-18 Effect of pre-ageing and natural ageing on the hardness of alloys (a) A2 and (b) A4.
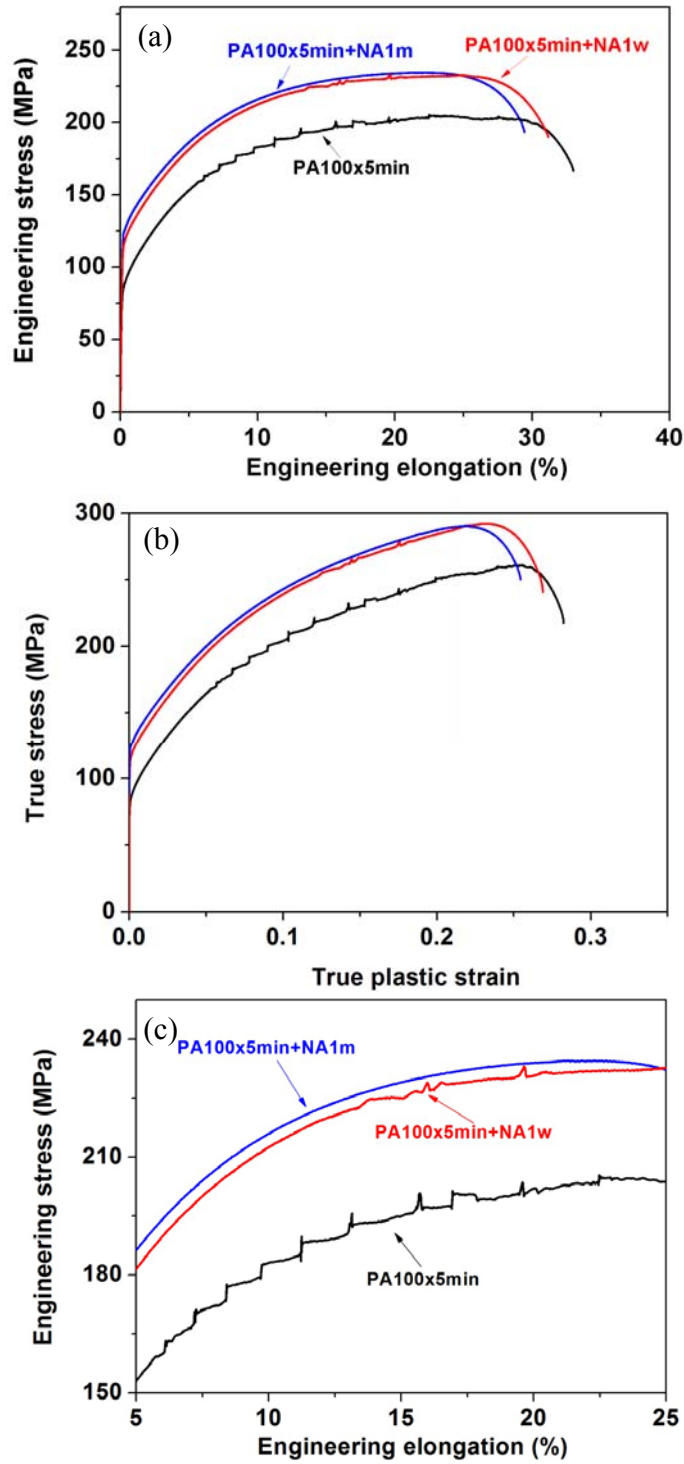
Fig. 5-19 Effect of natural ageing on the (a) engineering and (b) true stress-strain curves of alloy A2 pre-aged at 100 ºC for 5 min and (c) enlarged view of a segment of the diagram shown in (a).
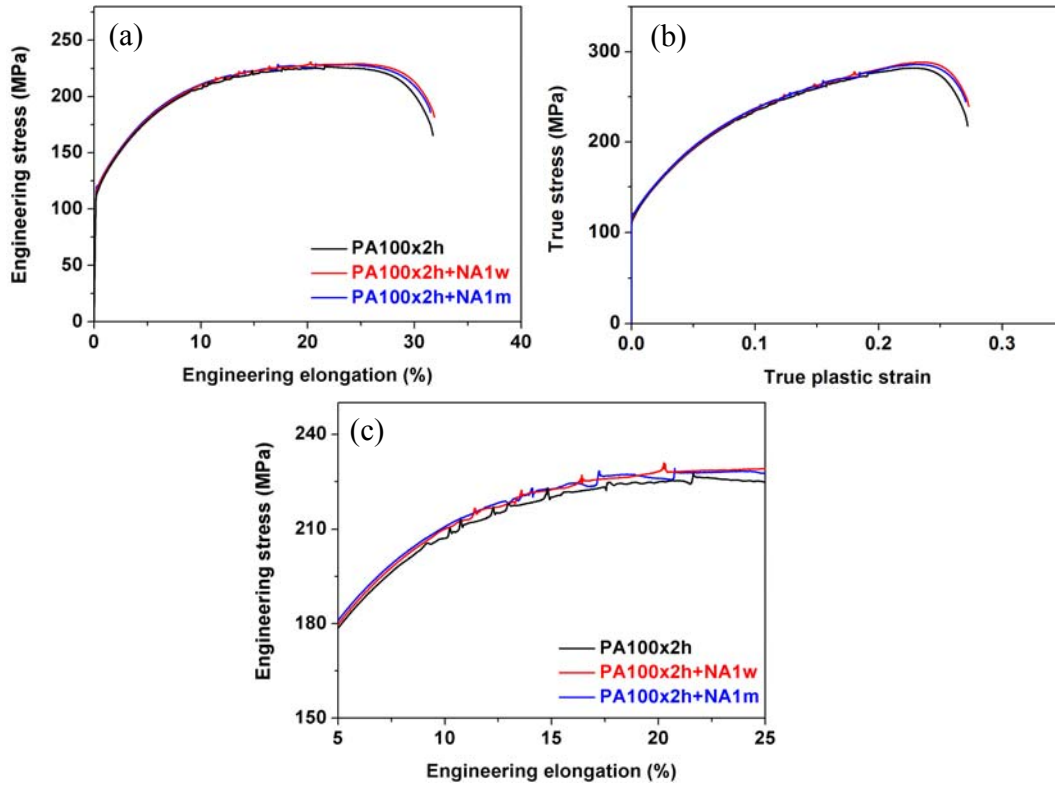
Fig. 5-20 Effect of natural ageing on the (a) engineering and (b) true stress-strain curves of alloy A2 pre-aged at 100 ºC for 2 h, and (c) enlarged view of a segment of the diagram shown in (a).
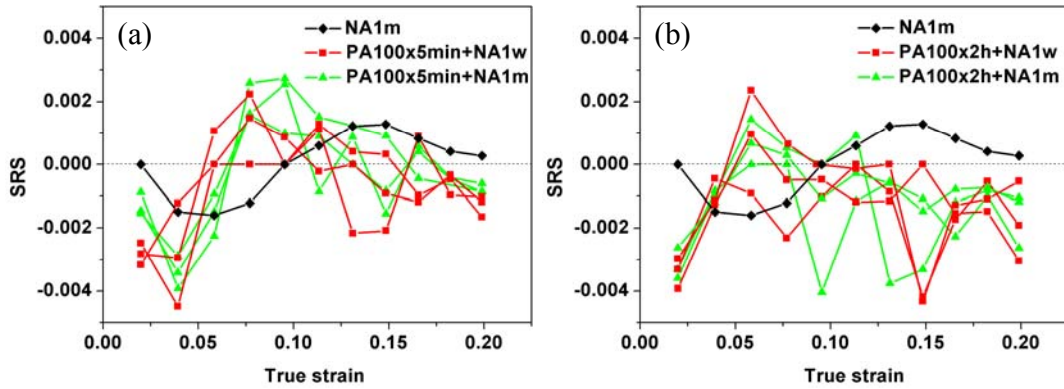
Fig. 5-21 Effect of natural ageing on the SRS of flow stress of alloy A2 pre-aged at 100 ºC for (a) 5 min and (b) 2 h.
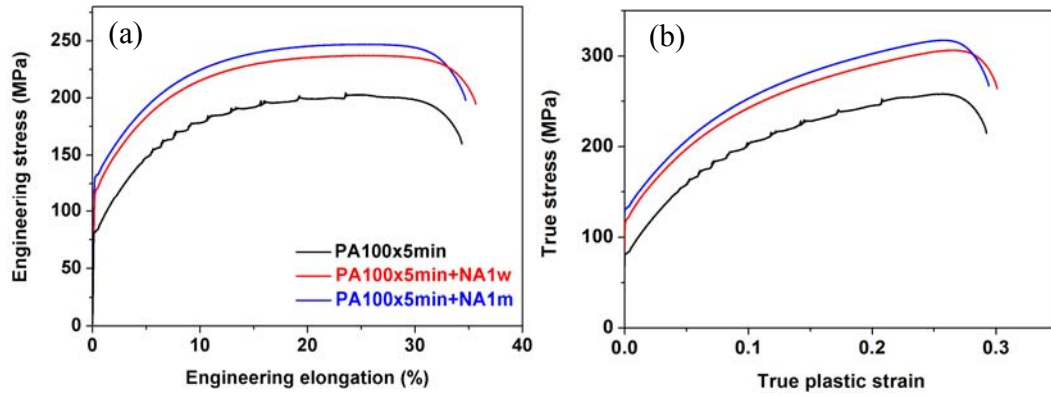
Fig. 5-22 Effect of natural ageing on the (a) engineering and (b) true stress-strain curves of alloy A4 pre-aged at 100 ºC for 5 min.
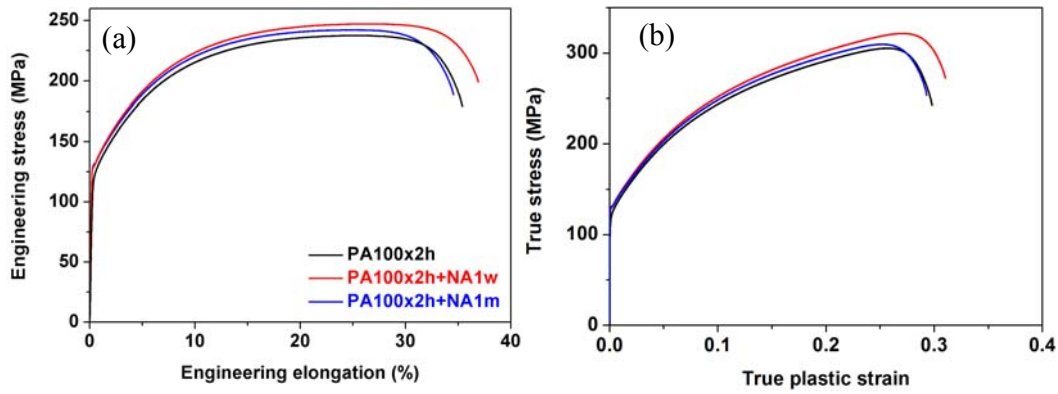
Fig. 5-23 Effect of natural ageing on the (a) engineering and (b) true stress-strain curves of alloy A4 pre-aged at 100 ºC for 2 h and.
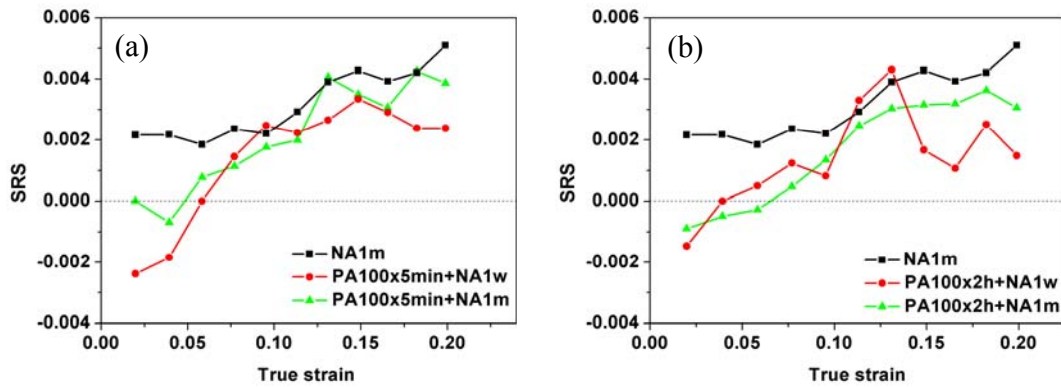
Fig. 5-24 Effect of natural ageing on the SRS of flow stress of pre-aged alloy A4.
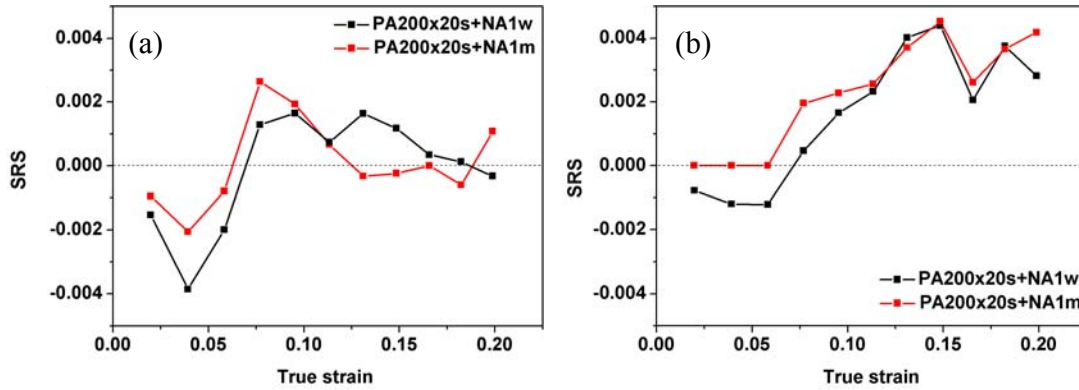
Fig. 5-25 Effect of natural ageing on the SRS of the flow stress of pre-aged alloys (a) A2 and (b) A4.

For longer pre-ageing time (i.e. not less than 2h at 100 ºC), Mechanism I may be still operating, provided excess vacancies are trapped in clusters. Those trapped-in excess vacancies would not contribute to the natural ageing process after pre-ageing regardless of the duration of natural ageing after pre-ageing. However, those excess vacancies can contribute to the development of DSA if vacancy-containing clusters are sheared by mobile dislocations, and vacancies are released from clusters to the matrix. In addition, Mechanism II may also be operating, although 3DAP results for the alloys A2 and A4 suggested that pre-aged samples (i.e. 2h at 100 ºC) do not necessarily contain more clusters than samples without pre-ageing [134]. However, considering the increased volume faction of cluster/precipitates with increasing pre-ageing time (i.e. 4h at 100 ºC), Mechanism II may also be operating.

For Mechanism I, why, after one week of natural ageing, pre-aged samples would contain more vacancies than samples without pre-ageing? To explain this, it is useful to consider the natural ageing behaviors of these alloys when there is no pre-ageing involved (i.e. the natural ageing process after quenching from solution treatment temperature). Several points can be put forward on the natural ageing behavior of these alloys:

- The PLC effect can be observed remarkably in as-quenched samples. With the natural ageing proceeds, the PLC effect gradually disappears due to the depletion of solutes/vacancies in the matrix. The depletion of vacancies is particularly important to the occurrence of PLC effect, since based on 3DAP results most of solutes (around 80%) was still retained in the matrix after one month of natural ageing [134];

- If natural ageing process after quenching is sluggish (or suppressed), then it would take more time for the disappearance of the PLC effect. For instance, alloy A3 with a sluggish natural ageing process showed the PLC effect after one day of natural ageing. By contrast, alloy A2 with a slightly faster natural ageing process did not show the PLC effect after one day of natural ageing (see Table 4-4). Note that alloy A3 is a low Mg content alloy, and alloy A2 is a high Mg content alloy. One would expect the PLC effect to be more significant in alloy A2 than in alloy A3.

- The sluggish natural ageing process can also be realised by low solution treatment temperature (i.e. 500 ºC other than 550 ºC). If samples were solution treated at 500 ºC, then the natural ageing process was more sluggish than that treated at 550 ºC (see Fig. 4-9). It would take more time for the PLC effect to disappear, so that, after one week of natural ageing, the PLC effect can be still observed in sample solution treated at 500 ºC (see Fig. 4-10). By contrast, no PLC effect was observed in sample solution treated at 550 ºC.

Based on the above experimental findings, the natural ageing process can be considered as a process of formation of clusters and removal of vacancies from the matrix. If the natural ageing process after quenching is suppressed (or sluggish), then both formation of clusters and removal of vacancies are expected to be suppressed. This may suggest samples have to be naturally aged longer time to remove the vacancies from the matrix. This probably explains why the alloys/samples with a sluggish natural ageing showed the PLC effect, while those with a fast natural ageing did not show the PLC effect after a certain natural ageing time.

Now the situation in the pre-aged alloys will be considered. In the pre-aged samples, the subsequent natural ageing process after pre-ageing is suppressed, compared to sample without pre-ageing. The PLC effect still gradually disappeared with natural ageing prolonging (see Fig. 5-19). However, due to the suppressed or sluggish natural ageing process, after one week of natural ageing, the PLC effect can still be observed in the pre-aged alloys. By contrast, no PLC effect was observed in the sample naturally aged for one week after quenching from solution treatment temperature. Therefore, the decreased SRS and

observed PLC effect in the pre-aged samples are believed to be caused by suppressed natural ageing process which delays the removal of vacancies from the matrix, thus retaining more vacancies after one week of natural ageing than in samples without pre-ageing. Those excess vacancies are expected to promote the development of DSA, and finally lead to the decreased SRS and the PLC effect. Also those excess vacancies can enhance the natural ageing process, thus a higher natural ageing response can be observed in the pre-aged samples than in samples without pre-ageing, if pre-aged samples were further naturally aged for one month after one week of natural ageing. It should be noted that those excess vacancies should exist as vacancy-solute complexes rather than quenched in vacancies [135]. This is the case when samples were pre-aged for a short time (i.e. 5 min or less than 2 h) at 100 ºC. If samples were pre-aged for a long time (i.e. more than 2 h), Mechanism I may still be operating provided excess vacancies are trapped in clusters. Therefore, there is no significant natural ageing response after pre-ageing regardless of the duration of natural ageing. The shearing of vacancy-containing clusters during deformation would release excess vacancies, and thus promote the DSA, which in turn, would lead to a decrease in the SRS and the occurrence of PLC effect.

Moreover, Mechanism I implies that as the natural ageing response decreases, the amount of DSA should be increase (due to more vacancies retained after one week of natural ageing), and consequently the SRS should become more negative. (Presuming, Mechanism I is operating regardless of pre-ageing time.) Here, natural ageing response is used to represent the degree of suppression of natural ageing process. A low natural ageing response means natural ageing process is efficiently suppressed. In order to better understand Mechanism I, the dependence of natural ageing response and the SRS at a strain of 0.02 on the pre-ageing time of alloys A2 and A4 after one week of natural ageing was studied, as shown in Fig. 5-26. It should be noted that the SRS at a strain of 0.02 was chosen to represent the degree of DSA, since at small strain the contribution of dislocation strengthening is assumed to be very small. As shown in Fig. 5-26, with increasing pre-ageing time, the natural ageing response decreases and the SRS tends to become more negative. The SRS reached its minimum value when the alloys were pre-aged for 1 h and the natural ageing response was ~ 3 HV_5. In this stage (Stage I), since a natural ageing response after pre-ageing can still be observed, the vacancy concentration after one week of natural ageing is therefore determined by the pre-

ageing and subsequent natural ageing, especially the latter. Although the sample after pre-ageing for a short time (i.e. 5 min at 100 ºC) is expected to have a higher vacancy concentration immediately after pre-ageing than the sample pre-aged for a longer time (i.e. 60 min at 100 ºC), a smaller natural ageing response in the latter sample would delay the removal of vacancies and retain a higher vacancy concentration after one week of natural ageing than in the former alloys with a larger natural ageing response. This high vacancy concentration could promote the DSA. Therefore, the former sample exhibited a higher SRS than the latter one. After Stage I, a re-increase in the SRS was observed with increasing pre-ageing time. In this stage (Stage II), the natural ageing response is almost zero. The annihilation of vacancies during natural ageing after pre-ageing is more effectively retarded in Stage II than in Stage I. Therefore, the vacancy concentration after one week of natural ageing is mainly determined by pre-ageing time. Consequently, it is not surprising that in Stage II, the SRS after one week of natural ageing increases with increasing pre-ageing time since the vacancy concentration gradually decreases during pre-ageing.
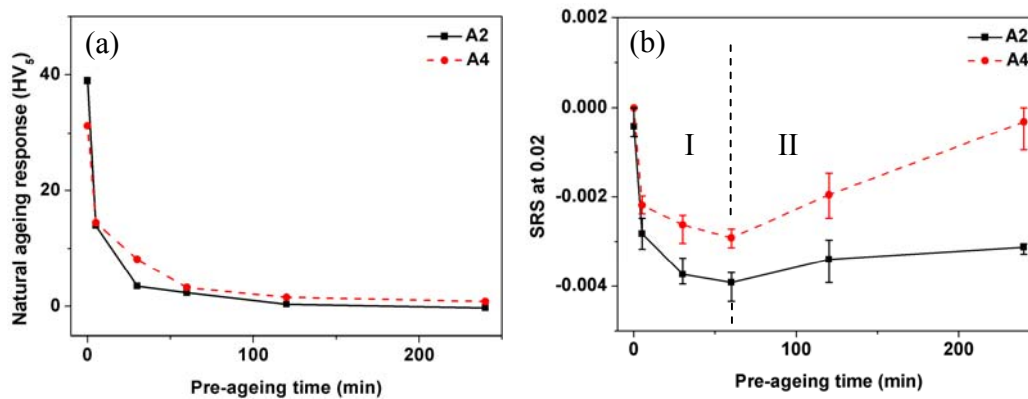
Fig. 5-26 Effect of pre-ageing time (at 100 ºC) on (a) the natural ageing response (after one week of natural ageing) and (b) the SRS at a strain of 0.02 for alloys A2 and A4 with further one week of natural ageing after pre-ageing treatment.

Finally, Mechanism I is summarised as follows: pre-ageing reduced the vacancy concentration in the matrix, compared to that in the as-quenched condition. Therefore, the SRS after pre-ageing was higher than in the as-quenched condition. However, during subsequent natural ageing (i.e. one week of natural ageing), the natural ageing process was retarded after pre-ageing, which delayed the removal of vacancies from the matrix and therefore retained more vacancies in the pre-aged sample than in the sample with one week

of natural ageing after quenching. Therefore, the former sample exhibited a lower (more negative) SRS than the latter one. The excess vacancies above the equilibrium vacancy concentration in the samples without pre-ageing may exist as solute-vacancy complexes or be bound with clusters. For instance, for pre-ageing for a short time (i.e. 5 min at 100 ºC), most of excess vacancies may exist as solute-vacancy complexes. By contrast, for pre-ageing for a long time (i.e. 2 h at 100 ºC), most of excess vacancies may be bound within clusters. The shearing of those vacancy-containing clusters during deformation releases vacancies, thus increasing the magnitude of DSA and decreasing the SRS. Fig. 5-27 schematically shows the dependence of the vacancy concentration and the SRS on the pre-ageing time based on Mechanism I. It should be noted that vacancy concentration here refers to concentration of free vacancies, vacancies in the complexes and/or clusters. In other words, vacancy concentration is the total concentration of vacancies in the sample. As shown in Fig. 5-27, with increasing pre-ageing time, the vacancy concentration immediately after pre-ageing decreases with pre-ageing time, and the SRS increases. If the pre-aged sample were further naturally aged for one week, then the vacancy concentration firstly increases with increasing pre-ageing time (Stage I). After reaching a maximum, the vacancy concentration decreases with increasing pre-ageing time (Stage II). The SRS of pre-aged samples after one week of natural ageing is expected to show an opposite trend with regard to the dependence of the vacancy concentration on the pre-ageing time. The increase in the vacancy concentration after one week of natural ageing in the Stage I is because the vacancy concentration is determined by natural ageing process after pre-ageing. With increasing pre-ageing time, the natural ageing process becomes more efficiently suppressed, and thus more vacancies are retained in the alloy. This leads to a decrease in the SRS in the Stage I. In the Stage II, since there is almost no natural ageing response after pre-ageing, the vacancy concentration after one week of natural ageing is determined by pre-ageing time. Therefore, a re-increase in the SRS can be observed since vacancies deplete with increasing pre-ageing time. There will be a moment when the SRS measured immediately after pre-ageing is the same as the SRS of pre-aged sample after one week of natural ageing when there is no natural ageing response after pre-ageing. After that moment, the SRS in these two conditions should evolve with the pre-ageing time in the same way.
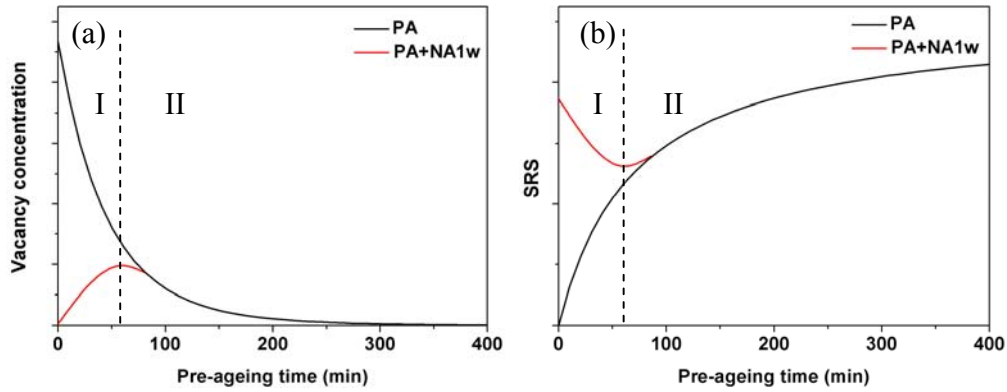
Fig. 5-27 Schematics showing the dependence of (a) the vacancy concentration in the alloy and (b) the SRS on the pre-ageing time at 100 ºC.

Furthermore, a stronger influence of pre-ageing on the SRS in the high Mg content alloy A2 than in the high Si content alloy A4 can be explained in two ways. Firstly, Si enhances the jump frequency of vacancies while Mg can trap vacancies and slow down their jump frequency [136]. In other words, vacancies can be more easily retained in the high Mg content alloys than in the high Si content alloys, which could give rise to a stronger DSA effect in the former alloys. Secondly, the characteristic waiting time of dislocations at pinning points being comparable to the characteristic diffusion time of Mg atoms to pinned dislocations should also contribute to the lower SRS of high Mg alloys. As shown in Fig. 5-28, even after ageing at 100 ºC for 1 month, DSA is still observable in alloy A2, which manifests itself as a decrease in the SRS with increasing strain.
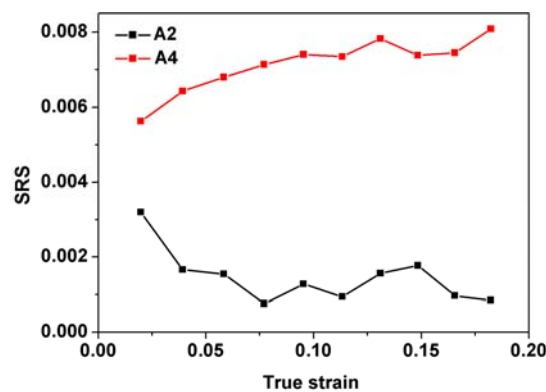
Fig. 5-28 The dependence of SRS on the true strain of alloys A2 and A4 pre-aged at 100 ºC for 1 month.

For the PLC effect observed in the pre-aged alloys, one should realise that the serrated yielding only occurs when the SRS drops below a certain negative value [59], i.e.

$$SRS < - (\Theta-\sigma)\Omega \qquad\qquad (5\text{-}1)$$

where Ω is a strain dependent quantity of the order of 10^{-4}. In this study, Ω was coarsely treated as a constant across different alloys and tempers. In other words, only the $\Theta-\sigma$ factor was considered. The dependence of $\Theta-\sigma$ on the true strain of the pre-aged alloys is shown in Fig. 5-29. On this basis, it is not surprising that the PLC effect was more readily observed in the high Mg content alloy A2 and low solute content alloy A3, since both of them exhibit lower $\Theta-\sigma$ levels than the other alloys. The magnitude of $\Theta-\sigma$, along with the increased DSA contribution to stress, can also be used to explain why the pre-aged alloys are more prone to the PLC effect. As shown in Fig. 5-30, for high Mg content alloy A2, the sample pre-aged at 100 ºC for 2 h exhibited the lowest magnitude of $\Theta-\sigma$ among the samples after the various tempers studied. Accordingly, serrated yielding was observed in the former sample, but not in the other two. For the low solute content alloy A3, the samples pre-aged at 100 ºC and 200 ºC showed similar levels of $\Theta-\sigma$, which was much lower than that of the sample without pre-ageing. Therefore, the PLC effect was observed in the pre-aged alloy A3. For the high Si content alloy A4, pre-ageing can even increase the $\Theta-\sigma$ level. Therefore, even though pre-ageing significantly reduced the SRS of the flow stress, the PLC effect was not observed in the pre-aged high Si content alloy A4.
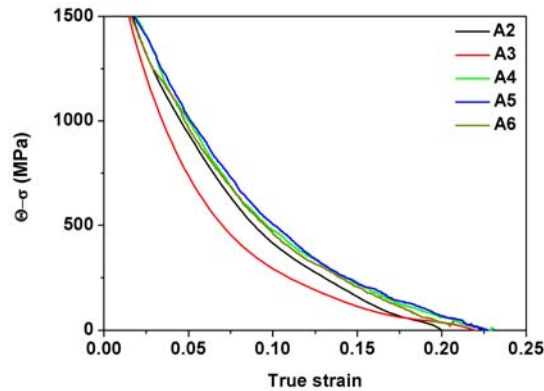
Fig. 5-29 The dependence of $\Theta-\sigma$ on the true strain of the alloys pre-aged for 2 h at 100 ºC followed by one week of natural ageing.
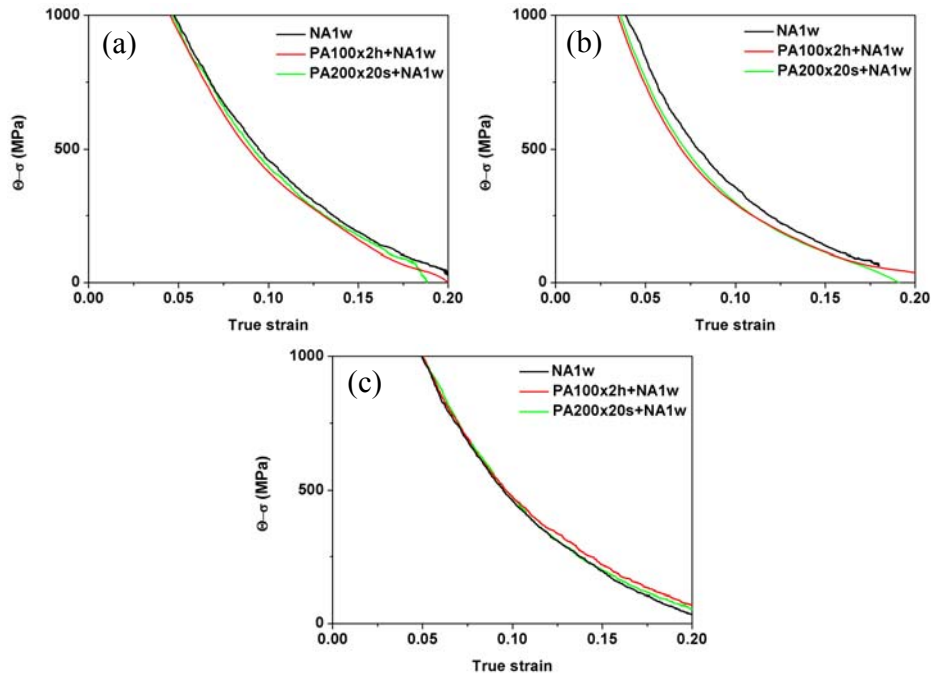
Fig. 5-30 The dependence of Θ-σ on the true strain of the pre-aged alloys:
(a) A2, (b) A3 and (c) A4.

The observed reduction in the SRS by pre-ageing, therefore, was found to decrease the post-uniform elongation, as shown in Fig. 5-31, and also the stretch formability, as shown in Fig. 5-15. The decrease in FLD_0 was more significant in the alloys pre-aged at 100 ºC for 2 h than in the alloys pre-aged at 200 ºC for 20s, since the decrease of SRS was more pronounced in the former alloys. The little influence of heat treatment on FLD_0 of alloy A3 will be explained by the work hardening behaviour of the alloy. The effect of pre-ageing on the stretch formability of 6xxx alloys was studied by Liu et al [18]. In reference [18], Erichsen dome height was used to represent the formability index. It was found that samples pre-aged at 170 ºC for 5 min exhibited a higher Erichsen dome height and lower yield strength than the sample without pre-ageing. Thus, the authors claimed that the low yield strength achieved by pre-ageing at 170 ºC for 5 min can improve the stretch forming performance of the alloys. However, it should be noted that a poor correlation between Erichsen dome height and press performance was recorded in [106, 107], which is also reviewed in Chapter 2. This may suggest that, although Erichsen dome height tests can provide a fast way to screening of different alloys, it is not a scientific way to evaluate the formability. We note that any declaration that low yield strength can improve the stretch formability is not necessarily correct, since stretch formability is determined by the work hardening and strain rate

hardening capabilities of the materials rather than by the strength level. It should be noted that low yield strengths could lead to a high work hardening capability provided that the work hardening rate is not decreased. Most importantly, the report in [18] did not supply information about the strain rate hardening behaviour of the alloys or provide correct information about the work hardening behaviour of the alloys.
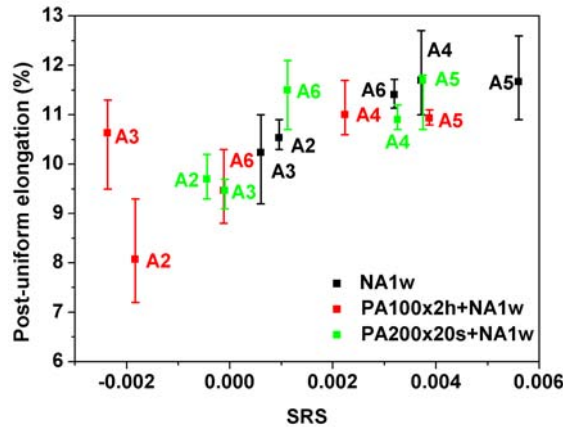
Fig. 5-31 The dependence of post-uniform elongation on the SRS at a strain of 0.2.

5.3.2 Work hardening behaviour

The instantaneous work hardening exponent at uniform stain ($n_{\varepsilon u}$) for the alloys in the different conditions is shown in Fig. 5-32. Comparing Fig. 5-32 with Fig. 5-13c, it can be seen that the dependence of $n_{\varepsilon u}$ on heat treatment is similar to the dependence of uniform elongation on heat treatment. This correlation between the working hardening exponent and uniform elongation follows from the Considère condition for the onset of necking under uniaxial tensile deformation. In other words, the uniform elongation results can be explained in terms of the work hardening behaviour. Furthermore, based on the response of $n_{\varepsilon u}$ to heat treatment, the six alloys studied may be categorised into two groups:

➢ Group 1, in which pre-ageing treatment slightly affects the work hardening capability, which is comprised of alloys A2 and A3. It can be seen that the pre-ageing treatment slightly reduces $n_{\varepsilon u}$ in alloy A2, and raises it in alloy A3 when the latter was pre-aged at 100 ºC for 2 h. In group 2, the PLC effect may occur depending on alloy composition and temper.

> ➢ Group 2, in which the pre-ageing treatment has little influence on the work hardening capability, i.e., high Si content alloys A4 and A5, and medium Mg/Si ratio alloy A6.
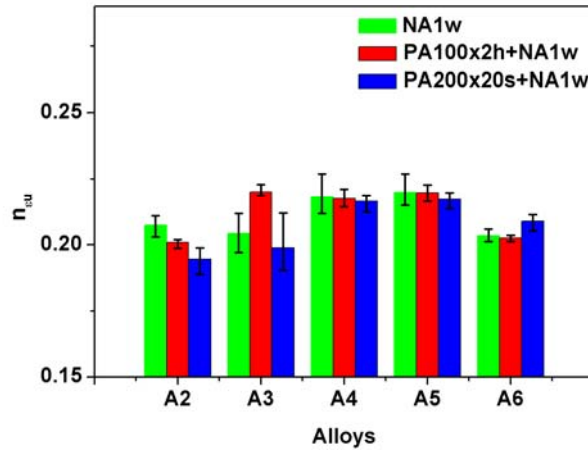
Fig. 5-32 Influence of heat treatment on $n_{\varepsilon u}$ for the different alloys.

The work hardening rate curves were further examined. As shown in Fig. 5-33, in group 1, pre-ageing significantly influences the work hardening behaviour of the alloys. More specifically, pre-aged alloy A2 shows a lower work hardening rate, especially at uniform strain and beyond the point of the onset of necking, than naturally aged alloy A2. The significant decrease in the strain rate sensitivity shown in Fig. 5-31 reduces the intrinsic work hardening capability of pre-aged alloy A2 at strains after the onset of necking, therefore contributing to the low work hardening rate after the onset of necking. For alloy A3, pre-ageing lowers the work hardening rate, especially in the sample pre-aged at 200 ºC for 20 s. It is interesting to observe that although the work hardening rate at strains before the onset of necking diminishes as a result of pre-ageing at 100 ºC for 2 h quite appreciably, the material can maintain the work hardening rate up to high strains after the onset of necking. In group 2, for high Si content alloys A4 and A5, the pre-ageing treatment has almost no influence on the work hardening rate curves. Therefore, pre-ageing has little effect on the uniform elongation. For medium Mg/Si ratio alloy A6, pre-ageing does not influence the work hardening behaviour within the uniform strain range. However, it appears that pre-ageing at 100 ºC for 2 h caused a fast drop in the work hardening rate after the uniform strain, which is attributed to a low strain rate sensitivity, cf. Fig. 5-31.
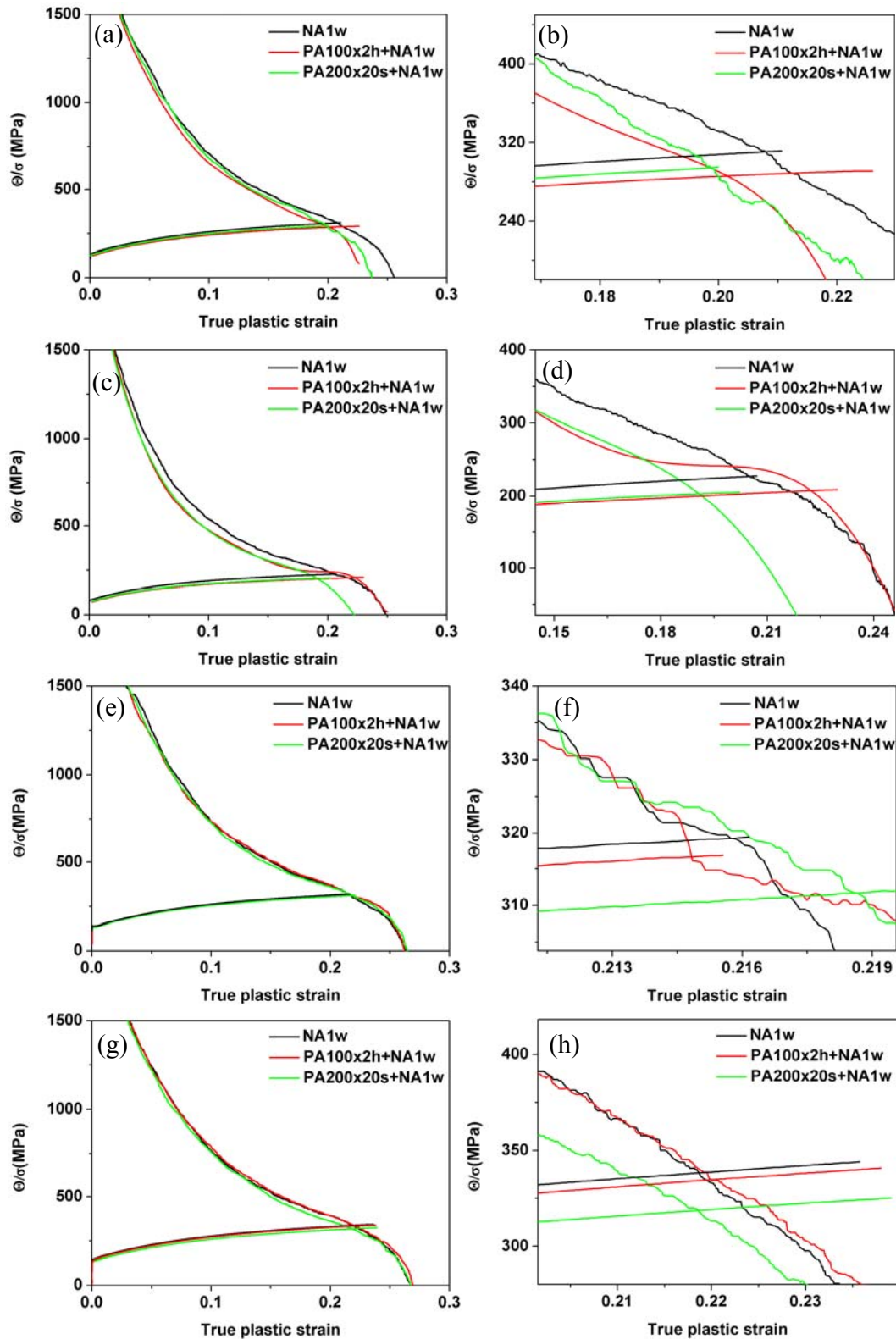
Fig. 5-33 Effect of heat treatment on the work hardening curves for alloys (a, b)A2, (c, d) A3, (e, f) A4, (g, h) A5 and (i, j) A6. Figures (b), (d), (f), (h) and (j) give an enlarged view of (a), (c), (e), (g) and (i), repectively.
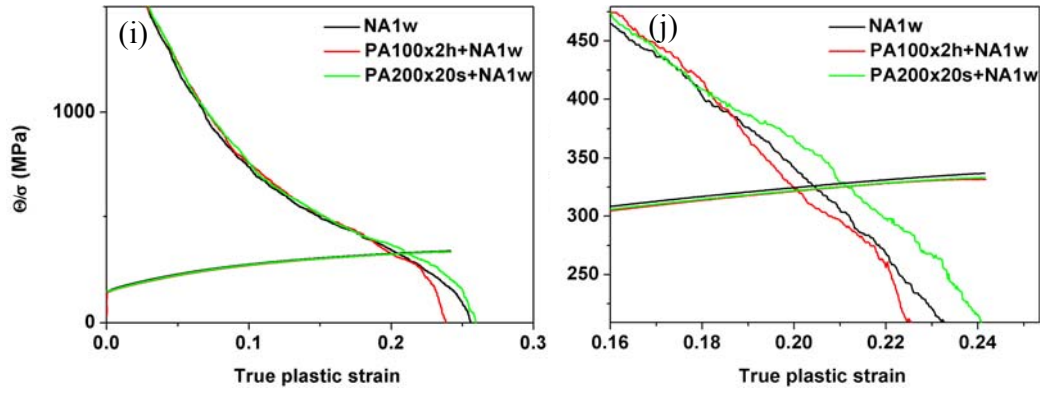
Fig. 5-33 continued
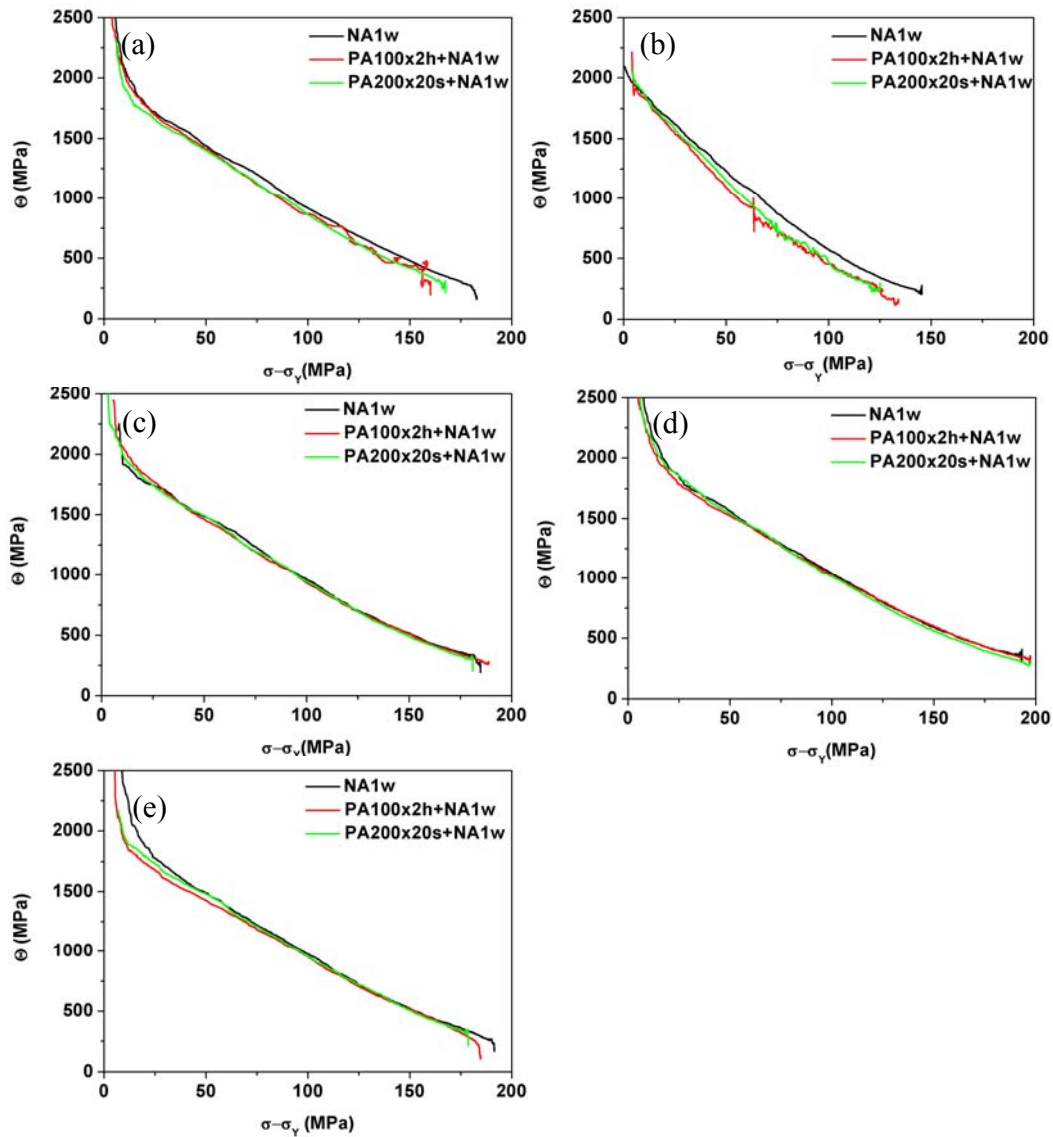
Fig. 5-34 Kocks-Mecking plots for the alloys studied in different conditions:
(a) A2, (b) A3, (c) A4, (d) A5 and (e) A6

The Kocks-Mecking plots representing the stress dependence of the work hardening coefficient for the alloys in the different conditions are shown in Fig. 5-34, and two important parameters (initial work hardening rate and dynamic recovery rate) for the work hardening extracted from the Kocks-Mecking plots are shown in Fig. 5-35.

● In group 1 (alloys A2 and A3), the initial work hardening rate was observed to be lower in both alloys when pre-aged at 200 ºC for 20 s and further naturally aged for one week, compared to samples without pre-ageing. A low initial work hardening rate can be correlated with low solute content in the alloys [15, 45, 48], which may suggests that pre-ageing at 200 ºC for 20 s decreases solute concentration in the matrix of alloys A2 and A3. If this is the case, then the rise of the dynamic recovery rate is not unexpected since a low solute concentration in the matrix would lead to a high dynamic recovery rate [48]. Therefore, pre-ageing at 200 ºC for 20 s slightly decreased the uniform elongation and FLD_0 of alloys A2 and A3. For alloys A2 and A3 pre-aged at 100 ºC for 2 h an increase in the Θ_{II} was observed, which may suggest the solute concentration in the matrix of pre-aged samples is higher than that in the samples without pre-ageing. However, high solute concentration in the pre-aged samples did not lead to a low dynamic recovery rate, as shown in Fig. 5-35b. This should be studied further, although similar trend was reported by Zolotorevsky *et al* [15]. Although as-quenched Al-Cu samples studied in [15] showed a higher initial work hardening rate than naturally aged samples, the former samples exhibited a higher dynamic recovery rate. It appears that the negative effect of high dynamic recovery rate on the uniform elongation and FLD_0 of alloy A2 pre-aged 100 at ºC for 2 h is higher than the beneficial effect of a large Θ_{II}, which led to a decrease in the uniform elongation and formability. For alloy A3, the effect of Θ_{II} on the uniform elongation and FLD_0 may be more important than the effect of dynamic recovery rate, therefore this pre-ageing treatment may increase the uniform elongation. However, pre-ageing at 100 ºC for 2 h had little influence on the formability. It appears that the improvement in work hardening is counterbalanced by a decrease in strain rate hardening in alloy A3 pre-aged at 100 ºC for 2 h. The greater effect of the work hardening capability than that of strain rate hardening capability on the stretch formability was also reported in [137]. Therefore, the overall effect of pre-ageing on the stretch formability of alloy A3 is fairly weak.

- In group 2 (alloys A4, A5 and A6), the initial work hardening rate of the pre-aged alloys was observed to be lower than that of the non pre-aged samples. Pre-ageing had little influence on the dynamic recovery rate. The observed reduction in Θ_{II} was found to decrease the formability, while having little influence on the uniform elongation. The low Θ_{II} for the pre-aged alloys may suggest a lower solute concentration in the matrix than in the alloys did not undergo pre-ageing.

Based on the analysis of the Kocks-Mecking plots, it appears that the pre-aged alloys after one week of natural ageing did not necessarily have a lower solute concentration in the matrix than that the alloys without pre-ageing. In fact, the solute concentration in the matrix is influenced by pre-ageing and subsequent natural ageing. Both pre-ageing and natural ageing after pre-ageing are expected to lower the solute content in the matrix. However, if the natural ageing process after pre-ageing is retarded by pre-ageing, then the pre-aged alloys after one week of natural ageing may have a higher solute content in the matrix than that in the alloys naturally aged for one week without pre-ageing. Furthermore, this result may possibly provide further evidence that the increased DSA effect by pre-ageing is caused by a high vacancy concentration rather than the variation in solute concentration in the matrix.
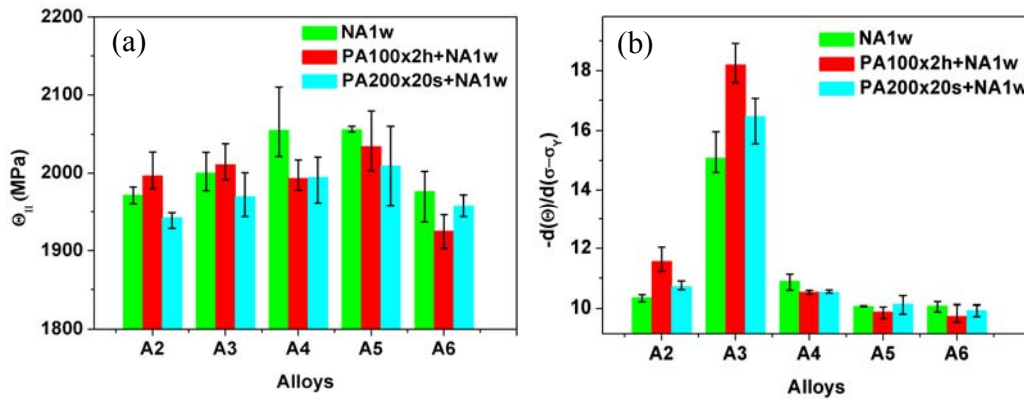
Fig. 5-35 Effect of heat treatment on the magnitude of Θ_{II} and $d(\Theta)/d(\sigma - \sigma_Y)$.

5.4 Summary

The effects of pre-ageing treatment on the tensile properties and stretch formability of five Cu-free alloys were studied. The work hardening and strain rate hardening behaviour of the alloys was used to explain the tensile ductility and stretch formability of the alloys. It was

found that although pre-ageing can significantly improve the paint bake response of the materials, pre-ageing deteriorates the stretch formability of the materials due to the decrease in the strain rate hardening and work hardening capability, particularly in alloys pre-aged at 100 ºC for 2 h, except for the low solute content alloy A3. In alloy A3, pre-ageing at 100 ºC for 2 h can improve the work hardening capability, although the strain rate hardening capability was decreased. It appears that the increase of the work hardening capability outstrips the drop of strain rate hardening capability in alloy A3 pre-aged at 100 ºC for 2 h, therefore resulting in a slightly improved formability after pre-ageing. Moreover, the decreased strain rate hardening was attributed to the increased DSA after pre-ageing. A model was proposed for the increased DSA according to which pre-ageing reduces the vacancy concentration in the matrix, compared to that in the as-quenched condition. Therefore, the SRS in the pre-aged alloys is higher than that of the as-quenched alloys. However, during the subsequent (i.e. one week) natural ageing, the natural ageing response was retarded in the pre-aged alloys, which delayed the removal of vacancies from the matrix. It is believed that the process retained more vacancies (residing in the solute-vacancy complexes or co-clusters) compared to the alloys after one week of natural ageing following quenching. Therefore, the pre-aged alloys exhibited a lower (more negative) SRS than the same alloys without pre-ageing (after one week of subsequent natural ageing).

Chapter 6 Microstructure and Formability of Al-Mg-Si-Cu Alloys

6.1 Introduction

In 6xxx series alloys, Cu is often added to enhance the precipitation hardening [95, 96], although the corrosion resistance tends to be degraded by the addition of Cu [97]. Cu additions are also expected to influence the stretch formability of 6xxx alloys since Cu was reported to have a positive effect on work hardening [48, 98] and a negative effect on the strain rate hardening [74]. In fact, it appears the effect of Cu on the stretch formability depends on the Mg/Si ratio in the 6xxx alloys. For instance, Cu additions were reported to increase LDH_0 of alloys with a medium Mg/Si ratio, while slightly decreasing that of alloys with a high and/or low Mg/Si ratio, although the work hardening exponent was seen to be increased by Cu additions regardless of the Mg/Si ratio in the alloys [13]. It should be noted that no strain rate hardening characteristics of alloys with different Mg/Si ratio were reported in the reference [13]. Moreover, Cu was reported to improve the tensile ductility, however to either increase or decrease the Erichsen dome height depending on the Cu content in the 6010-type alloys [138]. Tian *et al* [139] reported that Cu additions can increase the strength and decrease the Erichsen dome height of 6111-type alloys, although Erishsen test was not supposed to be a suitable method to evaluate stretch formability of the materials [19, 106]. Therefore, it is still unclear that how Cu additions influence the stretch formability of 6xxx alloys, and a better understanding on this aspect is needed.

In this chapter, three alloys A7, A8 and A10, which are Cu-containing versions of alloys A2, A6 and A4, respectively, were studied. The Cu-containing alloys were either naturally aged or pre-aged and subsequently aged naturally (the heat treatment parameters were similar to those employed for their Cu-free counterparts). The microstructural features (i.e. grain size, coarse particles, dispersoids) and texture were investigated. Moreover, the work hardening and strain rate hardening behaviours of the alloys were characterised to correlate the microstructural features with the formability results.

6.2 Results

6.2.1 Microstructure and texture of solution treated alloys

6.2.1.1 Grain structure

The grain structure of solution treated Cu-containing alloys is shown in Fig. 6-1. Comparing Fig. 6-1 with Fig. 4-4, it can be found that the addition of Cu slightly influences the average grain size of these alloys. For alloys A2 and A4, the addition of Cu slightly reduces the average grain size. For alloy A6, the addition of Cu increases the average grain size. However, the variation in the average grain size across the Cu-containing alloys is small (in the range of 30~41 μm), as is the case with the Cu-free alloys. This suggests that the difference in the average grain size should not be considered as an important factor that influences the formability.
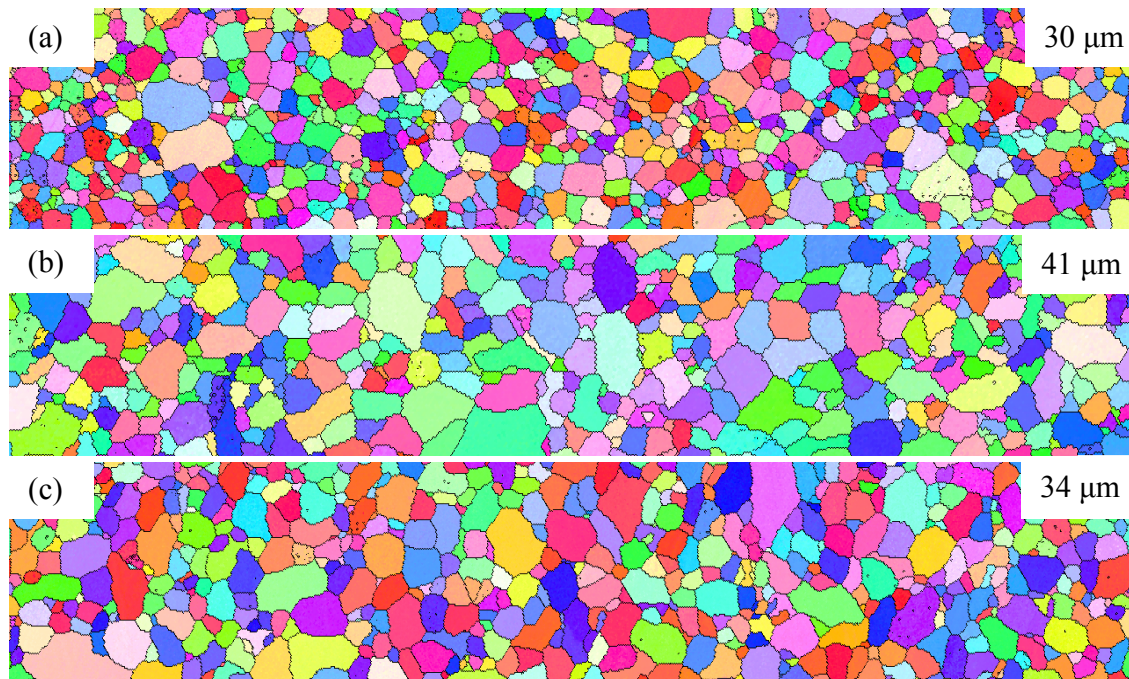
Fig. 6-1 Grain structure of alloys (a) A7, (b) A8 and (c) A10.
(Note: numbers in the upper right corners indicate the average grain size.)

6.2.1.2 Coarse particles and dispersoids

The morphologies of undissolved coarse particles observed in the Cu-containing alloys are shown in Fig. 6-2. Compared to the undissolved coarse particles present in the corresponding Cu-free alloys (see Fig. 4-2), the addition of Cu did not introduce new coarse particles. However, EDS results showed that the coarse particles in the Cu-containing alloys contain a small amount of Cu (~1 wt.%). In this case, the Fe-containing phase may be expressed as Al(Fe,Mn,Cu) Si [121].
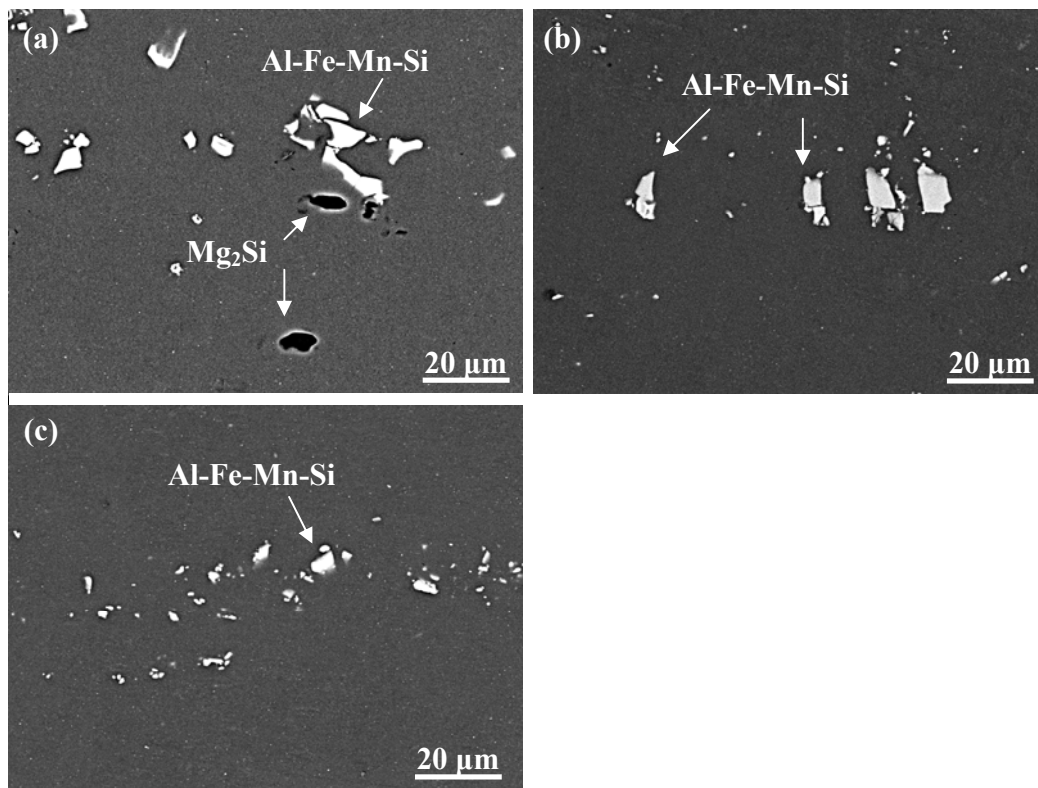
Fig. 6-2 Backscattered electron images showing undissolved coarse particles in the solution treated alloys (a) A7, (b) A8 and A10.

The distribution of dispersoids in the Cu-containing alloys is shown in Fig. 6-3. It can be seen that with decreasing Mg/Si ratio (from alloy A7 to A8, and further to A10) the distribution of dispersoids becomes more uniform and their number density increases. This trend is similar to the trend in the Cu-free alloys (from alloy A2 to A6, and further to A4), which suggests a similar mechanism is operating. Table 6-1 lists quantitative data for the dispersoids in the alloys, determined by image analysis of backscattered SEM images.

Compared to the dispersoids in the Cu-free alloys (see Table 4-2), it appears Cu has little influence on the number density of dispersoids, although in the high Mg/Si ratio alloy A2, Cu was observed to slightly reduce the number density of dispersoids.
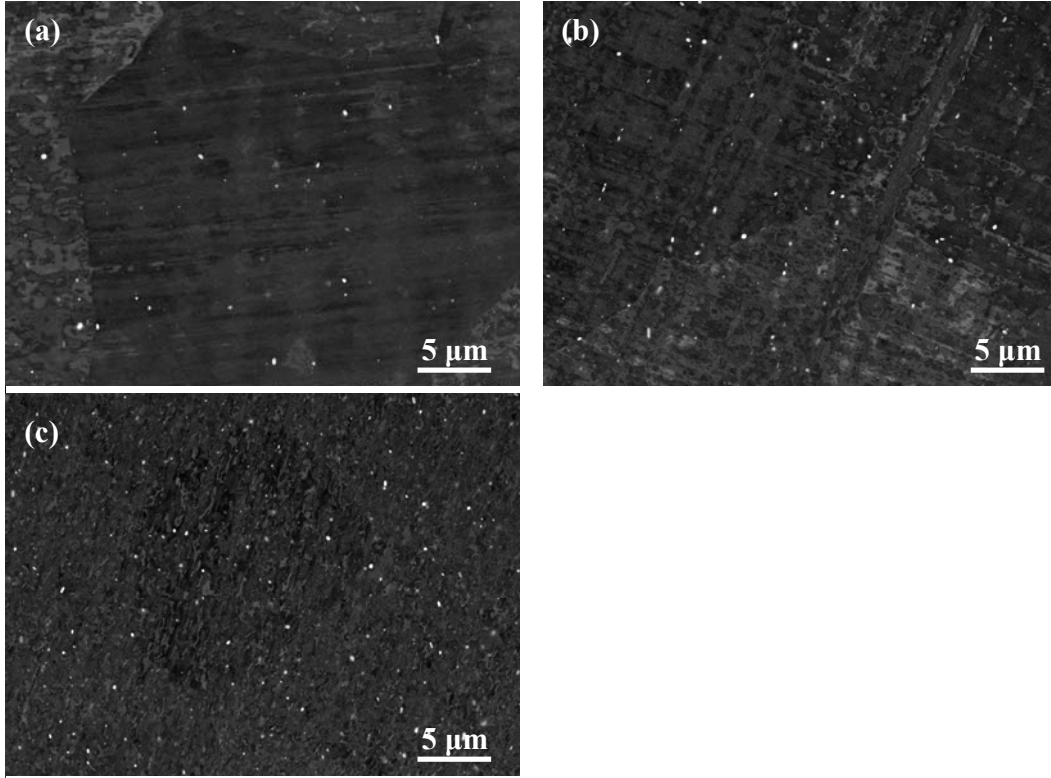
Fig. 6-3 Backscattered SEM images showing the distribution of dispersoids in the solution treated alloys: (a) A7 (b) A8 (c) A10.

Table 6-1 Quantitative data for dispersoids in the Cu-containing alloys.

Alloy	Area %	Number density per mm^2	Average diameter (μm)	Interpaticle distance (μm)
A7	0.63	1.7×10^5	0.21	1.72
A8	1.06	2.4×10^5	0.22	1.35
A10	1.06	3.1×10^5	0.20	1.22

6.2.1.3 Texture

Compared to the texture results presented for the Cu-free alloys (Fig. 4-5), Cu slightly decreases the maximum texture intensity in the high Mg/Si ratio alloy, but increases the maximum texture intensity in the medium and low Mg/Si ratio alloys, as shown in Fig. 6-4.

Table 6-2 lists the volume fractions of main texture components. As Cu has little influence on the texture of the alloys, the texture is not considered as a major factor that influences the formability of these alloys.

A7 (2.2)   A8 (2.7)   A10 (2.7)
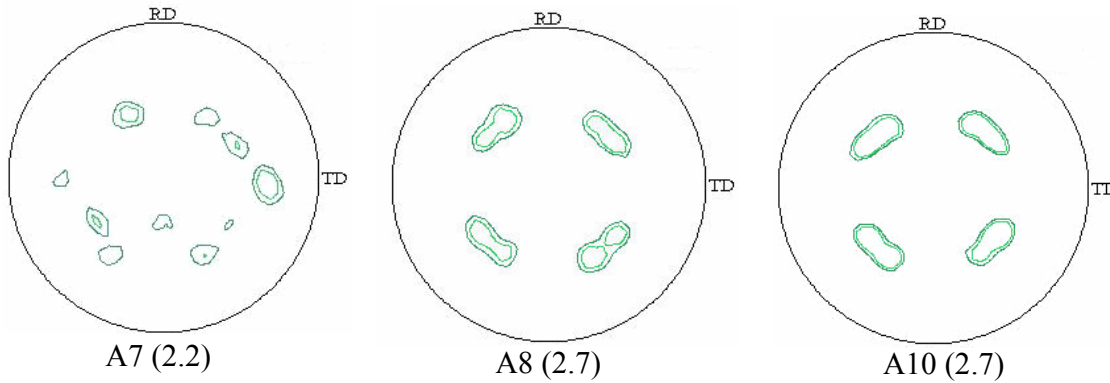
Fig. 6-4 {111} pole figures of experimental alloys in the T4 condition.
The number in parentheses represents the maximum texture intensity for each alloy.

Table 6-2 volume fractions of the main texture components based on bulk texture analysis.

Alloy	Texture components		
	{001}<100>	{001}<250>	{013}<100>
A7	5.14	8.19	/
A8	9.44	11.90	5.28
A10	9.82	11.96	5.46

6.2.2 Effect of Cu on the natural ageing response

Fig. 6-5 shows natural ageing curves for the Cu-containing alloys. For comparison, natural ageing curves for the corresponding Cu-free alloys are also presented in Fig. 6-5. As shown in Fig. 6-5, the natural ageing behaviour of Cu-containing alloys is similar to that of the Cu-free alloys, but it appears that Cu can slightly retard the natural ageing process regardless of the Mg/Si ratios in the alloys. Furthermore, the ratio $(H_i- H_l)/(H_w-H_l)$ was used to evaluate the natural ageing kinetics, where H_i is the hardness at a given time, H_w is the hardness after one week of natural ageing and H_l is the hardness at the beginning of natural ageing. The re-plotted results in Fig. 6-6 show that the natural ageing kinetics appear to be retarded by the addition of Cu. Moreover, it is interesting to observe that Cu additions can retard the natural ageing kinetics before one day of natural ageing in the alloy (A6) with medium Mg/Si ratio.

However, after one day of natural ageing, the natural ageing kinetics is indeed promoted by Cu so that after one week of natural ageing, the hardness of alloy A8 is noticeably higher than alloy A6.
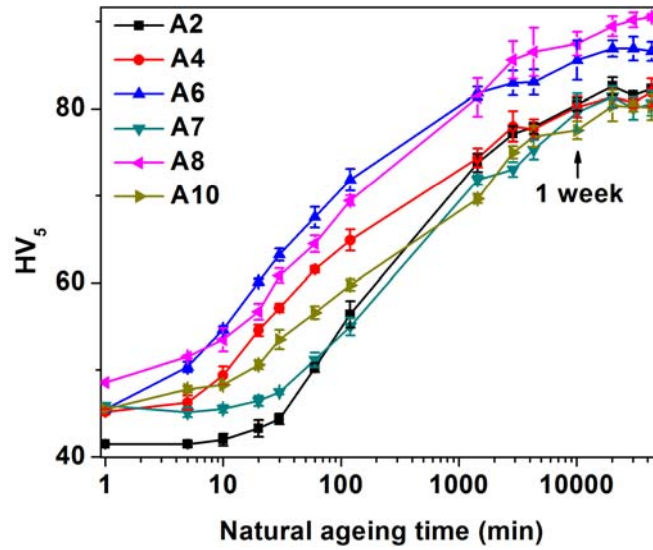
Fig. 6-5 Natural ageing curves of the alloys.
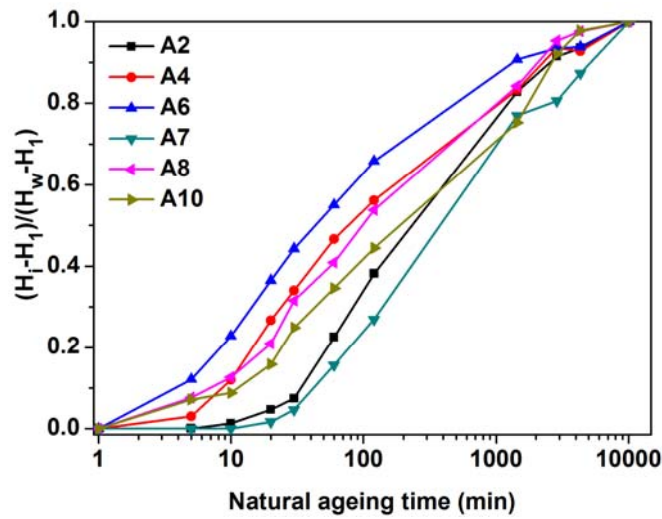
Fig. 6-6 Natural ageing kinetics of the alloys.

6.2.3 Effect of Cu on the tensile properties of naturally aged alloys

The mechanical properties of the alloys after one week of natural ageing were measured, as shown in Fig. 6-7. It can be seen that the addition of Cu has a larger influence on the tensile strength than on the yield strength, which indicates that Cu additions can influence the

dislocation strengthening. This will be discussed later in terms of effect of Cu additions on the work hardening capability. More precisely, the addition of Cu significantly increases the tensile strength of the alloys, and this increase was found to be largest at a Mg/Si ratio of around 1. On the other hand, the addition of Cu marginally decreases the yield strength of alloys A2 and A4, but clearly increases the yield strength of the medium Mg/Si ratio alloy A6. The addition of Cu is expected to increase the strength/hardness of as-quenched samples due to the solid solution strengthening, which is the case, as shown in Fig. 6-5. However, due to the sluggish natural ageing kinetics in the Cu-containing alloys, after one week of natural ageing, the hardness/strength of the alloys with Cu is equivalent as the Cu-free alloys. This is the case in the alloys with high or low Mg/Si ratio. In the medium Mg/Si ratio alloy A6, Cu additions promote the natural ageing kinetics after one day of natural ageing. Therefore, after one week of natural ageing, the strength/hardness of alloy A8 is higher than that of alloy A6. As for the tensile ductility, the addition of Cu slightly increases the uniform elongation but has almost no effect on the total elongation. These results are different from those in Reference [13]. In Reference [13], 0.2 wt.% Cu was reported to increase the strength, however, decrease the total elongation. Moreover, the addition of Cu was reported to only increase the uniform elongation when the alloy contains high or low Mg/Si ratios, although the work hardening exponent was increased by Cu regardless of the Mg/Si ratio in the alloys [13].
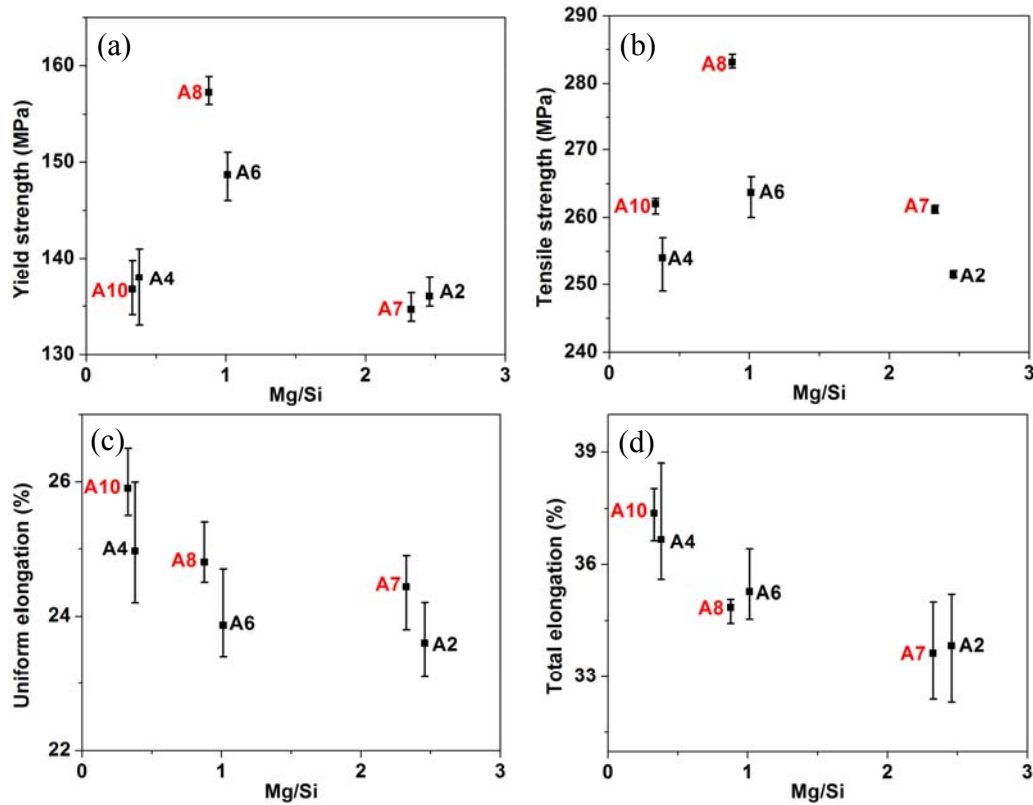
Fig. 6-7 Mechanical properties of the alloys after one week of natural ageing.

6.2.4 Effect of pre-ageing on the hardness and tensile properties of Cu-containing alloys

Without pre-ageing, the addition of Cu has little influence on the paint-bake response of the alloys (except for alloy A2), as shown in Fig. 6-8a. The addition of Cu in alloy A2 can even lead to a small but noticeable positive paint-bake response after one week of natural ageing. In other words, the retardation of negative effect of natural ageing on the paint-bake response by Cu is prominent in the high Mg content alloy. This may be attributed to the high vacancy concentration in the naturally aged alloy A7. This will be discussed later in terms of strain rate hardening behaviour of alloy A7. Like in the Cu-free alloys, pre-ageing treatments can significantly improve the paint bake response of the materials (Fig. 6-8b,c). The improvement in the paint bake response is more notable in the samples pre-aged at 100 ºC for 2 h than in the samples pre-aged at 200 ºC for 20 s. It appears that the addition of Cu has little influence on the paint bake response of pre-aged alloys except for alloy A10. In alloy A10, pre-ageing at 200 ºC for 20 s gives rise to a ~ 1 HV_5 paint bake response, while that for

alloy A4 is ~ 6 HV$_5$. The effect of pre-ageing on the mechanical properties of Cu-containing alloys and Cu-free alloys is shown in Fig. 6-9. As seen in Fig. 6-9, pre-ageing was found to reduce the strength after one week of natural ageing. As for the tensile ductility, pre-ageing can reduce both the uniform and the total elongation of alloy A10, but has little influence on the tensile ductility of alloy A8. It is interesting to observe that pre-ageing at 100 ºC for 2 h can even slightly raise the uniform and total elongations of alloy A7.
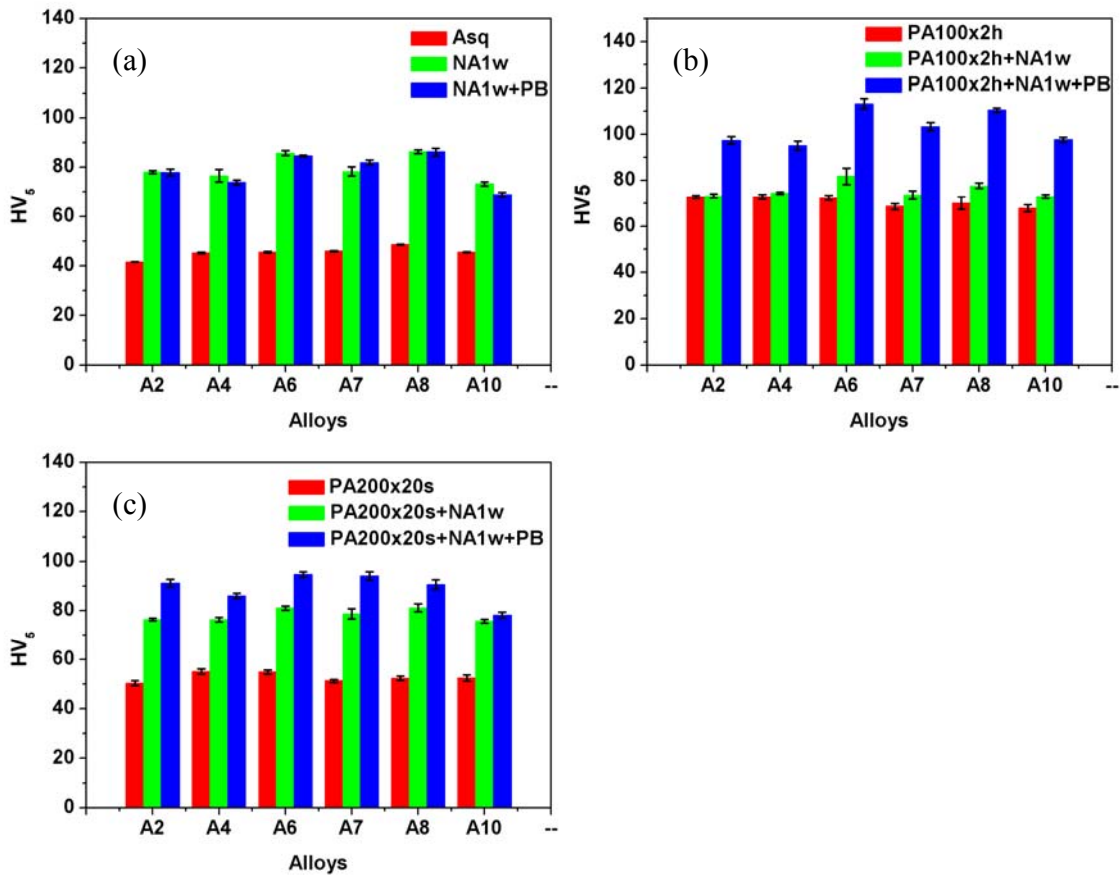
Fig. 6-8 Hardness of the alloys in different tempers.
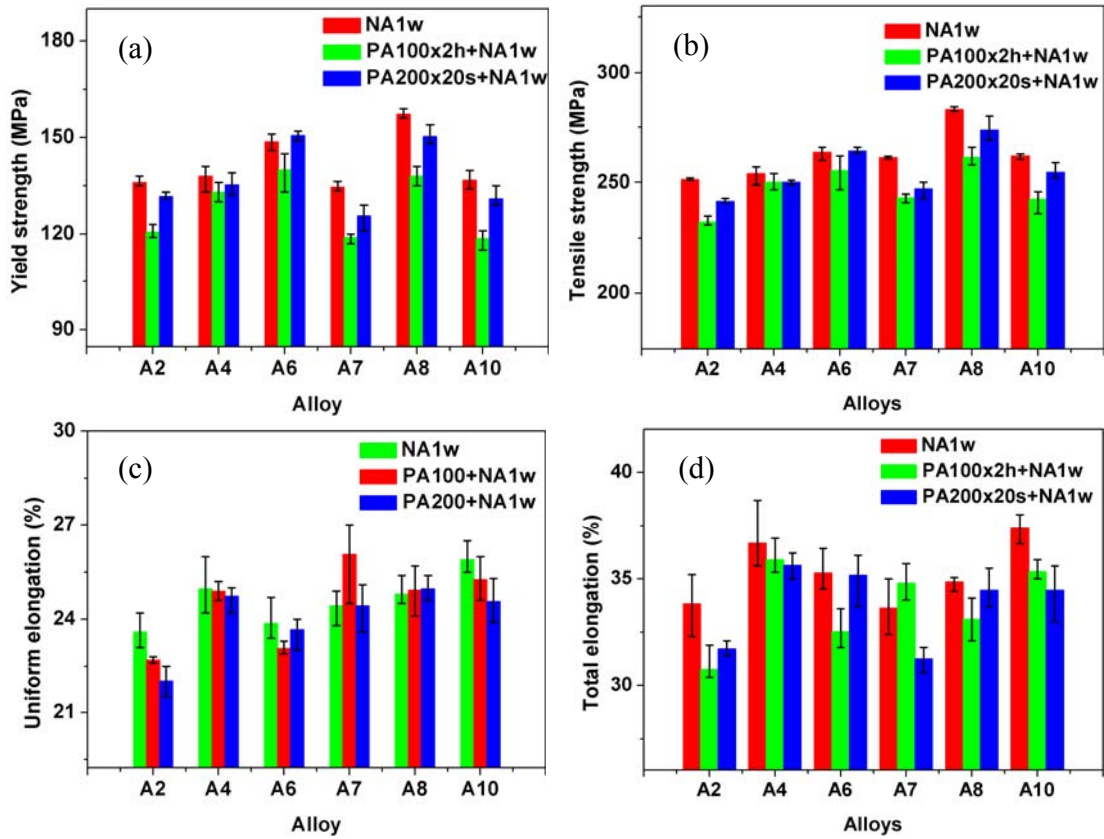
Fig. 6-9 Effect of pre-ageing on the tensile properties of the alloys

6.2.5 Effect of Cu and pre-ageing on the formability

The addition of Cu was found to improve the stretch forming performance of naturally aged the alloys, as shown in Fig. 6-10, although this improvement tends to decrease with decreasing Mg/Si ratio in the alloy. This observation is slightly different from the results in Reference [13]. In reference [13], it was reported that Cu can improve the LDH_0 in an alloy with a medium Mg/Si ratio, while leading to a decrease the LDH_0 in an alloy with high or low Mg/Si ratio. Furthermore, as in the Cu-free alloys, pre-ageing was found to decrease the formability of the Cu-containing alloys, as shown in Fig. 6-11.
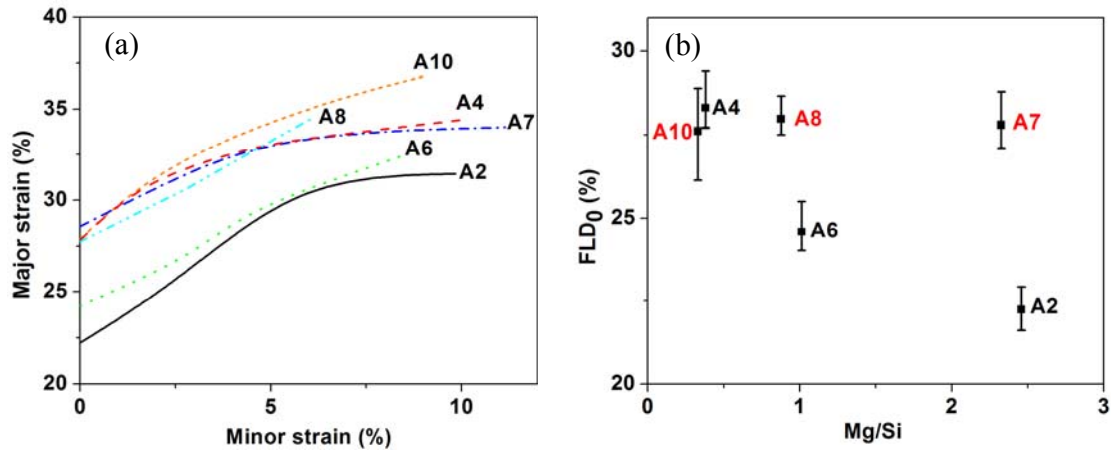
Fig. 6-10. (a) Right-hand side FLD and (b) FLD_0 of the alloys after 1 week of natural ageing.
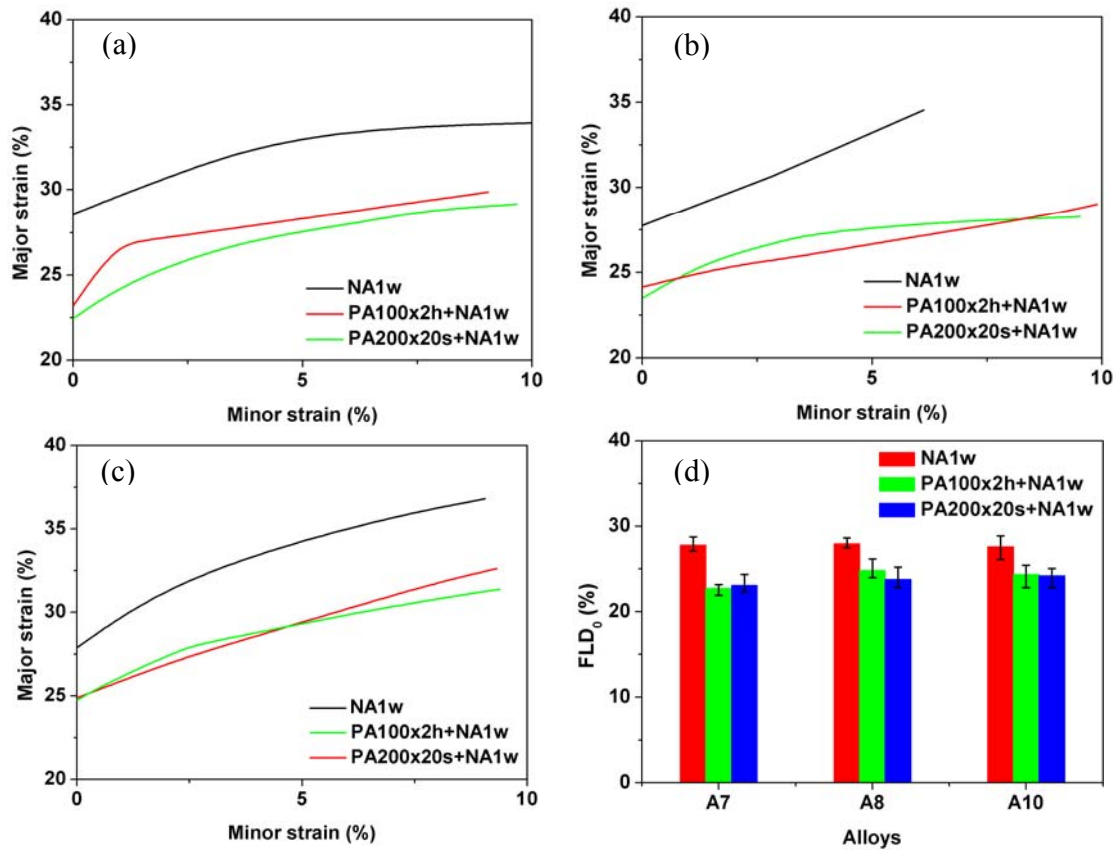
Fig. 6-11 Effect of heat treatment on the right-hand side of the FLD of alloys (a)A7, (b) A8 (c) A10 and FLD_0 results are shown in (d).

6.3 Discussion

6.3.1 Strain rate hardening behaviour

The dependence of the SRS of the flow stress of the alloys after one week of natural ageing on the strain is shown in Fig. 6-12. As seen in Fig. 6-12, after one week of natural ageing, the SRS of the flow stress of the alloys with low Mg/Si ratio is larger than that of the alloys with high Mg/Si ratio, especially at the large strains that are relevant for tensile ductility and formability. This is due to the faster natural ageing kinetics in the low Mg/Si ratio alloys, which has been discussed in Chapter 4. The addition of Cu slightly decreases the SRS, especially in the high Mg/Si ratio alloy A2. This is probably the reason why, after the onset of necking, alloy A7 shows a relatively faster decrease in the work hardening rate than the other two Cu-containing alloys A8 and A10 – since a negative SRS in alloy A7 is expected to strongly counter the intrinsic work hardening [7]. Note that alloys with higher strain rate sensitivity systematically exhibit a larger post-uniform elongation (Fig. 6-13). This is consistent with reports in the literature [8]. Since the strain rate hardening capability was decreased by Cu additions, the improvement in the formability will be explained in terms of the work hardening behaviour.
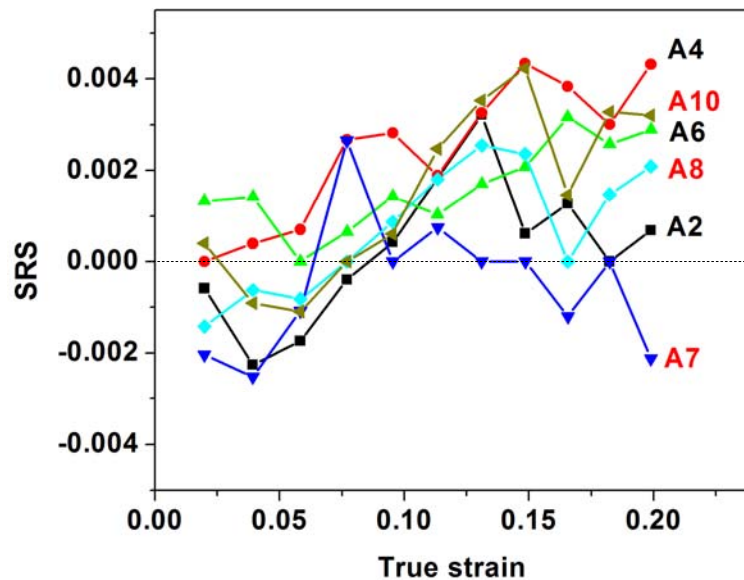
Fig. 6-12 The SRS of the flow stress for the alloys after 1 week of natural ageing.
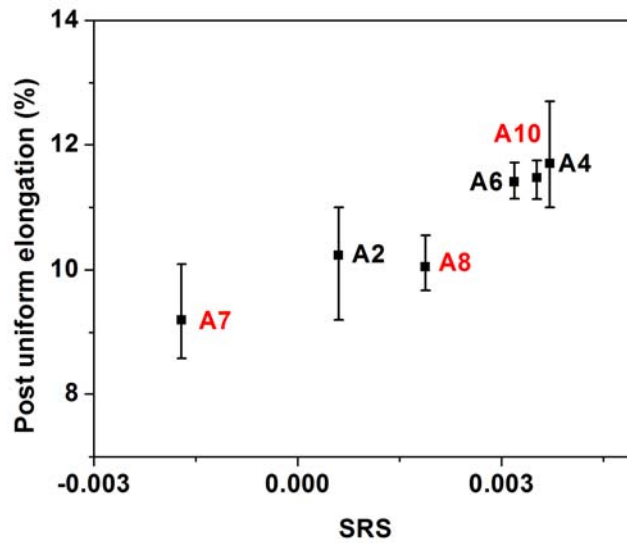
Fig. 6-13 The dependence of post-uniform elongation on the SRS of the flow stress of the alloys naturally aged for one week. The SRS was taken at a strain of 0.20.

The addition of Cu is always seen to decrease the SRS of the alloys irrespective of Mg/Si ratio in all the alloys. This effect is strongest in the high Mg/Si ratio alloy A2. This result is somewhat expected since the increase of solute content (i.e. Cu) will always tend to decrease the SRS due to a larger negative contribution of DSA to the SRS [74]. Furthermore, the retardation of the natural ageing process by Cu is expected to be another reason for the lower strain rate sensitivity. The retardation of natural ageing would delay the removal of mobile solutes and/or vacancies from the matrix, thus resulting in a larger contribution of DSA to the SRS. This retardation is seen from the hardness results (Fig. 6-5) and strain rate sensitivity results (Fig. 6-12 and Fig. 6-14). Fig. 6-14 shows the SRS of the flow stress of the alloys after one day and one month of natural ageing. From the strain rate sensitivity results, it is seen that the SRS of the Cu-containing alloys at small strains increases with prolonged natural ageing, but is always negative, except for alloy A8 after one month of natural ageing. For alloy A7, the SRS at small strains is even lower than that of A2 after one month of natural ageing. It is known that the mobility of Cu is much lower than that of Mg [140]. The effect of Cu alone is not expected to produce the negative SRS that is still observed after one month of natural ageing. Instead, Cu was reported to reduce the rate of migration of Mg and Si atoms, which retards the formation of Mg-Si clusters at room temperature [141]. Therefore,

the retardation of natural ageing by Cu additions observed here must also contribute to the low SRS in the Cu-containing alloys.
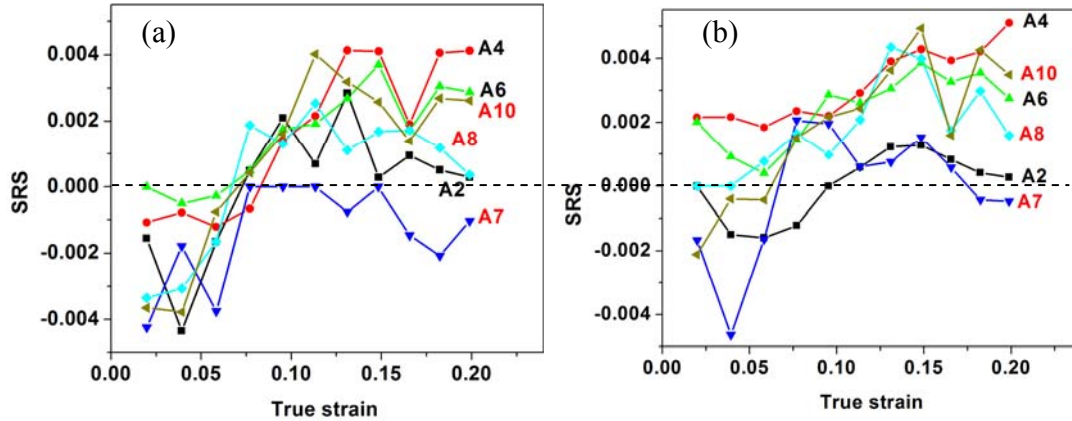
Fig. 6-14 The SRS of the flow stress for the alloys after (a) one day of natural ageing and (b) one month of natural ageing.

Moreover, the decrease in the SRS by the addition of Cu even led to the occurrence of serrated yielding in alloy A7 after one week of natural ageing, while the PLC effect was absent in the other two Cu-containing alloys (Fig. 6-15). Alloy A7 is the only alloy among the eight alloys studied where the PLC effect was observed after one week of natural ageing. After one month of natural ageing, the serrated yielding was still observable in alloy A7, as shown in Fig. 6-16. For the other seven alloys, the serrated yielding gradually disappeared with natural ageing due to the depletion of solute/vacancies in the matrix by clustering. After one week of natural ageing, no serrated yielding was observed in any alloys except for alloy A7. Therefore, the discontinuous yielding in alloy A7 after one week of natural ageing suggests a sluggish natural ageing process. In other words, natural ageing is retarded in alloy A7 by Cu additions. Although the serrated yielding was not observed in the other two Cu-containing alloys (A8 and A10) after one week of natural ageing, based on hardness results (Fig. 6-5) and the SRS results (Fig. 6-14), the natural ageing process should also be retarded. Moreover, the PLC effect observed in the alloy A7 after one week of natural ageing may suggest that alloy A7 retained more vacancies than in other alloys. Therefore, naturally aged alloy A7 showed an unusual positive paint bake response (since vacancies are believed to be important for the precipitation during artificial ageing [142]), while other naturally aged alloys had a negative PBR. In addition, the higher Θ-σ level for alloy A7 compared to that

for alloy A2 (see figure 6-17) suggests that a lower SRS is needed for the PLC effect to occur. This is indeed the case for alloy A7, as shown in Fig. 6-12.
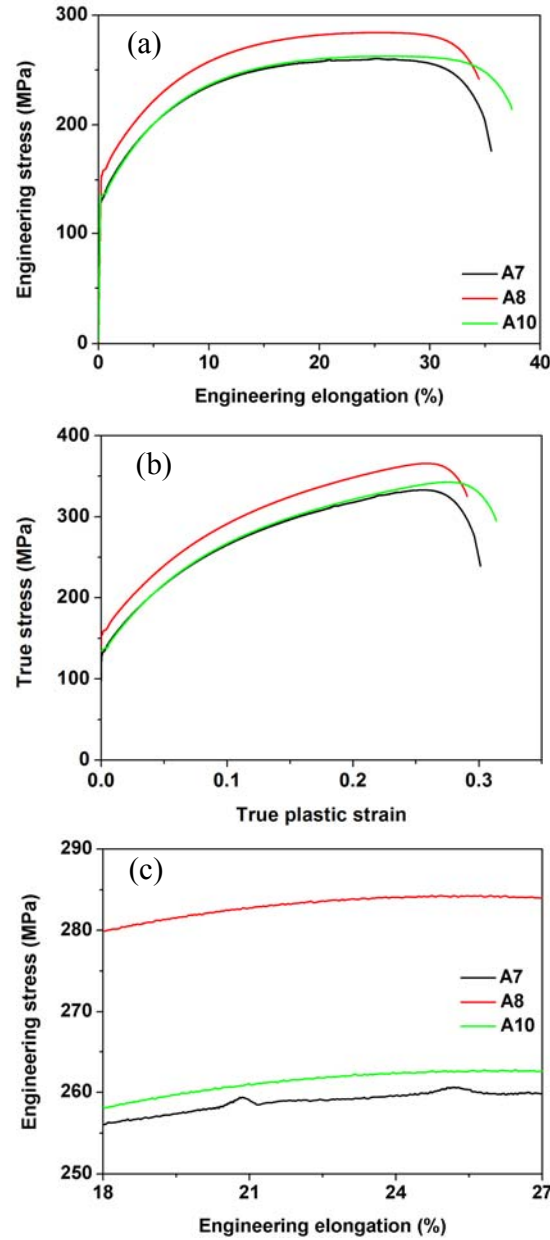
Fig. 6-15 (a) Engineering and (b) true stress-strain curves for the Cu-containing alloys after one week of natural ageing (c) enlarged view of (a).
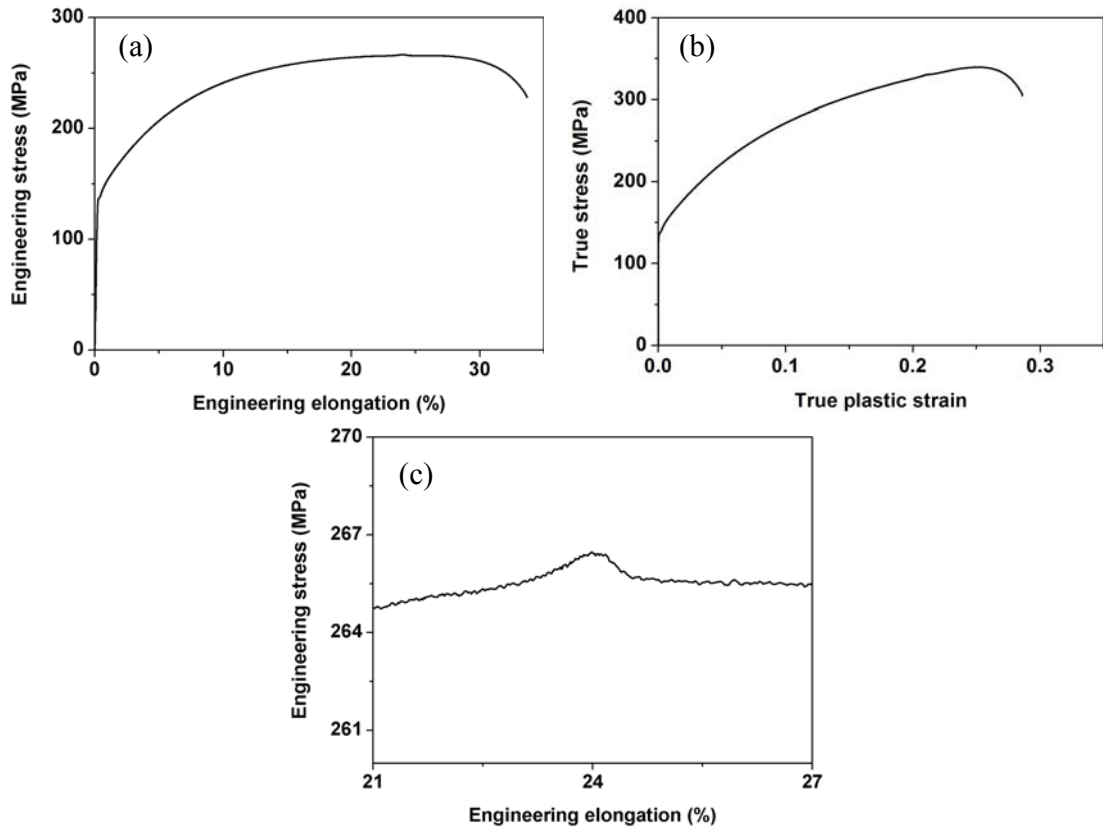
Fig. 6-16 (a) Engineering and (b) true stress-strain curves for the Cu-containing alloys after one month of natural ageing; (c) enlarged view of (a).
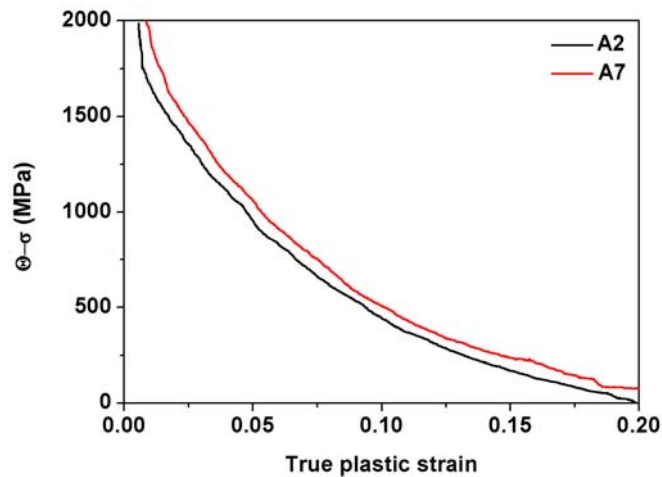
Fig. 6-17 The dependence of (Θ-σ) on the true plastic strain for alloys A2 and A7 after one week of natural ageing.

When the Cu-containing alloys were pre-aged, then, like in their Cu-free counterparts, a decrease in the SRS and the occurrence of the serrated yielding were observed, as shown in Fig. 6-18 and Table 6-3. The decrease in the SRS is more significant after pre-ageing at 100 ºC for 2 h than after pre-ageing at 200 ºC for 20 s. This result is not unexpected since pre-ageing at 200 ºC for 20 s results in a greater subsequent natural ageing response than does pre-ageing at 100 ºC for 2 h. Comparing Fig. 6-18 to Fig. 5-6 and Fig. 5-16, it can be seen that Cu additions can decrease the SRS after pre-ageing so significantly that serrated yielding can more readily observed in the Cu-containing alloys (see Table 5-1 and Table 6-3). Furthermore, the dependence of Θ-σ on the true plastic strain of the alloys in the different conditions is shown in Fig. 6-19. For alloy A7, the pre-aged samples showed a lower Θ-σ level than the samples without pre-ageing. Therefore, based on the criterion for the onset of PLC instability, the pre-aged samples are more prone to the PLC effect. For alloy A8, the pre-aged samples must have a lower SRS than the samples without pre-ageing to promote the occurrence of the PLC effect. For alloy A10, pre-ageing has little influence on the Θ-σ level, which means pre-ageing is not expected to influence the condition for the occurrence of the PLC effect. A similar strain rate hardening behaviour observed in the pre-aged Cu-containing alloys similar to that observed in the Cu-free alloys suggests that the same mechanism is operating.

Moreover, the decreased strain rate hardening capability of Cu-containing alloys after pre-ageing was found to correspond with a decrease in the post-uniform elongation and stretch formability, as shown in Figs. 6-11 and Fig. 6-20, respectively.
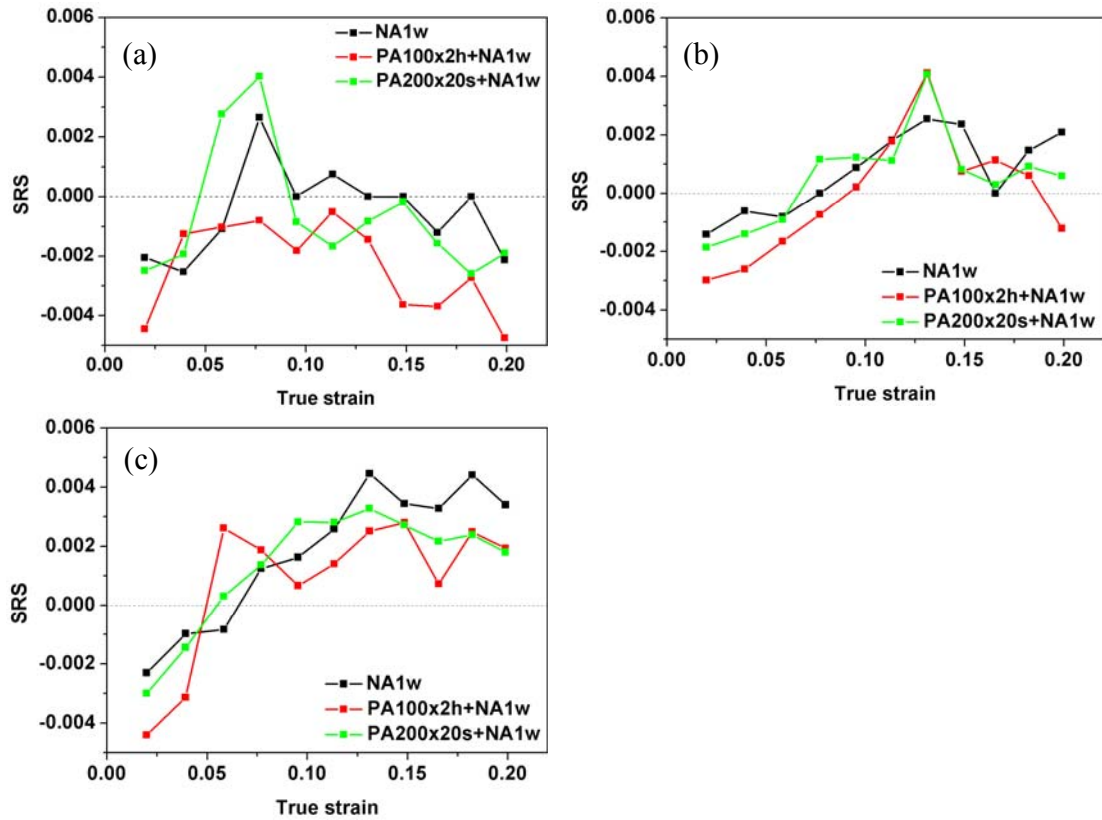
Fig. 6-18 The dependence of the SRS of the flow stress on the true strain for alloys (a) A7, (b) A8 and (c) A10.

Table 6-3 The observation of serrated yielding in the Cu-containing alloys.

Alloys	NA1w	PA100x2h+NA1w	PA200x20s+NA1w
A7	+	+	+
A8	-	+	-
A10	-	-	-

Note: - denotes that no serrated yielding was observed, + denotes that serrated yielding was observed.
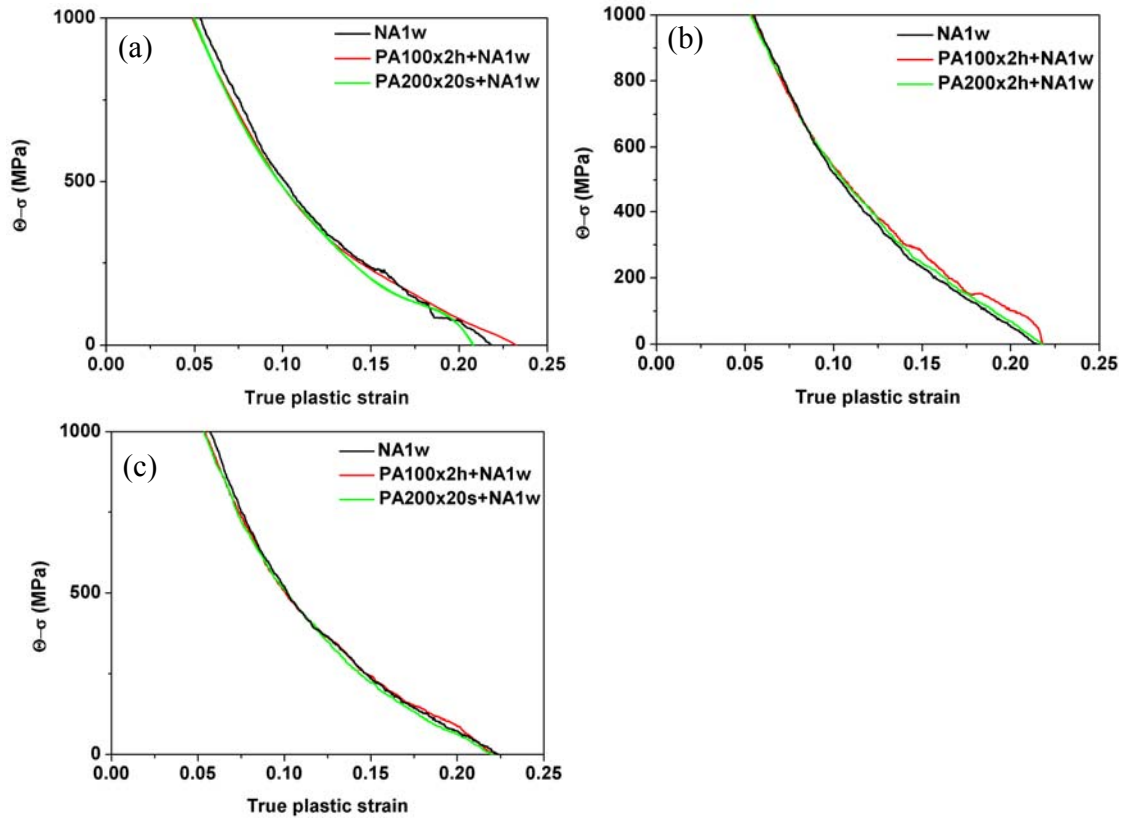
Fig. 6-19 The dependence of (Θ-σ) on the true plastic strain for the Cu-containing alloys (a) A7, (b) A8 and (c) A10.
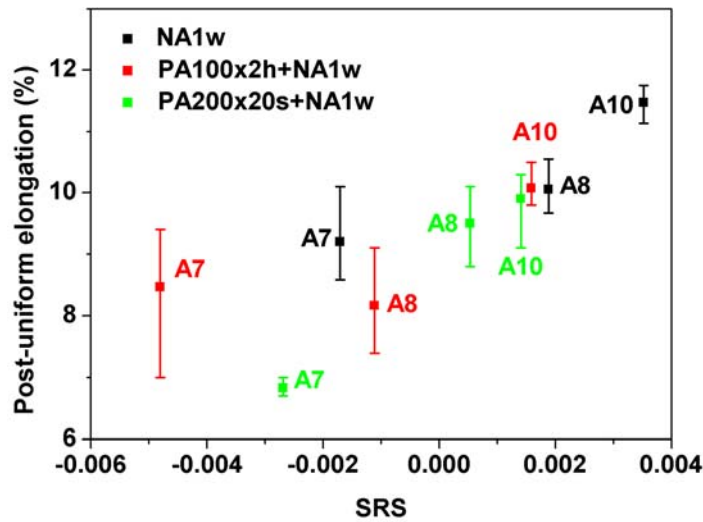
Fig. 6-20 The dependence of post-uniform elongation on the SRS at a strain of 0.2 for the Cu-containing alloys.

6.3.2 Work hardening behaviour

The average work hardening exponent (n-value) in the simplified description of work hardening by a power-law strain dependence of the flow stress (Ludwik equation) and the instantaneous work hardening exponent at the uniform strain ($n_{\varepsilon u}$) for the alloys after one week of natural ageing are shown in Fig. 6-21. It can be seen that alloying with Cu always enhances the work hardening capability regardless the magnitude of the Mg/Si ratio in the alloys. This is consistent with what is reported in reference [13]. The increased work hardening capability by Cu additions was also reported in reference [139]. Furthermore, comparing Fig. 6-21 with Fig. 6-7c, it can be found that the dependence of uniform elongation on the Mg/Si ratio is closer to the dependence of and $n_{\varepsilon u}$ on that ratio than to the Mg/Si dependence of the n-value. This further suggests that $n_{\varepsilon u}$ is a more suitable characteristic than the average n-value as a measure of the work hardening capability.
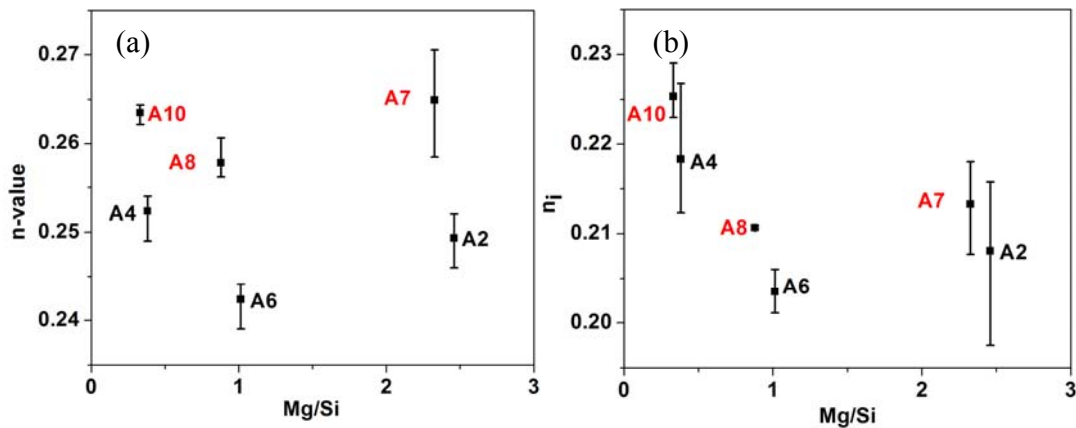
Fig. 6-21 (a) n-value and (b) n_i at uniform strain for the alloys after one week of natural ageing.

Further, the work hardening rate curves for the alloys after one week of natural ageing were examined. As shown in Fig. 6-22a, at first glance, the strain dependence of the work hardening rate is very similar for all the alloys. However, if the region near the onset of necking is enlarged, some differences are observed. As shown in Fig. 6-22b, the addition of Cu slightly increased the work hardening rate at strains close to the onset of necking. It is interesting to see that the alloys with Cu can still maintain a high work hardening rate at large strains after the onset of necking (except for alloy A7), which is believed to be important for the stretch formability [7, 16]. For alloy A7, after the onset of necking, the work hardening

rate dropped rapidly. This may be due to a negative SRS, which strongly counters the intrinsic work hardening capability [7].
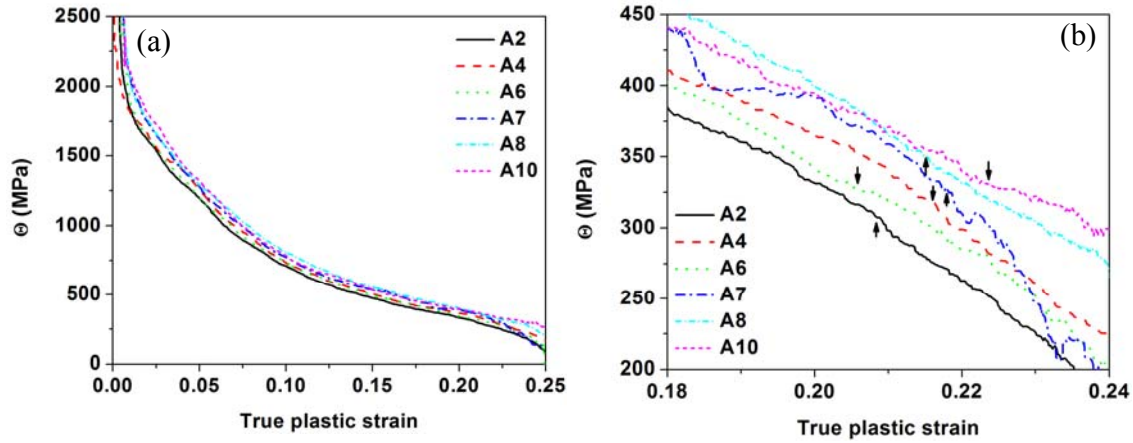
Fig. 6-22 (a) The dependence of work hardening rate on true plastic strain for the different alloys and (b) an enlarged view of (a) at strains close to uniform strains. The alloys were naturally aged for one week. Arrows in (b) indicate the uniform strain determined by the Considère necking criterion.
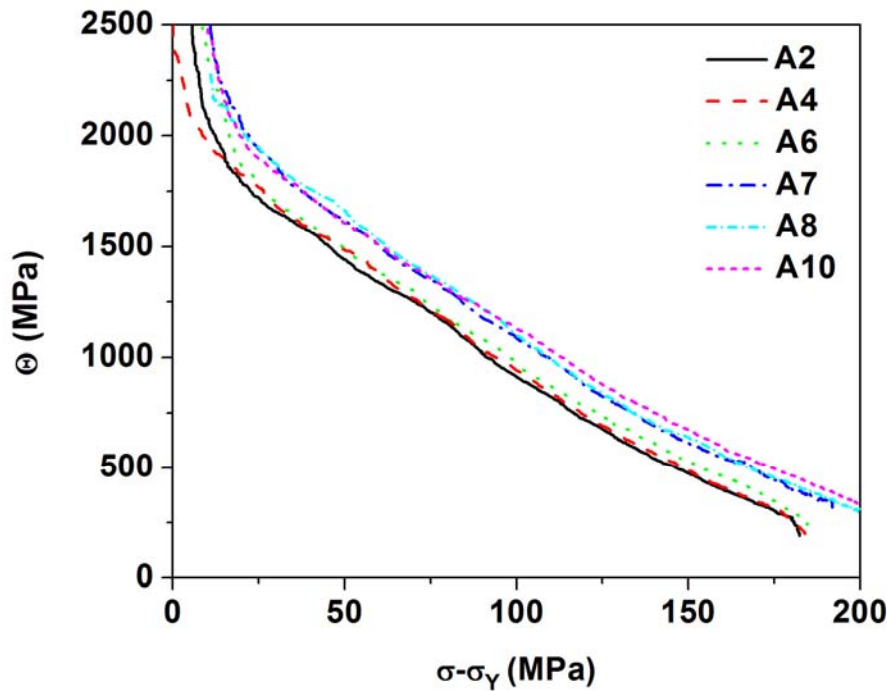
Fig. 6-23 The dependence of work-hardening rate on the flow stress (Kocks-Mecking plot). The alloys were naturally aged for one week.

The Kocks-Mecking plots for the alloys after one week of natural ageing are shown in Fig. 6-23. The graphs demonstrate that the addition of Cu raises the initial work-hardening rate significantly, but has little influence on the dynamic recovery rate.

Immediate observation of the experimental data obtained reveals some differences in the work hardening behaviour of these alloys. Still, a more detailed analysis involving modelling of the deformation behaviour of the alloys is required to establish the different contributions of microstructural features on the amount of work hardening. The Kocks-Mecking-Estrin model [39] was used to study the effect of Cu on the work hardening behaviour. The same procedure as the one employed in the Cu-free alloys was performed to determine the effect of Cu on the modelling parameters in Eq. 2-5. The contributions of dispersoids on the yield stress are listed in Table 6-4.

Table 6-4 Yield strength and σ_n of alloys A7, A8 and A10 after 1 week of natural ageing.

Alloy	Yield strength (MPa)	σ_n (Mpa)
A7	135	3.6
A8	157	4.6
A10	137	5.1

Fig. 6-24 shows the dependence of the coefficients k, k_1 and k_2 in the evolution equation for the dislocation density as determined by fitting the experimental curves to Eq. 2-5, on the magnitude of the Mg/Si ratio of the alloys. As shown in this figure, with decreasing Mg/Si ratio, a slightly higher k-value is found. This is attributed to the higher number density of dispersoids in the lower Mg/Si ratio alloys. It is interesting to note that k_1 slightly increases with decreasing Mg/Si ratio, and k_1 is markedly increased by the addition of Cu. In the classic work hardening theory, k_1 is independent of the solute content [39], although recent studies showed that k_1 can be influenced by the solute content (e.g. Cu content in Al alloys) [15] through its influence on k_1. As for the dynamic recovery rate k_2, there is a tendency that k_2 slightly decreases with growing Mg/Si ratio. The addition of Cu slightly reduces k_2 for alloys A2 and A6, but has no effect on alloy A4. These results explain, in terms of the Kocks-Mecking-Estrin model, why Cu additions can increase the work hardening capability of the alloys: the cause of increased strain hardening is that the addition of Cu can significantly increase the dislocation storage rate.
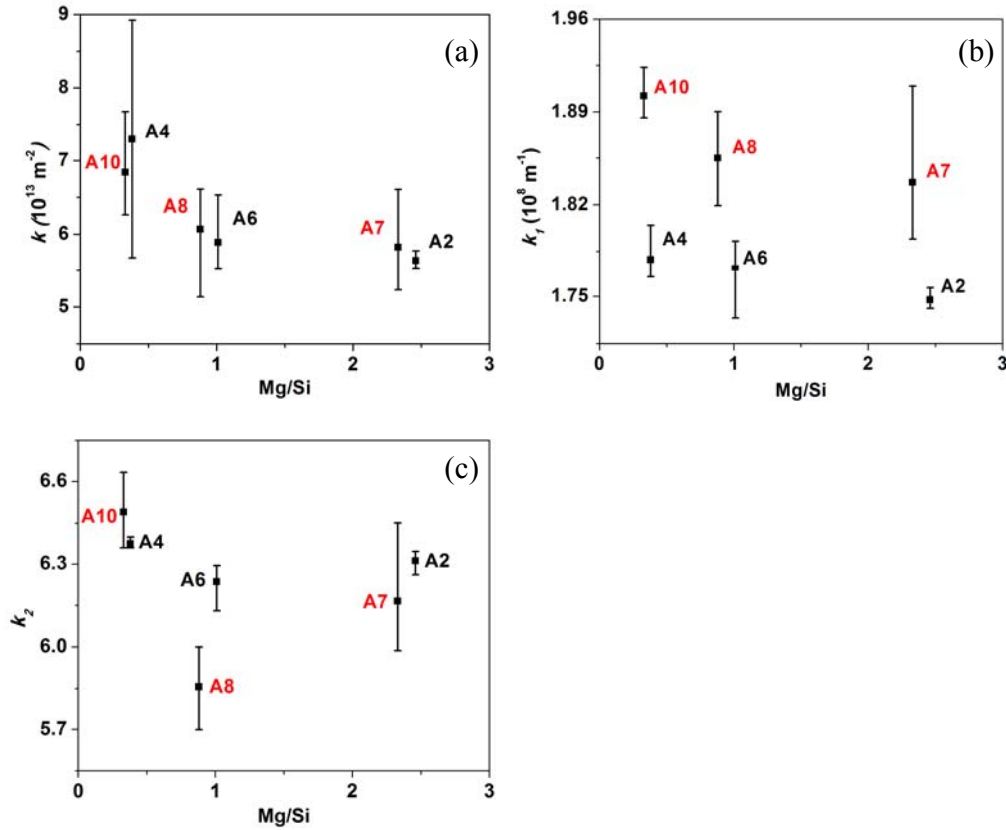
Fig. 6-24 The influence of Mg/Si ratio and Cu content on the parameters
(a) k, (b) k_1 and (c) k_2

Pre-ageing has a different influence on the work hardening capability of the Cu-containing alloys with different levels of the Mg/Si ratio, as shown in Fig. 6-25. For the low Mg/Si ratio alloy A10, pre-ageing slightly decreases $n_{\varepsilon u}$. Accordingly, a decrease in the uniform elongation and stretch formability were observed, as shown in Fig. 6-9c. For the medium Mg/Si ratio alloy A8 and the high Mg/Si ratio alloy A7, pre-ageing can even slightly increase $n_{\varepsilon u}$ (except for alloy A7 pre-aged at 200 ºC for 20 s). Comparing work hardening exponent results with the uniform elongation results for alloys A7 and A8 (see Fig. 6-9c), it is evident that the uniform elongation of alloys A7 and A8 is determined by work hardening capability.
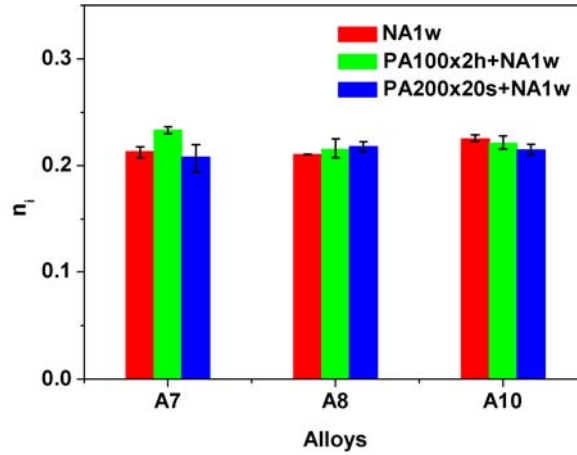
Fig. 6-25 Effect of pre-ageing on n_i at the uniform strain for alloys A7, A8 and A10 with and without pre-ageing as indicated.

The work hardening rate vs. strain curves for the pre-aged alloys are shown in Fig. 6-26. As seen in the figure, pre-ageing has little effect on the work hardening rate before the onset of necking, but slightly reduces the work hardening rate at the uniform strain. After the onset of necking, a faster decrease in the work hardening rate was observed in the pre-aged alloys than in the alloys without pre-ageing. As indicated above, this may be due to the low SRS (except for alloy A7 pre-aged at 100 ℃ for 2 h). For alloy A7 pre-aged at 100 ℃ for 2 h, the material has the ability to maintain the work hardening rate (albeit at a low level) up to relatively high strains, which is similar to alloy A3 pre-aged at 100 ℃ for 2 h. In these two alloys, a pronounced PLC effect was observed in the samples pre-aged at 100 ℃ for 2 h.
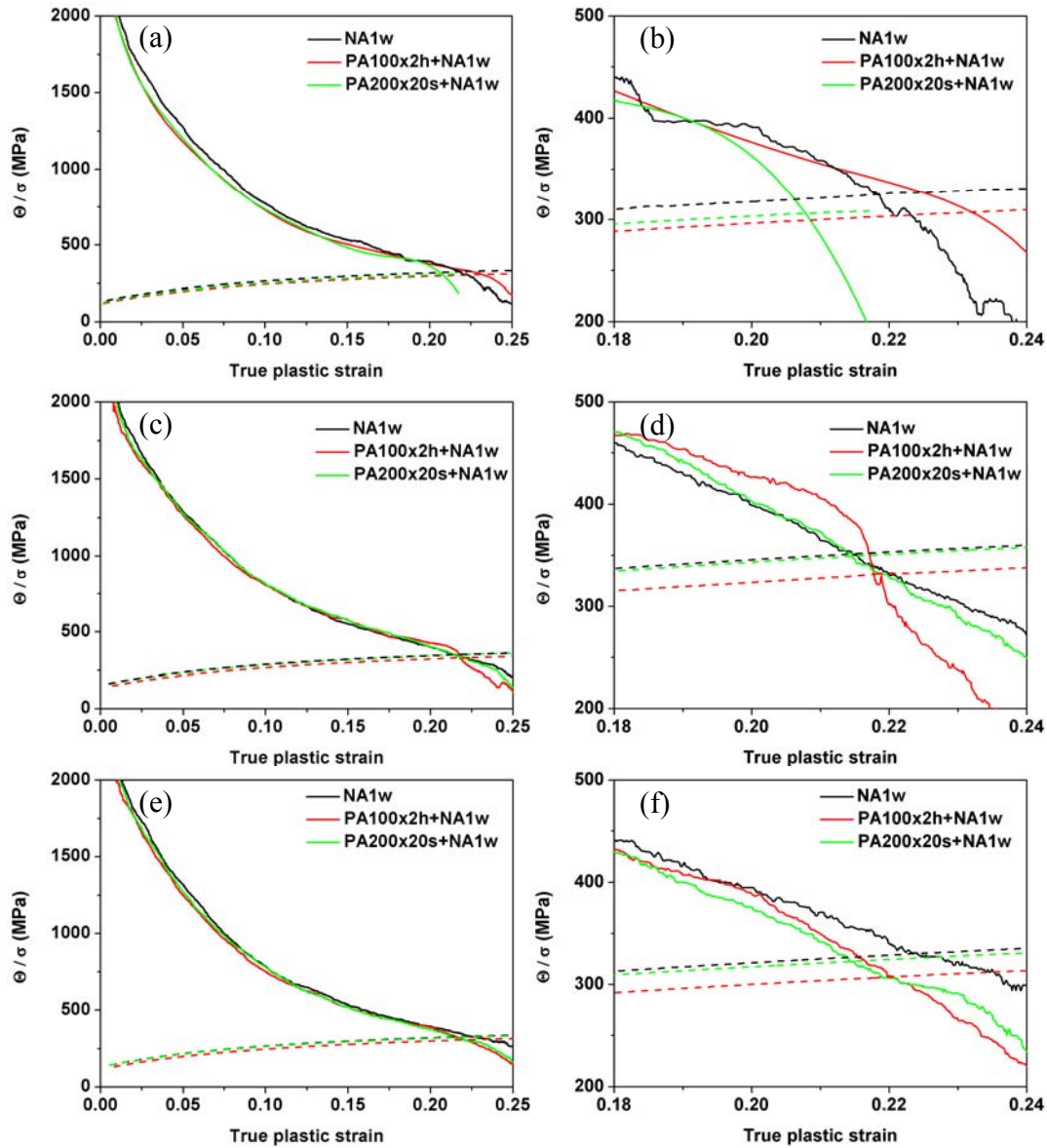
Fig. 6-26 Effect of pre-ageing on the work hardening rate curves of Cu-containing alloys (a, b) A7, (c, d) A8 and (e, f) A10. (b, d, f) are enlarged views of (a, c, f).
Note: the solid curves are work hardening rate curves, and dashed curves in the same color as solid curves are corresponding flow stress curves.

The Kocks-Mecking plots for Cu-containing alloys in the different tempers are shown in Fig. 6-27; the corresponding initial work hardening rate and dynamic recovery rate are presented in Fig. 6-28. At first glance, it appears pre-ageing has a noticeable influence on the initial

work hardening rate, while its effect on the dynamic recovery rate is small, as shown in Fig. 6-27. Detailed analysis on Fig. 6-27 reveals that pre-ageing slightly decreases the initial work hardening rate, but has little effect on the dynamic recovery rate (see Fig. 6-28). Therefore, in most cases, pre-ageing was found to have little influence on the uniform elongation or to slightly reduce it (except for alloy A7 pre-aged at 100 ºC for 2 h). One possible reason for the increased uniform elongation in alloy A7 pre-aged at 100 ºC for 2 h is a strong serrated yielding which inhibits the dynamic recovery process [44], thus leading to an increased work hardening capability [143, 144].

Therefore, pre-ageing was found to reduce the stretch formability of the Cu-containing alloys. This is associated with reduced work hardening and strain-rate hardening capabilities, especially the latter.
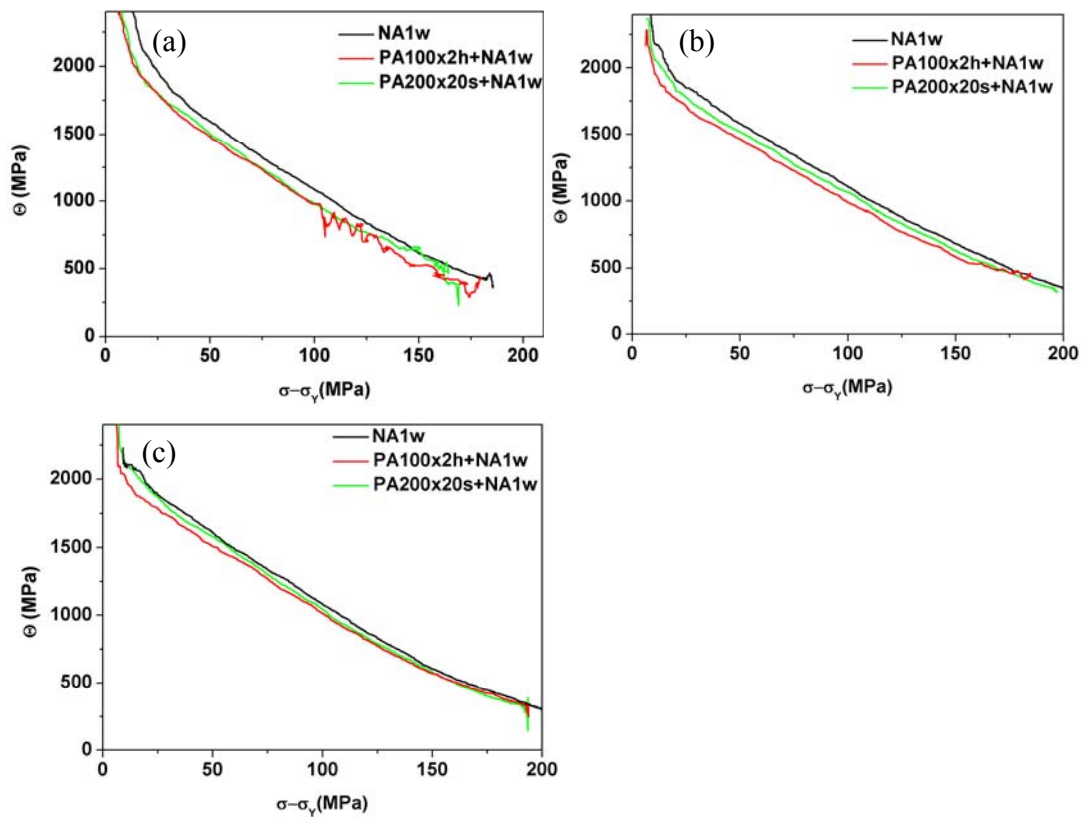
Fig. 6-27 Effect of heat treatment on the Kocks-Mecking plots for alloys (a) A7, (b) A8 and (c) A10.
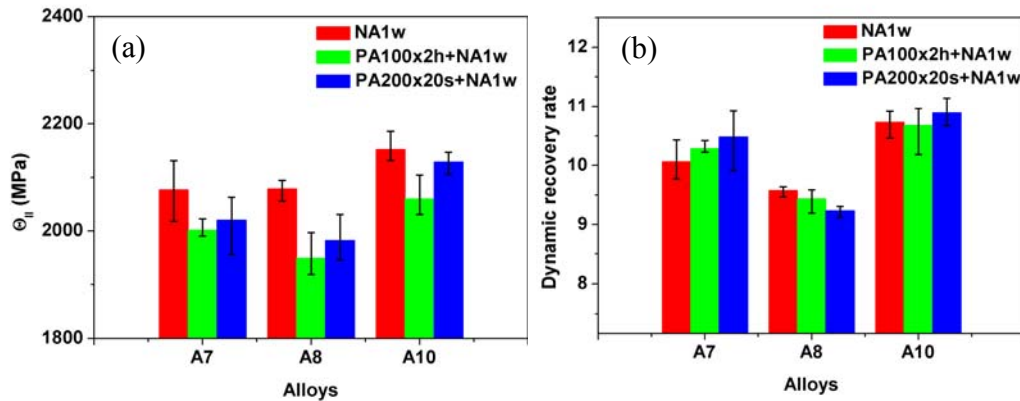
Fig. 6-28 Effect of heat treatment on the (a) initial work hardening rate and (b) dynamic recovery rate of the Cu-containing alloys

6.4 Summary

In this chapter, three alloys (A7, A8 and A10), which are Cu-containing versions of alloys A2, A6 and A4, respectively, were studied. The Cu-containing alloys were either naturally aged or pre-aged prior to natural ageing (the heat treatment parameters being similar to those employed for their Cu-free counterparts). The work hardening and strain rate hardening behaviour of the alloys was characterised to correlate the microstructural features with the formability. It was found that the addition of 0.3 wt.% Cu slightly decreases the strain rate sensitivity of the alloys, especially those with high magnitude of the Mg/Si ratio. The observed decrease in the strain rate hardening capability is believed to be associated with the high solute content and the retardation of natural ageing in the Cu-containing alloys. Despite this, alloying with Cu still enhances the stretch formability of the naturally aged alloys due to the increased work hardening capability. The enhancement of the work hardening rate stems from increased dislocation storage rate owing to copper content. However, this improvement in the stretch-formability diminishes with decreasing Mg/Si ratio, which suggests that the influence of strain rate hardening on the formability becomes more important at lower Mg/Si ratios. Pre-ageing of these alloys lowers their formability due to a decrease in their work hardening (except for alloy A7) and strain rate hardening capabilities. For the high Mg content alloy A7, pre-ageing at 100 ºC for 2 h even improved the work hardening capability. This is most likely due to a strong DSA effect in this alloy. Notwithstanding, this increased

work hardening pre-ageing at 100 ºC for 2 h resulted in a drop of the formability of alloy A7 due to a concomitant loss in strain rate hardening capability.

Chapter 7: Thermodynamic Modelling

7.1 Introduction

Based on the findings discussed so far, a high Si content is needed to maintain a high stretch formability, a high Si content in the 6xxx alloys is needed. Not only does an increase in the Si content raise the work hardening capacity of an alloy due to a decrease in the dynamic recovery rate, but it also enhances strain rate hardening by facilitating the formation of clusters that remove mobile solute atoms and vacancies from the solid solution. Furthermore, by increasing the Si content of the alloy, a high number density of dispersoids is promoted, which increases the storage rate of geometrically necessary dislocations. Collectively, these effects act to improve the stretch formability of the alloys. Moreover, the addition of Cu was also found to improve the stretch formability of the alloys due to the increased dislocation storage rate, especially in the alloys with medium and high Mg/Si ratios.

The High Mg content alloy A2 showed the lowest stretch formability among the alloys studied. However, the Mg and Si content of alloy A2 is out of the typical composition limit for Mg and Si in the commercial 6xxx alloys used for automotive panel applications. Therefore it is worthwhile to investigate whether the formability of alloy A2 can be improved by adjusting the alloy composition. This would provide information for the development of new 6xxx alloys for automotive body panels. To meet this end, thermodynamic modelling was employed to predict a microstructure that could improve the formability of alloy A2.

7.2 Results and discussion

7.2.1 Effect of alloy composition

Fig. 7-1 shows the influence of Mg, Si, Mn and Cu contents on the amount of undissolved Mg_2Si and Al(Fe,Mn)Si phases, as well as on the Si and Mg contents in solution in alloy A2 at 540 °C, as modelled by Thermocalc. It should be noted that the current Thermocalc predictions do not discriminate between fine-scale dispersoids and coarse Fe-phase particles. Hence Al(Fe,Mn)Si may refer to either, and the relative amount of each will depend on the processing history. Nevertheless, a predicted increase in the amount of Al(Fe,Mn)Si is

expected to result in an increase in the amount of fine-scale dispersoids, if the Si concentration in the matrix is predicted to increase. This has been confirmed experimentally as listed in Tables 4-1 and 4-2. Moreover, there are two reasons to perform the thermodynamic modelling at 540 °C. Firstly, it is believed that Al(Fe,Mn)Si dispersoids are mainly formed during the homogenisation treatment [81]. In this study, the maximum homogenisation temperature was 540°C. Secondly, it appears that the solution treatment at 550 °C for 30 min employed in this study can only dissolve the finer Mg_2Si particles (which probably were formed during the thermo-mechanical treatment after homogenisation [26]), while the coarse Mg_2Si particles, due to the insufficient solution treatment, still remain undissolved, as shown in Figs. 4-1a and 7-2. Even though the solution treatment temperature is 10°C higher than the homogenisation temperature, there should be very little difference between the equilibrium values at 540 °C and the actual value after only 30 min at 550 °C because the solvus temperature is close to 550 °C and therefore the dissolution rate at this temperature is sluggish. Moreover, one should also consider that the solution treatment time is only 30 min, which may not bring the system to the equilibrium state at 550 °C.

As shown in Fig. 7-1, the microstructure of alloy A2 is expected to be modified by composition modifications. More precisely, decreasing the Mg content in alloy A2 can increase the amount of Al(Fe,Mn)Si slightly and reduce the amount of undissolved Mg_2Si (Fig. 7-1a). Decreasing the alloy Mg content is also predicted to raise the amount of Si in solid solution due to the release of Si from the undissolved Mg_2Si, as well as to decrease the amount of Mg in solution (Fig. 7-1b). This could enhance the natural ageing kinetics and the precipitation conditions for dispersoids. Not only does the increased Mn content effectively promote the formation of Al(Fe,Mn)Si, but it can also reduce the formation of undissolved Mg_2Si (Fig. 7-1c). However, an increase in the Mn content is also predicted to increase the amount of Mg and reduce the amount of Si in solid solution (Fig. 7-1d), which may reduce the SRS of the flow stress. Furthermore, the amounts of both Al(Fe,Mn)Si and undissolved Mg_2Si are predicted to rise with increasing Si content in the alloy (Fig. 7-1e). This increase in Si content would also raise the amount of Si in solution and diminish the amount of Mg in solution (Fig. 7-1f). This would increase the SRS of the flow stress of the alloy after one week natural ageing. It appears that the influence of Cu on the amounts of phases and the solute concentrations in the matrix is relatively small compared to that of other elements.

Nevertheless, adding Cu to alloy A2 is predicted to decrease the amount of Mg_2Si, thus slightly promoting the formation of Al(Fe,Mn)Si and increasing the Mg and Si concentrations in the matrix (Fig. 7-1g, h). This suggests that adding Cu to alloy A2 may improve the stretch formability due to the increased amount of Al(Fe,Mn)Si and Si concentration in the matrix. However, it should be noted that the increasing Cu content is also predicted to increase the Mg concentration in the matrix, which may decrease the SRS of the flow stress and formability. In fact, the addition of Cu (alloy A7) did improve the stretch formability of alloy A2, due to the increased dislocation multiplication by Cu atoms. While it appears other factors (amount of Al(Fe,Mn)Si and the Mg and Si concentrations in the matrix) had little influence on the stretch formability of alloy A2.
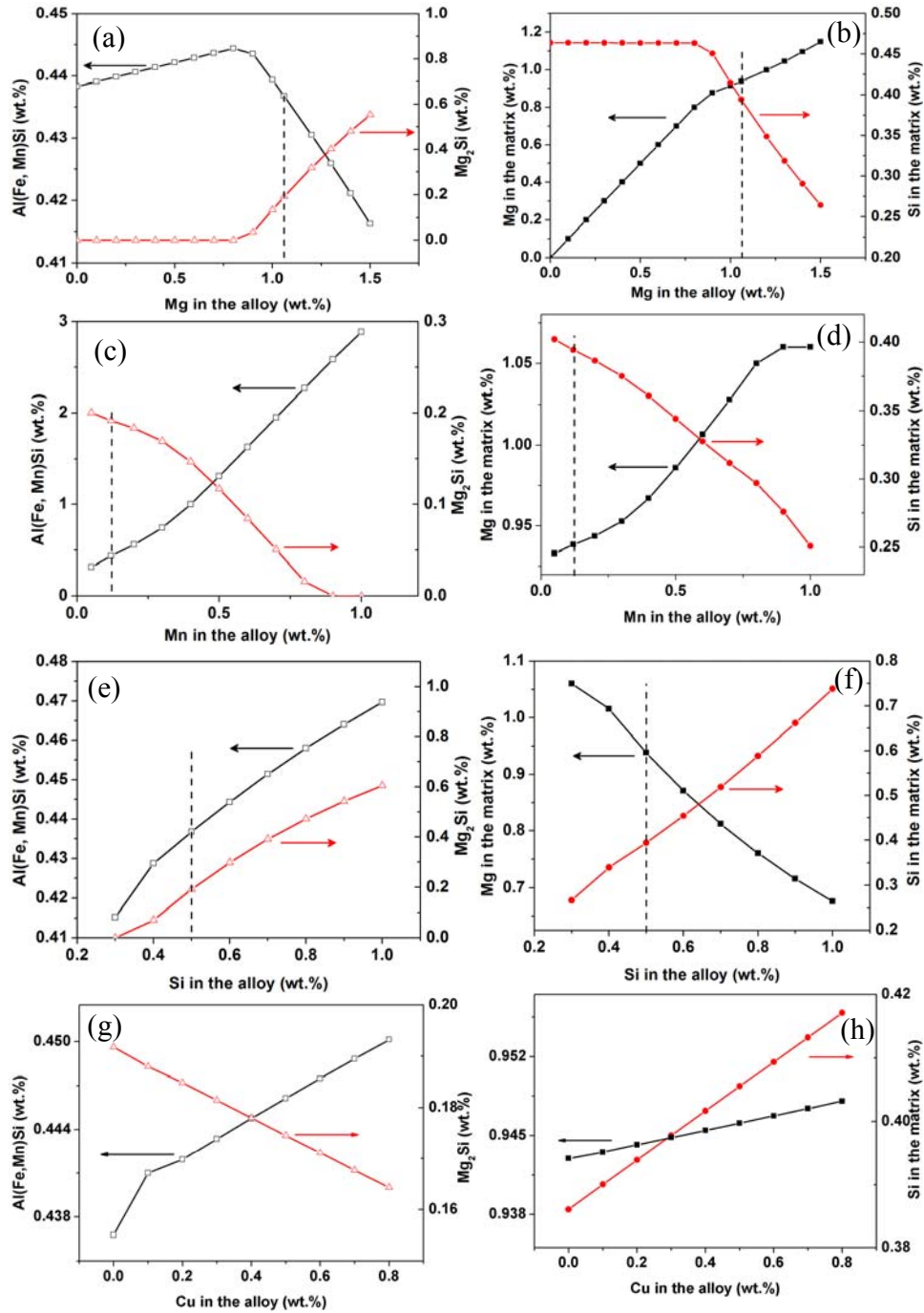
Fig. 7-1 Influence of (a,b) Mg (c, d) Mn, (e, f) Si and (g, h) Cu content on the amount of undissolved Al(Fe,Mn)Si and Mg$_2$Si, as well as the amount of Si and Mg in solid solution for alloy A2 at 540 °C predicted by Thermocalc. The vertical dashed lines represent the composition of alloy A2.
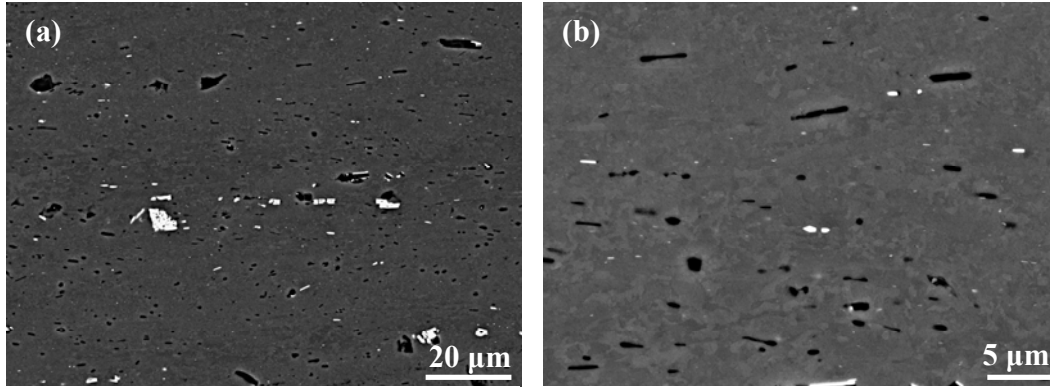
Fig. 7-2 (a) Backscattering SEM image showing Mg_2Si (black) and Fe-containing phase (white) in as-rolled alloy A2 (b) enlarged view of (a).

7.2.2 Effect of homogenisation/solution treatment temperature

The effect of homogenisation/solution treatment temperature on the amount of undissolved phases and solute concentration in the matrix of alloy A2 is shown in Fig. 7-3 (for a scenario where the homogenisation temperature is the same as the solution treatment temperature). As shown in Fig. 7-3, the Mg_2Si phase is predicted to be fully dissolved into the matrix at 560 °C. Therefore, the Mg content in the matrix reaches a maximum at 560 °C. The Si content in the matrix almost reach maximum at 560 °C, and further increasing the temperature does not significantly increase the Si concentration in the matrix. It should be noted that melting is expected to start when the temperature is higher than 600 °C. The increased Mg and Si concentrations in the matrix are expected to increase the natural ageing response, therefore resulting in a higher SRS after one week of natural ageing. The increased solute concentration should also increase the work hardening capability of the material. Apart from the solute effects, increasing the solution treatment temperature is also expected to increase the amount of quenched-in-vacancies (for a give fast quench rate). This would further increase the natural ageing response. As for the Al(Fe,Mn)Si phases, it is predicted that the equilibrium amount of Al(Fe,Mn)Si phases will decrease with increasing temperature. This suggests that a high homogenisation temperature is not good for the precipitation of Al(Fe,Mn)Si dispersoids, which is consistent with the reported findings in the reference [81]. In reference [81], the number density of dispersoids was reported to decrease with increasing homogenisation temperature. Although a high number density of dispersoids was reported to homogenise the dislocation slip [54], based on the Kocks-Mecking-Estrin model, the

contribution of dispersoids to the work hardening is much smaller than that of solute atoms. Therefore, even though a higher temperature would decrease the amount of Al(Fe,Mn)Si particles, the increased solute concentration would still enhance the work hardening capability.
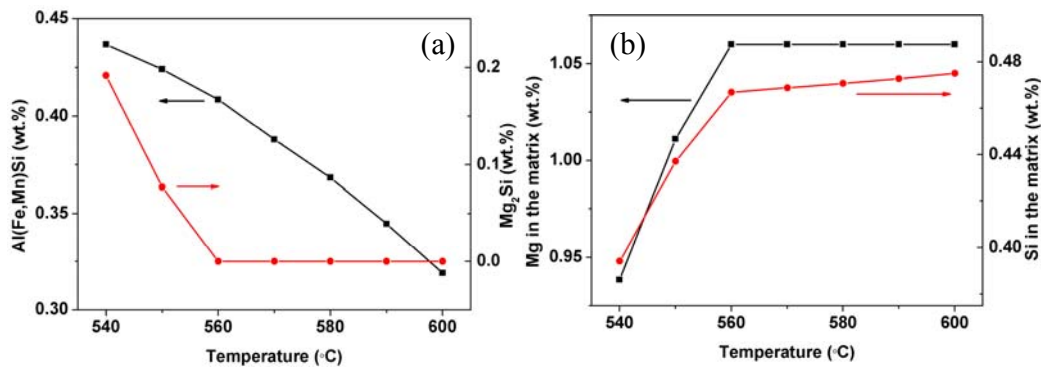
Fig. 7-3 Effect of solution treatment temperature on the amount of undissolved Al(Fe,Mn)Si and Mg_2Si, as well as the amount of Si and Mg in solid solution for alloy A2.

7.3 Summary

Thermodynamic modelling was employed to predict microstructures that could improve stretch formability of the high Mg content alloy A2. It was found that decreasing the alloy Mg content is predicted to decrease the amount of Mg in solution and to increase the amount of Si in solid solution due to the release of Si from any undissolved Mg_2Si. This could enhance the natural ageing kinetics and the precipitation conditions for dispersoids, thus improving the stretch formability of alloy A2; An increased Mn content has two effects: (i) it effectively promotes the formation of Al(Fe, Mn)Si, and (ii) it can reduce the amount of undissolved Mg_2Si. However, an increase in the Mn content is also predicted to increase the amount of Mg and reduce the amount of Si in solid solution, which may reduce the SRS of the flow stress. It appears whether Mn can improve the formability depending on which factors (the increased amount of Al(Fe, Mn)Si and the variation of solute concentration in the matrix) are more important. Furthermore, the amounts of both Al(Fe, Mn)Si and undissolved Mg_2Si are predicted to rise with increasing Si content in the alloy. This increase in Si content would also raise the amount of Si in solution but decrease the amount of Mg in solution. This would increase the SRS of the flow stress of the alloy after one week natural ageing. Therefore, an

increased Si content is expected to improve the stretch formability of alloy A2. Adding Cu to alloy A2 is also predicted to modify the microstructures, which could influence the formability. Moreover, increasing the homogenisation and/or solution treatment temperatures would also improve the stretch formability, due to the increased solute concentration in the matrix.

Chapter 8: Conclusions and Recommendations for Future Work

8.1 Conclusions

The ultimate goal of this study was to determine the mechanisms underlying the effect of alloy composition and heat treatment on the stretch formability of 6xxx alloys. To meet this goal, eight 6xxx alloys with systematically varying Mg, Si, Cu contents and magnitude of the Mg/Si ratio were studied. The alloys were either naturally aged or were subjected to pre-ageing at 100 ºC for 2 h or at 200 ºC for 20 s prior to natural ageing. The following conclusions about the mechanisms governing stretch formability of 6xxx alloys can be drawn.

- **Increasing the Si content of the alloy significantly improves the stretch formability of the alloys due to the increased work hardening and strain rate hardening capabilities.**

Not only does an increase in the Si content (alloys A3 to A4, and further to A5) raise the work hardening capacity of an alloy due to a decrease in the dynamic recovery rate, but it also enhances strain rate hardening by facilitating the formation of clusters that remove mobile solute atoms and vacancies from the solid solution. Furthermore, by increasing the Si content of the alloy, the occurrence of a high number density of dispersoids is promoted, which increases the storage rate of geometrically necessary dislocations. Collectively, these effects act to improve the tensile ductility and stretch formability of sheet products manufactured from these alloys.

- **Increasing the Mg content of the alloy has little influence on the tensile ductility and stretch formability.**

Increasing the alloy Mg content (from alloy A3 to A2) has little influence on the work hardening capability and slightly decreases the strain rate hardening capability. The decrease in the strain rate hardening is due to a strong interaction between Mg atoms and mobile dislocations, which provides a large negative contribution of dynamic strain ageing to the strain rate sensitivity of the flow stress. The overall effect of work hardening and strain rate

hardening resulted in little improvement in the tensile ductility and stretch formability with increasing Mg additions.

- **<u>Decreasing the Mg/Si ratio improves the tensile ductility and stretch formability.</u>**

Decreasing the Mg/Si ratio (from alloys A2 to A6, and further to A4) can increase work hardening capability, due to the increased dislocation storage. Decreasing the Mg/Si ratio can also improve the strain rate hardening capability, which is associated with enhanced natural ageing kinetics that speeds up the removal of mobile solutes and vacancies form the matrix. As a result, the stretch formability was found to be improved by decreasing the magnitude of the Mg/Si ratio.

- **<u>The addition of Cu leads to improved stretch formability due to increased work hardening capability.</u>**

Cu was found to increase the work hardening capability due to an enhancement in the dislocation storage rate. Therefore, a slight improvement in the uniform elongation was observed to result from Cu additions. However, Cu additions slightly decrease the SRS of the alloys, especially in alloys with high Mg content. The reduced SRS is associated with the increased solute content and the retardation of natural ageing by Cu. The net effect of work hardening and strain rate hardening is an improvement in the stretch formability, although this improvement tends to diminish with decreasing Mg/Si ratio.

- **<u>Although pre-ageing can significantly improve the paint-bake response after natural ageing, it deteriorates the stretch formability.</u>**

The main purpose of pre-ageing is to reduce the negative effect of natural ageing on the paint-bake response of 6xxx alloys. However, pre-ageing was found to reduce the stretch formability by decreasing the work hardening and strain rate hardening of the alloys. The decreased work hardening is due to the solute depletion in the matrix. The reduced strain rate hardening is attributed to the increased DSA, which is an unexpected result revealed by experiment. A mechanism was proposed to explain the observed strain rate hardening behaviour: after natural ageing (particularly for short ageing times), pre-aged samples may contain more vacancies than samples without pre-ageing. The excess vacancies may exist as

mobile solute-vacancy complexes or be bound with co-clusters, depending on the pre-ageing time. These excess vacancies increase the magnitude of DSA in pre-aged and subsequently naturally aged samples.

- **Solutes in solution are the major factor that controls the stretch formability.**

Solutes (i.e. Si, Mg and Cu) in solution are the most important factor governing the stretch formability of 6xxx alloys through their effect on the work hardening and strain rate hardening capabilities.

For work hardening, the Kocks-Mecking-Estrin model provides a way to separate the individual contributions of different microstructural features (i.e. solutes and dispersoids) on the amount of work hardening. Solutes are the major factor that influences the work hardening behaviour. Among Si, Mg and Cu alloying elements, Cu is the most efficient element for increasing the dislocation storage rate. The second and third ones are Si and Mg, respectively. Both Si and Mg atoms increase the work hardening rate by reducing dynamic recovery, owing to their inhibiting effect on dislocation cross-slip. Cu has little influence on dynamic recovery, but contributes efficiently to work hardening still. Thus, as was shown in Chapter 6, alloying with Cu raises the stage II hardening rate, as reflected in the increased dislocation storage coefficient k_1.

Although work hardening provides a positive contribution to the SRS, DSA is also a crucial factor, as it gives rise to a negative contribution to the SRS. The degree of DSA is determined by the specific solute species involved and its concentration. For instance, Mg atoms increase DSA more strongly than Si and Cu atoms do, which is due to a strong interaction between Mg atoms and mobile dislocations. The degree to which a specific solute species influences the natural ageing kinetics will also influence the magnitude of DSA. As discussed in Chapter 5, sluggish natural ageing kinetics normally leads to more pronounced DSA, which is the case in the alloys with high Mg and/or Cu contents. By contrast, a high Si content enhances the natural ageing kinetics and therefore decreases the magnitude of the DSA effect.

- **Vacancies are another important factor that influences the stretch formability.**

This may be the first time that the role of vacancies as an important factor affecting the stretch formability of 6xxx alloys was highlighted. The effect of vacancies on the stretch formability is through their influence on the strain rate hardening capability. The importance of this is specially highlighted when the alloy is pre-aged. It was proposed that pre-aged samples should contain more vacancies than samples without pre-ageing. This degrades the strain rate hardening capability and therefore decreases the formability.

- **The formability of high Mg content 6xxx alloy can be improved by alloy composition adjustments.**

Based on the knowledge derived from the experimental and constitutive modelling results, thermodynamic modelling was shown to be a very useful tool for designing an alloy with improved formability. The thermodynamic modelling results suggest that the stretch formability of the high Mg content alloy A2 could be improved by increasing increasing the Si, Cu and Mn contents and/or decreasing the alloy Mg content in the alloy.

In fact, while the high Mg content 6xxx alloy A2 showed an inferior stretch formability, the addition of Cu to alloy A2 was found to improve the formability of alloy A2 to a level similar to that of the high Si content alloys. Another interesting feature is that the addition of Cu to alloy A2 did not increase the yield strength. In other words, with Cu, the high Mg content alloy still has a similar strength level as the high Si content alloy. This means that, with Cu, the Mg-rich 6xxx alloy A2 has the same potential for automotive outer panels as the conventionally used Si-rich alloys. However, another issue arising from the addition of Cu is that of potential surface quality problems after forming due to the occurrence of the PLC effect. This issue may be solved by decreasing the Mg content and/or increasing the Si content slightly. It may also be avoided by controlling the strain rate during stamping. Although the thermodynamic modelling results suggest that the stretch formability of alloy A2 can be improved by compositional adjustments, possible issues related to other aspects of formability arising from the improved stretch formability should also be considered.

- **Comments on the current commercial alloys for automotive outer panels.**

This work has provided a rationale for the fact that most of the commercial 6xxx alloys for automotive panels are Si-rich alloys (i.e. 6016 and 6022) rather than Mg-rich alloys. From a formability point of view, this is because Si-rich alloys exhibit a superior stretch formability.

Moreover, practically, the original purpose of adding Cu to the medium Mg/Si ratio alloy 6111 was to improve the paint-bake performance [138]. In this study, the addition of Cu was also found to be beneficial to the stretch formability. However, the addition of Cu in alloys with a medium Mg/Si ratio (e.g. A8) can significantly increase the strength. Therefore, the bending performance of alloy 6111 is worse than that of alloys 6016 and 6022 [21] since a bad bending performance tends to correlate with a high yield strength [10] and the yield strength of the former material is much higher than that of the latter two materials. The addition of Cu to low Mg/Si ratio alloys was found not to increase the stretch formability or the strength. Therefore, in alloys 6016 and 6022 (low Mg/Si ratio alloys), the Cu content is much lower than that in medium alloy Mg/Si ratio alloys like 6111.

As a general conclusion, it can be stated that the current study has provided a substantial database for an important range of Al alloys of the 6xxx series in terms of their mechanical properties and formability. The effect of the composition, particularly the Mg/Si ratio and alloying with Cu, and ageing regimes on the work hardening and strain rate hardening behavior and the ensuing uniaxial ductility and stretch formability of the alloys has been thoroughly investigated. The value of the thesis is seen in a mechanism-based interpretation of the observed material behaviour. The results provide information for a rational approach to alloy selection for automotive body panel applications. However, it should be noted that the technical processes employed in this study are different from industrial processes (e.g. lab-scale permanent mold casting *vs.* industrial direct-chill casting, and differences in some other processing parameters). This means that any attempts to use the experimental results from this PhD project for industrial purposes should not be made without considering these differences.

8.2 Recommendations for future work

8.2.1 The role of vacancies in the increased DSA observed after pre-ageing

In Chapter 5, a higher vacancy concentration in the pre-aged samples exceeding that in the samples without pre-ageing was suggested as a mechanism for the increased DSA observed in pre-aged samples. The proposed mechanism was verified by some indirect experiments (tensile testing and hardness testing), and appears to explain the proposed mechanism in terms of increased DSA in the pre-aged alloys. However, this mechanism is still somewhat speculative, and further, more elaborate, experiments are needed to verify whether the vacancy concentration in the pre-aged samples is indeed higher than in the samples which did not undergo pre-ageing. In fact, the role of vacancies in the increased DSA can be studied by positron annihilation lifetime spectroscope (PALS). PALS is a non-destructive nuclear technique which is used in solid state physics, materials science, chemistry, etc. due to its unique sensitivity to open volume defects such as atom-sized vacancies [136]. Therefore, the PALS method has been used in the study of the role of vacancies on the natural ageing processes in Al-Mg-Si alloys [145, 146], and ageing kinetics in Al-Cu alloy [147].

In future work, PALS experiments should be carried out on alloys A2 and A4 pre-aged at 100 ºC for 5 min or 2 h, and on the same alloys without pre-ageing. It was interesting to see that samples pre-aged for 5 min showed a much greater natural ageing response than samples pre-aged for 2 h during one week of natural ageing to one month of natural ageing. The excess vacancies in samples pre-aged for 5 min may exist as solute-vacancy complexes, while the excess vacancies in samples pre-aged for 2 h may be bound in co-clusters. It is believed this was the reason why a different natural ageing response was observed during one week of natural ageing to one month of natural ageing. PALS experiments would firstly help to confirm whether pre-aged samples do indeed contain more vacancies than samples without pre-ageing, and identify the locations of these vacancies. Secondly, the PALS experiments would also help determining the differences in the vacancy concentrations and locations in samples that were pre-aged for 5 min as opposed to 2 h.

8.2.2 Optimising the heat treatment parameters for industrial application

The effects of the two kinds of pre-ageing treatments considered (i.e. 2 h at 100 ºC or 20 s at 200 ºC) on the formability were investigated. It was found that pre-ageing, especially at 100 ºC for 2 h, can improve the paint-bake response of the material. However, pre-ageing was also found to decrease the stretch formability of the material (especially when the material was pre-aged at 100 ºC for 2 h), mainly due to a decrease in the strain rate hardening capability.

In order to improve the stretch formability, pre-ageing parameters must be modified to reduce the degree of decrease in the strain rate hardening capability. From Fig. 5-26, it is evident that the strain rate hardening capability can be improved if the sample is pre-aged at 100 ºC for more than 2 h or less than 30 min. However, pre-ageing for more than 2 h may lead to a decrease in the work hardening capability due to the depletion of solutes from solution. Moreover, pre-ageing for more than 2 h or less than 30 min may result in a decrease in the paint-bake response, as shown in Fig. 5-1. This suggests that both the paint-bake performance and the formability must be considered when modifying the pre-ageing parameters. Alternatively, pre-ageing at less than 100 ºC (i.e. 70 ºC) for a long time may lead to a good combination of paint-bake response and formability. An improvement in the paint-bake response by pre-ageing at 70 ºC for 17 h was reported in Reference [95]. Meanwhile, pre-ageing at less than 100 ºC for a long time may not significantly deplete the solute from solution, thereby limiting the decrease in the work hardening capability. Furthermore, pre-ageing at a low temperature for a long time may anneal out more vacancies than pre-ageing at 100 ºC for 2 h. Thus, the decrease in the stretch formability may be less than after pre-ageing at 100 ºC for 2 h. This is probably the reason why pre-ageing at 82 ºC for 8 h was employed by Alcoa to enhance the overall formability [148].

For pre-ageing treatments at 200 ºC (which are more suitable for in-line treatments), a longer pre-ageing time of about 2-5 minutes may be suitable for a good combination of paint-bake response and formability [5].

A modification of the solution treatment temperature may also be beneficial for improving the formability. In Chapter 4, it was shown that a relatively low solution treatment

temperature would promote the occurrence of the PLC effect. Thus, a high solution treatment temperature (i.e. > 550 ºC) with modified pre-ageing parameters may lead to a good combination of paint-bake response and formability.

Any future work in this respect should therefore focus on determining the optimum combinations of solution treatment and pre-ageing for given alloy compositions. Depending on the industrial application, suitable high temperature and/or low temperature pre-ageing treatments can be explored in more detail, guided by the results obtained in this thesis. Firstly, the effect of solution treatment temperature on the work hardening and strain rate hardening behaviours of naturally aged samples will be studied. A suitable solution treatment temperature will be chosen. Then the effect of pre-ageing time at relatively low temperature (i.e. 70 ~ 90 ºC) and at 200 ºC on the paint-bake response, work hardening and strain rate hardening behaviours should be studied. Several suitable pre-ageing parameters, which provide a good combination of paint-bake response, work hardening and strain rate hardening capabilities need to be chosen for further FLD tests.

References

1. W.S. Miller, L. Zhuang, et al., *Recent development in aluminium alloys for the automotive industry.* Materials Science and Engineering: A, 2000. **280**(1): p. 37-49.

2. G. Bavies, *Materials for automobile bodies*. 2012, Great Britain: Butterworth-Heinemann.

3. *Aluminum in cars-European Aluminum Association*. 2008; Available from: www.alueurope.eu/pdf/Aluminium_in_cars_Sept2008.pdf.

4. J. Hirsch, *Aluminum alloys for automotive application.* Materials Science Forum, 1997. **242**: p. 33-50.

5. Y. Birol, *Pre-aging to improve bake hardening in a twin-roll cast Al–Mg–Si alloy.* Materials Science and Engineering: A, 2005. **391**(1–2): p. 175-180.

6. S.S. Hecker, *Formability of Aluminum Alloy Sheets.* Journal of Engineering Materials and Technology, 1975. **97**(1): p. 66-73.

7. J.E. Bird and J.L. Duncan, *Strain hardening at high strain in aluminum alloys and its effect on strain localization.* Metallurgical Transactions A, 1981. **12**(2): p. 235-241.

8. A.K. Ghosh, *The Influence of Strain Hardening and Strain-Rate Sensitivity on Sheet Metal Forming.* Journal of Engineering Materials and Technology, 1977. **99**(3): p. 264-274.

9. A. Sachdev, *Development of an aluminum sheet alloy with improved formability.* Metallurgical and Materials Transactions A, 1990. **21**(1): p. 165-175.

10. S.M. Hirth, G.J. Marshall, et al., *Effects of Si on the aging behaviour and formability of aluminium alloys based on AA6016.* Materials Science and Engineering: A, 2001. **319–321**(0): p. 452-456.

11. P.W. Beaver and B.A. Parker, *Medium strength formable aluminium alloys: an exercise in alloy design.* Materials Science and Engineering, 1986. **82**(0): p. 217-224.

12. H. Liu, W. Song, and G. Zhao, *Pre-aging and microstructures properties on 6000 series aluminium alloys for automotive body sheets.* The Chinese Journal of Nonferrous Metals, 2005. **15**(2): p. 270-276.

13. S.J. Murtha, *New 6xxx aluminum alloy for automotive body sheet applications.* SAE Techn. Paper 950718, 1995.

14. J. Bottema, C. Lahaye, and C. Other, *Recent developments in AA6016 aluminum type body sheet product.* . SAE Techn. Paper 981007, 1998.

15. N.Y. Zolotorevsky, A.N. Solonin, et al., *Study of work hardening of quenched and naturally aged Al–Mg and Al–Cu alloys.* Materials Science and Engineering: A, 2009. **502**(1–2): p. 111-117.

16. K. Campbell, L. Dover, et al., *Influence of heat treatment on the formability of al-Mg-Si alloys.* Metals Forum 2, 1979. **2**: p. 229-235.

17. J.D. Embury and J.L. Duncan, *Formability maps.* Annual Review of Materials Science, 1981. **11**: p. 502-521.

18. H. Liu, G. Zhao, et al., *Effects of different tempers on precipitation hardening of 6000 series aluminium alloys.* Transactions of Nonferrous Metals Society of China, 2007. **17**(1): p. 122-127.

19. S.S. Hecker, *A cup test for assessing stretchability.* Metals Engineering Quarterly, 1974. **14**: p. 30-36.

20. D. Daniel, R. Shahani, et al., *Develpment of 6xxx alloy aluminium sheet for autobody outer panels:bake hardening, formability and trimming performance.* SAE Techn. Paper 1999-01-3195, 1999.

21. R.G. kamat, J.F. Butler, et al., *Alloy 6022-T4E29 for automotive sheet applications.* Materials Science Forum, 2002. **396-402**: p. 1591-1596.

22. S.K. Das, Materials Forum, 2006: p. 1239-1244.

23. *Aluminium in cars-unlocking the light-weighting potential.* Available from: http://www.alueurope.eu/wp-content/uploads/2012/10/EAA-Aluminium-in-Cars-Unlocking-the-light-weighting-potential.pdf.

24. J. Hirsch, *Automotive trends in aluminium - the european perspective.* Materials Forum, 2004. **28**: p. 15-23.

25. D. Daniel, J.L. Hoffmann, et al., *Optimisation of 6016 aluminium alloy selection for outer panels.* SAE Techn. Paper 2002-01-2012, 2002.

26. O. Engler and J. Hirsch, *Texture control by thermomechanical processing of AA6xxx Al–Mg–Si sheet alloys for automotive applications—a review.* Materials Science and Engineering: A, 2002. **336**(1–2): p. 249-262.

27. R.P. Garrett, J. Lin, and T.A. Dean, *An investigation of the effects of solution heat treatment on mechanical properties for AA 6xxx alloys: experimentation and modelling.* International Journal of Plasticity, 2005. **21**(8): p. 1640-1657.

28. A. Sachdev, *Development of an aluminum sheet alloy with improved formability.* Metallurgical Transactions A, 1990. **21**(1): p. 165-175.

29. C. Lahaye, J. Bottema, and P.D. Smet, *Improved AA5182 aluminum alloy as a preferred choice for critical forming operations.* SAE Technical paper 1999-01-3173, 1999.

30. J.D. Embury, W.J. Poole, and D.J. Lloyd, *The work hardening of single phases and multi-phase aluminum alloys.* Mater. Sci. Forum, 2006. **319-521**: p. 71-78.

31. Y. Du, Y.A. Chang, et al., *Diffusion coefficients of some solutes in fcc and liquid Al: critical evaluation and correlation.* Materials Science and Engineering: A, 2003. **363**(1–2): p. 140-151.

32. D.H. Kang, D.W. Kim, et al., *Relationship between stretch formability and work-hardening capacity of twin-roll cast Mg alloys at room temperature.* Scripta Materialia, 2009. **61**(7): p. 768-771.

33. D.J. Lloyd, *The work hardening of some commercial Al alloys.* Materials Science Forum, 2006.

34. U.F. Kocks and H. Mecking, *Physics and phenomenology of strain hardening: the FCC case* Progress in Materials Science, 2003. **48**: p. 171-273.

35. W.J. Poole and J.D. Embury, *Work hardening in aluminium alloys*, in *Fundamentals of Aluminium Metallurgy*, R. Lumley, Editor. 2010, Woodhead Publishing. p. 307.

36. U.F. Kocks, *Laws for work-hardening and low-temperature creep.* Journal of Engineering Materials and Technology, 1976. **98**: p. 76-85.

37. A. Rollett and U.F. Kocks, *A review of the stage of work hardneing.* Materials Science Forum, 1993. **35-36**: p. 1-18.

38. Y. Estrin, *Dislocation Density Related Constitutive Modeling*, in *Unified Constitutive Laws of Plastic Deformation*, A.S. Krausz and K. Krausz, Editors. 1996, Academic Press. p. 69.

39. Y. Estrin and H. Mecking, *A unified phenomenological description of work hardening and creep based on one-parameter models.* Acta Metallurgica, 1984. **32**(1): p. 57-70.

40. L.M. Cheng, W.J. Poole, et al., *The influence of precipitation on the work-hardening behavior of the aluminum alloys AA6111 and AA7030.* Metallurgical and Materials Transactions A, 2003. **34**(11): p. 2473-2481.

41. A. Deschamps, F. Bley, et al., *In-situ small-angle X-ray scattering study of dynamic precipitation in an Al-Zn-Mg-Cu alloy.* Philosophical Magazine, 2003. **83**(6): p. 677-692.

42. A. Deschamps, M. Niewczas, et al., *Low-temperature dynamic precipitation in a supersaturated AI-Zn-Mg alloy and related strain hardening.* Philosophical Magazine A, 1999. **79**(10): p. 2485-2504.

43. C.G. Schmidt and A.K. Miller, *The effect of solutes on the strength and strain hardening behavior of alloys.* Acta Metallurgica, 1982. **30**(3): p. 615-625.

44. J.G. Morris, *Dynamic strain aging in aluminum alloys.* Materials Science and Engineering, 1974. **13**(2): p. 101-108.

45. C.R. Hutchinson, J.D.C. Teixeira, and L. Bourgeois. *Dynamically responding microstructures: a means to simultaneously achieve high strength and high elongation in Al alloys?* in *11th international conference on Al alloys*. 2008. Anchen.

46. A.M. Garde, A.T. Santhanam, and R.E. Reed-Hill, *The significance of dynamic strain aging in titanium.* Acta Metallurgica, 1972. **20**(2): p. 215-220.

47. J.D.C. Teixeira, Y. Brechet, et al., *The strain hardening behaviour of supersaturated Al-Cu alloys.* ICAA.

48. Y. Chen, M. Weyland, and C.R. Hutchinson, *The effect of interrupted aging on the yield strength and uniform elongation of precipitation-hardened Al alloys.* Acta Materialia, 2013. **61**(15): p. 5877-5894.

49. M. Tiryakioglu and J.T. Staley, *Physical Metallurgy and the effect of alloying additions in aluminium alloys*, in *Handbook of Aluminum: Vol. 1: Physical Metallurgy and Processes*, G.E. Totten and D.S. MacKenzie, Editors. 2003. p. 99.

50. T. Narutani and J. Takamura, *Grain-size strengthening in terms of dislocation density measured by resistivity.* Acta Metallurgica et Materialia, 1991. **39**(8): p. 2037-2049.

51. J.D. Meakin and N.J. Petch, *Strain-hardening of polycrystals: The α-brasses.* Philosophical Magazine, 1974. **29**(5): p. 1149-1156.

52. D.J. Lloyd. *Strain localisation and shear banding in aluminum alloys*. in *Formability and Metallurgical Structure*. 1986. Orlando, USA: The Metallurgical Society.

53. W.J. Poole, X. Wang, et al., *The shearablenon-shearable transition in AlMgSiCu precipitation hardening alloys: implications on the distribution of slip, work hardening and fracture.* Philosophical Magazine, 2005. **85**(26-27): p. 3113-3135.

54. J.M. Dowling and J.W. Martin, *The influence of Mn additions on the deformation behaviour of an Al-Mg-Si alloy.* Acta Metall., 1976. **24**: p. 1147-1153.

55. A.K. Busby, L. Edwards, and J.W. Martin, *Effect of aging and dispersoid content on tensile properties of Al–0·6Mg–1 Si alloys.* Materials Science and Technology, 1986. **2**(4): p. 363-367.

56. G.B. Gibbs, *Thermodynamic analysis of dislocation glide controlled by dispersed local obstacles.* Materials Science and Engineering, 1969. **4**(6): p. 313-328.

57. A. Seeger, *CXXXII. The generation of lattice defects by moving dislocations, and its application to the temperature dependence of the flow-stress of F.C.C. crystals.* Philosophical Magazine Series 7, 1955. **46**(382): p. 1194-1217.

58. R.A. Mulford, *Analysis of strengthening mechanisms in alloys by means of thermal-activation theory.* Acta Metallurgica, 1979. **27**(7): p. 1115-1124.

59. Y. Estrin and L.P. Kubin, *Continuum Models for Materials with Microstructure*, in *Continuum Models for Materials with Microstructure*, H.B. Mühlhaus, Editor. 1995, Wiley. p. 395.

60. A.H. Cottrell, *DISLOCATIONS AND PLASTIC FLOW IN CRYSTALS*. 1965: Clarendon Press.

61. A.H. Cottrell, *LXXXVI. A note on the Portevin-Le Chatelier effect.* Philosophical Magazine Series 7, 1953. **44**(355): p. 829-832.

62. L.P. Kubin and Y. Estrin, *Dynamic strain ageing and the mechanical response of alloys.* J. Phys. III, 1991: p. 929-943.

63. P.G. McCormigk, *A model for the Portevin-Le Chatelier effect in substitutional alloys.* Acta Metallurgica, 1972. **20**(3): p. 351-354.

64. A. van den Beukel, *Theory of the effect of dynamic strain aging on mechanical properties.* physica status solidi (a), 1975. **30**(1): p. 197-206.

65.   R.A. Mulford and U.F. Kocks, *New observations on the mechanisms of dynamic strain aging and of jerky flow.* Acta Metallurgica, 1979. **27**(7): p. 1125-1134.

66.   P. Rodriguez, *Serrated plastic flow.* Bulletin of Materials Science, 1984. **6**(4): p. 653-663.

67.   L.P. Kubin and Y. Estrin, *Evolution of dislocation densities and the critical conditions for the Portevin-Le Châtelier effect.* Acta Metallurgica et Materialia, 1990. **38**(5): p. 697-708.

68.   A. Yilmaz, *The Portevin–Le Chatelier effect: a review of experimental findings.* Science and Technology of Advanced Materials, 2011. **12**(6): p. 063001.

69.   A. Van Den Beukel, *On the mechanism of serrated yielding and dynamic strain ageing.* Acta Metallurgica, 1980. **28**(7): p. 965-969.

70.   Y. Brechet and Y. Estrin, *On the influence of precipitation on the Portevin-Le Chatelier effect.* Acta Metallurgica et Materialia, 1995. **43**(3): p. 955-963.

71.   Y. Brechet and Y. Estrin, *On a pseudo-Portevin-Le Chatelier effect.* Scripta Metallurgica et Materialia, 1994. **31**(2): p. 185-190.

72.   P.G. Mccormick. *Negative strain rate sensitivity and the develpment of localised yielding.* in *Formability and Metallurgical Structure.*

73.   J.M. Robinson, *Serrated flow in aluminium base alloys.* International Materials Reviews, 1994. **39**(6): p. 217-227.

74.   L.R. Morris, R. Iricibar, et al., *Formability of Aluminum sheet alloys.* 1982.

75.   R.P.a.D. Ganguli, *The forming limits of aluminum-magnesium alloy sheet in biaxial tension.* Journal of the Institute of Metals, 1972. **100**: p. 289-295.

76.   A. Deschamps, S. Esmaeili, et al., *Strain hardening in relation to microstructure in precipitation hardening materials.* J. Phys. IV France, 2000. **10**: p. 151-156.

77.   H.J. Harun and P.G. McCormick, *Effect of precipitation hardening on strain rate sensitivity and yield behaviour in an Al-Mg-Si alloy.* Acta Metallurgica, 1979. **27**(1): p. 155-159.

78.   I.R. Dover, J.D. Embury, and J.L. Duncan, *The influence of microstructure on the formability and fracture of an aluminum-copper alloy (2036).* J. Applied Metalworking, 1980. **1**: p. 24-33.

79. Q. Zhao and B. Holmedal, *Modelling work hardening of aluminium alloys containing dispersoids.* Philosophical Magazine, 2013. **93**(23): p. 3142-3153.

80. R.E. Sanders, *Microstructure, slip distribution, and strain hardening in aluminium alloys*, in *Formability of Metallic Materials*. 2000.

81. K. Strobel, E. Sweet, et al., *Dispersoids phases in 6xxx series aluminium alloys.* Mater. Sci. Forum, 2010. **654-656**: p. 926-929.

82. S.A. Court, K.M. Gatenby, and D.J. Lloyd, *Factors affecting the strength and formability of alloys based on Al-3 wt.% Mg.* Mater. Sci. Eng. A, 2001. **319-321**: p. 443-447.

83. P.L. Sun, E.K. Cerreta, et al., *The effect of grain size, strain rate, and temperature on the mechanical behavior of commercial purity aluminum.* Metallurgical and Materials Transactions A, 2006. **37**(10): p. 2983-2994.

84. Y. Estrin, M. Murashkin, and R. Valiev, *Ultrafine-grained aluminium alloys: processes, structural features and properties*, in *Fundamentals of Aluminium Metallurgy: Production, Processing And Applications*

R. Lumley, Editor. 2011. p. 468–503.

85. Q. Wei, S. Cheng, et al., *Effect of nanocrystalline and ultrafine grain sizes on the strain rate sensitivity and activation volume: fcc versus bcc metals.* Materials Science and Engineering: A, 2004. **381**(1–2): p. 71-79.

86. O. Saray, G. Purcek, et al., *Formability of Ultrafine-Grained Interstitial-Free Steels.* Metallurgical and Materials Transactions A, 2013. **44**(9): p. 4194-4206.

87. D.V. Wilson, A.R. Mirshames, and W.T. Roberts, *An experimental study of the effect of sheet thickness and grain size on limit-strains in biaxial stretching* International Journal of Mechanical Sciences, 1983. **25**: p. 859-870.

88. R.C. Dorward, *Forming characteristics of coarse and fine-grained AA 2024 aluminum alloy sheet.* Journal of Materials Engineering and Performance, 1994. **3**: p. 115-121.

89. A. Korbel, J.D. Embury, et al., *Microstructural aspects of strain localization in Al Mg alloys.* Acta Metallurgica, 1986. **34**(10): p. 1999-2009.

90. D.V. Wilson, W.T. Roberts, and P.M.B. Rodrigues, *Effect of Grain anisotropy on limit strains in biaxial stretching: part i. influence of sheet thickness and grain size in weakly textured sheets.* Metall. Trans. A 1981. **12**: p. 1595-1602.

91. C.S. Man, *On the r-value of textured sheet metals.* International Journal of Plasticity, 2002. **18**(12): p. 1683-1706.

92. S. Mishra and C. Darmann, *Role and control of texture in deep-drawing steels.* International Materials Reviews, 1982. **27**(1): p. 307-320.

93. K.O. Pedersen, O.G. Lademo, et al., *Influence of texture and grain structure on strain localisation and formability for AlMgSi alloys.* Journal of Materials Processing Technology, 2008. **200**(1–3): p. 77-93.

94. K. Yoshida, T. Ishizaka, et al., *The effects of texture on formability of aluminum alloy sheets.* Acta Materialia, 2007. **55**(13): p. 4499-4506.

95. M. Murayama, K. Hono, et al., *The Effect of Cu Additions on the Precipitation Kinetics in an Al-Mg-Si Alloy with Excess Si.* Metallurgical and Materials Transactions A, 2001. **32**(2): p. 239-246.

96. W.F. Miao and D.E. Laughlin, *Effects of Cu Content and Preaging on Precipitation Characteristics in Aluminum Alloy 6022.* Metallurgical and Materials Transactions A, 2000. **31**(2): p. 361-371.

97. G. Svenningsen, M.H. Larsen, et al., *Effect of high temperature heat treatment on intergranular corrosion of AlMgSi(Cu) model alloy.* Corrosion Science, 2006. **48**(1): p. 258-272.

98. E. Brünger, O. Engler, and J. Hirsch, *Al-Mg-Si sheet alloys for autobody applications*, in *Virtual fabrication of aluminium products: microstructural modeling in industrial aluminum fabrication processes*, J. Hirsch, Editor. 2006, Wiley-Vch. p. 51-63.

99. F. Ozturk, E. Esener, et al., *Effects of aging parameters on formability of 6061-O alloy.* Materials & Design, 2010. **31**(10): p. 4847-4852.

100. T.R. Thomson, G. Glover, and R. Jackson, *The formability of sheet steels.* BHP Technical Bulletin, 1974. **18**: p. 15-19.

101. R.S. Brammar and D.A. Harris, *Production and properties of sheet metal and aluminium alloys for forming applications.* Journal of the Australian Institute of Metals, 1975. **20**: p. 85-100.

102. P.W. Beaver, *The formability of wrought aluminum alloys*. 1980, Monash University. p. 278.

103. H.J.B. D. Banabic, K. Pohlandt, A. E. Tekkaya, *Formability of metallic materials: plastic anisotropy, formability testing, forming limits*. 2000.

104. ASTM standard E643-09, *Standard test method for ball punch deformation of metallic sheet material*. 2009.

105. D. Banabic, *Forming limts of sheet metal*, in *Formability of metallic materials: plastic anisotropy, formability testing, forming limits*
D. Banabic, Editor. 2000, Springer-Verlag Berlin Heidelberg Germany. p. 173-214.

106. J.A. Schey, *Formability determination for production control*. Journal of Materials Processing Technology, 1992. **32**(1–2): p. 207-221.

107. M. Safaeirad, M.R. Toroghinejad, and F. Ashrafizadeh, *Effect of microstructure and texture on formability and mechanical properties of hot-dip galvanized steel sheets*. Journal of Materials Processing Technology, 2008. **196**(1–3): p. 205-212.

108. K. Narasimhan, M.P. Miles, and R.H. Wagoner, *A better sheet-formability test*. Journal of Materials Processing Technology, 1995. **50**(1–4): p. 385-394.

109. D. Banabic, *Sheet Metal Forming Processes*. 2010: Springer Berlin Heidelberg.

110. K.J. Kim, C. Kim, et al., *Formability of Aluminum 5182-Polypropylene Sandwich Sheet for Automotive Application*. Journal of Solid Mechanics and Materials Engineering, 2008. **2**(4): p. 574-581.

111. R. Ayres, W. Brazier, and V. Sajewski, *Evaluating the GMR-Limiting Dome Height Test as a new measure of press formability near plane strain*. Journal of Applied Metalworking, 1978. **1**(1): p. 41-49.

112. A.s. E646-00, *Standard test method for tensile stain-hardening exponents (n-values) of metallic sheet metals*.

113. A.s. E517-00, *Standard test method for plastic strain ratio r for sheet metal*.

114. R. Stevenson, *Correlation of tensile properties with plane-strain, limiting dome height*. Journal of Applied Metalworking, 1984. **3**(3): p. 272-280.

115. M.P. Miles, J.L. Siles, et al., *A better sheet formability test*. Metallurgical Transactions A, 1993. **24**(5): p. 1143-1151.

116. M.M. Moshksar and S. Mansorzadeh, *Determination of the forming limit diagram for Al 3105 sheet.* Journal of Materials Processing Technology, 2003. **141**(1): p. 138-142.

117. E. Hsu, J.E. Carsley, and R. Verma, *Development of Forming Limit Diagrams of Aluminum and Magnesium Sheet Alloys at Elevated Temperatures.* Journal of Materials Engineering and Performance, 2008. **17**(3): p. 288-296.

118. S.S. Hecker. *Experimental studies of sheet stretchability.* in *Formability: Analysis, modelling and experimentation.* 1977.

119. F. Casari, M. Tassan, et al., *Effect of punch diameter, grid dimension and lubrication on forming limit diagram.* Journal of Testing and Evaluation, 2006. **34**: p. 1-7.

120. L.M. Brown. *Precipitation and dispersion hardening.* in *ICSMA 5.* 1979. Aachen: Pergamon.

121. *TTAL6, TT Al-based alloys database, version 6.0, ThermoTech Ltd., Surrey Technology Center, Guildford, United Kindom, 2007.*

122. N.C.W. Kuijpers and F.J. Vermolen, *The dependence of the -AlFeSi to -Al(FeMn)Si transformation kinetics in Al–Mg–Si alloys on the alloying elements.* Mater. Sci. Eng. A, 2005. **394**: p. 9-19.

123. M.J. Starink, L.F. Cao, and P.A. Rometsch, *A model for the thermodynamics of and strengthening due to co-clusters in Al–Mg–Si-based alloys.* Acta Materialia, 2012. **60**(10): p. 4194-4207.

124. P.M. Rodrigues, *A new 6xxx series aluminium car body sheet alloy.* Sheet Metal Industries, 1984. **6**: p. 492-495.

125. Y. Huang and F.J. Humphreys, *The effect of solutes on grain boundary mobility during recrystallization and grain growth in some single-phase aluminum alloys.* Materials Chemistry and Physics, 2012. **132**: p. 166-174.

126. D.J. Lloyd, *The deformation of commercial aluminum-magnesium alloys.* Metallurgical Transactions A, 1980. **11**(8): p. 1287-1294.

127. P.W. Beaver, *Localized thinning, fracture and formability of alumnum sheet alloys in biaxial tension.* Journal of mechanical working technology, 1982. **7**: p. 215-231.

128. M.S. Duesbery, *Dislocation motion, constrictiona and cross-slip in fcc metals.* Modelling Simulation in Materials Science Engineeing, 1998. **6**: p. 35-49.

129. W.F. Hosford, *Mechanical behavior of materials.* 2005: Cambridge university press.

130. A.K. Gupta, D.J. Lloyd, and S.A. Court, *Precipitation hardening in Al–Mg–Si alloys with and without excess Si.* Materials Science and Engineering: A, 2001. **316**(1–2): p. 11-17.

131. J.D. Embury and J.L. Duncan, *Formaiblity maps.* Annual Review of Materials Science, 1981. **11**: p. 505-521.

132. D.M. Riley and P.G. McCormick, *The effect of precipitation hardening on the portevin-le chatelier effect in an Al-Mg-Si alloy.* Acta Metallurgica, 1977. **25**(2): p. 181-185.

133. H. Zhong, P. Rometsch, and Y. Estrin, *The Influence of Si and Mg Content on the Microstructure, Tensile Ductility, and Stretch Formability of 6xxx Alloys.* Metallurgical and Materials Transactions A, 2013. **44**(8): p. 3970-3983.

134. P.A. Rometsch, S.X. Gao, and M.J. Couper, *Effect of Composition and Pre-Ageing on the Natural Ageing and Paint-baking Behaviour of Al-Mg-Si Alloys*, in *ICAA13: 13th International Conference on Aluminum Alloys*. 2012, John Wiley & Sons, Inc. p. 15-20.

135. J. Banhart, C.S.T. Chang, et al., *Natural Aging in Al-Mg-Si Alloys – A Process of Unexpected Complexity.* Advanced Engineering Materials, 2010. **12**(7): p. 559-571.

136. M. Liu, Y. Yan, et al., *Influence of Mg and Si on Cluster Formation in Al-Mg-Si Alloys Studied by Positron Annihilation Lifetime Spectroscopy*, in *ICAA13: 13th International Conference on Aluminum Alloys*. 2012, John Wiley & Sons, Inc. p. 1131-1137.

137. C. Lahaye and J. Bottema, *Improved AA5182 aluminium alloys as a preferred choice for critical forming operations.* SAE Techn. Paper 1999-01-3173, 1999.

138. P.E. Fortin, M.J. Bull, and D.M. Moore, *An optimized aluminum alloy (x6111) for auto body sheet application.* SAE Techn. Paper 830096, 1983.

139. N. Tian, G. Zhao, et al., *Effect of Cu content on the formability and bake-hardening ability of Al-1.0Mg-1.0Si-0.6Mn aluminium alloys sheet.* Journal of Materials and Metallurgy, 2010. **9**: p. 133-142.

140. M. Mantina, Y. Wang, et al., *First principles impurity diffusion coefficients.* Acta Materialia, 2009. **57**(14): p. 4102-4108.

141. D.K. Chatterjee and K.M. Entwistle, *A study of the effect of magnesium loss and of the addition of copper on the ageing of aluminium-magnesium-silicon alloys.* Journal of the Institute of Metals, 1973. **101**.

142. S. Pogatscher, H. Antrekowitsch, et al., *Mechanisms controlling the artificial aging of Al–Mg–Si Alloys.* Acta Materialia, 2011. **59**(9): p. 3352-3363.

143. S. Allain, F. Danoix, et al., *Static and dynamical ageing processes at room temperature in a Fe25Ni0.4C virgin martensite: effect of C redistribution at the nanoscale.* Philosophical Magazine Letters, 2012. **93**(2): p. 68-76.

144. I.S. Kim and M.C. Chaturvedi, *Serrated flow in Inconel 625.* Transaction of the Japan Institute of Metals, 1987. **28**(3): p. 205-212.

145. J. Banhart, M.D.H. Lay, et al., *Kinetics of natural aging in Al-Mg-Si alloys studied by positron annihilation lifetime spectroscopy.* Physical Review B, 2011. **83**(1): p. 1-13.

146. J. Banhart, M. Liu, et al., *Study of ageing in Al–Mg–Si alloys by positron annihilation spectroscopy.* Physica B: Condensed Matter, 2012. **407**(14): p. 2689-2696.

147. A. Somoza, A. Dupasquier, et al., *Positron-annihilation study of the aging kinetics of AlCu-based alloys. I. Al-Cu-Mg.* Physical Review B, 2000. **61**(21): p. 14454-14463.

148. U. Ali and G.F. Wyatt-Mair, *In-line method of making heat treated and annealed aluminium alloy sheet.* US patent US7182825, 2007.